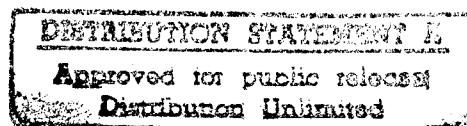NASA Conference Publication 2122

Part I

Cryogenic Technology

Proceedings of
a conference held at
Langley Research Center
Hampton, Virginia
November 27-29, 1979

FOR EARLY DOMESTIC DISSEMINATION

Because of its significant early commercial potential, this information, which has been developed under a U.S. Government program, is being disseminated within the United States in advance of general publication. This information may be duplicated and used by the recipient with the express limitation that it not be published. Release of this information to other domestic parties by the recipient shall be made subject to these limitations.

Foreign release may be made only with prior NASA approval and appropriate export licenses. This legend shall be marked on any reproduction of this information in whole or in part.

Date for general release ___March 1982.___

NASA

NASA Conference Publication 2122

Part I

Cryogenic Technology

Proceedings of
a conference held at
Langley Research Center
Hampton, Virginia
November 27-29, 1979

NASA

National Aeronautics
and Space Administration

**Scientific and Technical
Information Office**

1980

PREFACE

The proceedings of the NASA Conference on Cryogenic Technology held at Langley Research Center on November 27-29, 1979, are in this NASA Conference Publication.

The purpose of the conference was to provide early dissemination of new cryogenic technology generated by the design and construction of the National Transonic Facility and review of plans and programs essential to its operation and utilization. This was the first conference held specifically for this purpose.

The technical papers reported resulted from in-house efforts and covered a wide variety of subjects where new technology had evolved as a consequence of the cryogenic test environment. The general areas covered by sessions were:

    I. Overviews
   II. Mechanical/Structural Design
  III. Systems Design
   IV. Instrumentation
    V. Model/Sting Technology

The efforts of the review committee, session chairmen, and speakers contributing to the technical excellence and professional character of the conference are especially appreciated.

Certain commercial materials are identified in the proceedings in order to specify adequately the materials investigated in the developmental work. In no case does such identification imply recommendation or endorsement of the product by NASA, nor does it imply that the materials are necessarily the only ones or the best ones available for the purpose. In many cases equivalent materials are available and would probably produce equivalent results.

Robert R. Howell
Conference Chairman

CONTENTS

Part I

*Papers 17 to 29 are presented under separate cover.

vi

SESSION I - OVERVIEWS

EVOLUTION OF THE CRYOGENIC WIND TUNNEL AND EXPERIENCE

WITH THE LANGLEY 0.3-METER TRANSONIC CRYOGENIC TUNNEL

Robert A. Kilgore
NASA Langley Research Center

SUMMARY

This paper traces some of the key events in the evolution of the cryogenic wind tunnel leading up to the decision in the United States to build the National Transonic Facility (NTF), the first major wind tunnel especially designed to take advantage of cryogenic operation. The NTF, which is the subject of this conference, will not only close the Reynolds number gap, but will also provide for the exploitation of other unique research capabilities made possible by cryogenic operation. A brief overview is given of the cryogenic wind tunnel projects around the world in order to illustrate the profound impact the cryogenic tunnel concept is having on wind tunnel development. This paper also reviews some of our experiences with the Langley 0.3-Meter Transonic Cryogenic Tunnel (TCT), the tunnel in which the cryogenic wind tunnel concept was verified at transonic speeds, thereby making possible the decision to build the NTF.

INTRODUCTION

Reynolds number has long been recognized as an important scaling parameter in wind tunnel testing. As shown in Figure 1, dynamic similarity between the flow over the vehicle in flight and the flow over the model in the wind tunnel requires the Reynolds numbers to be equal. It is also well known that at transonic speeds in air, equality of Reynolds number is not enough. To insure dynamic similarity for compressible fluids there is the additional requirement that the Mach numbers be equal. Over the years, as aircraft speeds have increased, we have been able to build tunnels capable of matching flight values of Mach number. The main difficulty in trying to simulate flight conditions in the wind tunnel is therefore one of achieving adequate values of Reynolds number to assure dynamic similarity.

The need for increased capability in terms of test Reynolds number has been recognized since the earliest days of testing sub-scale models. Today, the need for increased test Reynolds number capability is especially acute. Modern aircraft wings encounter, even by design, large areas of complex transonic flows involving, as illustrated in Figure 2, interactions between recompression shocks and the boundary layer which can be highly sensitive to Reynolds number. The interest in high angle of attack

aerodynamics and the resulting Reynolds number sensitive flows about the fuselage forebody is but one other example of the urgent need for improved wind tunnel simulation.

Previous attempts to provide high Reynolds number transonic tunnels have been seriously limited by the large drive power required for transonic tunnels which has made it necessary to use relatively small tunnels, and therefore relatively small models. This difference between model and full-scale size has created the so-called "Reynolds number gap", the difference between our present capability and full-scale Reynolds number.

The Reynolds number gap in the U.S. at subsonic and transonic speeds is illustrated in Figure 3. The problems actually caused by, or at least attributed to, the Reynolds number gap have been numerous and are well documented.[1,2] Several of these are listed in Figure 4. Perhaps the best known example is that of the C-141 aircraft shown in Figure 5. In this case, the relatively thicker boundary layer of the low Reynolds number tunnel tests caused the recompression shock to be located 20 percent farther forward on the wing of the model than on the wing of the aircraft in flight. As a result of this lack of proper simulation of flight Reynolds number in the wind tunnel, there was a 9-month delay in the initial operational availability of the C-141.

Of the various ways of increasing Reynolds number that have been tried or proposed for closing the Reynolds number gap for transonic tunnels, cooling the test gas to cryogenic temperatures (150 K or less) appears to be the best solution in terms of model, balance and sting loads, as well as capital and operating cost. In addition, having temperature as an independent test variable offers some new and unique aerodynamic testing capabilities which, in some instances, may be of equal importance with the ability to achieve full-scale Reynolds number. Personnel at the NASA Langley Research Center have been studying the application of the cryogenic wind tunnel concept to various types of high Reynolds number transonic tunnels since the autumn of 1971 and, through extensive theoretical and experimental studies, have successfully demonstrated both the validity and practicality of the concept.[3-6] As a result of this work, the first major transonic tunnel especially designed to take advantage of cryogenic operation is now under construction here at the Langley Research Center. This tunnel, the National Transonic Facility (NTF), will provide an order of magnitude increase in Reynolds number capability over existing tunnels in the United States when it becomes operational in 1982 and will close the Reynolds number gap.

This paper traces some of the key events in the evolution of the cryogenic wind tunnel leading up to the decision in the U.S. to build the NTF. A brief overview is given of the cryogenic wind tunnel projects around the world in order to illustrate the profound impact the cryogenic tunnel concept is having on wind tunnel development. This

paper also reviews some of our experiences with the 0.3-m transonic cryogenic tunnel (TCT), the tunnel in which the cryogenic wind tunnel concept was verified at transonic speeds, thereby making possible the decision to build the NTF.

SYMBOLS

a	speed of sound
c	chord of two-dimensional airfoil
$\bar{c}$	mean geometric chord
C_p	pressure coefficient, $\dfrac{p - p_\infty}{q_\infty}$
E	modulus of elasticity
ι	linear dimension of model
M	Mach number
p	pressure
q	dynamic pressure, $1/2\ \rho V^2$
Q	q/q_∞
R	Reynolds number, $\dfrac{V}{a}$
T	temperature, K
x	linear dimension
α	angle of incidence
δ	boundary layer thickness
μ	viscosity
ρ	density

Subscripts

max	maximum
min	minimum
t	stagnation conditions
∞	free stream

EVOLUTION OF THE CRYOGENIC WIND TUNNEL

1870-1920

The origin of the highly sophisticated National Transonic Facility, as well as the origin of all other wind tunnels, is to be found in a very simple wind tunnel built one hundred and nine years ago in Greenwich, England. It was in 1870 that the first wind tunnel was built under the direction of a marine engineer with a keen interest in aeronautics, Mr. F. H. Wenham, who had the support and financial backing of the Aeronautical Society of Great Britain (now the Royal Aeronautical Society) and the help of Mr. John Browning.[7] A photograph of Wenham is presented in Figure 6. Unfortunately, no photograph or detailed description of this historic tunnel has been found and we can only speculate on its appearance. The only description we have is the following: "By means of a fan-blower, a current of considerable force was directed through a trunk ten feet long by eighteen inches square."[8]

The first tests were on five flat plates fixed at various angles to the wind on a horizontal arm outside the tunnel, but in the airstream. The test results were published by the Aeronautical Society in its Annual Report for 1871 and it was not long before other, presumably more sophisticated, wind tunnels were being built and put to use.

It soon became obvious that the testing of either full-scale components or sub-scale models under the controlled conditions of a wind tunnel offered many advantages over earlier methods of testing. By the end of the first world war the wind tunnel was firmly established as an essential tool and, by 1920 or so, there were large low-speed tunnels in regular use at the major aeronautical laboratories around the world. However, as airships and airplanes increased in both size and speed and became more sophisticated, some of the limitations and disadvantages of testing in wind tunnels were becoming serious problems.

1920-1945

In several of the aeronautical papers[9-11] written around 1920, the following "problems" are listed as common to even the best wind tunnels of that era:

low Reynolds number
flow unsteadiness
wall interference
support interference

As you can see, the major problems we have with the wind tunnels of today were also recognized in the wind tunnels of 60 years ago. It is only fair to note that these problems are still with us not through a lack of

effort in trying to solve them during the last 60 years. Rather, they are still with us due to their complexity as well as to the fact that, with some, their magnitude and nature have changed with increasing flight speed and aircraft size. Thus, we find that many of the solutions that were developed and found to be adequate at low speeds are of little or no use today. Each of the "problems" listed above has been, and could again be, the subject of an entire conference. However, our primary interest at this conference is related to the single problem of "low Reynolds number" and what has been done about its solution.

Increasing Reynolds Number by Increasing Pressure

A practical solution to the problem of low Reynolds number for low speed tunnels was conceived early in 1920 by Dr. Max Munk[12] here at Langley when it was the Langley Memorial Aeronautical Laboratory of the N.A.C.A. After considering many fluids that might be substituted for air in a wind tunnel in order to increase the test Reynolds number, Munk decided the only reasonable choice would be the "new" fluid he would obtain by compressing air. This new fluid, compressed air, has increased density but essentially unchanged viscosity and speed of sound.

As can be seen from Figure 7, any increase in Reynolds number brought about solely through pressurization is a result of increasing the inertia force term of the equation for Reynolds number. As shown in the lower left of Figure 7, the problem with this solution is the fact that the desired increase in Reynolds number is accompanied by a commensurate and undesirable increase in drive power and in dynamic pressure, q, with increases in model, balance, and sting loads. Munk circumvented to some extent the problem of increased power and q by taking advantage of the fact that Mach number did not have to be matched between the tunnel tests and the full-scale low-speed airplanes of the 1920's. As shown in the lower right of Figure 7, Munk recognized that testing 1/10-scale models at a pressure of 20 atmospheres and at 1/2 of the full-scale speed made it possible to achieve full-scale values of Reynolds number with drive power only 2 1/2 times and model loads only 5 times those experienced in conventional unpressurized tunnels. Munk's suggested solution was realized in 1921 with the construction of the second wind tunnel at Langley Field, the N.A.C.A. variable density wind tunnel (VDT). A sectional view of the VDT is shown in Figure 8 and a photograph is shown in Figure 9. The influence of the high operating pressure is evident in the design of the annular-return tunnel within the very sturdy pressure vessel.

Problems with High Pressures.- When compressibility effects become important, both flight Reynolds number and flight Mach number must be matched in the wind tunnel. Thus, for much of todays testing, we are not able to take advantage of Munk's idea of simply reducing velocity

in order to keep power and dynamic pressure within reasonable bounds. Some of the problems that can arise when excessively high pressure is used to increase test Reynolds number are illustrated in Figure 10. In addition to increasing wing deflection with increasing q, it may be necessary to drastically modify the shape of the aft portion of the model fuselage to accomodate the more robust support sting. In addition, the larger sting can seriously distort the flow field. To avoid these problems, the use of high test pressures is generally avoided except for tests at very low speeds.

Increasing Reynolds Number by Reducing Temperature

Consideration of operating at low temperatures in order to increase the Reynolds number capability of a wind tunnel came in 1920 when W. Margoulis, a Frenchman working as an "aerodynamical expert" in the Paris Office of the NACA, pointed out that using a heavy gas (such as CO_2) and cooling the gas to 253 K would increase the test Reynolds number and reduce the drive power requirements for fan-driven tunnels.[13,14] He concluded that the moderate benefits resulting from cooling to 253 K were not worth the effort. Other researchers of that time[12,15] knew of Margoulis' work. However, it appears that they too believed the benefits of moderate cooling not worth the effort and, so far as we know, no attempt was made at that time to cool the test gas in a wind tunnel below ambient conditions.

That Reynolds number increases as total temperature is reduced is a well known fact to any wind tunnel operator who has had to calculate Reynolds number for the relatively moderate temperature variations encountered in conventional tunnels. However, at first glance, it is no more obvious to us today than it was to our counterparts in 1920 whether or not the benefits of reducing temperature are worth the effort. To see more clearly what the benefits of cooling might be and to understand where the benefits come from, we need to take a closer look at how the individual terms in the equation for Reynolds number, as well as how Reynolds number itself, vary with both temperature and pressure.

The equation for Reynolds number can be written

$$R = \frac{\text{inertia force}}{\text{viscous force}} = \frac{\rho V^2 \iota^2}{\mu V \iota} = \frac{\rho V \iota}{\mu} = \frac{\rho M_a \iota}{\mu}$$

To the first order μ and a are not functions of pressure while ρ is directly proportional to pressure. Thus, as previously noted, increasing pressure produces an increase in Reynolds number by increasing the inertia force with a commensurate increase in drive power and q, which causes a highly undesirable increase in model, balance, and sting loads. Also, to the first order, $\rho \propto T^{-1}$, $\mu \propto T^{0.9}$ and, for a constant Mach number, $V \propto T^{0.5}$. Thus, decreasing temperature leaves the inertia force, and hence the model, balance, and sting loads, unchanged at a

8

given Mach number due to the compensating effects of ρ and V^2. The increase in Reynolds number with decreasing temperature is thus due strictly to the large reduction in the viscous force term as a result of the reduction in μ and V with temperature.

The fact that Reynolds number can be increased without using a pressurized gas also gives rise to important advantages with regard to reducing the tunnel shell stresses and therefore reducing the capital cost.

The effect of a reduction in temperature on the gas properties, test conditions, and drive power are illustrated in Figure 11. For comparison purposes, a stagnation temperature of 322 K for normal ambient temperature tunnels is assumed as a datum. It can be seen that cooling the test gas sufficiently results in an increase in Reynolds number by more than a factor of 6 with no increase in dynamic pressure and with a large reduction in the required drive power. To obtain such an increase in Reynolds number without increasing either the tunnel size or the operating pressure while actually reducing the drive power is extremely attractive and makes the cryogenic approach to a high Reynolds number transonic tunnel much more desirable than previous approaches.

In Margoulis' time, however, the ability to cool to cryogenic temperatures anything as large as even a small wind tunnel was impractical. Since Margoulis suggested cooling to 253 K, we can safely assume that cooling a tunnel to such a temperature was practical. However from Figure 11, we can see that this relatively small amount of cooling produces only a slight increase in Reynolds number. We, like Margoulis and others of his time, must conclude that the benefits of only moderate cooling are not worth the effort.

1945-1971

As with many good ideas, that of cooling the test gas to increase Reynolds number seems to have been independently recognized and proposed by several people before finally being put into practice.

Margoulis' idea of 1920 appears to have been forgotten until some 25 years later when, in 1945, a theoretical study by Smelt[16] again pointed out that the use of heavy gases and reduced temperatures would permit large reductions in wind-tunnel size and power requirements in comparison with a wind tunnel operated at normal temperature and the same pressure, Mach number, and Reynolds number. The study by Smelt was presumably a case of the independent re-invention of a good idea since Margoulis was not cited. During a visit to Langley in 1975, Dr. Smelt stated that the lack of a practical means of cooling a reasonable size wind tunnel to cryogenic temperatures and the unavailability of suitable structural materials precluded application of the cryogenic wind-tunnel concept at the time of his work. The apparent lack of interest in overcoming these practical problems and applying the cryogenic concept in 1945 was

probably due to the fact that the Reynolds number gap was not as great in 1945 as it is today since aircraft of that time were generally smaller than those of today and were not being designed to operate with local transonic flows. It also appears that the excellent study by Smelt did not in later years receive the wide recognition it deserved due to its security classification. Smelt's paper was, in fact, finally declassified and made available to the public just this year, 34 years after it was written!

As noted by Goodyer[17], "we can perhaps excuse ourselves for missing these proposals, the first [Margoulis] on the count of obscurity, the second [Smelt] because most researchers were denied access by its security classification. However, we are guilty of ignoring another airing of the proposal in the text Wind-Tunnel Technique by Pankhurst and Holder[18]. Through 1 1/2 pages in their 700 page book published in 1952 they outlined the concept and its advantages. It seems we all failed to recognize and exploit this approach".

Rush's Compressor Test Rig

In 1962 C. K. Rush of the National Research Council of Canada built a compressor test rig which appears to have been the first practical application of the cryogenic concept for aerodynamic measurements.[19] According to Rush, "The project had its origin in a suggestion from Dr. D. C. MacPhail who was director of the Mechanical Engineering Division of the NRC at that time (around 1961)." But for the absence of a test section, Rush's test rig would have been the first cryogenic wind tunnel. The test rig, shown in Figure 12, consisted of a single-stage compressor pumping air through a closed circuit containing an air-liquid nitrogen heat exchanger which cooled the air in the rig to about 125 K. By operating at these very low temperatures, Rush, taking advantage of the reduction in the speed of sound at reduced temperatures, was able to achieve dynamic similarity with a substantial reduction in both rotational speed and the power required to drive the compressor. In this application of the cryogenic concept, Rush's main interest was in the reduction of rotational speed and the attendant reduction in impeller loading which allowed him to test various compressor configurations using impellers of easily machined materials.

1971-1975

So far as I know, the next step in the evolution of the cryogenic wind tunnel took place here at Langley in October 1971. Dr. M. J. Goodyer of the University of Southampton, England, who was working with us at the time as a NRC Associate, suggested, independently, the use of either air or nitrogen at cryogenic test temperatures as a way of increasing the test Reynolds number in the small tunnels equipped with magnetic-suspension and balance systems.[4] By 1971, the availability of liquified

gases in large quantities and the wide-spread application of cryogenic technology in government and industry made Goodyer's proposal seem reasonable not only for the tunnels of modest size equipped with magnetic suspension and balance systems, but also for large tunnels that would be capable of testing models of full-scale values of Reynolds number.

I was fortunate to be working with Goodyer at the time on the magnetic-suspension and balance research. Because of the urgent need for a reasonable size transonic tunnel capable of full-scale, or near full-scale Reynolds numbers, the work on magnetic-suspension and balance systems was temporarily set aside as we established a small team of Langley researchers to solve, hopefully, any practical problems we might find in trying to make the cryogenic wind tunnel concept work.

Low Speed Cryogenic Tunnel

By January of 1972, the concept had at last been turned into hardware with the successful operation of a low-speed cryogenic tunnel here at Langley.[4] This tunnel was used for a variety of so-called "proof-of-concept" tests through the spring and summer of 1972.

Description of the Low-Speed Tunnel.- The low-speed tunnel was a single-return fan-driven tunnel with a 7" x 11" (17.8 cm x 27.9 cm) closed-throat test section. The atmospheric tunnel could be operated at Mach number from near zero to 0.2 over a temperature range from 333 K to 80 K. The low-speed tunnel was adapted from an existing 1/24 - scale model of the Langley V/STOL tunnel and was therefore aerodynamically representative of modern low-speed tunnel practice.

A sketch of the low-speed cryogenic tunnel circuit is shown in Figure 13. A photograph of the tunnel being insulated is shown in Figure 14 and a photograph of the insulated tunnel and test apparatus as it appeared in the spring of 1972 is shown in Figure 15. Materials of construction included wood, plywood, plexiglas, mild and stainless steels, aluminum, brass, copper, and fiberglas reinforced plastic. The fan blades were made of laminated wood.

Viewing ports were provided to allow inspection of key areas of the tunnel circuit including the test section, spray zones, corner vanes, screen section, and contraction section. The viewing ports consisted of either 3 or 4 layers of plexiglas separated by air gaps. Thermal insulation for the remainder of the circuit was a 3" to 4" (7.6 cm to 10.2 cm) layer of expanded styrofoam applied to the outside of the tunnel structure with a 0.005" (0.0127 cm) thick polyethylene vapor barrier on the outside.

The tunnel was cooled and the heat of compression added to the stream by the drive fan was removed by spraying liquid nitrogen (LN_2) at about 78 K directly into the tunnel circuit in either of the two locations shown in Figure 13. Complete evaporation of the liquid nitrogen was achieved down to the lowest temperature explored of 80 K.

The rate of cooling of the tunnel circuit was such that, for example, a temperature of 116 K could be stabilized within 10 minutes of the initiation of cooling from room temperature. The tunnel was operated at temperatures from 333 K to 80 K. The lower temperature is very close to the saturation temperature of nitrogen of 77.4 K at 1 atmosphere. At 80 K the Reynolds number is increased by a factor of about 7 over that achieved at normal tunnel temperatures and the same Mach number. Approximately 40 hours of tunnel operation were at cryogenic temperatures, that is, below 150 K. At the reference station in the test section the test temperature was held to within about ± 1 K by automatic on-off control of one or more nitrogen injection nozzles. Much closer temperature control was achieved by injecting a slight excess of liquid nitrogen and establishing temperature equilibrium at the desired test temperature by modulating the heat input from a simple wire-grid electrical heater which was built into the tunnel in the low-speed end of the return leg of the circuit. Using this technique, test temperatures within about ± 0.22 K of the mean could be maintained.

Boundary-Layer Experiment.- One of the first experiments needed was one which would demonstrate that the true aerodynamic effects of Reynolds number increases are indeed provided by temperature reduction to cryogenic levels in nitrogen. Clearly an aerodynamic experiment was required in which there would be a change in some measurable aerodynamic parameter solely due to change in Reynolds number. Further, the change in the measured parameter should be reasonably sensitive to and vary predictably with Reynolds number. We decided on a simple boundary-layer experiment in which the variation of a measure of boundary-layer thickness, δ, with Reynolds number would be compared with theory. For maximum sensitivity, we decided to make the measurements in a laminar boundary layer since δ varies as $R_x^{-1/2}$ for a laminar boundary layer but only approximately as $R_x^{-1/5}$ for a turbulent boundary layer.

A small diameter pitot-tube (0.0330 cm o.d. and 0.0165 cm i.d.) was mounted as a Preston tube against a flat plate in the test section. The pitot-tube was mounted at a fixed position 3.261 cm from the rounded leading edge of the plate. The longitudinal location of the pitot-tube was such that it would lie in a laminar portion of the boundary layer over a wide range of conditions in the test section. A sketch of the experimental arrangement is shown in Figure 16.

In the tunnel, Reynolds number was varied by temperature or by M_∞. Changes in the ratio of the dynamic pressure of the pitot-tube to the

12

free-stream dynamic pressure indicate changes in boundary layer thickness and therefore changes in Reynolds number. Details of the experiment and the analysis are presented in reference 20 and will not be repeated here. The zero pressure gradient form of the Pohlhausen laminar boundary layer velocity profile was adopted in order to allow a curve to be fitted to data taken with the tunnel running warm. This eliminated the need to estimate effective values for x and y from the geometry of the plate and pitot-tube. A constant required for the curve fitting was obtained very simply from determining at ambient temperature the ratio of q in the boundary layer to q in the free-stream in the limit as Mach number was reduced to zero. The ratio $Q = q/q_{\infty}$ is simply a function of Reynolds number. Therefore there is a unique relationship between Q and either R_x or unit Reynolds number, independent of test temperature and Mach number, provided that the flow can be treated as incompressible. In addition to the measurements made at ambient temperature, further measurements were made with this simple set-up at test temperatures of 227.6 K, 144.3 K, and 95.9 K. At these temperatures, test Reynolds number is increased relative to its value at 322 K, at the same Mach number, by the factors 1.569, 2.950, and 5.350 respectively. Therefore, to achieve the same Reynolds number (and the same boundary layer thickness and Q) the test Mach number must be reduced by the above factors. The curves on Figure 17 correspond to the reduced-temperature test conditions which were obtained in this way.

The experimental data at 227.6 K is in good agreement with the theoretical curve, and the data at the two lower temperatures are in fair agreement. The experimental data was a confirmation of the magnitude of the theoretical predictions of the increase of Reynolds number with M_{∞} at constant temperature, but, more importantly, a first experimental confirmation of the valid effect of increases of Reynolds number with decreasing temperature at constant M_{∞}.

Strain-Gage Balance Experiment.- Most wind-tunnel testing involves the measurement of forces and moments on models using sting-mounted internal strain-gage balances. In order to determine if conventional strain-gage balance techniques might be used to make force and moment measurements at cryogenic temperatures, a 11.4 cm span sharp leading-edge 74° delta-wing model was tested on an existing water-jacketed strain-gage balance in the cryogenic tunnel. Since the purpose of this test was to investigate any possible adverse effects of temperature on the measuring techniques rather than the effects of Reynolds number on the aerodynamics of the model, a sharp leading-edge 74° delta-wing model was chosen since it is known that, except for the usual effects of friction drag, the aerodynamic characteristics of this shape are relatively insensitive to Reynolds number. A photograph of the model, balance, and supporting sting is presented in Figure 18. The strain-gage elements of the balance were heated and insulated from the cryogenic environment by a jacket through which was circulated water at approximately 294 K. The quadrant shown in Figure 18 allowed model incidence to be changed from -4° to $+22^o$.

Some of the aerodynamic test results are presented in Figure 19 as the variation of C_m, C_L, and C_D with α for various test conditions. As can be seen, there is good agreement between the data obtained at stagnation temperatures from 322 K to 111 K. Based on the results of these tests, we concluded that there should be no fundamental or insurmountable practical difficulties in obtaining force and moment data in a cryogenic tunnel using conventional strain-gage balance techniques.

In addition to the two "proof-of-concept" experiments, other experiments were made in the low-speed cryogenic tunnel. The conclusions drawn from the experiments as well as from the day-to-day operation of the low-speed tunnel were as follows:

1. Cooling with liquid nitrogen is practical. Rapid cool-down rates may be achieved. Following purging of the tunnel circuit with dry nitrogen before cool-down, the gas stream in the test section remains clear and free from frost. Liquid nitrogen completely evaporates even at test temperatures close to the liquid temperature. The test temperature can be controlled with acceptable limits either manually or automatically. The temperature distribution in the test section is satisfactory.

2. Satisfactory insulation techniques exist. Viewing ports are easily constructed and maintained clear.

3. A fan-driven tunnel is satisfactory at cryogenic temperatures. Drive power and fan speed vary with temperature in accordance with simple theory.

4. Pressure measurements may be made at cryogenic temperatures. Satisfactory results are obtained by locating the pressure transducer outside the tunnel at ambient temperature and connecting the transducer to the sensor in the circuit by a short length of tubing.

5. There is good agreement between theoretical predictions and experimental measurements of the development of laminar boundary layers at cryogenic temperatures.

6. Conventional strain-gage balances can be used for model testing. A satisfactory arrangement is to maintain the strain-gage balance at ambient temperatures by heating.

0.3-m Transonic Cryogenic Tunnel

Based on the experience and confidence gained with the low-speed cryogenic tunnel, a larger tunnel capable of being pressurized and operated at transonic speeds and especially designed for cryogenic operation was built and put into operation at Langley during 1973.[21] This

pilot transonic pressurized cryogenic tunnel, now known as the 0.3-m transonic cryogenic tunnel (TCT), has been used since August of 1973 to validate cryogenic nitrogen as a transonic test gas, develop cryogenic instrumentation and testing techniques, determine possible operating limits set by condensation or other real-gas effects, study various tunnel control schemes, and gain experience in the operation of a cryogenic nitrogen-gas transonic wind tunnel. In addition, it has been used for a variety of aerodynamic tests that could take advantage of either the high unit Reynolds number or the extremely wide range of Reynolds number available. A photograph of the 0.3-m TCT with a 3-dimensional test section, taken during initial assembly, is shown in Figure 20. A photograph of the 0.3-m TCT as it looks today, equipped with a 2-dimensional test section, is shown in Figure 21. Details of our experiences with the 0.3-m TCT will be given in subsequent sections of this paper as well as in other papers to be given during this conference.

Additional Advantages of a Cryogenic Tunnel

The Langley researchers soon recognized that the high Reynolds number capability at reasonable model loads and the reduced capital and operating costs were not the only advantages of a cryogenic wind tunnel. Very important additional advantages are offered due to the fact that a cryogenic tunnel with the independent control of Mach number, temperature, and pressure has the unique capability to determine independently the effect of Mach number, Reynolds number, and aeroelastic distortion on the aerodynamic characteristics of the model. It is believed that this new and unique aerodynamic testing capability may be, in some instances, of equal importance with the ability to achieve full-scale Reynolds number.

In order to illustrate these additional research advantages, a typical constant Mach number operating envelope for the 0.3-m TCT is presented in Figure 22. The envelope shows the range of dynamic pressure and Reynolds number available for sonic testing. It is bounded by the maximum temperature boundary (340 K), the minimum temperature boundary (chosen to avoid saturation at free-stream conditions), the maximum pressure boundary (6.0 atm), and the minimum pressure boundary (1.0 atm).

With such an operating capability, it is possible, for example, to determine at a constant Mach number the true effect of Reynolds number on the aerodynamic characteristics of the model without having the results influenced by changing model shape due to changing dynamic pressure, as is the case in a conventional pressure tunnel.* This ability to make pure Reynolds number studies is of particular importance, for example, in research on the effects of the interaction between the shock and the boundary layer. As indicated on the envelope, pure aeroelastic studies may be made under conditions of constant Reynolds number. In addition, combinations of R and q can be established to represent accurately

---

*There will be a slight variation of the modulus of elasticity E of most model materials with temperature. To correct for this variation in E, the dynamic pressure q may be adjusted by varying total pressure so that the ratio q/E remains constant over the Reynolds number range.

the variations in flight of aeroelastic deformation and changes in Reynolds number with altitude. Similar envelopes are, of course, available for other Mach numbers.

The National Transonic Facility

Along with the early experimental work on cryogenic tunnels, there was a parallel theoretical study by Adcock[3,22] of the so-called "real gas effects" resulting from operating a transonic tunnel using nitrogen gas at cryogenic temperatures. Adcock's studies, combined with the experimental verification of the cryogenic tunnel concept at transonic speeds in the 0.3-m TCT, had a far reaching effect. Several proposed ambient temperature intermittent high Reynolds number tunnels, both in the U.S. and in Europe, were abandoned as the superiority of the cryogenic concept became more widely recognized[23-26]. A direct and most significant outcome of this work was the decision in 1975 to build a single large transonic cryogenic tunnel to meet the high Reynolds number testing needs of the United States. Implementation of this decision is evidenced by the construction at Langley, now well underway, of the National Transonic Facility. Subsequent papers in this conference will describe in detail the design and construction of the NTF. The one further comment I will make is to note that the NTF construction site is conveniently located adjacent to the 0.3-m TCT, as can be seen in the photograph of the NTF construction site presented as Figure 23. The two liquid nitrogen storage tanks for the 0.3-m TCT can be seen in the lower right of the photograph with the tunnel itself just out of sight to the right of the tanks.

1975-Present

The general acceptance of the validity of the cryogenic wind tunnel concept, which we now enjoy, has not always been present. Following the low-speed cryogenic tunnel work at Langley in 1972, the rest of the world took, at best, a "wait and see" attitude toward cryogenic tunnels. The bold decision by Langley management to proceed with a pilot transonic cryogenic tunnel was made in spite of much skepticism and some ridicule expressed by persons not fully aware of the low-speed experimental work or the theoretical work which fully justified extension of the proof-of-concept studies to transonic speeds. However, following the transonic proof-of-concept research in 1973 and 1974, the acceptance of the cryogenic tunnel concept has been rapid, as evidenced by the fact that over 20 cryogenic tunnels of various types have either been placed in service or planned at research establishments around the world. This is graphically illustrated in Figure 24, which shows the number of cryogenic tunnels as a function of time. The numbers within the symbols refer to table I which gives the location, actual or anticipated date of initial cryogenic operation, and other information for each of the tunnels.

The present worldwide interest in cryogenic wind tunnels was very much in evidence in Southampton, England, at the First International Symposium on Cryogenic Wind Tunnels held in the spring of 1979.

Thirty six technical papers were presented at the symposium which was attended by 88 researchers representing 34 organizations in 9 countries. Those in attendance were, of course, only the "tip of the iceberg", being the visible representatives of several hundred people, worldwide, who are now working on cryogenic wind tunnel projects.

An additional indication of the high level of activity related to cryogenic tunnels is seen in the large number of recent papers cited in reference 27, a bibliography on cryogenic wind tunnels which has just been published.

So much for the evolution and current state of the cryogenic wind tunnel concept. The remainder of this paper will review some of our experiences with the Langley 0.3-m transonic cryogenic tunnel, the tunnel in which the cryogenic wind tunnel concept was verified at transonic speeds, thereby making possible the decision to build the NTF and leading, directly or indirectly, to the present high level of activity around the world related to cryogenic wind tunnels.

EXPERIENCE WITH THE LANGLEY 0.3-m TRANSONIC CRYOGENIC TUNNEL

As previously mentioned, following the successful completion of the low-speed cryogenic tunnel work in the summer of 1972, we decided to build a relatively small continuous-flow fan-driven transonic cryogenic pressure tunnel. This pilot transonic cryogenic tunnel was needed in order to extend the design and operational experience with a cryogenic tunnel to the pressure and speed range contemplated for a large high Reynolds number transonic cryogenic tunnel. The specific purposes envisioned for the pilot transonic cryogenic tunnel were to demonstrate in compressible flow that the results obtained when Reynolds number is increased by reducing temperature are equivalent to those obtained when Reynolds number is increased by increasing pressure, to determine experimentally any limitations imposed by liquefaction, to verify engineering concepts with a realistic tunnel configuration, and to provide additional operational experience. Design of the transonic cryogenic tunnel began in December of 1972 and initial operation began in August of 1973. The first run at cryogenic temperatures (150 K or lower) was made on October 16, 1973, less than two years after we started work on the cryogenic tunnel concept. Figure 25 shows a sketch of the 0.3-m TCT surrounded by photographs illustrating some of the uses to which the tunnel has been put since 1973. Figure 26 shows several photographs of models that were tested when the tunnel was equipped with the original 3-dimensional octagonal test section. In the summer of 1976 the 3-dimensional test section was

replaced with a 20 by 60-cm 2-dimensional test section. The sketch and photographs of Figure 27 illustrate a few of the jobs that have been done since 1976 in the 2-dimensional test section. Some of the work, such as that on strain-gage balances, will be described in other papers at this conference and will not be discussed further in this paper. I will, however, briefly describe some of our proof-of-concept work at transonic speeds, some work done in support of the NTF, and some of our work that relates directly to the cost of operation of a cryogenic tunnel.

Description of the 0.3-m TCT

The 0.3-m transonic cryogenic tunnel is a single-return fan-driven tunnel originally built with a slotted, octagonal test section measuring 34 cm from flat to flat. The fan is driven by a 2.2-MW variable-frequency motor which is capable of operating the tunnel in its present two-dimensional test section configuration at Mach numbers from about 0.05 to about 1 at stagnation pressures from slightly greater than 1 atm to 6 atm over a stagnation temperature range from about 78 K to 340 K. The ranges of pressure and temperature provide the opportunity of investigating Reynolds number effects by temperature and pressure independently over almost a 6 to 1 range of Reynolds number. As was the case with the low-speed tunnel described in reference 4, the wide range of operating temperatures is obtained by spraying liquid nitrogen (LN$_2$) directly into the tunnel circuit to cool the structure and the gas stream and to remove the heat of compression added to the stream by the drive fan. The tunnel was designed so that the contraction, test section, and diffuser could be easily removed in order to allow for alternate test sections. Figure 28 shows sketches of the tunnel circuit with the original 3-dimensional octagonal test section and the 2-dimensional test section insert. A more detailed description of the 0.3-m transonic cryogenic tunnel and its ancillary equipment can be found in reference 21.

Operation and Performance of the 0.3-m TCT

Much of the information being obtained from the 0.3-m TCT relates to the operation and performance of the tunnel itself. The data for the most part consist of the usual tunnel calibration information but with particular emphasis being placed on identifying any problems related either to the method of cooling or to the wide range of operating temperature.

Temperature Versus Time During a Typical Run

Typical of some of the performance information obtained from the 0.3-m TCT is the record of stream and tunnel wall temperature as a function of time shown in Figure 29. This figure will also serve to illustrate the various phases of operation during a typical run. The tunnel had not been opened to the atmosphere prior to the run illustrated so the prerun

purging operation described in reference 21 was not necessary. The tunnel is normally cooled down at a rate of about 10 K/minute or less to avoid excessive thermal stresses in the tunnel structure. This particular cool-down is fairly typical and took about 40 minutes. Near the end of the cool-down, the cooling rate was reduced to enable the tunnel wall and stream temperatures to equalize. Figure 30 shows the temperature difference between the wall and stream for this run. Note that at one time during the cool-down there was a "lag" of about 83 K between the wall and stream. During the 52 minute test time, however, the differences between the wall and stream temperatures were maintained with 10 K. The normal run procedure has been to keep the wall and the stream at about the same temperature. It should be noted, however, that to date there has been no evidence of any aerodynamic discrepancies due to differences in temperature between the wall and stream. In the example shown in Figure 29, there were eight different test conditions established at temperatures from 86 K to 103 K, pressures between 4.31 and 5 atmospheres, and Mach numbers from 0.740 to 0.755. If a tunnel entry is required, the normal procedure is to warm the tunnel to ambient temperatures at a rate roughly equal to the cool-down rate. It has recently been proven in the 0.3-m TCT that the tunnel can be left at cryogenic temperatures when not running without damage to the tunnel or any of its subsystems. If tunnel entry is not required at the end of the day, this procedure avoids the time and expense of warm-up and cool-down.

The major conclusions with respect to operation and performance of the 0.3-m TCT to be made after over 3000 hours of running at cryogenic temperature are as follows:

1. Purging, cooldown, and warmup times are acceptable and can be predicted with good accuracy.

2. Liquid nitrogen requirements for cooldown and running can be predicted with good accuracy.

3. Cooling with liquid nitrogen is practical at the power levels required for transonic testing. Test temperature is easily controlled and good temperature distribution obtained by using a simple nitrogen injection system.

4. Test-section flow quality is good over the entire range of operating conditions.

The experimental data on which these conclusions are based as well as other information related to the operational and performance characteristics of the 0.3-m TCT have been reported in references 5, 6, and 21 and will not be discussed further in this paper.

19

Aerodynamic Experiments in the 0.3-m TCT

In addition to the experimental results related to the operational and performance aspects of the cryogenic tunnel, there have been a series of aerodynamic experiments primarily aimed at determining the validity and practicality of the cryogenic concept in compressible flow. In the following sections will be presented some of the results of these validation experiments.

Validation Airfoil Pressure Tests

Based on the real-gas studies of reference 22, there is little doubt that airfoil pressure distributions measured for given values of Reynolds number and Mach number should be the same at cryogenic and ambient temperature conditions. However, in order to provide experimental verification of this equivalence, the pressure distribution on a two-dimensional airfoil has been measured in the 0.3-m TCT at ambient and cryogenic temperatures under conditions of constant Reynolds number and Mach number.

A modified NACA 0012-64 airfoil having a 13.72-cm chord was used for the two dimensional airfoil pressure tests. The airfoil spanned the octagonal test section and was fastened to the walls in such a way that incidence could be varied. An airfoil somewhat larger than would normally be tested in this size tunnel was selected in order to allow for more accurate model construction, a reasonable number of pressure orifices, and higher chord Reynolds number. The fact that the relatively high ratio of chord to tunnel height might result in wall-induced interference was of no particular concern since the tests were being made only to determine whether the airfoil pressure distribution was modified in any way by real-gas effects associated with testing at cryogenic temperatures. The pressure distribution data should therefore be looked at from the point of view of agreement or lack of agreement between data obtained at ambient and cryogenic conditions and the results used only as an indication of the validity of the cryogenic concept. The conditions selected to insure a valid and critical cryogenic evaluation were:

1. Ambient and cryogenic temperature tests were made in the same tunnel on the same model at the same Mach number and Reynolds number.

2. The airfoil was tested with free transition to allow any possible temperature effect on boundary-layer development.

3. The symmetrical airfoil was tested at zero incidence to eliminate any shape or incidence change due to the dynamic pressure differences between the ambient and cryogenic temperature conditions.

4. Free-stream Mach number exceeded the Mach number normal to the leading edge of typical near-sonic transport designs.

A comparison of the pressure distribution for ambient and cryogenic temperature tests at a free-stream Mach number of 0.85 is shown in Figure 31. For this comparison, the same chord Reynolds number was obtained at each temperature by an appropriate adjustment of pressure. As can be seen, there is excellent agreement between the pressure distribution obtained at ambient and cryogenic conditions. This is considered to be a valid check in view of the large variation in the gas properties over this large temperature and pressure range. In addition, this agreement is particularly significant with regard to setting tunnel conditions when one considers, for example, the large variation of the speed of sound with temperature and the sensitivity of the airfoil pressure distribution to changes in Mach number.

This distribution, $M_\infty = 0.85$ is of special significance since the pressure distribution shows the flow to be supersonic over a large portion of the airfoil, reaching a local Mach number of about 1.22 just ahead of the strong recompression shock. This type of flow, typical of super-critical flows, should be extremely sensitive to any anomalous behavior of the test gas due to operation at cryogenic temperatures. The almost perfect agreement in the pressure distributions provides experimental confirmation that nitrogen at cryogenic temperatures behaves like a perfect gas and is therefore a valid transonic test gas as predicted by the real-gas studies.

Boattail Afterbody Pressure Tests

Tests have been made in the 0.3-m transonic cryogenic tunnel to determine the effect of varying Reynolds number on the boattail drag of two wing-body configurations as well as on several isolated boattail configurations. Photographs of two of the models used for these tests are shown in Figure 26. The Reynolds number, based on the distance from the nose to the beginning of the boattail, was varied from about 2.6 million to about 132 million by changing unit Reynolds number by a factor of about 25 and by changing model length by a factor of 2. Included in this paper is an example of the test results which relates to the validity of the cryogenic concept. The complete test results have been reported in papers by Reubush and Putnam.[28,29,30]

Shown in Figure 32 are the boattail pressure coefficient distributions for a circular arc-conic boattail at a Mach number of 0.6 and a Reynolds number of about 10.5 million. The shape of the distribution clearly indicates flow separation toward the rear of the boattail. The distribution shown with circular symbols was obtained at a stagnation pressure of 1.2 atm at a stagnation temperature of 117 K while the distribution shown with square symbols was obtained at a stagnation pressure of 5.0 atm at a stagnation temperature of 311 K. These data show nearly identical pressure distributions for ambient and cryogenic conditions and thus provide further substantiation that there are no undesirable effects in using nitrogen at cryogenic temperatures to achieve high Reynolds number data even in the presence of separated flow.

NTF Cooling Coil Tests

Gaseous nitrogen has been shown to be a valid test gas at temperatures ranging from higher than ambient to just above those resulting in the onset of condensation effects. From an economic standpoint, however, it is desirable to include an efficient chilled water heat exchanger in the circuit of cryogenic wind tunnels such as the NTF in order to provide a test capability at low and moderate Reynolds numbers in air as well as in nitrogen at ambient temperatures. The Reynolds number range of a cryogenic pressure tunnel such as the NTF far exceeds the aerodynamic design requirements for conventional cooling coils and an improper selection could compromise the high Reynolds number efficiency of the tunnel. It is essential, therefore, in the selection of a cooling coil design, to determine the aerodynamic characteristics over the entire operating range of the tunnel.

William B. Igoe of the NASA Langley Research Center has made a study of various cooling coils being considered for the NTF. The unique features of the 0.3-m TCT provided the capability to assess the aerodynamic behavior of the cooling coils from very low to full-scale Reynolds numbers. A photograph of one of the cooling coil models installed in the two-dimensional test section is shown in Figure 33. The tube bundle models completely spanned the width of the test section. The pressure drop, flow uniformity, turbulence, and noise characteristics were determined using total and static pressure measurements, thermocouples, two-component hot wire probes, and microphones. The hot wire probes consisted of crossed, platinum-coated 5 micron tungsten wire with an effective length-to-diameter ratio of about 250. It is obvious from this instrumentation inventory that specialized measurements can be made in cryogenic test environments.

The test conditions covered during the cooling coil studies included variation in Reynolds number from about 0.4×10^6 to 28×10^6, variation in Mach number from 0.01 to 0.10 (corresponding to the low velocity area of the NTF), variation in stagnation pressure from 1 to 5 atmospheres, and variation in stagnation temperature from 100 K to 300 K. The Reynolds number based on hydraulic tube diameter varied from about 6×10^3 to 4×10^5. One fortunate aspect of this test was the fact that the 0.3-m TCT did not impose severe dynamic loading on the models. This advantage eased model construction and also proved to be beneficial from the instrumentation standpoint. For example, there was no hot wire breakage due to adverse test conditions.

Some representative examples of the pressure loss and longitudinal turbulence data obtained on a six-row, round tube bundle and on a four-row, elliptical tube bundle are also shown in Figure 33. From the standpoint of cooling and hydraulic characteristics, both of these configurations would meet the NTF requirements. It is obvious from the

sample results that there are significant effects of Reynolds number on the coil configurations. At low Reynolds number, there is virtually no difference in the turbulence characteristics of the two coil configurations. At full scale Reynolds number, however, the elliptical coil has the lower level of turbulence as well as significantly lower pressure loss. On the basis of these tests, the elliptical coil configuration was selected for use in the NTF.

Saturation Boundary Tests

As noted in reference 3, the saturation boundary for nitrogen is well defined and any possible effect of liquefaction of the test gas can easily be avoided if the maximum local Mach number on the model is known. As shown in Figure 34, for a given size tunnel and a constant operating pressure, a significant increase in test Reynolds number is possible if the saturation boundary may be crossed in these localized high Mach number regions. For example, if the test temperature for sonic testing is selected to avoid the saturation boundary based on free-stream Mach number, the test Reynolds number is about 30% greater than could be achieved at the same stagnation pressure had the test temperature been selected to avoid the saturation boundary based on a maximum local Mach number of 1.7. In order to determine if such an increase in test Reynolds number could safely be realized, an experiment was needed to investigate the feasibility of testing under conditions of local supersaturation.

The pressure distribution of an airfoil having a strong recompression shock should provide a sensitive indicator of condensation, which would be expected to occur in the low-pressure region ahead of the shock. Therefore, the airfoil pressure model previously described was used also in a series of supersaturation tests.

Some data obtained during the initial operation of the 0.3-m TCT indicated that several degrees of local supersaturation had no effect on the pressure distribution over the airfoil. However, these early tests covered only a limited Mach number range and total temperatures only low enough to result in operation down to free-stream saturation conditions.

Because of the potential increase in Reynolds number capability that results from operation below local saturation conditions, an experimental program has been undertaken in the 0.3-m TCT to extend the saturation studies to cover a wider range of test conditions. Studies have been made at constant test-section Mach numbers of 0.75, 0.85, and 0.95 at total pressures from 1.2 to 5.0 atmospheres with temperature to within 2 K of settling chamber saturation. The temperature at which condensation effects perturb the flow is determined at a constant Reynolds number by reducing total temperature and pressure until the pressure distribution over the airfoil deviates from the pressure distribution obtained with unsaturated conditions. The results of

these studies have been reported by Hall.[31] Some of the Mach number 0.85 results from reference 31 are included herein to illustrate the technique used for these studies as well as to illustrate the potential benefit of operation beyond both the local and free-stream saturation boundaries.

For these tests with the airfoil at zero incidence, the maximum local Mach number over the airfoil was 1.22. The three saturation boundaries of interest - local, free-stream, and settling chamber - are shown as a function of total pressure in Figure 35.

To determine the total temperature at which condensation effects begin as a function of total pressure, six paths of constant Reynolds number were investigated. A reference pressure distribution was taken above the upper saturation boundary shown in Figure 35 if it was possible to do so within the pressure envelope of the tunnel. The six paths of constant Reynolds number and the total conditions sampled are shown in Figure 36.

To determine if condensation effects were, in fact, perturbing the flow over the airfoil, pressure distributions obtained at the different total temperatures along a constant Reynolds number line were compared to the reference pressure distribution. Even though the agreement between the reference distribution and those distributions considered to be affected by condensation in many cases appeared to be within the experimental accuracy of the data, there was always a systematic positive shift in the pressure coefficient from the 20% chord position of the airfoil back to the recompression shock.

By making similar comparisons along each of the constant Reynolds number paths shown in Figure 36 Hall was able to define the conditions under which "possible" condensation effects were present over nearly the entire pressure range of the tunnel. A conservative experimental lower limit to tunnel operation was then obtained by plotting, as shown in Figure 37, the total conditions where the first "possible" effects of condensation were observed in the pressure distributions. As noted by Hall, the operating boundary defined by this locus of points is considered conservative since, in fact, the differences in pressure distributions even for those comparisons labeled "possible effect" may be insignificant to the aircraft designer.

For the particular airfoil used for these tests, there appear to be no serious condensation problems associated with testing at temperatures far below the saturation boundary associated with the high local Mach number over the airfoil. No low-temperature effects were observed until total conditions were at least 2 K below those which produced saturated flow in the test section. For the conditions of this experiment, the ability to operate below the local saturation boundary allowed an increase in test Reynolds number of 17% for a constant total pressure over the pressure range from 1.2 to 4.5 atmospheres. If, instead of holding total pressure constant, test Reynolds number is held

constant, the ability to operate with saturated flow allows a reduction in total pressure of more than 17%.

CONCLUDING REMARKS

Based on theoretical studies and experience with a low-speed cryogenic tunnel and with the Langley 0.3-Meter Transonic Cryogenic Tunnel (TCT), the cryogenic concept has been shown to offer many advantages with respect to the attainment of full-scale Reynolds number at reasonable levels of dynamic pressure in a ground-based facility. The unique modes of operation which are available only in a pressurized cryogenic tunnel make possible for the first time the separation of Mach number, Reynolds number, and aero-elastic effects. By reducing the drive-power requirements to a level where a conventional fan-drive system may be used, the cryogenic concept makes possible a tunnel with high productivity and run times sufficiently long to allow for all types of tests at reduced capital costs and, for equal amounts of testing, reduced total energy consumption in comparison with other tunnel concepts.

The 0.3-m TCT has provided experimental verification of the validity of the cryogenic concept at transonic speeds at operating pressures up to 6 atmospheres. In over 3000 hours of operation at cryogenic temperatures, the 0.3-m TCT has also been used to develop solutions to many of the practical problems related to the operation of a pressurized transonic cryogenic tunnel. These include the areas of instrumentation, control systems, test techniques, and model construction techniques.

The Langley Research Center has been selected as the site of a new fan-driven high Reynolds number transonic tunnel to meet the research and development needs of NASA, the Department of Defense, and industry. The new tunnel will take full advantage of the cryogenic wind-tunnel concept, will have a 2.5- by 2.5-m test section, and will be capable of operating at stagnation pressures up to 8.8 atmospheres. This new tunnel, to be known as the National Transonic Facility, will provide an order of magnitude increase in Reynolds number capability over existing transonic tunnels in the United States.

Based on our experience with the 0.3-m TCT and the theoretical "real-gas" studies that have been made since 1972, we are confident that we will know how to efficiently use the NTF when it becomes operational in 1982 and be able to take advantage of the new and unique testing capabilities it offers.

REFERENCES

1. Heppe, Richard R.; O'Laughlin, B. D.; and Celniker, Leo: New Aeronautical Facilities - We Need Them Now. Astronaut. & Aeronaut. Vol. 6, No. 3, Mar. 1968, pp. 42-54.

2. Hills, R.: The Need for a Large Transonic Wind Tunnel in Europe: A Summary of the Report of an AGARD Working Group (LaWs). AIAA Paper No. 74-630, July 1974.

3. Adcock, Jerry B.; Kilgore, Robert A.; and Ray, Edward J.: Cryogenic Nitrogen as a Transonic Wind-Tunnel Test Gas. AIAA Paper No. 75-143, Jan. 1975.

4. Goodyer, M. J.; and Kilgore, R. A.: The High Reynolds Number Cryogenic Wind Tunnel. AIAA Paper 72-995, 7th Aerodynamic Testing Conference, Palo Alto, Calif., Sept. 13-15, 1972. Also, AIAA Journal, vol. 11, no. 5, May 1973, pp. 613-619.

5. Kilgore, Robert A.; Adcock, Jerry B.; and Ray, Edward J.: Simulation of Flight Test Conditions in the Langley Pilot Transonic Cryogenic Tunnel. NASA TN D-7811, 1974.

6. Ray, Edward J.; Kilgore, Robert A.; and Adcock, Jerry B.: Analysis of Validation Tests of the Langley Pilot Transonic Cryogenic Tunnel. NASA TN D-7828, 1975.

7. Pritchard, J. Laurence: A Century of British Aeronautics - The Royal Aeronautical Society 1866 - 1966. Journal of the Royal Aeronautical Society, Vol. 70, No. 661, Jan. 1966.

8. Sixth Annual Report of the Aeronautical Society of Great Britain (for the year 1871), pp. 75-78.

9. Munk, Max.: On a New Type of Wind Tunnel. NACA TN No. 60, May 1921.

10. Hall, Robert: Applying the Results of Experiments on Small Models in the Wind Tunnel to the Calculation of Full-Scale Aircraft. NACA TM No. 84, April 1922. (From "Premiér Congres International de la Navigation Aérienne," Vol. I, pp. 1-13.)

11. Lepre, M.: Trend to be Given Aerodynamical Research and Experiment. NACA TM No. 209, June 1923. (From L'Aérophile, March 1-15, 1923.)

12. Munk, Max. M.; and Miller, Elton W.: The Variable Density Wind Tunnel of the National Advisory Committee for Aeronautics. NACA Report No. 227.

26

13. Margoulis, W.: Nouvelle Méthode d'essai de Modèles en Souffleries Aérodynamiques. (A New Method of Testing Models in Wind Tunnels.) Compts Rendus Acad. Sci. Vol. 171, 1920, pp. S997-999, Sèance du 22 Nov. 1920.

14. Margoulis W.: A New Method of Testing Models in Wind Tunnels. NACA-TN-52, Aug. 1921.

15. Hersey, Mayo Dyer: Variation of Fluid Properties in Aerodynamics. International Air Congress, London, 1923.

16. Smelt, R.: Power Economy in High-Speed Wind Tunnels by Choice of Working Fluid and Temperature. British R.A.E. Rep. no. Aero. 2081, Aug. 1945.

17. Goodyer, M. J.: The evolution of the Cryogenic Wind Tunnel. Paper No. 1, First International Symposium on Cryogenic Wind Tunnels, Southampton, England, April 3-5 1979.

18. Pankhurst, R. C.; and Holder, D. W.: Power Economy by Reduction of Stagnation Temperature. Wind Tunnel Technique, Sir Issac Pitman and Sons, Ltd., London, 1952, pp. 45-47.

19. Rush, C. K.: A Low Temperature Centrifugal Compressor Test Rig (Mechanical Engineering Report). National Research Council of Canada Rep. MD-48: NRC-7776, Nov. 1963, 57 pp.

20. Kilgore, Robert A.: The Cryogenic Wind Tunnel for High Reynolds Number Testing. Ph. D. Thesis, University of Southampton, 1974. (Available as NASA TM X-70207.)

21. Kilgore, Robert A.: Design Features and Operational Characteristics of the Langley 0.3-Meter Transonic Cryogenic Tunnel. NASA TN D-8304, 1976.

22. Adcock, Jerry B.: Real-Gas Effects Associated with One Dimensional Transonic Flow of Cryogenic Nitrogen. NASA TN D-8274, Dec. 1976.

23. Whitfield, Jack D.; Schueler, C. J.; and Starr, Rogers F.: High Reynolds Number Transonic Wind Tunnels - Blowdown or Ludwieg Tube? Facilities and Techniques for Aerodynamic Testing at Transonic Speeds and High Reynolds Number. AGARD CP No. 83, Aug. 1971, pp. 29-1 - 29-17.

24. Evans, J. Y. G.: A Scheme for a Quiet Transonic Flow Table for Model Testing at High Reynolds Number. Facilities and Techniques for Aerodynamic Testing at Transonic Speeds and High Reynolds Number, AGARD CP No. 83, Aug. 1971, pp. 35-1 - 35-5.

25. Carriere, P.: "The Injector-Driven Wind Tunnel," ONERA Paper, LaWs Paper No. 127, Oct. 1972. Published in AGARD Report R-600-72.

26. Ludwieg, H., Grauer-Carstensen, H., and Lorenz-Meyer, W.: "Project Study of a Large European Transonic Ludwieg Tube Wind Tunnel." DFVLR/AVA 06272A 14, June 1972 and Sept. 1972, LaWs Paper Nos. 98 and 98A. Published in AGARD Report R-600-72.

27. Tuttle, Marie H.; and Kilgore, Robert A.: Cryogenic Wind Tunnels - A Selected, Annotated Bibliography. NASA TM 80168, Oct. 1979.

28. Reubush, D. E.; and Putnam, L. E.: An Experimental and Analytical Investigation of the Effect on Isolated Boattail Drag of Varying Reynolds Number up to 130 Million. NASA TN D-8210, May 1976.

29. Reubush, D. E.: Effect of Reynolds Number on the Subsonic Boattail Drag of Several Wing-Body Configurations. NASA TN D-8238, July 1976.

30. Reubush, D. E.: An Experimental Investigation to Validate the Use of Cryogenic Temperatures to Achieve High Reynolds Numbers in Boattail Pressure Testing. NASA TM X-3396, Aug. 1976.

31. Hall, Robert M.: Onset of Condensation Effects With an NACA 0012-64 Airfoil Tested in the Langley 0.3-Meter Transonic Cryogenic Tunnel. NASA TP-1385, 1979.

TABLE I.– TABULAR SUMMARY OF CRYOGENIC WIND TUNNELS, NOVEMBER 1979

Information sequence: Orqanization; speed; test section size; run date below
150 K (actual or forecast); drive; "pressure" if above atmospheric.

Tunnels which have run to date.

1. NASA-LRC; low speed; 0.22m; Jan. 31, 1972; fan.
2. NASA-LRC; transonic; 0.3m; Oct. 16, 1973; fan; pressure.
3. DFVLR; transonic and supersonic; 8.3mm; June 25, 1976; blowdown; pressure.
4. University of Southampton; low speed; 0.1m; March 4, 1977; fan.
5. Douglas Aircraft; transonic; 1 foot; May 20, 1977; blowdown; pressure.
6. ONERA; T'2 transonic; 0.1m; June 1977; induction; pressure.
7. University of Illinois; low speed; 0.86m; Aug. 17, 1978; fan.
8. University of Southampton; transonic; 8.3mm; March 1, 1979; free piston; pressure.
9. ONERA-CERT; low speed; free jet; blowdown; pressure.
10. ONERA-CERT; transonic; 0.12m; July 1979; fan; pressure.

Tunnels under design or construction, in order of estimated completion date.

11. NASA-LRC; low speed; 0.05m; Dec. 1979; blowdown.
12. Douglas Aircraft; transonic; 4 foot; Dec. 1979; blowdown; pressure.
13. I.H.I. (Japan); low speed; 0.56m; March 1980; fan; pressure.
14. Tsukuba National University (Japan); low speed; 0.8m; March 1980; fan; pressure.
15. College of Aeronautics (U.K.); transonic; mid 1980; free piston; pressure.
16. NASA-LRC; transonic; 0.05m; late 1980; fan; pressure.
17. ENSAE-CERT; transonic; 0.23m; late 1980; fan; pressure.
18. Pilot ETW; transonic; 0.25m; 1981; fan; pressure.
19. NASA-LRC; NTF transonic; 2.5m; July 1982; fan; pressure.
20. ETW; transonic; 1.79m; 1984; fan; pressure.
21. B.Ae. Warton; transonic; 1.2m; 1984?; blowdown; pressure.
22. Boeing; BHRT transonic and supersonic; 4 foot; 1984?; blowdown; pressure.
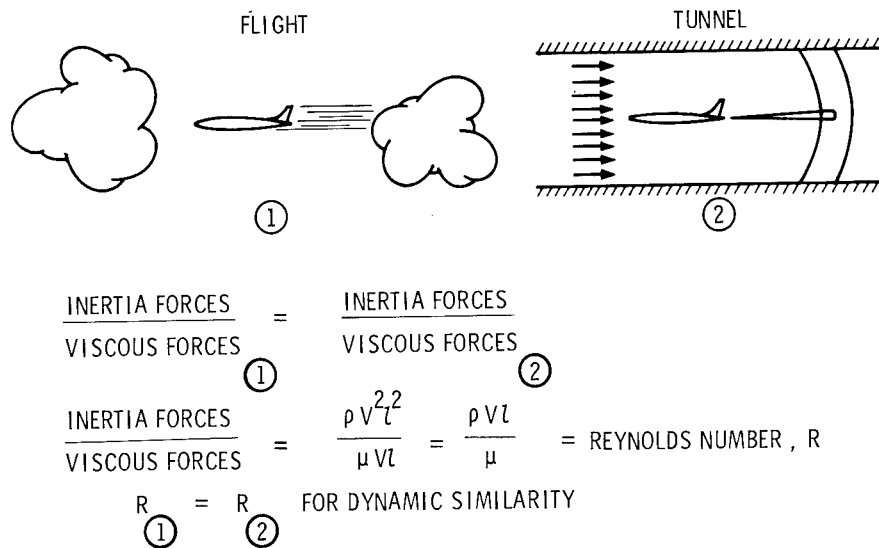
FLIGHT   TUNNEL

$$\frac{\text{INERTIA FORCES}}{\text{VISCOUS FORCES}}_{①} = \frac{\text{INERTIA FORCES}}{\text{VISCOUS FORCES}}_{②}$$

$$\frac{\text{INERTIA FORCES}}{\text{VISCOUS FORCES}} = \frac{\rho V^2 l^2}{\mu V l} = \frac{\rho V l}{\mu} = \text{REYNOLDS NUMBER , R}$$

$$R_{①} = R_{②} \quad \text{FOR DYNAMIC SIMILARITY}$$

Figure 1.- Dynamic similarity of viscous flows.
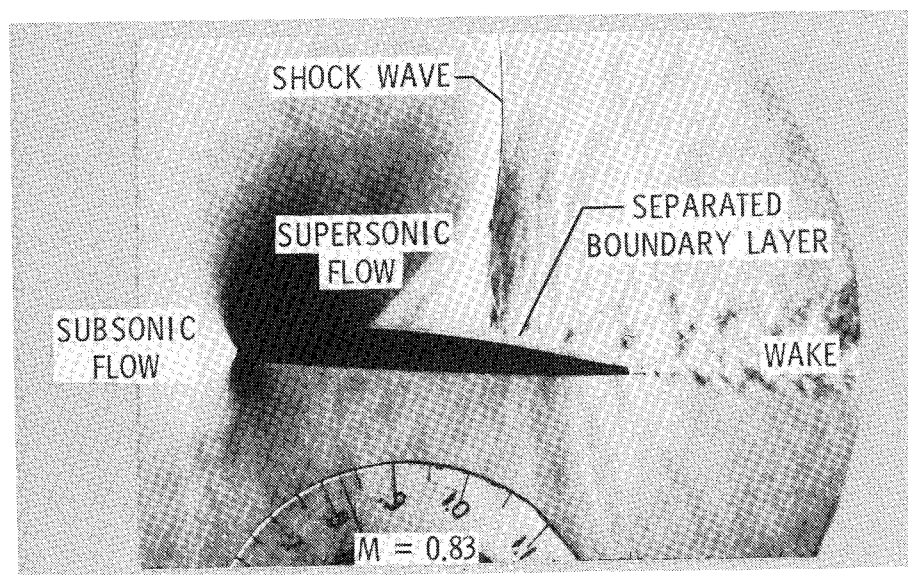
Figure 2.- Complex transonic flow.
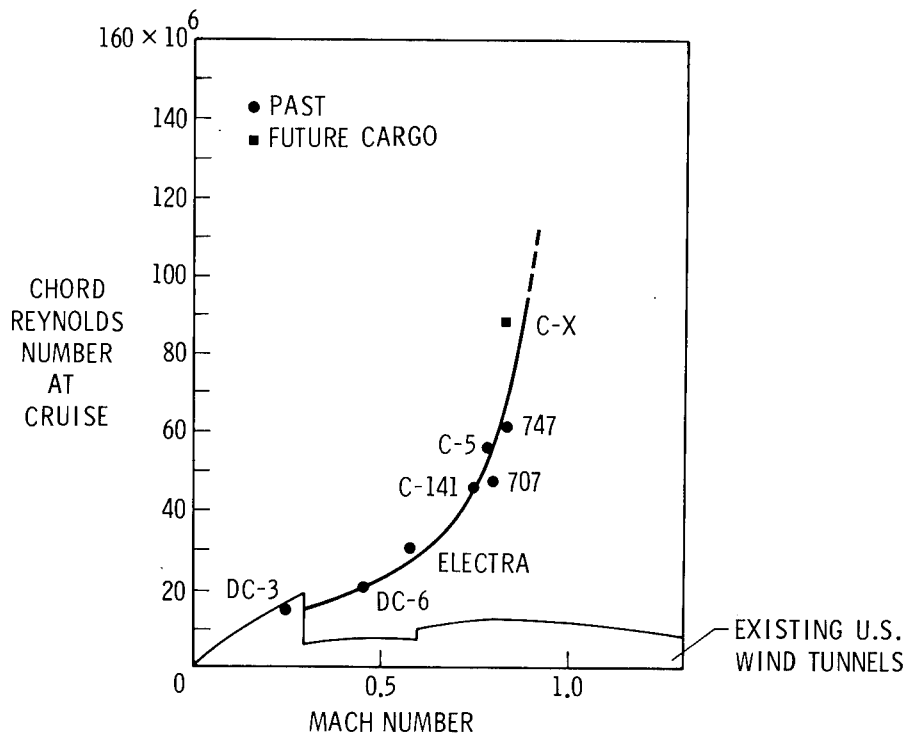
Figure 3.- The growing Reynolds number gap.

AIRCRAFT	PROBLEMS
C-141	WING FLOW INCORRECTLY PREDICTED. STABILITY, STRUCTURAL LOADS AND PERFORMANCE AFFECTED.
F-111	TRANSONIC-FLOW INTERFERENCE EFFECTS INCORRECTLY PREDICTED. AIRFRAME DRAG UNDERESTIMATED.
B-58 B-70 YF-12	IMPROPER AERODYNAMIC OPTIMIZATIONS AT TRANSONIC SPEEDS. LOW TRANSONIC ACCELERATION MARGIN RESULTED IN RANGE AND MANEUVERABILITY LIMITATIONS REDUCING AIRCRAFT EFFECTIVENESS.
F-102	TRANSONIC DRAG RISE IMPROPERLY PREDICTED CAUSED MAJOR RECONFIGURATION FOLLOWED BY REPLACEMENT BY F-106. TRANSONIC BASE DRAG PROBLEMS PLAGUED BOTH AIRCRAFT.

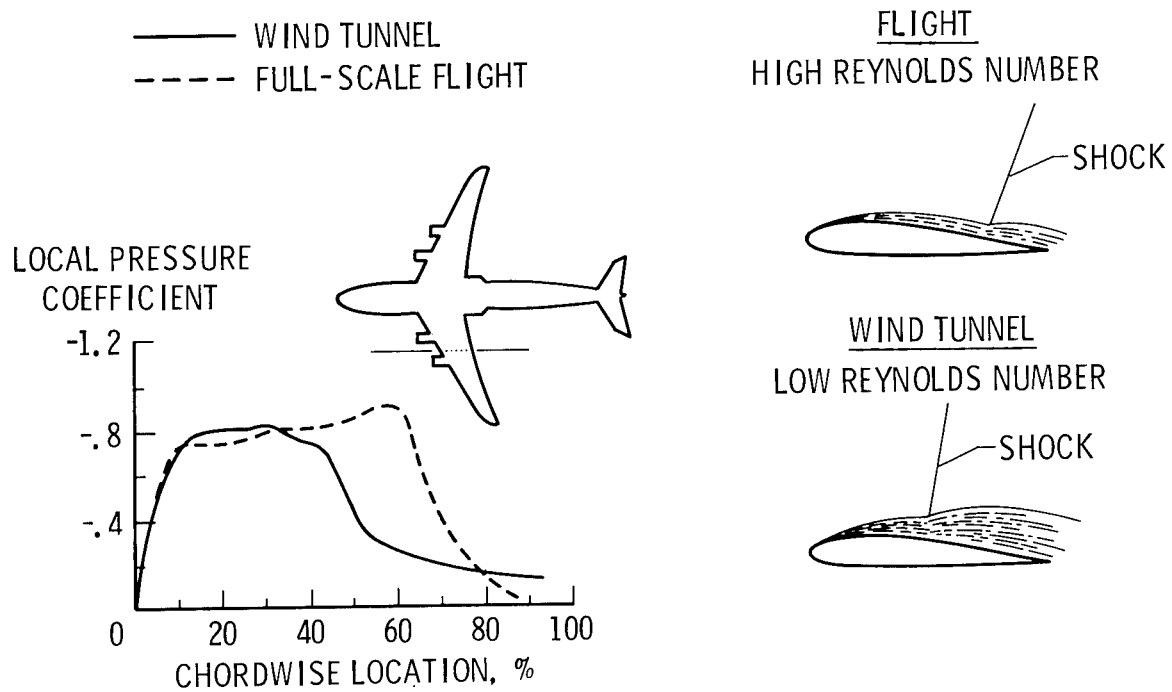Figure 4.- Problems attributed to scale effects.

WIND TUNNEL

FULL-SCALE FLIGHT

FLIGHT
HIGH REYNOLDS NUMBER

SHOCK

LOCAL PRESSURE
COEFFICIENT

-1.2

-.8

-.4

0   20   40   60   80   100

CHORDWISE LOCATION, %

WIND TUNNEL
LOW REYNOLDS NUMBER

SHOCK

Figure 5.- C-141 problems.

F. H. WENHAM
1824 - 1908

Figure 6.- F. H. Wenham, builder of the first wind tunnel.

$$R = \frac{\text{INERTIA FORCE}}{\text{VISCOUS FORCE}} = \frac{\rho V^2 l^2}{\mu V l} = \frac{\rho V l}{\mu}$$

$$\text{MODEL LOADS} \propto q = \frac{\rho V^2}{2}$$

$$\text{TUNNEL POWER} \propto qV = \frac{\rho V^3}{2}$$

MUNK PROPOSED USING COMPRESSED AIR AS A WAY OF INCREASING DENSITY, ρ, TO INCREASE R.

- MODEL = 1/10 FULL SCALE
- VELOCITY = FLIGHT VELOCITY
- PRESSURE = 10 atm

- MODEL = 1/10 FULL SCALE
- VELOCITY = 1/2 FLIGHT VELOCITY
- PRESSURE = 20 atm
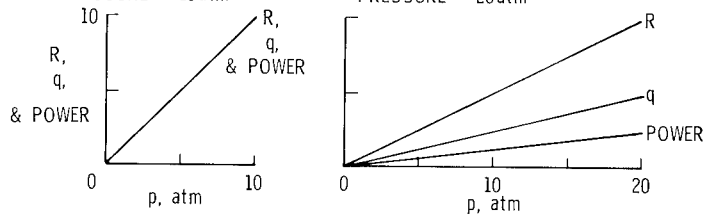
Figure 7.- Variable density tunnel concept.

A-Synchronous motor
B-Lift balance
B₀-Drag balance
C-Entrance cone
C-Exit cone
C-Outer cone
C-Inner cone

D-Deflector
E-Experiment chamber
F-Model
G-Angle of attack mechanism
H-Primary ring honeycomb
H-Secondary honeycomb
J-Oil-seal mechanism

K-Door
L-Vertical rod
M-Dead-air space
N-Weight
P-Propeller, 2-blade, 7 ft
Q-Revolution counter
R-Balance ring
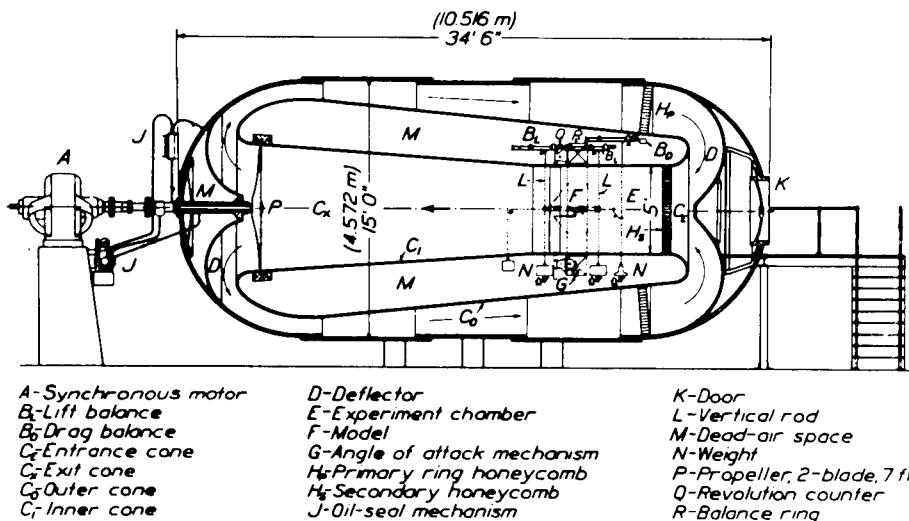
Figure 8.- Sectional view of NACA variable density wind tunnel, 1921.

33
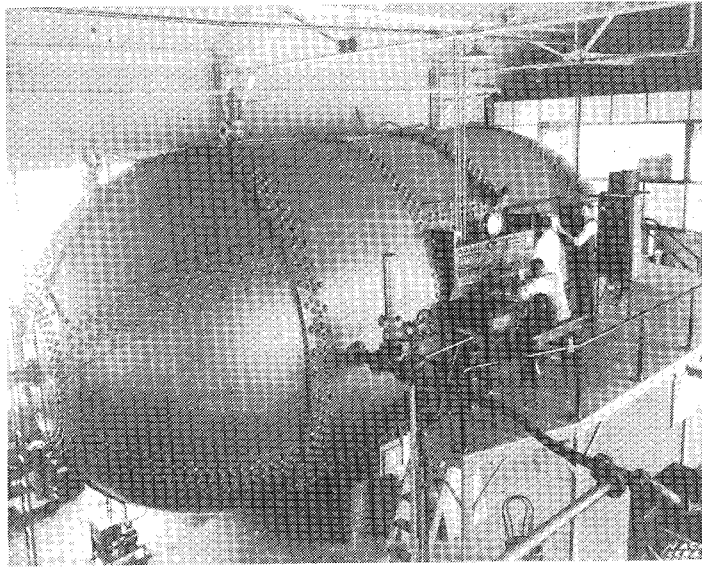
Figure 9.- NACA variable density wind tunnel, 1921.

● Wing and balance stress

● Wing distortion

● Sting interference
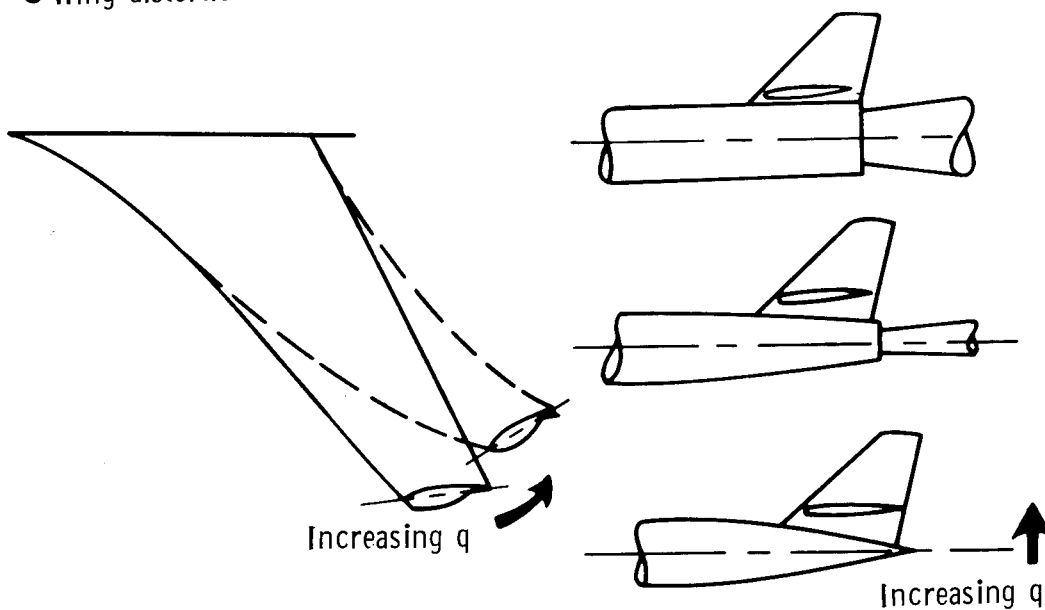
● Fuselage distortion

Increasing q

Increasing q

Figure 10.- Some problems with high dynamic pressures.

● $R = \dfrac{\text{INERTIA FORCE}}{\text{VISCOUS FORCE}} = \dfrac{\rho V^2 l^2}{\mu V l} = \dfrac{\rho V l}{\mu} = \dfrac{\rho Ma l}{\mu}$

● MODEL LOADS $\propto q = \dfrac{\rho V^2}{2} = \dfrac{\rho M^2 a^2}{2}$

● TUNNEL POWER $\propto qV = qMa$

FOR CONSTANT MODEL SIZE, PRESSURE, AND MACH NUMBER:
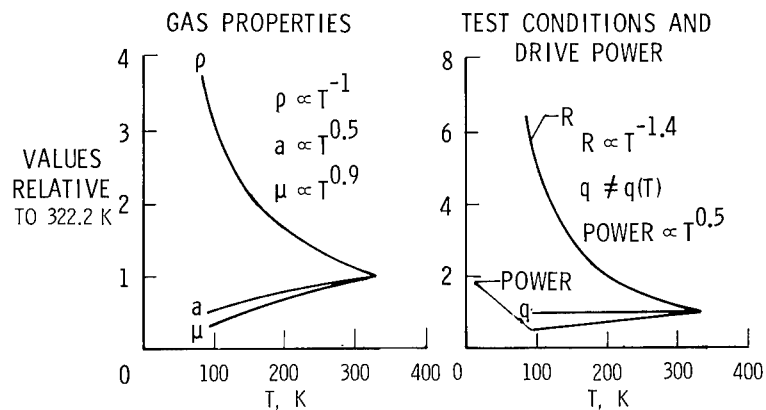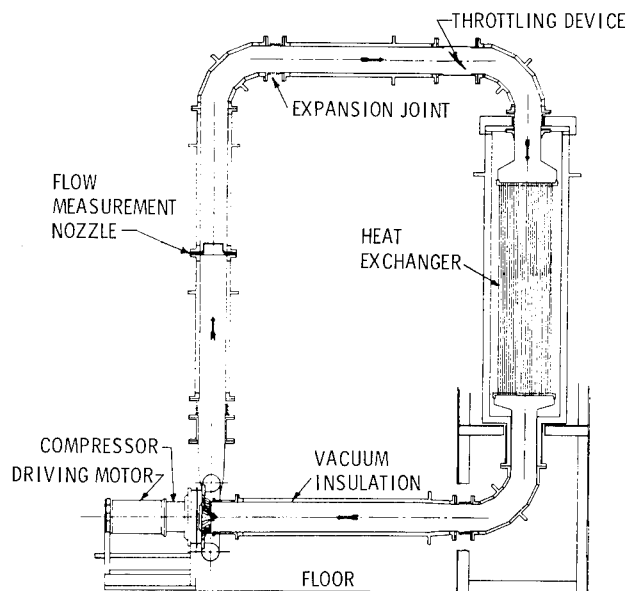

Figure 11.- Cryogenic tunnel concept.

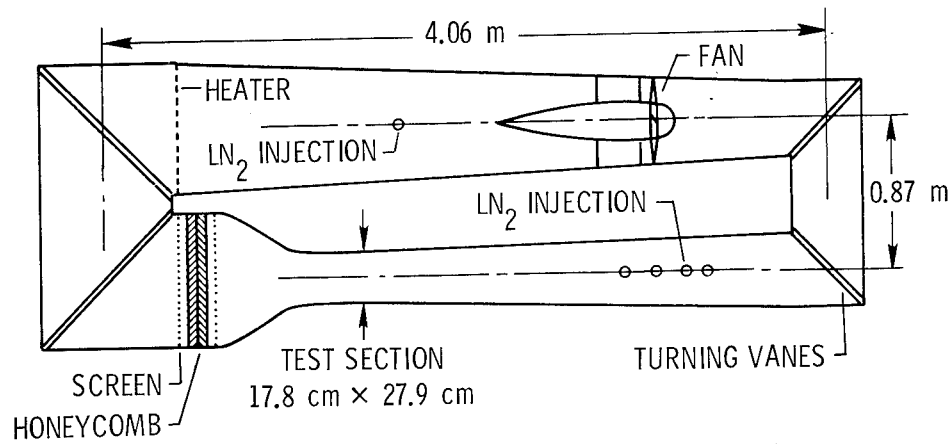Figure 12.- Rush's low temperature compressor test rig, 1962.

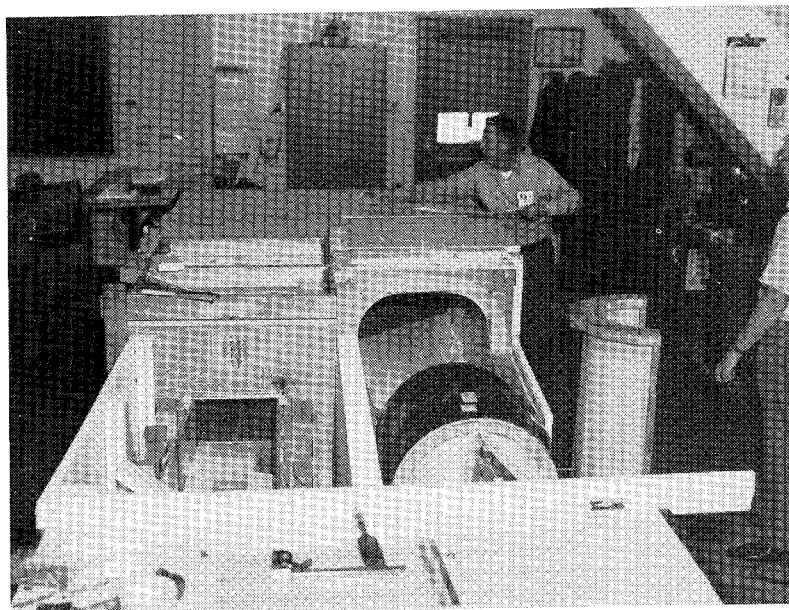Figure 13.- Low-speed cryogenic tunnel circuit, 1972.

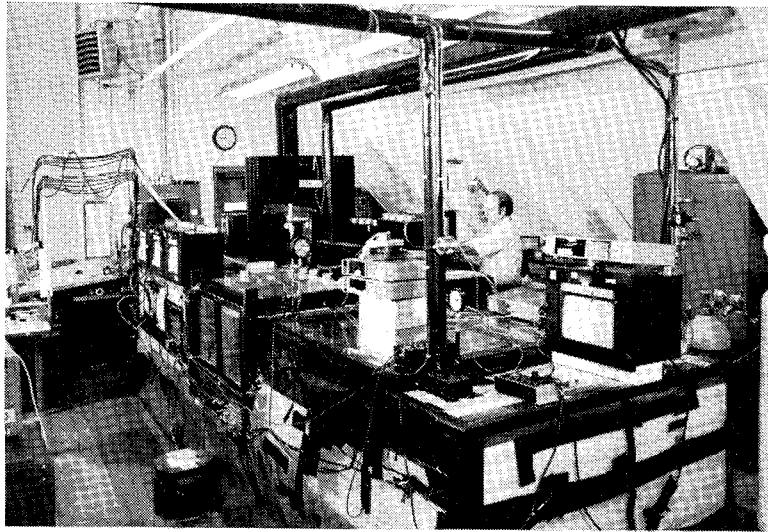Figure 14.- Low-speed cryogenic tunnel being insulated, 1971.

36

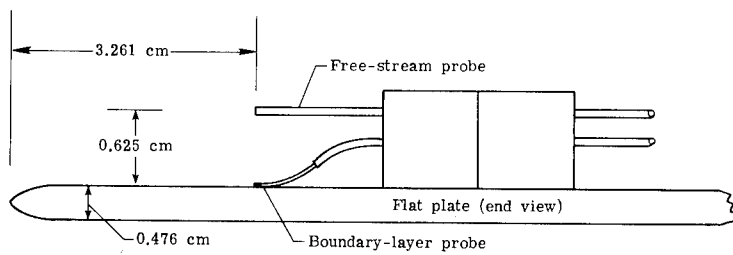Figure 15.- Insulated low-speed cryogenic tunnel and test apparatus, 1972.
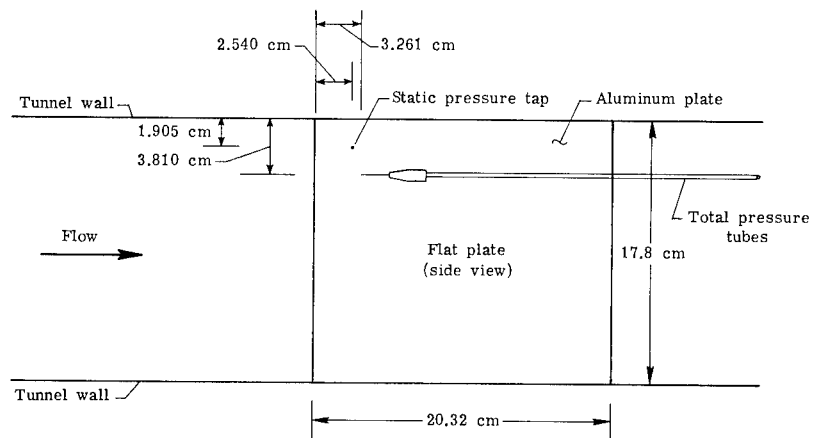

Figure 16.- Sketch of plate and probes used in boundary-layer experiment.

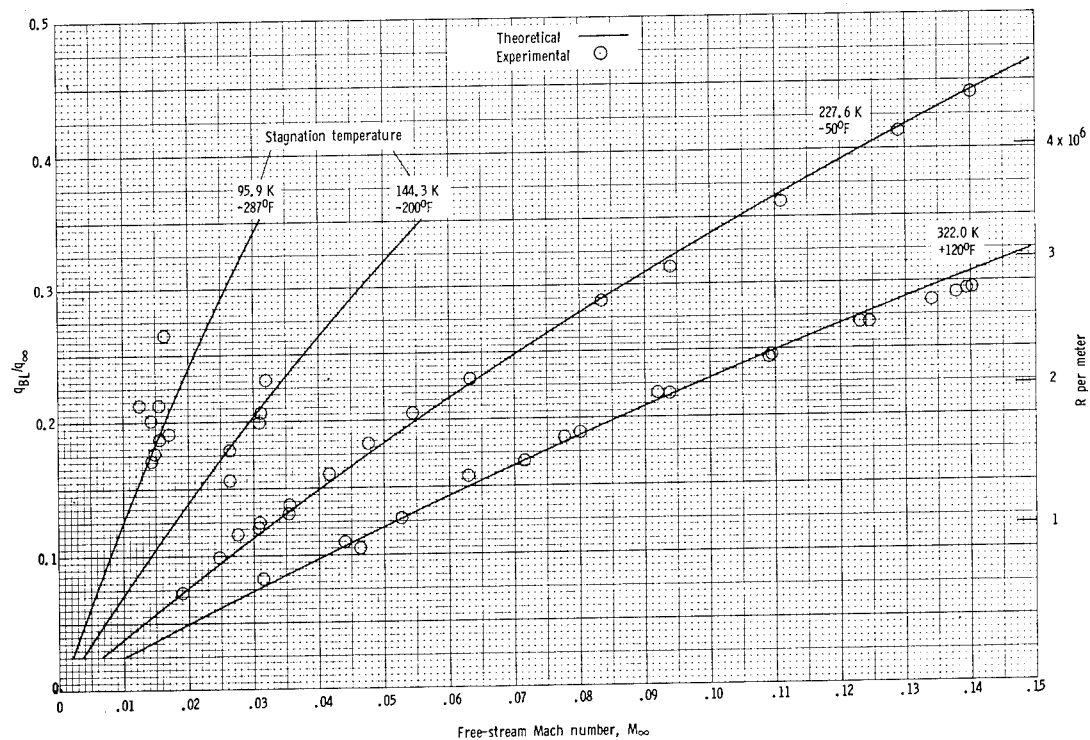Figure 17.- Theoretical and measured variation of the ratio of dynamic pressure in a laminar boundary layer to free-stream dynamic pressure as a function of Mach number and stagnation temperature.
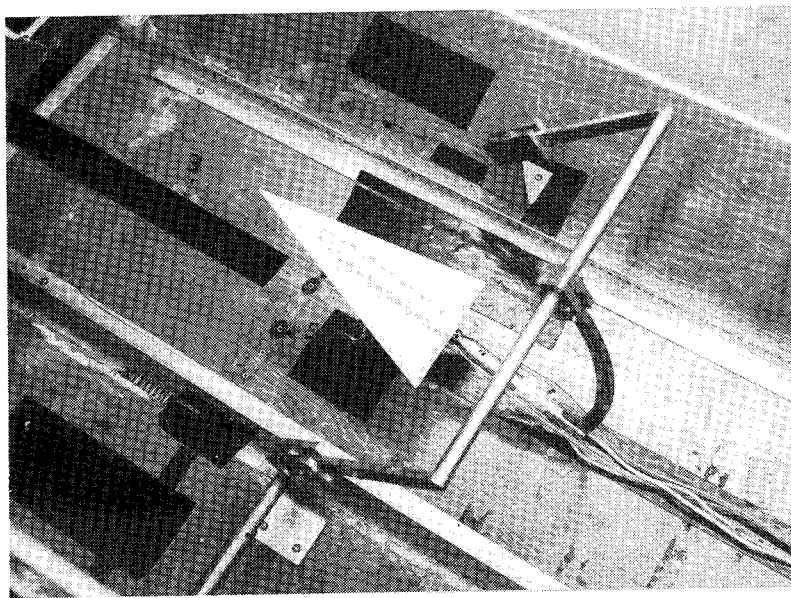
Figure 18.- Delta-wing model on water jacketed balance in low-speed cryogenic tunnel.
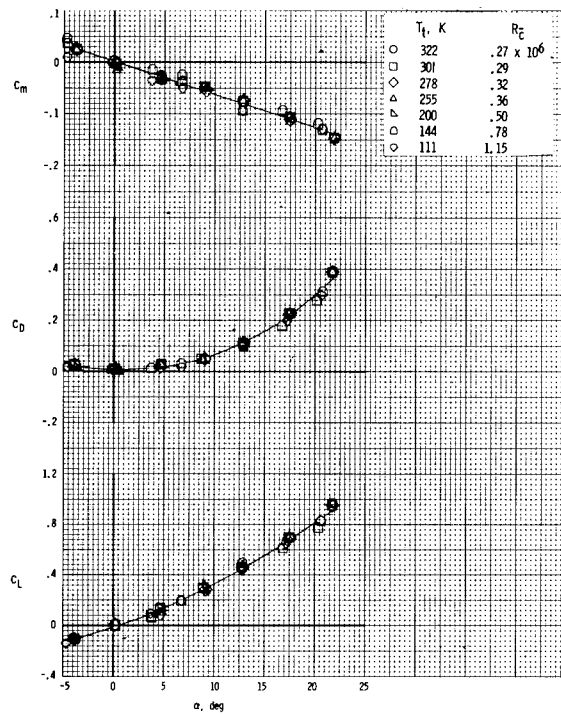
Figure 19.— Results from balance tests in low-speed cryogenic tunnel.
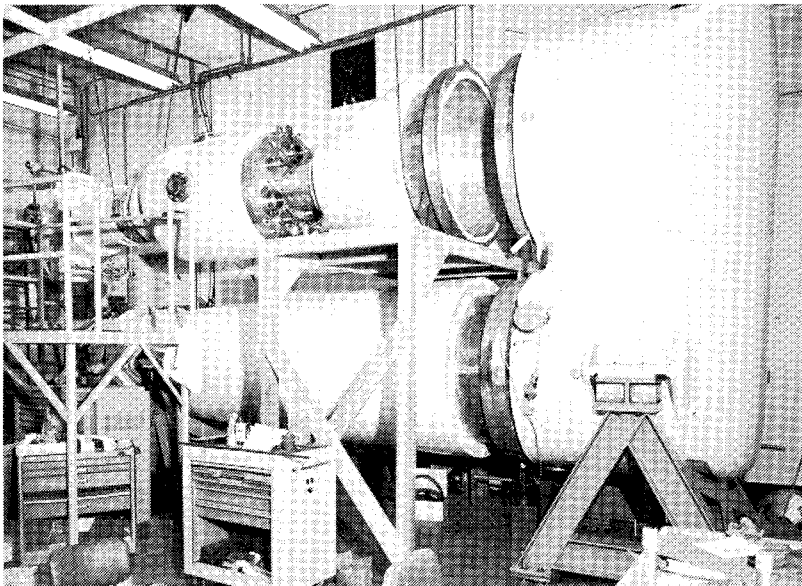
Figure 20.— Initial assembly of 0.3-m transonic cryogenic tunnel, 1973.
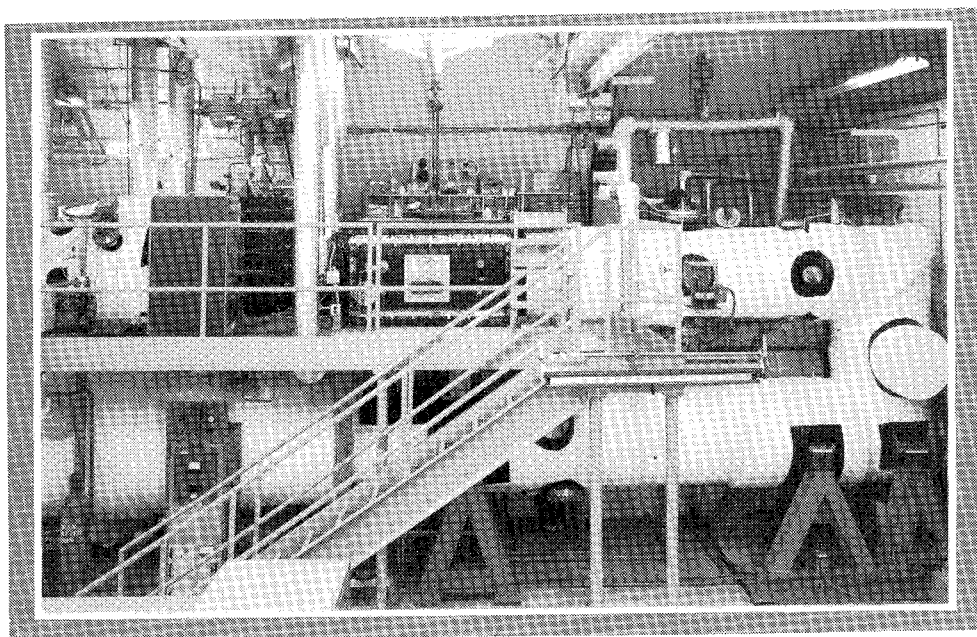
Figure 21.- View of 0.3-m transonic cryogenic tunnel, 1979.
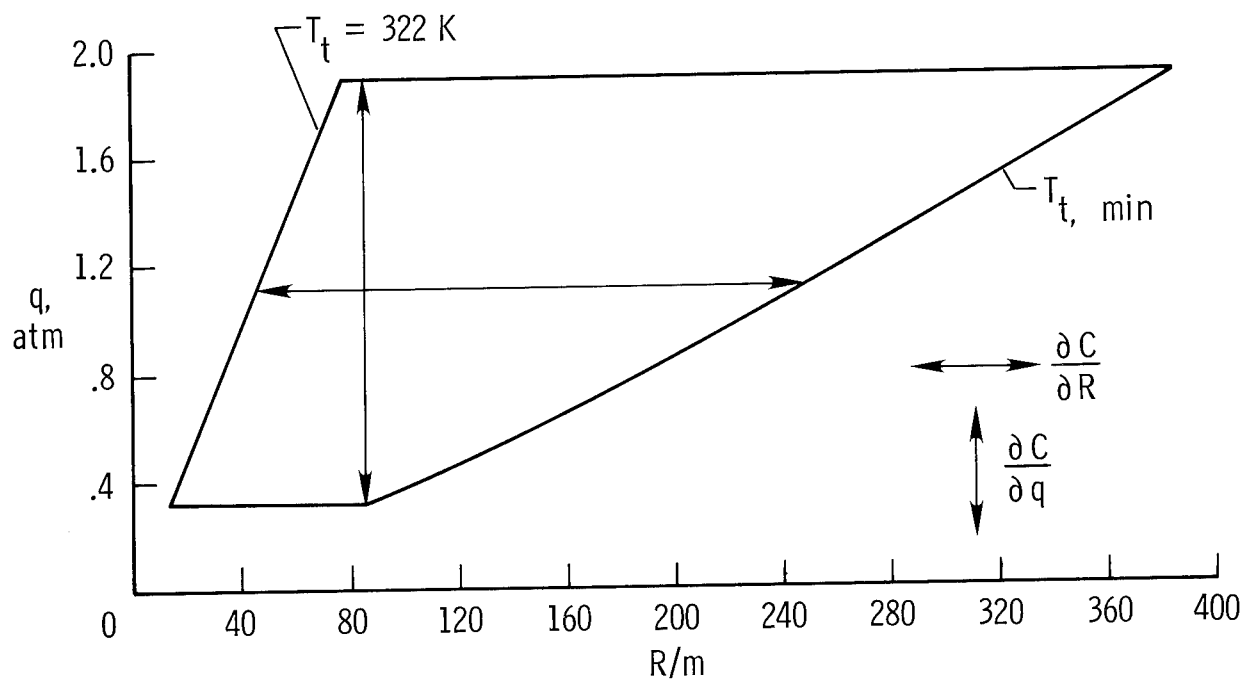
Figure 22.- Constant Mach number operating envelope for 0.3-m TCT.
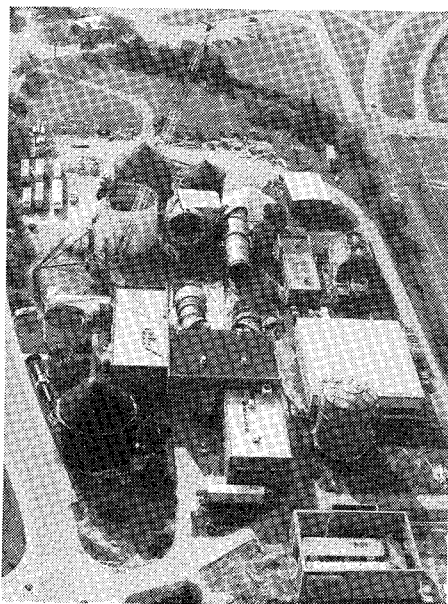
Figure 23.- View of NTF construction site, October 1979.
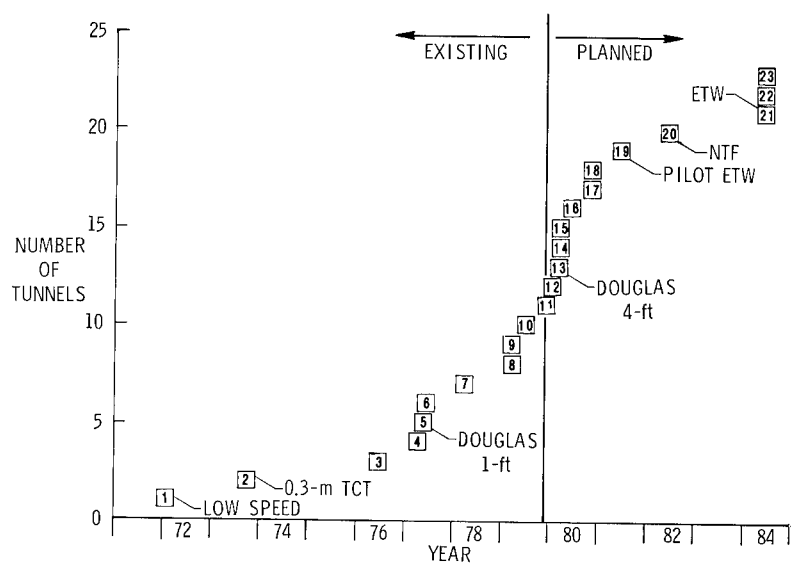
Figure 24.- Cryogenic wind tunnels as a function of time.
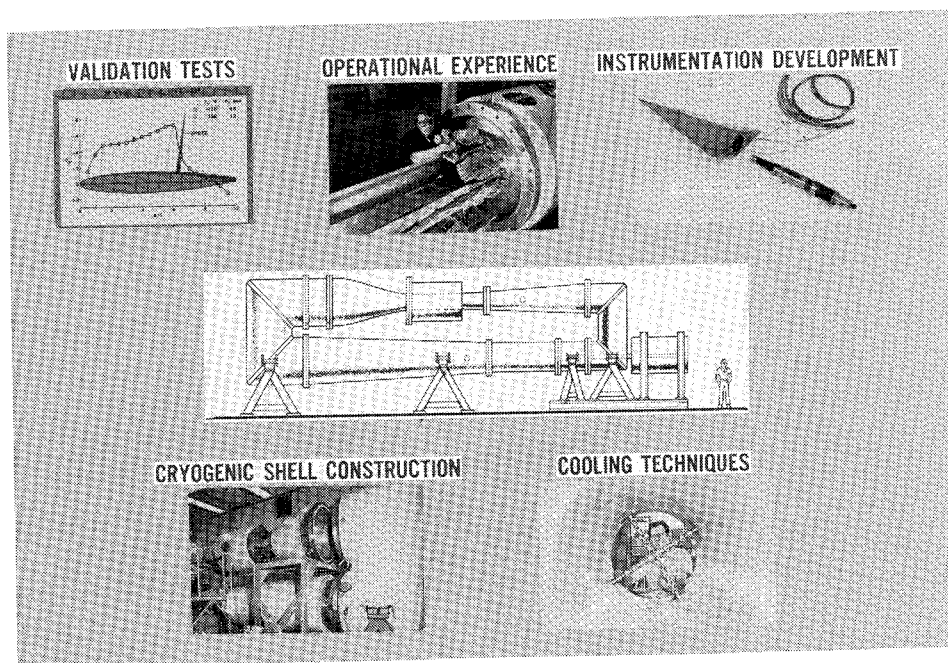
Figure 25.- 0.3-m transonic cryogenic tunnel activities.
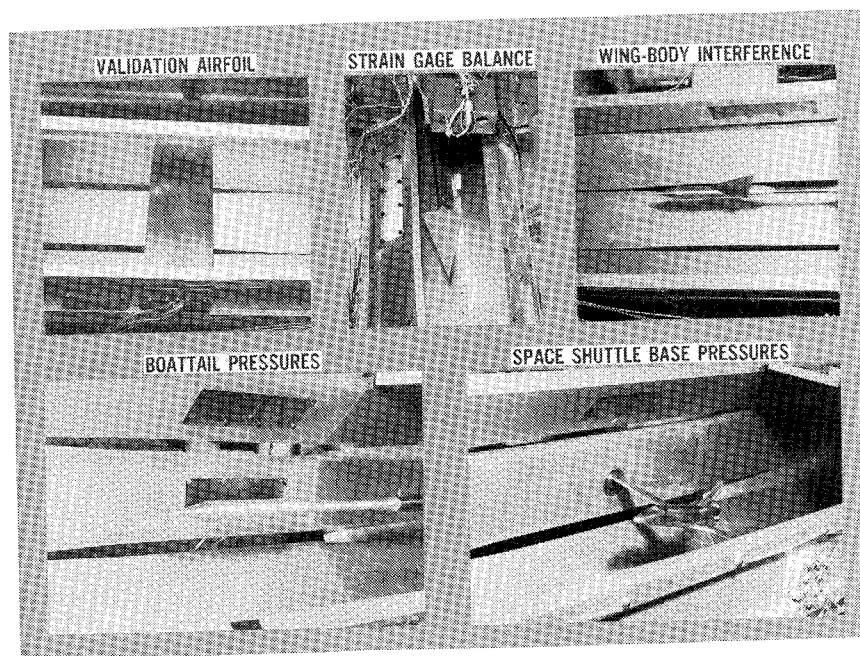
Figure 26.- Examples of tests made in 0.3-m TCT with original
octagonal test section.
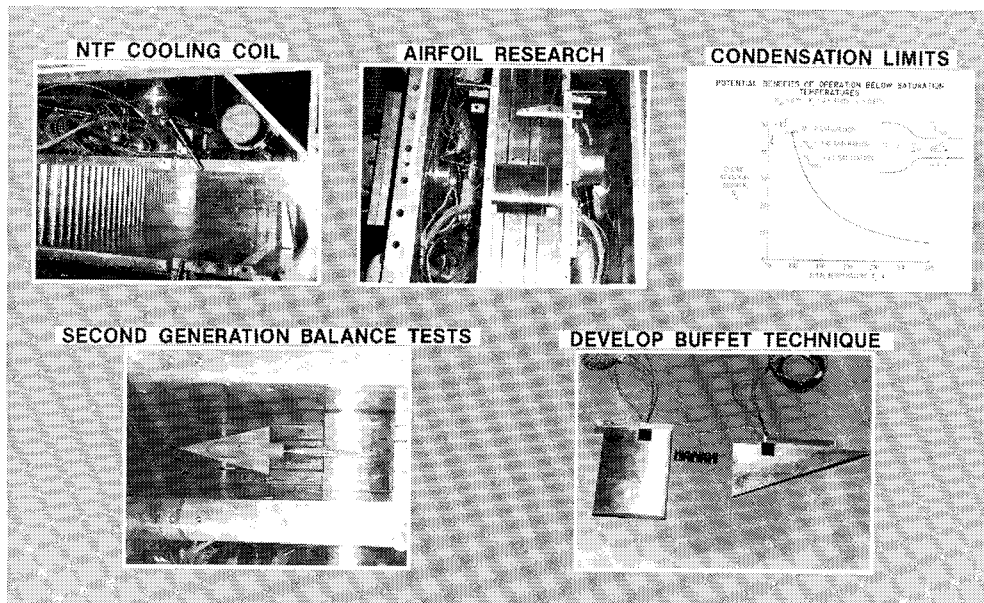
Figure 27.- Examples of tests made in 0.3-m TCT with 2-dimensional test section.
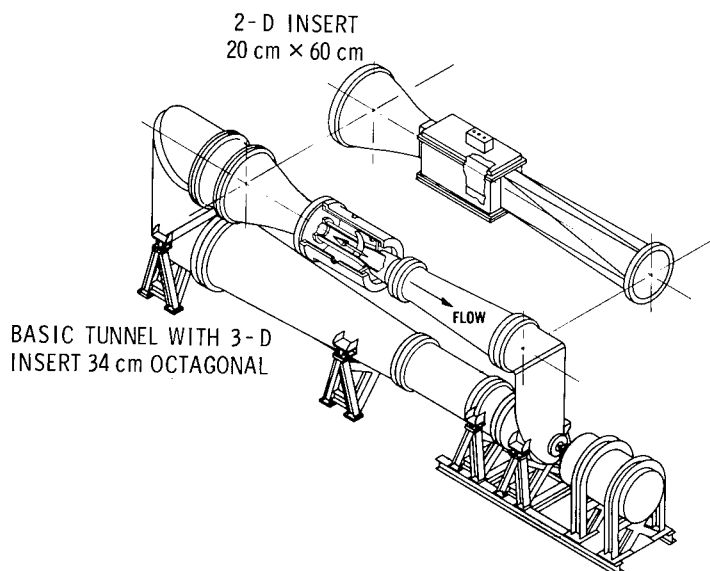
Figure 28.- Interchangeable test section capability, 0.3-m TCT.
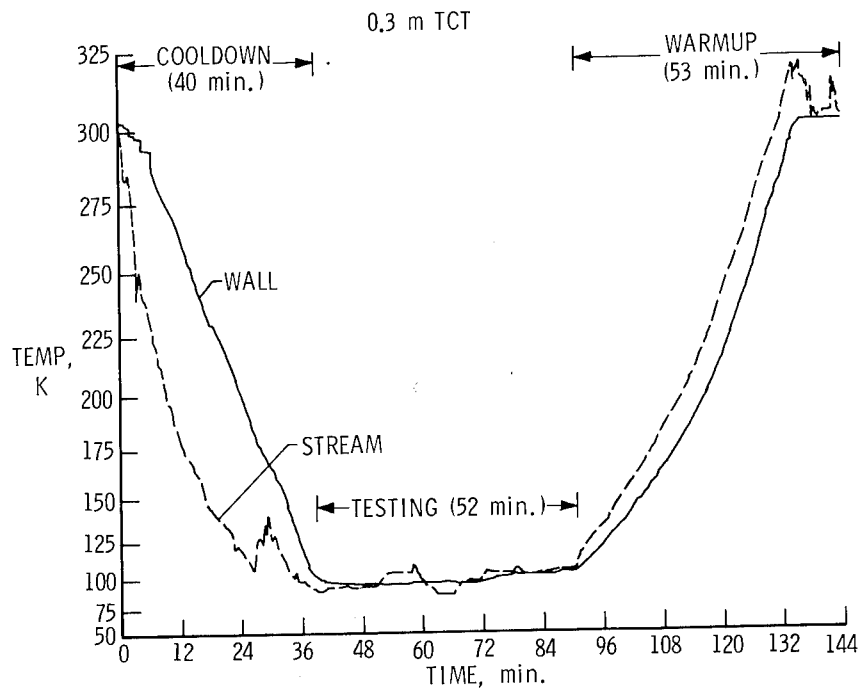
0.3 m TCT

Figure 29.- Stream and wall temperature as a function of time during a typical run.

0.3-m TUNNEL, DATA FROM A TYPICAL RUN
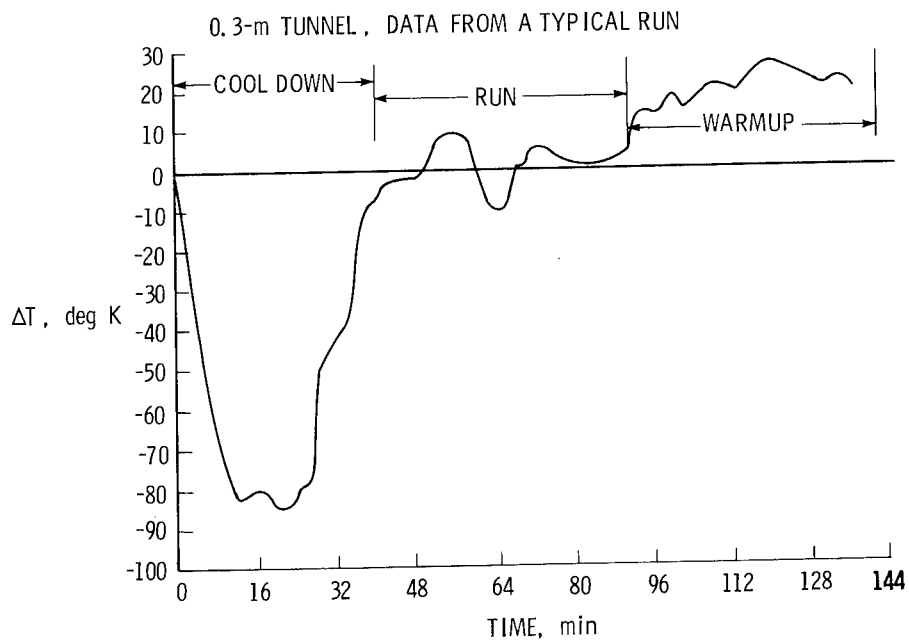
Figure 30.- Temperature difference between wall and stream.

M = 0.85, α = 0°, R$_C$ = 8.5 × 10⁶

	T$_t$, K	P$_t$, atm
O	322.2	4.9
□	116.7	1.2

SHOCK

C_p

SUPERSONIC

SUBSONIC

SUBSONIC

X/C
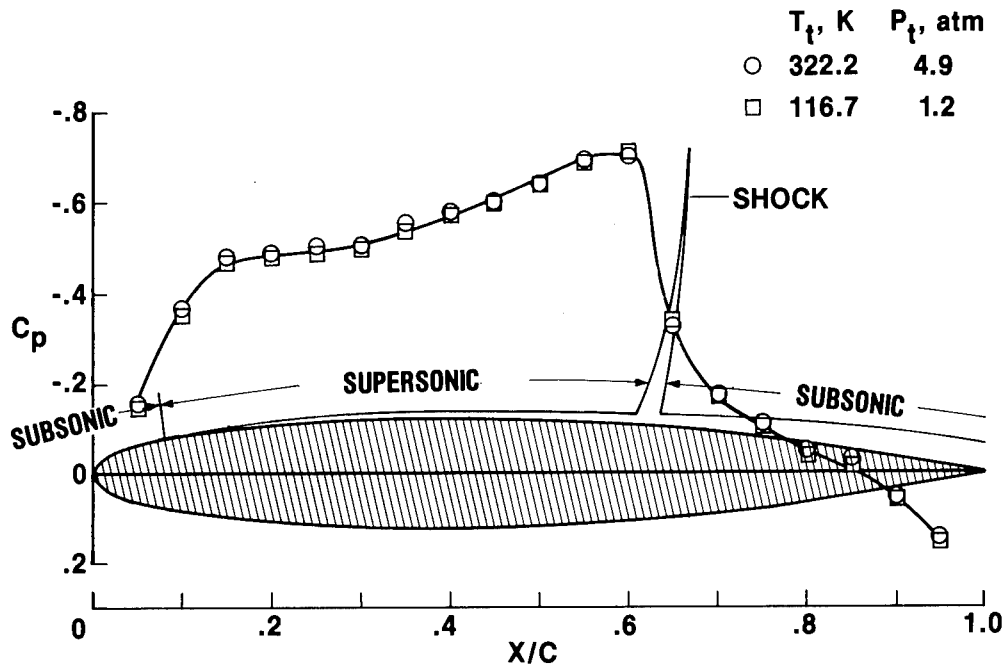
Figure 31.- Pressure distributions on validation airfoil in 0.3-m TCT.

$M_\infty = 0.6$

$C_{p,\beta}$

x/d_m

d_m

x

R × 10⁻⁶	T$_t$	P$_t$	C$_{D,\beta}$
O 10.43	117K	1.2 atm	0.010
□ 10.99	311K	5.0 atm	.010
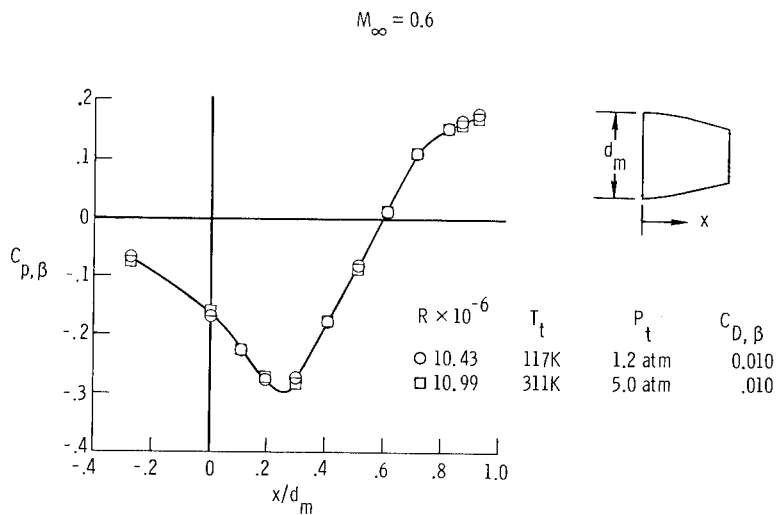
Figure 32.- Boattail pressures for a circular arc-conic boattail at cryogenic and ambient conditions.

FLOW →

COOLING COIL MODEL

HOT WIRE SUPPORT

WAKE RAKE

PRESSURE LOSS

$\dfrac{\Delta p_t}{q}$

.16 TURBULENCE
.08 $\dfrac{u'}{U}$
.04

6 ROW CIRCULAR

4 ROW ELLIPTICAL
FULL-SCALE

R/m
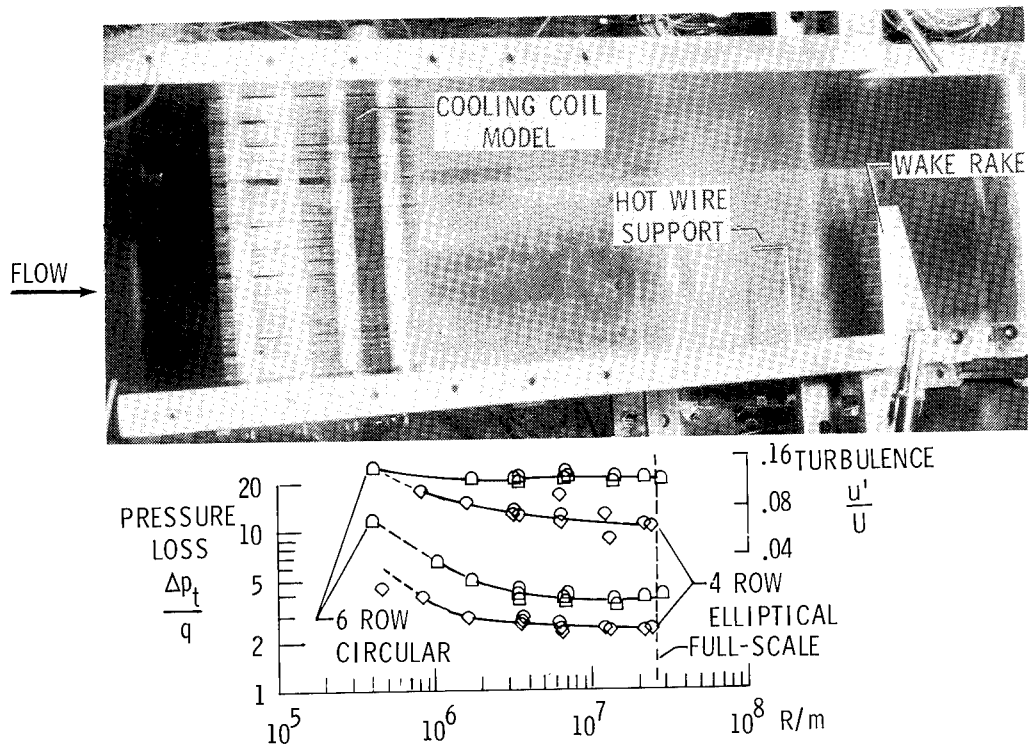
Figure 33.- Results obtained in full-scale cooling coil study, 0.3-m TCT.

$M_\infty = 0.85$, $P_t = 4.5$ ATMS, $C = 0.137$ m

$M = 0$ SATURATION

$M_\infty = 0.85$ SATURATION

$M_{L_{max}} = 1.2$ SATURATION

$M \sim 0$ $M_\infty \rightarrow$ $M_{L_{max}}$

CHORD REYNOLDS NUMBER, R_c

TOTAL TEMPERATURE, T_t, K

Figure 34.- Potential benefits of operation below saturation boundaries.

46
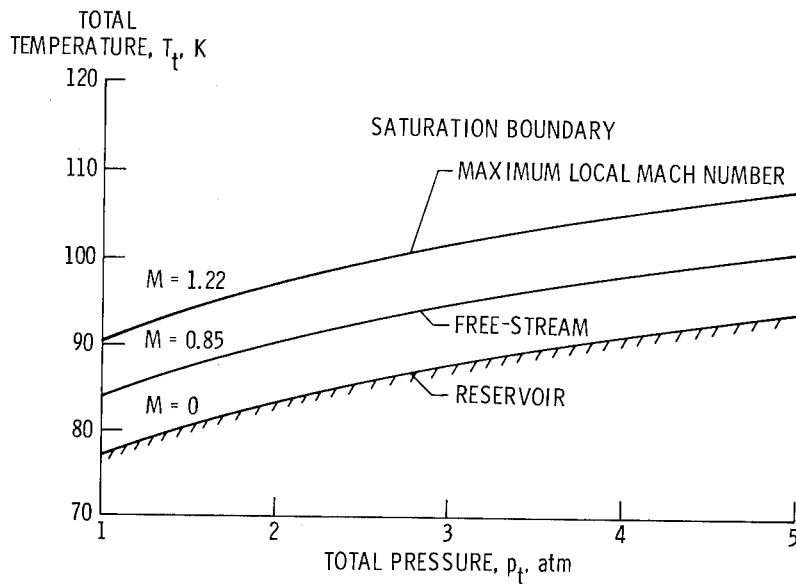
Figure 35.- Saturation boundaries of interest as a function of total pressure, $M_\infty = 0.85$.
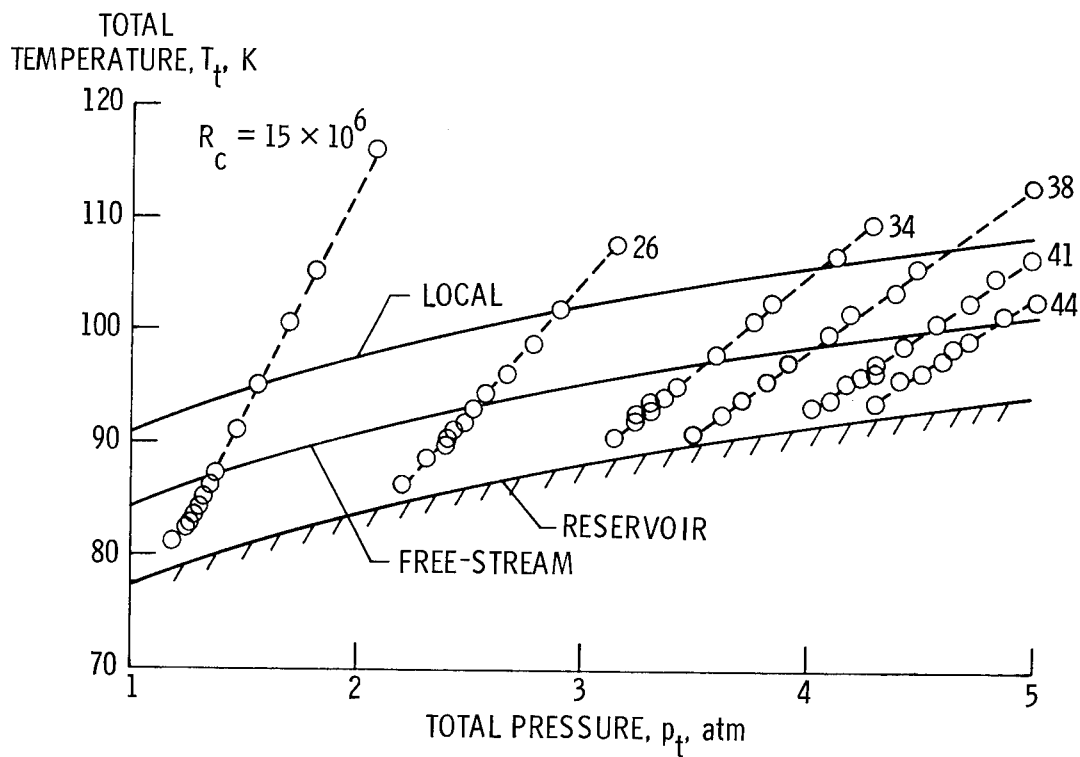
Figure 36.- Paths of constant Reynolds number showing total conditions sampled, $M_\infty = 0.85$.
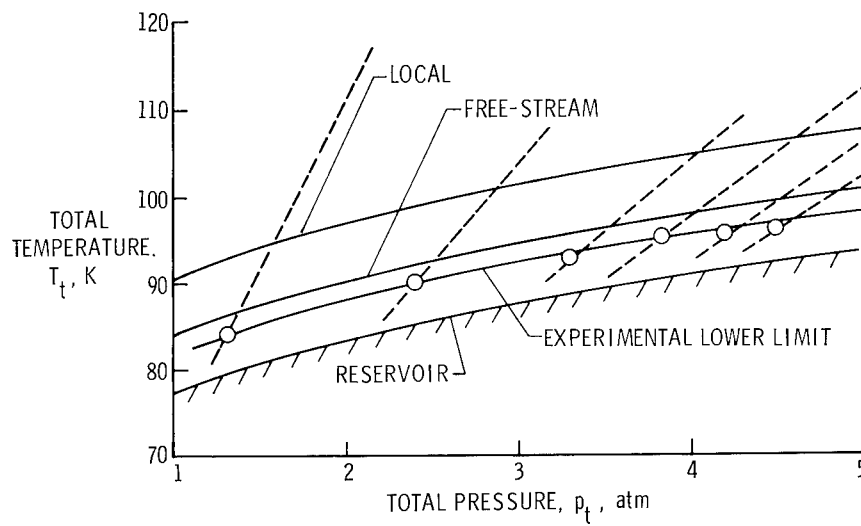
Figure 37.- Experimental lower limit at which pressure distributions
begin to differ from their references.

OVERVIEW OF ENGINEERING DESIGN AND OPERATING CAPABILITIES OF THE NATIONAL TRANSONIC FACILITY

Robert R. Howell
Langley Research Center

SUMMARY

An overview of the engineering design of the National Transonic Facility is presented. The overview includes a summary of the design goals and criteria, pertinent design details and the projected facility performance.

The facility will afford the nation a markedly improved capability to test at or near full scale Reynolds number and to assess the effects of Reynolds number, Mach number and model deformation on the aerodynamics of configurations.

The facility design is complete and its construction is approximately 50 percent complete. It is scheduled to become operational in 1982.

INTRODUCTION

The design of the National Transonic Facility (NTF) represents a major undertaking. It represents the effort and contributions of approximately 200 people and spanned a period of about 4 years. A recounting of the design details is beyond the scope of this conference. We have elected, therefore, to focus the following papers on design areas that are impacted by the cryogenic environment or are unique and unusual. As a consequence, large portions of the NTF design will not be discussed in any detail.

This paper will provide an overview of the systems and components which make up the facility so that it is clear how subsequent detailed papers contribute to the overall facility definition.

Some of the important milestones in the chronology of the NTF design are presented in figure 1. Early conceptual studies contributing to the design of the National Transonic Facility began in 1972. However, actual preliminary design did not begin until 1974. In November 1974 -- becaus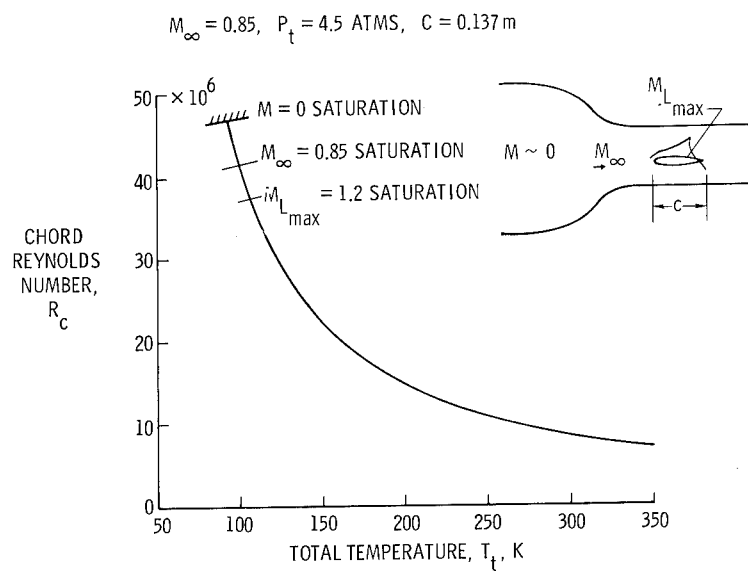e of inflationary cost trends -- design activities became dormant while a special ad hoc facilities review panel of the joint Air Force/NASA Aeronautics and Astronautics Coordinating Board (AACB) reassessed the national need for high Reynolds number testing and defined a wind tunnel with requirements to meet those needs. As a consequence of this panel's

activity, the National Transonic Facility was proposed in July 1975 and in November 1975 the National Transonic Facility Project was approved. The design of the NTF is currently complete.

DESIGN GOALS AND CRITERIA

As mentioned earlier, the Facilities Review Panel of the AACB produced, in July 1975, a set of performance criteria for the National Transonic Facility which established firm guidelines for its location, the type of wind tunnel and its major characteristics (see fig. 2). Additionally, it specified a productivity which implied a work capability considerably greater than existing wind tunnels.

More specifically, the criteria define a closed circuit transonic wind tunnel having a test section cross section 2.5 meters square, capable of operating at temperatures down to 78 K (140°R) and at pressures up to 8.8 bar (130 psia), as required to produce a chord Reynolds number of 120×10^6 (based on 0.25 meters) at Mach number of 1.0. To achieve the annual productivity goal of 8000 polars (or 100,000 data measurement points) the control and operation of this tunnel, as well as the data acquisition process, must be largely automated. Additionally, the facility design must include features which will permit quick changes to models to minimize loss of testing time. General requirements for safe operation and the criteria for environmental impact were added to the performance requirements. This expanded set of criteria, together with budget and operating cost constraints, formed the broad criteria for the design.

DESIGN IMPLEMENTATION

The A/E selected to perform the design was the Ralph M. Parsons Company and their associate FluiDyne Engineering Corporation. All of the design work required could not be accomplished under contract because of the design budget constraints. This made it necessary to split the design effort between the A/E and NASA (fig. 3). The A/E work was also split between Parsons and FluiDyne. NASA Langley Research Center took the responsibility for the aerodynamic design, the design of specific items, most of the detailed systems analysis and all of the verification and developmental testing. Additionally, the NASA team was responsible for monitoring and reviewing the A/E design progress and participating in the design decisions and concept selections. Parsons was generally responsible for the design of all components and systems external to the pressure shell. FluiDyne was responsible for the design of all internal components including the large doors in the plenum shell and design of the control system. You will note that three internal components; the cooling coil, rapid diffuser and turning vanes were transferred to Parsons to more equally balance the workload. The shell design was shared between the firms.

Thus, the design that evolved was the product of a team composed of two A/E firms and NASA-Langley -- all contributing to different facets of the total design problem. The final design process started in November 1975. The A/E work on the basic design was completed in May 1978. Since that time, Langley has continued to massage the design of certain packages in an attempt to minimize cost and to maximize the competition for the procurement packages. Eighty-five percent of the design is currently under contract. The remaining major packages will be advertised in the spring of 1980.

THE DESIGN

Major parts of the facility design were amenable to standard engineering practices and techniques. However, where systems were required to operate in the cryogenic environment, unusual analysis seemed required to alleviate concerns. These systems will be the subject of subsequent papers in these proceedings.

Capital cost was a major driver in concept and technique selection and operating cost was a factor in the establishment of goals and criteria for the efficiency of the operating systems. Additionally, as always, there was the ever present concern for operational safety.

Site Selection

Site selection (fig. 4) was impacted by the determination that the existing 4' X 4' Supersonic Pressure Tunnel could be decommissioned and certain of its systems made available for use by the NTF. As a consequence of this decision, the two existing drive motors and their speed control system, the cooling towers and associated pumping equipment and the office and motor buildings were contributed to the NTF project -- greatly reducing the out-of-pocket cost of the facility.

The disadvantages of the site were associated with its proximity to the highway and a residential area. As it turned out, the problems connected with the site would have had to be addressed regardless of where the facility was located.

Pressure Shell

The geometry of the pressure shell (fig. 5) is controlled largely by the requirement to minimize capital cost and provide efficient aerodynamic lines. The aerodynamic lines evolved as a consequence of trying to minimize internal volume, which is tied directly to cost, while satisfying the criteria of 2.5 m square test section with near minimum drive horsepower and better than average flow quality. A fairly short circuit was achieved by using what is called a rapid diffuser at the entrance to the settling

chamber. The rapid diffuser requires a uniform resistance across its exit to assure the absence of flow separation. In our design, the cooling coil is used to provide the required resistance, as well as to provide heat removal during tunnel operation with air as the test medium.

The cooling coil is followed by 4 anti-turbulence screens and a 15 to 1 contraction to the nozzle throat. The high speed diffuser and the low speed diffuser are designed to be near optimum conical diffusers. The pressure shell closely conforms to the shape of the aerodynamic lines, except in areas where internal plumbing or operating equipment is required.

The pressure shell is required to contain the working gas with temperatures between 353 K (635°R) and 78 K (140°R) at pressures between 0.5 bar (8 psia) and 8.8 bar (130 psia). At the onset, it was clear that an insulation system was required to minimize the energy transfer to the gas in the cold state. In the process of analyzing the effectiveness of the insulation in various locations relative to the shell, it was recognized that the energy required to change the temperature of the shell was quite large. Since certain types of tests envisioned required rapid changes in working gas temperature and pressure while operating, it was cost effective to insulate the shell from temperature changes. Thus, the decision was made to place the insulation inside the shell. As a consequence, the shell normally remains at near atmospheric temperature.

Despite the internal insulation, the shell has been designed for exposure to the test medium temperature excursions and is capable of withstanding liquid nitrogen spills internally. Therefore, the structural integrity of the pressure shell is not dependent upon the integrity of the insulation system. Because of the 8.8 bar (130 psi) maximum operating pressure with nitrogen gas in the shell, structural integrity of the vessel is a concern. Excellence in design and fabrication of the vessel was assured by imposing ASME Pressure Vessel Code requirements. The vessel design has been subjected to a stress analysis that is in accordance with ASME Section VIII, Division II Code. The vessel will be fabricated, inspected, tested, and stamped for Section VIII, Division I, of the ASME Unfired Pressure Vessel Code. It will be the first wind tunnel ever known to receive a code stamp. Additionally, a fatigue analysis has been performed on the vessel which indicates a 50 year service life before fatigue should become a concern. A periodic inspection program will assure fatigue never becomes a safety problem.

Insulation System

The internal insulation system design (fig. 6) was complicated by the necessity for the insulation material to be capable of withstanding the 8.8 bar (130 psi) operating pressure and rapid pressure and temperature changes. Additionally, there is a requirement that the tunnel be capable of operating with air at pressure. This latter requirement establishes the potential of a fire hazard because of increased oxygen availability in

pressurized air. Thus, in addition to having the desired insulating characteristics, the insulation material was required to be self-extinguishing at elevated pressure, have sufficient compressive strength to withstand 8.8 bar (130 psi) with margin of safety, and have adequate tensile strength to prevent fatigue cracks due to thermal stress. The insulation system is a laminated composite of rigidized closed cell foam, fiberglass, and adhesive. The system is bonded to the inner surface of the shell and further retained by a mechanical system which forms the flow surface. The flow liner is supported by a fiberglass-epoxy structure attached through links and clips to the pressure shell. The liner is aluminum plate. The mechanical system is designed to breath thermally in response to differences in temperature between the shell and internal gas and is vented to avoid excessive pressure load due to rapid changes in working pressure.

Internal Structures

Although the pressure shell is insulated from the working gas and consequently remains at near ambient temperature, there are structures inside the tunnel which, by virtue of their function, must feel the temperature. These structures (fig. 7) include the turning vanes, the nacelle and fan shrouds and the structures which define the settling chamber and high speed leg of the tunnel. All of these structures must accommodate large and rapid temperature changes and, as a consequence, were designed to alleviate and/or accommodate thermal stress. Their design required extensive combined stress analysis including transient thermal effects. Aluminum alloys were used as the structural material primarily because of their high thermal conductivity and relatively low cost.

Test Section

The test region of the tunnel (fig. 8) is one of the most complicated internal structures because of the many remotely adjustable parts. The test section is 2.5 meters square. All four walls are slotted. The top and bottom wall angles relative to tunnel centerline are adjustable about a hinge line at their upstream end (Station 0). The flow re-entry flaps at the downstream end of each slot are also adjustable. The upstream sections of the entire sidewall are on a vertical track which permits it to be lowered for ready access to the model. To permit insertion of access tubes (described later), the diagonal corner fillets are also required to fold out of the way. The top and bottom walls of the model support section also pivot about a hinge line at station 11.8 meters (38.6 ft).

The actuators for these movable components are electro-mechanical jacks. Problems resulting from the cryogenic temperature were avoided by encapsulating the actuators in a thermal enclosure and controlling the internal temperature with electric heaters.

The large circular arc angle-of-attack strut is supported on sets of bearing pads located at top and bottom. It is driven by a large hydraulic cylinder attached to the plenum shell beneath the test section.

Test Section Isolation System

Early in the design process, it became obvious that even though the cryogenic approach was most cost effective of all approaches considered, high Reynolds number tests would be more expensive than conventional wind tunnel tests, and we would need to take advantage of every opportunity to reduce operating cost. One cost effective system included in the design of the NTF is the system for test section plenum isolation which permits changes to be made to the model while the remainder of the tunnel circuit is pressurized with cold nitrogen gas (fig. 9).

To achieve test section isolation, the contraction and high speed diffuser are uncoupled and moved away from the plenum bulkheads on a sliding pad-rail system. The large dished heads (valves) are raised, positioned, and dogged to each bulkhead opening. These heads isolate the plenum volume from the rest of the circuit. The plenum volume is then vented to the atmosphere. When the pressure in the plenum reaches atmosphere, the model access system can be activated. This system (figs. 10a and 10b) is composed of two tubes having rectangular cross sections and doors at the outer ends. They are mounted in the opening of the 2.74 m by 3.66 m doors. These doors can be unseated and moved on internal tracks to their open position. The side wall of the test section is lowered and the two access tubes slowly inserted. When these two tubes meet in the center of the test section, they capture the model in the tube and seal around the model sting. The tube volume is then purged with air to provide a working environment, the end doors are open to allow a through passage. The model is conditioned for change. To go back into operation the process is reversed.

The design of the test section and test section isolation system is complicated by the cryogenic environment. It was found necessary to maintain a thermal environment for all of the actuators. Design technology for seals which seat and reseat in a cryogenic environment was not available. Large static seals required around the bulkhead also exceeded existing experience. As a consequence, we have had to perform design verification/ development work in these areas.

The Upstream Nacelle

The upstream nacelle structure (fig. 11) houses the main radial bearing for the fan shaft and its lubrication system. It also contains the inlet guide vane actuator ring and its hydraulic system. Because of the need to avoid cryogenic temperature on the bearing lubrication and hydraulic systems, the internal volume will be maintained at 292 K (525°R)

or above. This criterion made it necessary to insulate this structure internally like the pressure shell. The volume contains thermostatically controlled electric heaters to maintain temperature. It is sealed, generally, except for a vent to the upstream side of the fan disk.

The internal volume of the upstream nacelle is the location where some of the major inspection and maintenance work will be carried out. These inspections include the fan blades and hub, the shaft bearing and lube system and the fan shaft.

Internal Noise Treatment

The structures upstream and downstream of the fan were designed to accommodate noise attenuation panels. The fan was recognized as a major source of both external and internal noise. Since there were criteria for noise levels in the settling chamber as well as environmental constraints for the far field noise, we elected to attenuate the noise near the source using resonator panels submerged within the aerodynamic lines of the nacelles and flow liners.

The other major noise source inside the tunnel is the ventilated test section. However, little is currently known about possible noise treatment for this source and none was attempted in the basic design.

Drive System

The fan drive system, figure 12, makes use of the two existing variable speed induction motors and their speed control. These two motors have a combined maximum rating of 52×10^6 W (70,000 hp) for 10 minutes. At any given Mach number (fan compression ratio) the rotational speed of a fixed geometry fan system must be adjusted to compensate for the change in speed of sound with temperature. Since power available from the motors is related to the rotational speed, there is a need to shift gears to achieve the desired power operating envelope. The final design provides a two-gear ratio clutch arrangement (figs. 12 and 13). The higher gear ratio was selected to provide adequate compression ratio for tunnel operation with air at ambient temperature. This permits the NTF to be operated as a conventional wind tunnel and overlap the Reynolds number capability of most other tunnels in the United States. The lower gear ratio was picked to meet requirements at cryogenic-high Reynolds number conditions. So, at maximum speed for the low gear ratio, the additional power required to develop the 120×10^6 at M = 1.0 was added. The additional motor is synchronous; so, Mach number control is achieved with the inlet guide vanes only. The synchronous motor is brought to speed and synchronized using the induction motors.

Cryogenic System (LN$_2$ Supply and Vent)

The liquid nitrogen supply system is shown schematically as figure 14. It is composed of the LN$_2$ storage tank, pumps and appropriate valves. There is a vaporizer system to keep the ullage in the supply tank at atmospheric pressure while liquid is being removed. Liquid nitrogen is sprayed into the tunnel circuit upstream of the fan to establish and maintain cryogenic temperatures. The heat of vaporization is used to absorb energy to reduce or maintain temperature. The injection system is shown schematically as figure 15. The system is composed of 12 separate supply pipes (3 at each of the 4 quadrants). The flow in each pipe can be adjusted to maximize the flexibility in the distribution of LN$_2$ injected. Both the flow in each pipe and the injection pressure can be varied by changing the injection nozzles. Pressure in the tunnel is maintained by venting at the large end of the tunnel. Where constant operating temperature and pressure are required, venting mass flow is equal to the injected liquid mass flow and is directly proportional to the power absorbed by the fan. The maximum mass flow through the system is approximately 454 kg/sec (1000 lbs per sec). In the design, three pumps are used instead of a single large one for reasons of cost and efficiency. The smallest pump is used for tunnel cooldown. The other two are either used separately or together depending on flow rate requirements. The vent system discharges from the tunnel through two control valves into a muffler vessel which is used to attenuate valve noise and exhausts into the base of a 36.6 meter (120 foot) high vent stack. The momentum of the discharge from the tunnel is used to induce air into the base of the stack. The system is designed to assure that the mixture of air and nitrogen at the discharge of the stack has sufficient oxygen to sustain life. The minimum upward velocity at discharge is 21.3 m/sec (70 ft/sec) which assures adequate mixing with surrounding air so that no thermal problem will occur if the plume returns to ground level. For low pressure operation of the tunnel, four axial flow fans pump air up the stack and provide the required momentum at the discharge. These fans also provide the safety system for any nitrogen leaks within the vent system enclosure by pumping the nitrogen gas up the stack. In addition to confining cryogenic nitrogen from leaks, the enclosure also serves to attenuate the far field noise.

Air System

The air system (fig. 16) serves two purposes. One purpose is to provide air for purging nitrogen out of spaces and conditioning for personnel entry. These spaces include the volume housing the isolation valves, the plenum, and the nacelle volumes. The other purpose is to provide for pressurization of the circuit when required for air operation. The incoming air is heated to replace energy loss due to pressure reduction and then distributed to the various use points. The air enters the system at 124 bar (1800 psi) and is reduced after heating to 10.3 bar (150 psi) for distribution. The purge air is under flow control for safety.

Water Systems

The water systems (fig. 17) are closed, treated systems used to transfer heat from the tunnel through the cooling coil when the tunnel is operated in the conventional air mode and to transfer heat from a number of heat exchangers which cool various lubrication and hydraulic systems. The system uses existing cooling towers, pumps and supply and return piping. New piping has been provided near the use point as required.

Building

The building addition (figs. 18, 19, and 20) is a conventional structure sized to provide a model preparation shop and buildup rooms (designated as user space) on the first floor. The buildup rooms permit aerodynamic test models to be built up on support stings and to permit instrumentation and operating systems to be checked out in a secure space (as may be required for proprietary models). Each of the buildup rooms provide connections to the data recording system for the tunnel so that calibrations, deflections, etc., can be recorded and processed like data from the tunnel. Behind the model preparation shop, there is a high bay which covers the tunnel test region. There is a large pit in this area which accommodates the hydraulic actuators for the model angle-of-attack system and the test section side walls.

The second floor of the building addition provides space for the tunnel control room and model installation area. Models on a handling dolly will be raised from the first floor to the second floor and placed in the tunnel through a large 2.75 m (9 ft) by 3.66 m (12 ft) door on the side of the test section plenum. The model preparation process is configured to accommodate four separate models in the building at one time -- one in test and three others in different stages of preparation in the rooms below. In general, the building design presented no significant technical concerns. However, we did require that low areas in the building be provided with oxygen monitors and alarms and forced exhaust systems to avoid the potential hazard of inadvertent nitrogen accumulation within the building.

The control room is sized to accommodate all of the equipment required for automated control and data acquisition. It is designed with a raised floor to allow wiring beneath the floor. A layout of the cabinets and consoles is shown as figure 21. The arrangement permits several pre- or post-test activities to proceed simultaneously without interference. For example, checkout of the tunnel control system and the model instrumentation can occur simultaneously with the calibration of a model balance in the buildup room below.

During the operation of the tunnel, process monitoring stations are provided for the operating crew as well as the test crew and data and software personnel.

Controls and Data Acquisition System

The basic control loop employed in the control of the NTF is shown in figure 22. Each control variable such as pressure, temperature, or Mach number has its own servo control loop. Each loop stands alone and is stabilized and managed by a microprocessor. A sequencer is used to assess the status of the tunnel and equipment. It contains the necessary interlocks to assure safe operation of the loops.

In addition, there is a programable computer which permits an input of test conditions, model attitudes, dwell times, etc., and allows the tunnel to be operated in an automatic mode.

Computers are used for control and management of the automation of the tunnel control and data processing. Note that in addition to control and management, the computers are required to provide feedback to displays for monitoring purposes. Displays will generally be on cathode ray tubes.

A summary schematic of the total control and data system complex is shown on figure 23. Four medium size computers are interconnected such that information can be interchanged between them. Two of the computers are allocated to data acquisition and management and two are allocated to tunnel process control and monitoring. There is a shared pool of peripheral equipment including plotters, line printers, CRT's, etc. You will note that there is an interconnecting switch for each pair of computers which permits either computer to do either job. This affords the capability of operating with one computer doing both jobs at some reduced capability. As mentioned earlier, the arrangement also permits several pre- or post-test activities to proceed without interference.

PROJECTED PERFORMANCE

Now that the design of the National Transonic Facility has been described in an overview fashion, it is appropriate to briefly describe the overall performance of the facility as compared to the goals originally set for it.

Reynolds Number Capability

The primary goal for the facility was to enhance the nation's ability to simulate full scale Reynolds numbers in a wind tunnel. As mentioned in the beginning, the facility must be capable of achieving a Reynolds number of 120×10^6 at M = 1.0 based on a model chord of 0.1 the test section width (or 0.25 m). The design performance map for a Mach number of 1.0 is shown as figure 24. In this format, performance is presented as an envelope of operation in terms of stagnation pressure, Reynolds number, and temperature.

The boundaries on the operating envelope, as indicated by the dashed line, consist of inlet guide vane angle limit on the left which results in a minimum temperature at which the fan can achieve the required compression ratio at the fixed rpm, the maximum power available (the curved dashed line at the upper left) the maximum operating pressure for the shell (8.8 bar), and the minimum operating temperatures which for this case have been set as those required to produce condensation at a local Mach number of 1.4.

The cryogenic wind tunnel differs from the conventional tunnel by virtue of its having temperature as an operating variable. Most conventional wind tunnels operate at near atmospheric temperature or near the maximum temperature line shown. It should be noted that the goal of 120×10^6 Reynolds number for the NTF is achieved at the maximum operating pressure and minimum temperature.

An operating envelope, such as the one shown, has been developed for each Mach number. An overall envelope of the maximum Reynolds number for the Mach number range of the facility is shown as figure 25. Presented is Reynolds number as a function of Mach number. The Mach 1.0 performance is indicated for reference.

The boundary on this overall operating envelope is the maximum operating pressure for the pressure shell (8.8 bar), the maximum fan power available (93×10^6 W) and the limiting compression ratio of the fan. At the bottom of the figure is an envelope of the current Reynolds number capability of all known wind tunnels. It is noted that the National Transonic Facility affords an order of magnitude improvement in Reynolds number capability at transonic speed over existing wind tunnels.

For reference, this operating envelope has been transposed to the Reynolds number gap figure used by Kilgore in figure 26. In this figure, the cruise Reynolds number for various existing and projected transport airplanes has been plotted at their cruise Mach number. As can be seen, the full scale cruise Reynolds number for these airplanes fall within the operating envelope of the NTF.

The ability of the NTF to perform full scale Reynolds number tests is indicated on figure 27, where flight at full scale and test at model scale are compared. The airplane used in this comparison is the well known Boeing 747. On the left of the figure is a plot of the airplane flight envelope in terms of altitude versus Mach number. Lines of constant Reynolds number are shown within the flight boundary. On the right, the flight envelope has been superimposed on the NTF test envelope which is presented in terms of Reynolds number and Mach number for a properly sized model. The part of the flight boundary covered by the NTF test boundary is where full scale flight Reynolds numbers can be achieved. The maximum test boundary has also been transferred to the flight envelope on the left to show the full scale Reynolds number test capability in that format. As you can see, the tunnel will not provide full scale Reynolds numbers for low altitude flight of this airplane. However, it does provide correct

simulation in the high performance region of the envelope which includes the cruise point. This region is by far the most important region insofar as aircraft design and efficiency are concerned. At the bottom of the figure, on the right again, for reference, is the envelope of Reynolds number capability as it exists today.

CONCLUDING REMARKS

The engineering design of the National Transonic Facility has been described in an overview manner. This facility will afford the nation a markedly improved capability to test at or near full scale Reynolds number and to assess the effects of Reynolds number, Mach number, and model deformation on the aerodynamics of configurations. The facility design is complete and its construction is approximately 50 percent complete. It is scheduled to become operational in 1982.

- 1972 – CONCEPTUAL STUDIES

- APRIL 1974 – DETAIL DESIGN STARTED

- NOV. 1974 – JULY 1975 – AACB FACILITIES REVIEW PANEL ACTIVITIES

- JULY 1975 – NTF PERFORMANCE CRITERIA

- NOV. 1975 – NTF PROJECT APPROVAL

- MAY 1978 – A/E WORK COMPLETE

- NOV. 1979 – NTF DESIGN COMPLETE

Figure 1.– Chronology of some important milestones in
design of National Transonic Facility.

A SINGLE TRANSONIC TEST FACILITY IDENTIFIED AS
THE NATIONAL TRANSONIC FACILITY (NTF)

CRYOGENIC CONCEPT

CHARACTERISTICS:

TEST SECTION SIZE	2.5 m SQUARE
DESIGN PRESSURE	9 BAR
DESIGN MACH NUMBER RANGE	0.2 – 1.2
STREAM FLUID	NITROGEN
BASIC DRIVE POWER	9×10^7 W
PRODUCTIVITY/EFFICIENCY	8000 POLARS/yr
REYNOLDS NUMBER	120×10^6 (M = 1.0)

LOCATED AT LANGLEY RESEARCH CENTER

_____

SAFE OPERATION

SATISFY ENVIRONMENTAL IMPACT CRITERIA

CONSTRUCT WITHIN BUDGET

Figure 2.– Recommended characteristics for National Transonic Facility.

A/E		NASA
RMP CO.	FEC	LaRC
DEMOLITION & FOUNDATIONS	PRESSURE SHELL (HIGH SPEED LEG)	AERODYNAMIC DESIGN
BLDG & SITES	TEST SECTION & MODEL SUPPORT	ALL FINITE ELEMENT MODELING AND ANALYSIS
PRESSURE SHELL (EXCEPT FOR HIGH SPEED LEG)	TEST SECTION ISOLATION SYSTEM	STRESS THERMAL
RAPID DIFFUSER	MODEL SUPPORT STRUT & ACTUATOR	DYNAMIC FATIGUE
COOLING COIL	CONTRACTION & HIGH SPEED DIFFUSER	FRACTURE MECH.
TURNING VANES		FAN HUB AND BLADES
FAN DRIVE SYSTEM	NACELLES & SHROUDS	MODEL ACCESS TUBES
VENT SYSTEM	SCREENS & SUPPORT	MODEL ROLL DRIVE
LN_2 TANK	LN_2 INJECTION SYSTEM	CONTROL ROOM
LN_2 SUPPLY SYSTEM	INSULATION SYSTEM	INSTRUMENTATION & DATA ACQUISITION
WATER SUPPLY SYSTEM	HYDRAULIC SUPPLY SYSTEM	SEALS
AIR SUPPLY SYSTEM (EXTERNAL)	INTERNAL AIR DISTRIBUTION	NOISE CONTROL
ELECTRICAL SUPPLY SYSTEM	PROCESS CONTROLS (HARDWARE)	CONTROL LOGIC
		SAFETY ANALYSIS
		SOFTWARE
		ALL VERIFICATION TESTING

Figure 3.- Division of responsibilities in design of National Transonic Facility.
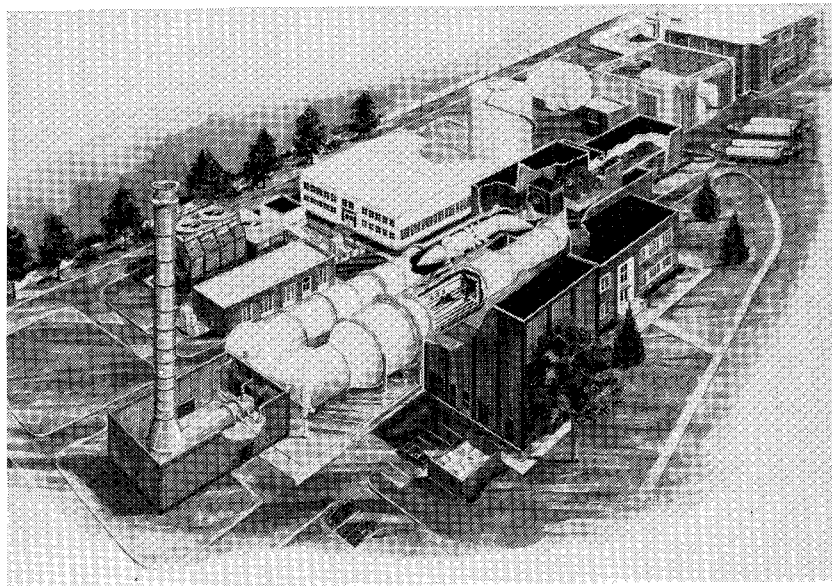
Figure 4.- Perspective of National Transonic Facility on site of Langley 4 ft. by 4 ft. Supersonic Pressure Tunnel.
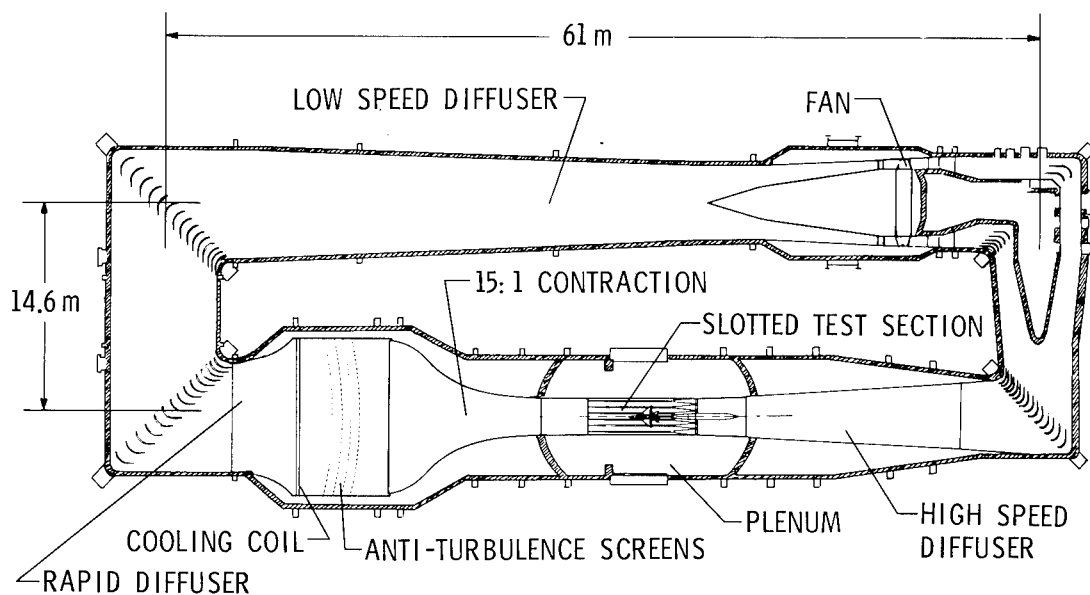
Figure 5.- Plan view of tunnel circuit showing pertinent dimensions and components - National Transonic Facility.
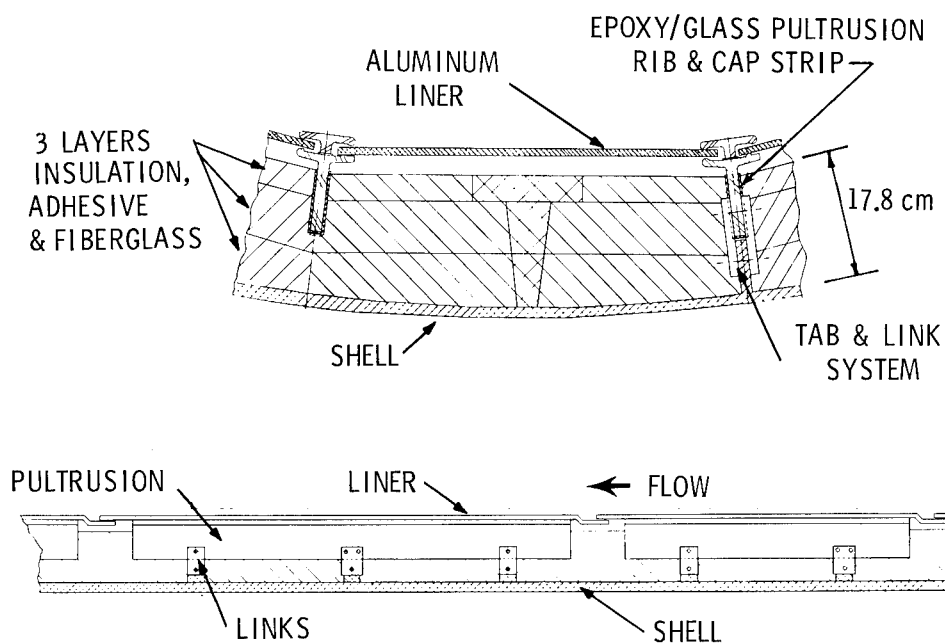
Figure 6.- Schematic showing typical sections of internal insulation system of National Transonic Facility.
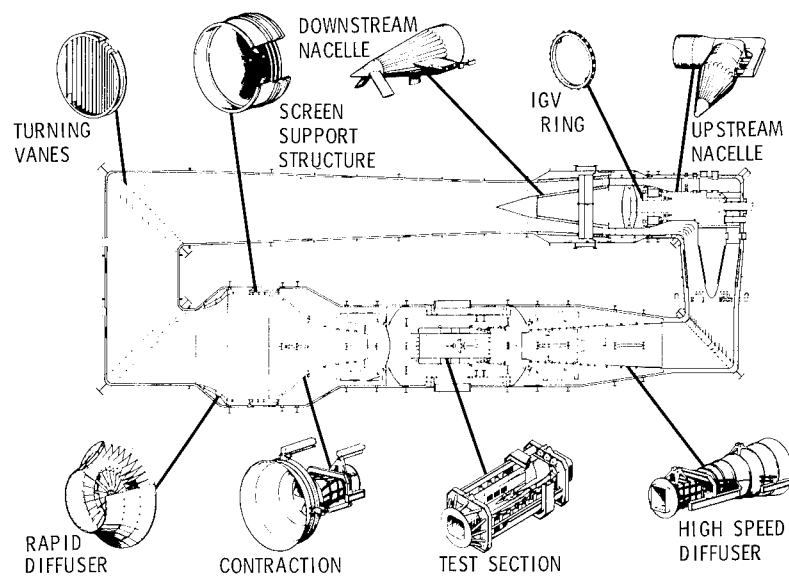
Figure 7.- Schematic showing location and perspective of internal structural components.
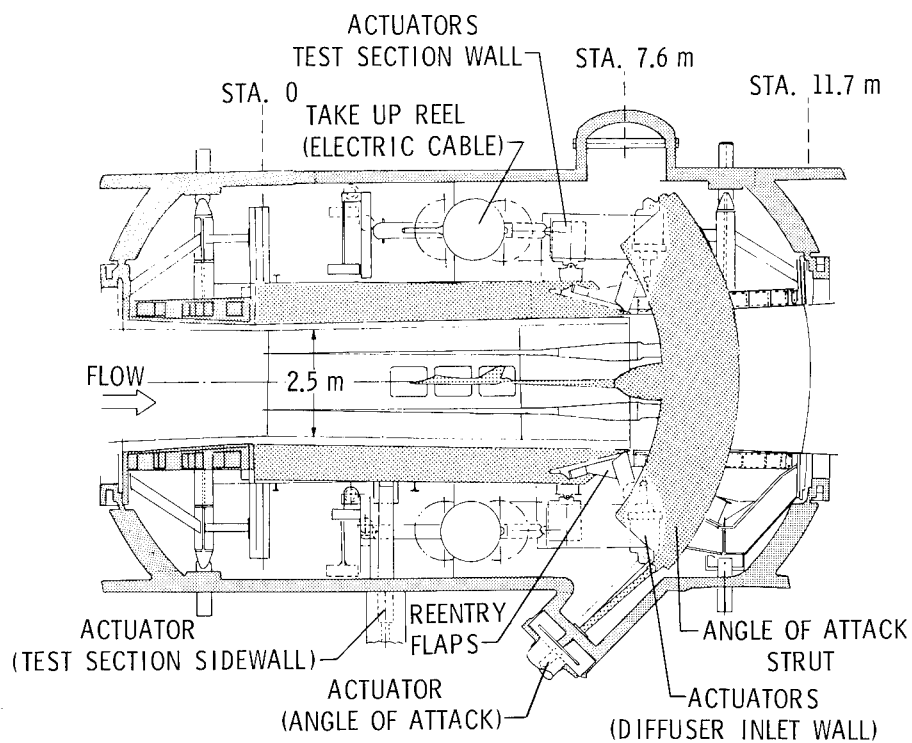
Figure 8.- Longitudinal section of test section and plenum of National Transonic Facility showing movable parts and actuators.
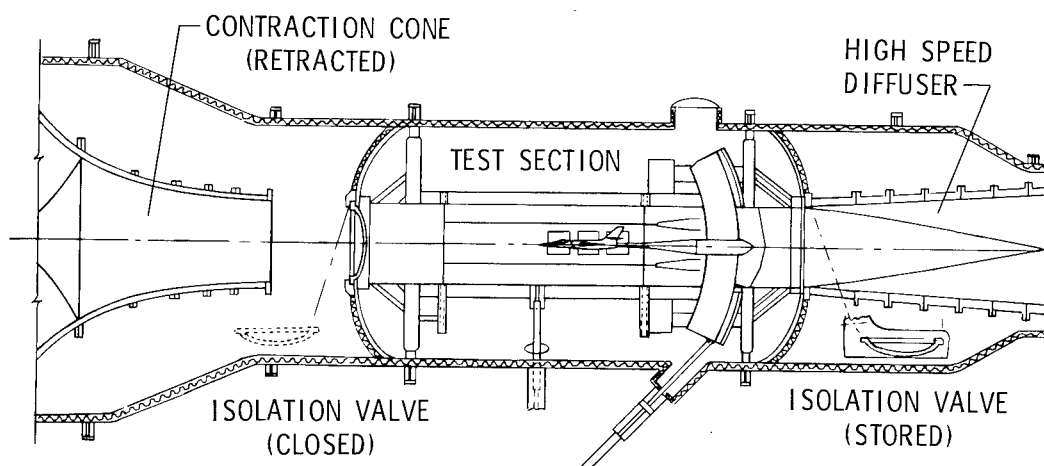
Figure 9.- Schematic showing basic arrangement for isolating
the plenum volume for model access.
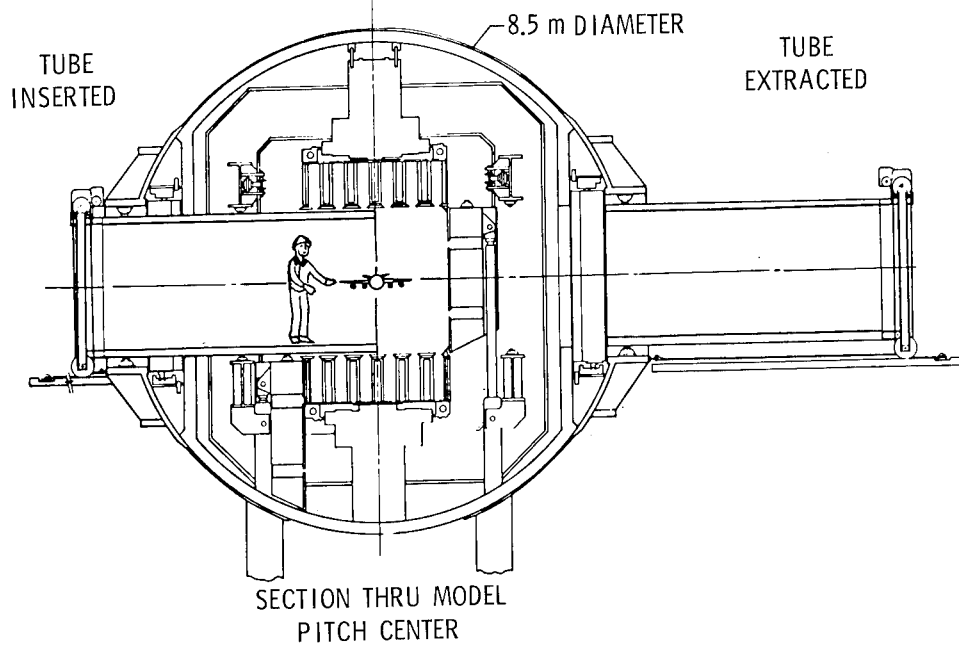
(a) Cross section through model pitch center.
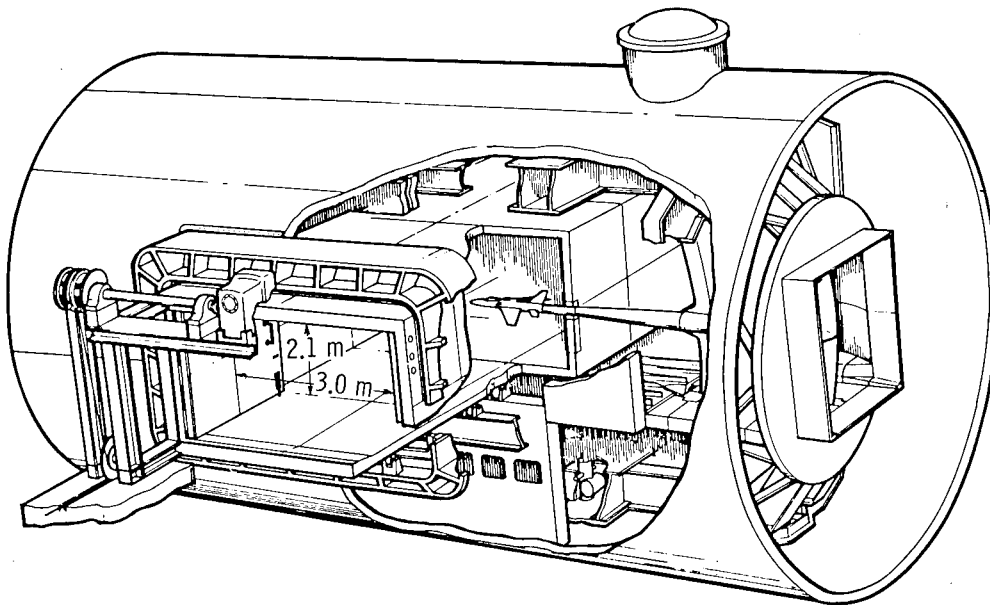
(b) Perspective showing access tubes in place.

Figure 10.- Schematic of model access system.
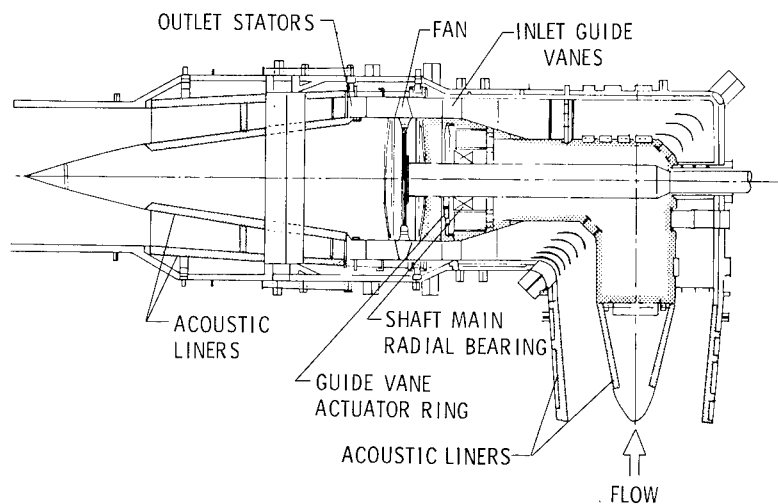
Figure 11.- Plan view of nacelle-fan region of tunnel circuit.
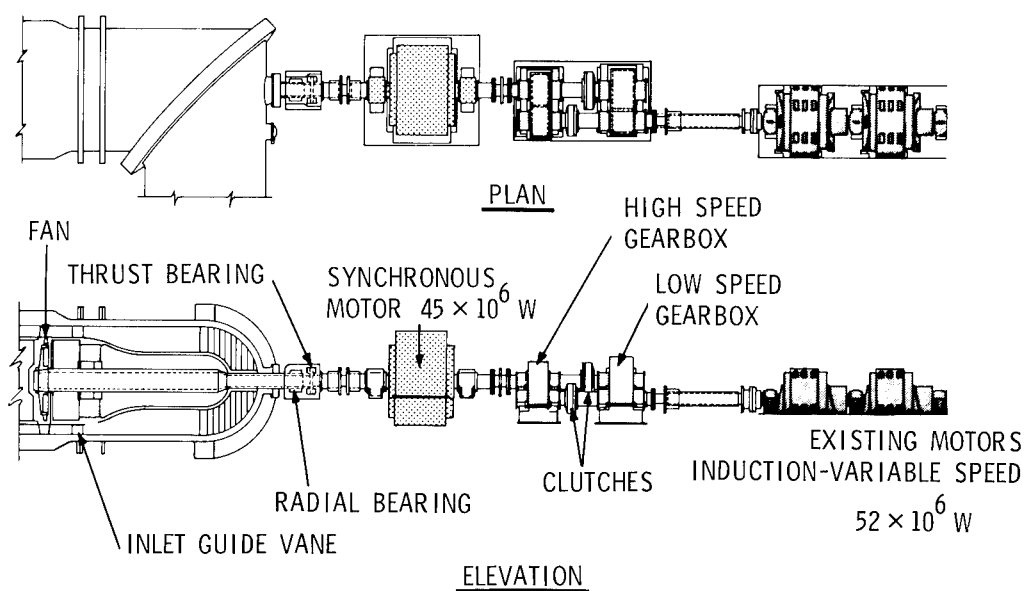
Figure 12.- Schematic showing drive system component arrangement.
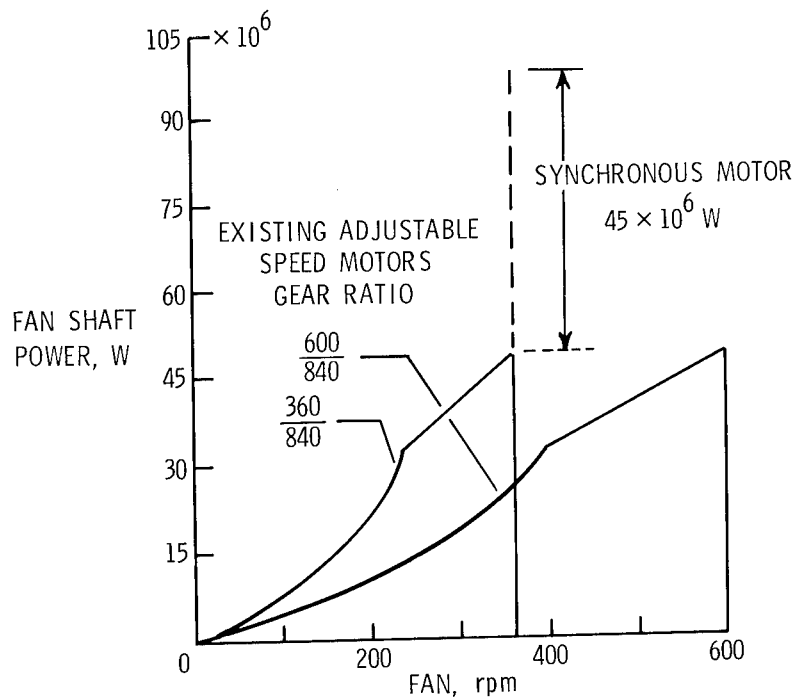
Figure 13.- Variation of fan drive horsepower with fan
rotational speed.
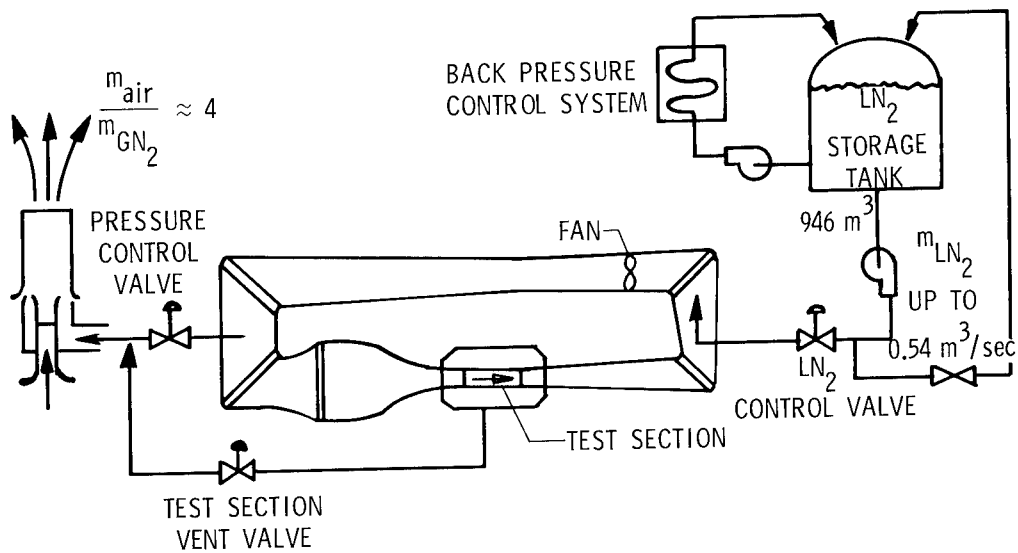
Figure 14.- Schematic showing basic nitrogen supply
and vent systems. (All components not shown.)
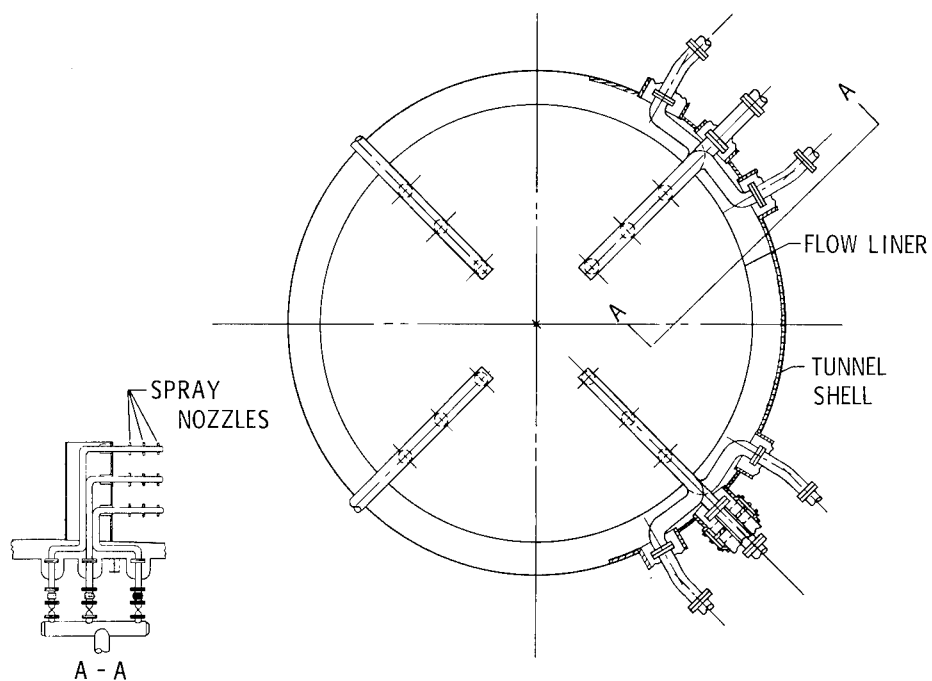
Figure 15.- Schematic showing liquid nitrogen system arrangement.
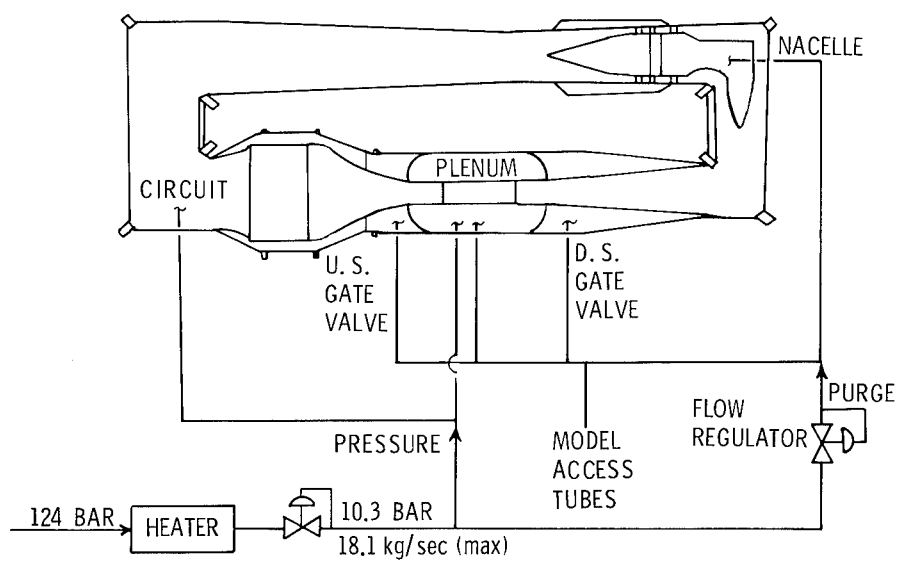
Figure 16.- Schematic showing basic air supply system.
(All components not shown.)

HEAT REMOVAL FROM THE TUNNEL (COOLING COIL)

- $0.44 \text{ m}^3/\text{sec}$
- 4.5 BAR
- 7.5×10^6 W

HEAT REMOVAL FROM MECHANICAL EQUIPMENT

- $0.18 \text{ m}^3/\text{sec}$
- 4.5 BAR
- 7.5×10^6 W

Figure 17.- Basic design performance characteristics for two cooling water systems.

EAST-WEST SECTION
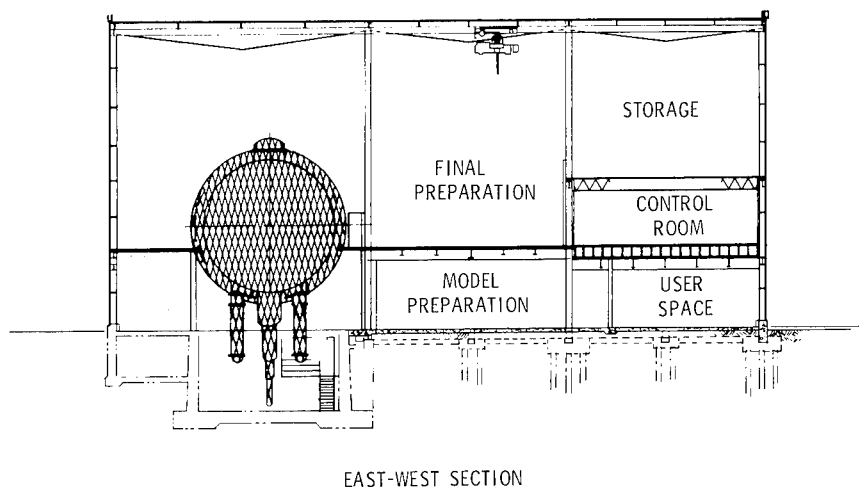
Figure 18.- Cross section of building addition showing space arrangement and location of tunnel test section.
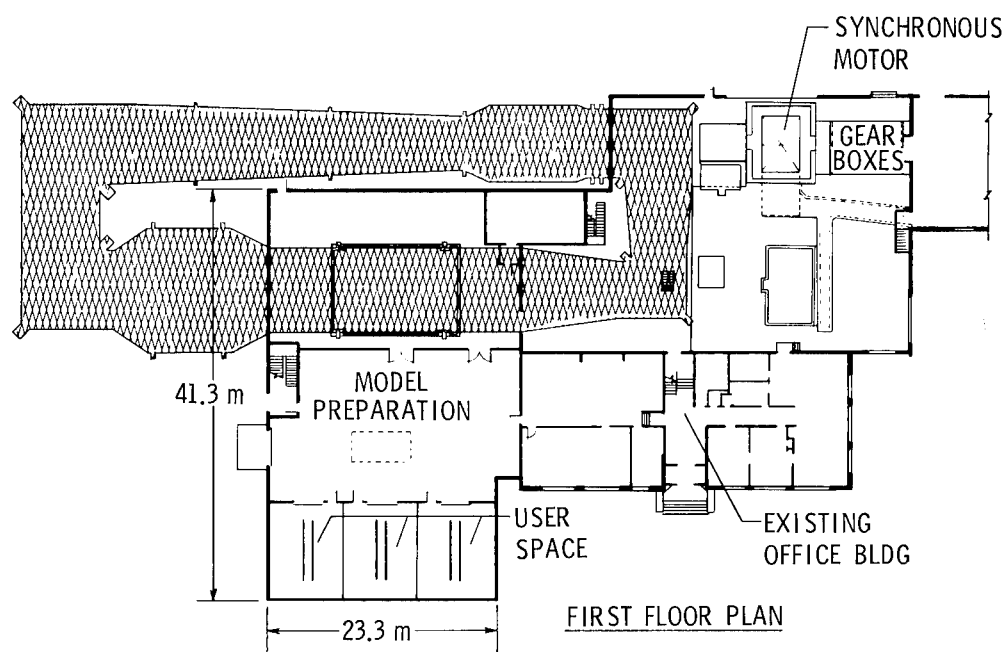
Figure 19.- Plan of building showing first floor space.
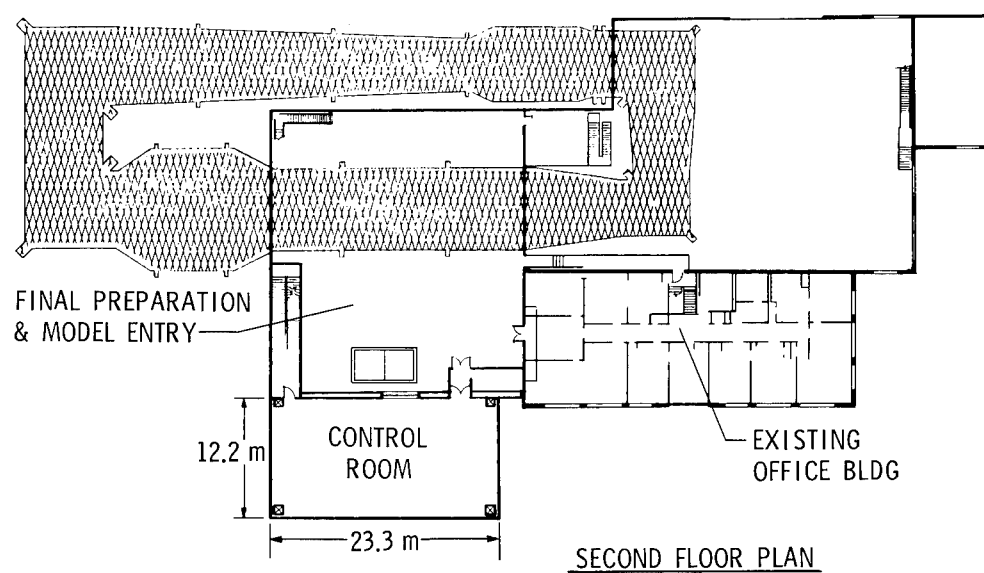
Figure 20.- Plan of building showing second floor space.
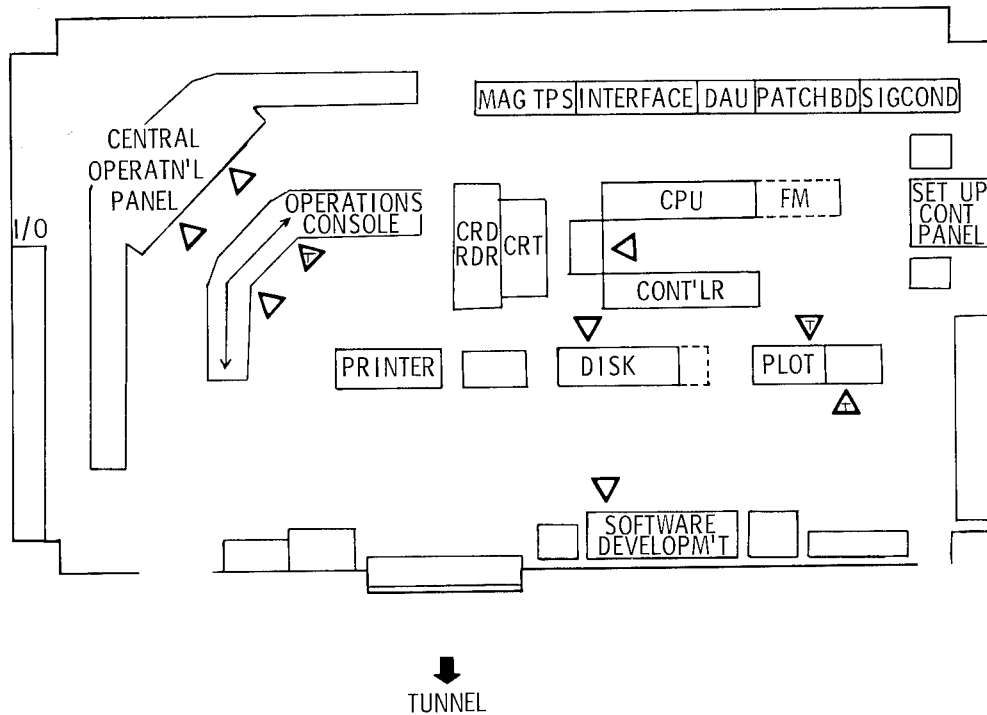
Figure 21.- Current layout of equipment in control room showing typical operator stations.
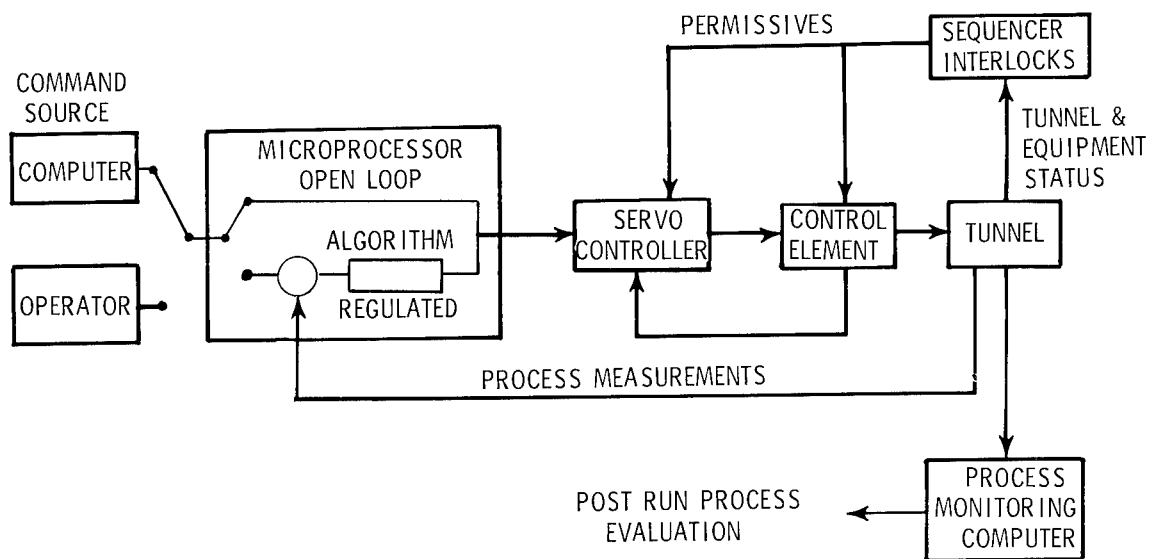
Figure 22.- Schematic diagram showing basic approach to control of variables.

COMPUTER TO COMPUTER LINKS

```
┌──────────┐   ┌──────────┐            ┌──────────┐   ┌──────────┐
│   DATA   │   │   DATA   │            │ PROCESS  │   │ PROCESS  │
│ACQUISITION│  │MANAGEMENT│            │ CONTROL  │   │ MONITOR  │
│ COMPUTER │   │ COMPUTER │            │ COMPUTER │   │ COMPUTER │
└──────────┘   └──────────┘            └──────────┘   └──────────┘
```

| BUS TRANSFER SWITCHES | PERIPHERAL SELECTOR SYSTEM | BUS TRANSFER SWITCHES |

| RESEARCH MEASUREMENT SUBSYSTEMS | COMMUNICATIONS SUBSYSTEM | SHARED PERIPHERAL POOL | CONTROL VARIABLE MICRO-COMPUTERS | PROCESS MEASUREMENT SUBSYSTEM | PROCESS SEQUENCERS |

Figure 23.- Block diagram showing link and switch
arrangement for National Transonic Facility
computer complex.

$$M = 1.0, \ \bar{c} = 0.1 \sqrt{A_{TS}}$$
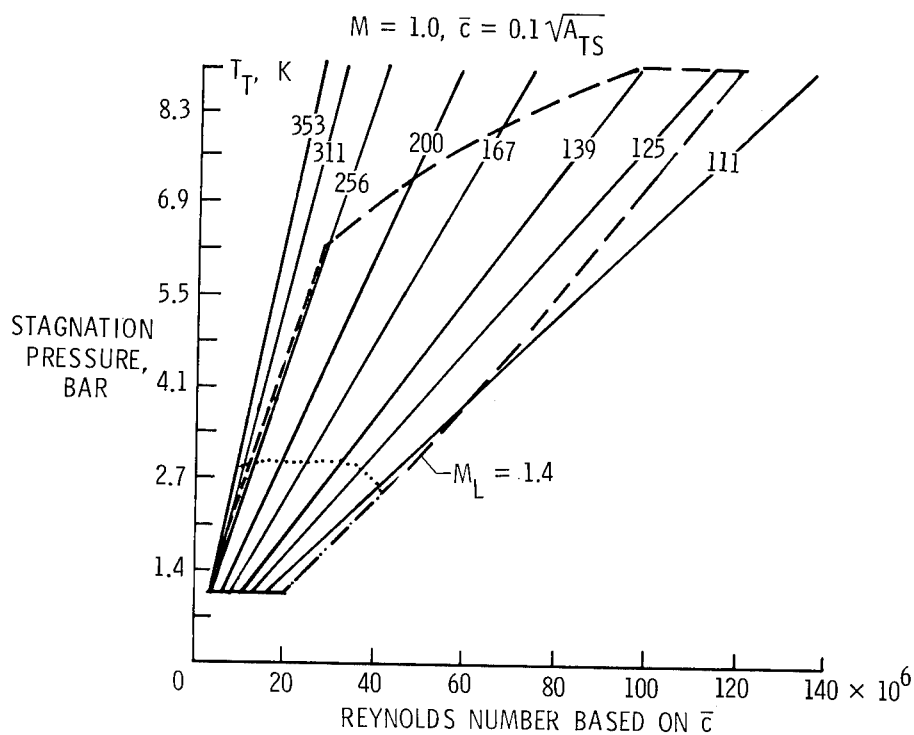
Figure 24.- Variation of Reynolds number with stagnation
pressure and temperature in National Transonic Facility.

73

$$\bar{c} = 0.25 \text{ m}$$
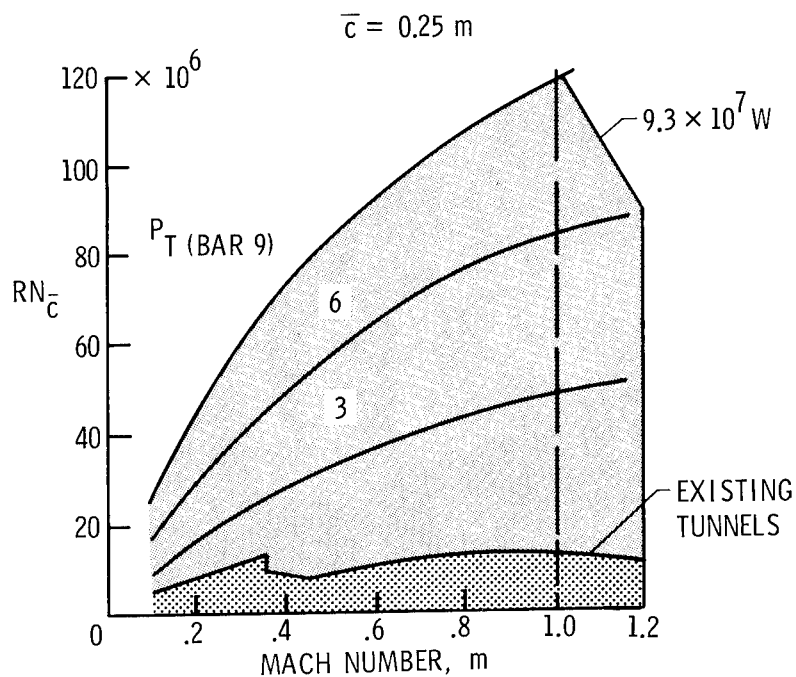
Figure 25.- Variation of maximum Reynolds number with Mach number for National Transonic Facility as compared with all existing tunnels.
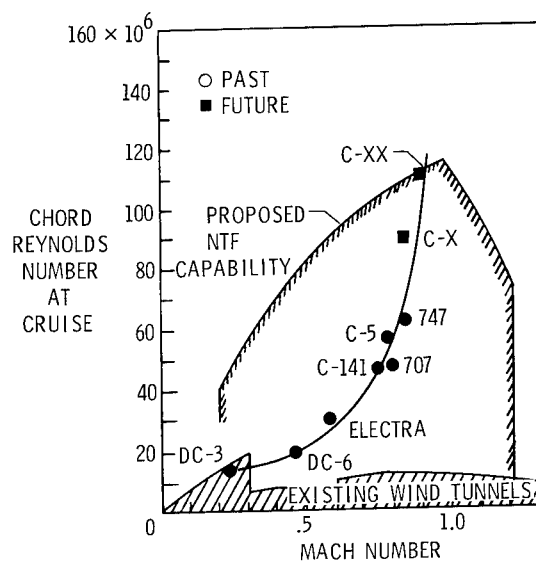
Figure 26.- Flight cruise Reynolds numbers for existing and projected transport aircraft compared with test Reynolds number capability of National Transonic Facility.
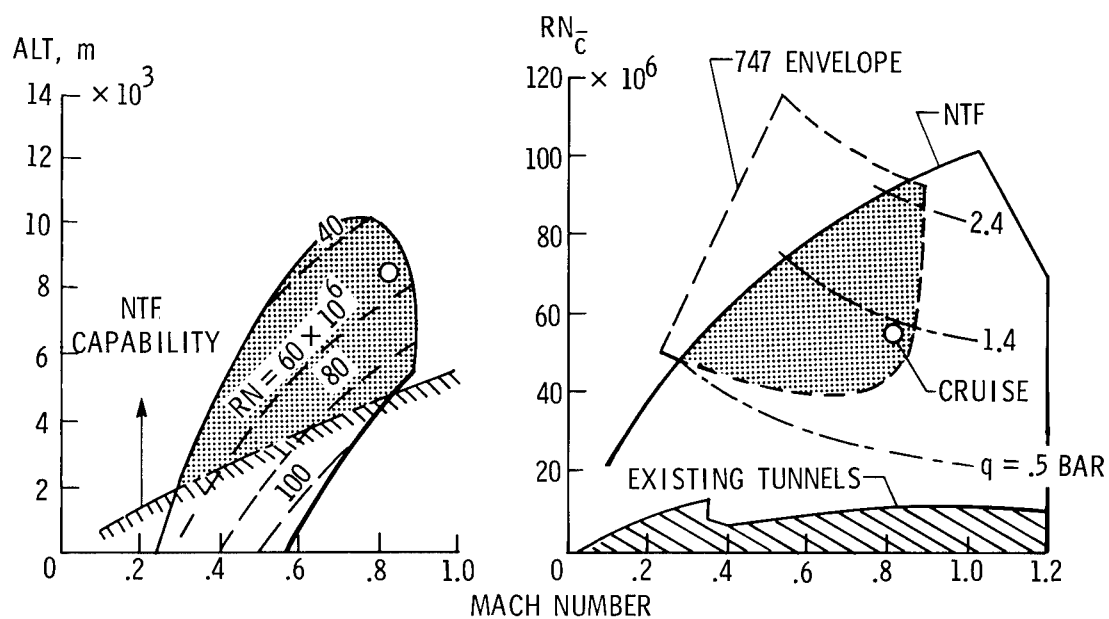
Figure 27.- Comparison of full scale flight envelope of
Boeing-747 aircraft with full scale Reynolds number
test envelope provided by National Transonic Facility.

PERSPECTIVE ON NATIONAL TRANSONIC FACILITY

OPERATING COST

Robert R. Howell
Langley Research Center

One of the concerns expressed by most potential users of the National Transonic Facility (NTF) is whether the cost of testing will be prohibitive. It is therefore timely to take a practical look at the basic operation from a cost point of view.

The basic operation of the NTF will be similar to any other transonic wind tunnel. Its controls and automation may be somewhat more sophisticated and, therefore, may require somewhat more maintenance than simpler tunnels. The cost per occupany hour, however, is not expected to be greatly different than for currently existing tunnels. Because of the attempts made to enhance data gathering efficiency, one might expect that the total tunnel occupancy cost for a given set of data could be less for the NTF.

The other cost which must be added to occupancy cost is the cost of the liquid nitrogen consumed in the users test program. Based on an assumed liquid nitrogen cost of 80¢ per kilogram ($70 per ton), the operating cost in dollars per second is presented as a function of Reynolds number in figure 1. The maximum cost rate is about $30/second or about $18,000 for 10 minutes. Cost rate is directly related to the drive power required for testing and the maximum rate at the upper operating boundary. Drive power and cost rates required decrease rapidly, moving down from the boundary (fig. 2). For example, a model of the Boeing 747 airplane can be tested at full scale Reynolds number at a cost rate of about $10 per second or $6000 for 10 minutes.

Thus, the Reynolds number requirements of a users test program will largely determine what the liquid nitrogen cost will be. Moreover, there appears to be a significant range of test Reynolds number capability which can be explored without significant cost concern.

$LN_2 = 80 \, \text{¢/kg ($70/ton)}$
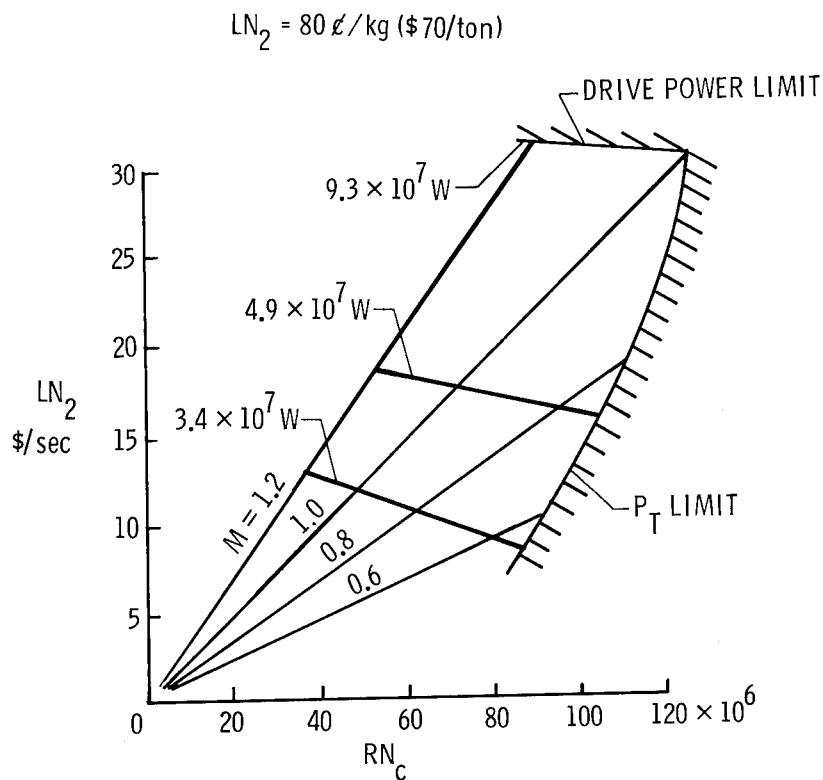
Figure 1.– Plot of LN_2 cost rate versus Reynolds number for the NTF showing different levels of test Mach number and drive power.

$\bar{c} = 0.3 \, \text{m}$
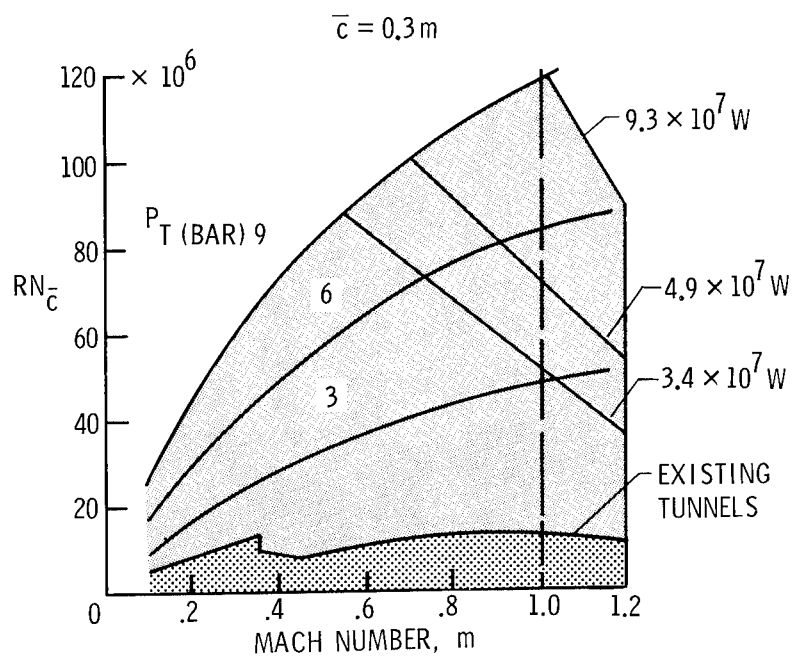
Figure 2.– Plot of maximum Reynolds number versus Mach number for the NTF showing levels of power required.

USE OF THE NATIONAL TRANSONIC FACILITY AS A NATIONAL TESTING FACILITY

Robert E. Bower
Langley Research Center

SUMMARY

Special capabilities of the NTF are reviewed to encourage potential
users to start planning for future tests. Specific areas of research and
development are suggested. User concerns such as tunnel productivity,
data quality, and procedures for proposing specific experiments are discussed.
Participation by the scientific community in this opportunity for transonic
research is encouraged, and mechanisms for implementation are offered.

INTRODUCTION

The National Transonic Facility (NTF) is expected to come on-line in
late 1982. It was designed from the start to be a national testing facility,
satisfying the research and development needs of NASA, DOD, industry and
universities. This conference will provide much technical information
regarding the design of the NTF. The purpose of this paper is to encourage
potential users to start thinking now about how they will want to use its
special capabilities (fig. 1). Some of these special capabilities will be
reviewed as well as specific areas of research and development that are pro-
posed for the NTF. Concerns of the users will be discussed in regard to
tunnel productivity, data quality and procedures for proposing specific
experiments.

SPECIAL CAPABILITY OF THE NTF

The NTF offers, for the first time, simulation of full scale Reynolds
numbers in the critical flight regimes of most current and planned aerospace
vehicles (fig. 2). An additional and highly important benefit of cryogenic
facilities, however, is the independent variation of both pressure and
temperature. This opens up a test envelope never before available in
large transonic test facilities. In addition to being able to vary Mach
number at constant Reynolds number and constant dynamic pressure to study
compressibility effects, Reynolds numbers can now be varied independent of
Mach number and dynamic pressure to study viscous effects. By varying
dynamic pressure at constant Mach and Reynolds numbers, pure aeroelastic
effects can be explored. This is important since model deflection effects
can be equally important to Mach number or Reynolds number effects.

An example of this special capability is shown in figure 3. The wide range of temperatures available in the NTF can be used for tunnel wall interference studies by testing models of various sizes at constant Mach and Reynolds numbers and constant dynamic pressure, q. Since in conventional tunnels q must vary to maintain constant Reynolds number, the important effects of aeroelasticity or Reynolds number cannot be separated from the basic problem of wall interference.

AREAS FOR RESEARCH AND DEVELOPMENT

Areas envisioned for research and development in the NTF are shown in figure 4. Approximately 50 percent of the test time will be devoted to systems development and evaluation. Current aircraft which have critical transonic flight regimes are probably less than optimum because of the lack of full scale Reynolds number wind tunnel data. It is not clear in all cases, however, that test Reynolds number, per se, will satisfy the aircraft designer in his need for high Reynolds number aerodynamic data. Also, due to cost and availability of the NTF, the designer will be very selective in its use.

In component studies, preliminary design assessment, configuration development, and final evaluation, aerodynamic needs will vary with the type of aircraft under consideration. In the case of a commercial transport, prime candidates for study in the NTF are cruise drag, buffet marings, flutter boundaries and dynamic air loads, pressure distributions and structural loads, control surface hinge moments, propulsion integration effects, low-speed maximum lift and drag levels, high-lift device performance and low-speed stall and stability and control characteristics. In the case of military fighters, important areas which are Reynolds number dependent are high angle-of-attack performance near stall, spin characteristics, and boattail nozzle drag.

A high Reynolds number research conference was held at Langley in October 1976 to address those areas shown under research and technology in figure 4 (ref. 1). The recommendations of this conference will be treated in some detail as it is forming the basis for the NASA research program in NTF.

Fluid Mechanics and Aerodynamics

In the case of fluid mechanics and aerodynamics (fig. 5), it was recommended that prime emphasis be placed on basic studies of turbulent boundary layers, separated flows, and vortex flows, since these underlie almost all practical aerodynamic problems. Indeed, it is the plea of most of the scientific community that sufficient time be scheduled in the early utilization of the NTF to understand basic aerodynamic phenomena as well

as understand thoroughly the characteristics of the tunnel. NASA plans to respond to this important request.

The second item for study listed in figure 5 is the support of computational aerodynamics. Notice the use of the word support. Computational aerodynamics should be thought of as a partner with testing in aircraft design and it is the intelligent aerodynamicist who will select the proper balance in the use of each of these tools to take advantage of their special capabilities. The NTF can offer special inputs to the theory, e.g., turbulence modeling. Some specific theory validation experiments include high-aspect-ratio wing body combinations, high lift systems on high-aspect-ratio wings, and low-aspect-ratio moderately and highly swept wings.

The third area in fluid mechanics and aerodynamics emphasizes the important role of the NTF in increasing the usefulness of existing tunnels. Recommended experiments include Reynolds number scaling techniques, aeroelastic effects and support and wall interference.

Propulsion Aerodynamics

Recommended propulsion aerodynamic studies for the NTF are shown in figure 6. They include the effects of Reynolds number on the drag of simple afterbody models incorporating simulated jets and on inlet transonic drag. It is important to explore propulsive lift concepts at high Reynolds numbers. Finally, a correlation is needed of propulsion aerodynamic test data from wind tunnel and flight tests at or near flight Reynolds number conditions.

It is the strong opinion of the propulsion integration researchers that a large amount of precursor research and development work needs to be undertaken so that the NTF can be utilized for propulsion aerodynamics research within a reasonably short time after it is placed in operation. A good example is the need for studies to determine the requirements for achieving valid jet simulation.

Dynamics and Aeroelasticity

Specific NTF experiments in dynamics and aeroelasticity are listed in figure 7. They concern the important areas of unsteady aerodynamics, buffet and flutter. The NTF is expected to be very useful for investigations of the Reynolds number effects on the unsteady air loads needed in aeroelastic analyses. One such program is already underway at Langley.

Buffet studies and flutter clearance testing require aeroelastically scaled models. In the NTF, this presents both advantages and problems. The model technology required for aeroelastic studies at cryogenic temperatures is beyond the state of the art and it is not clear how complex or expensive

the models may be. On the positive side, however, the ability to vary fluid temperature in the NTF independent of Mach number permits the key scaling parameter of mass density ratio to be satisfied at all major points of the airplane flight envelope with a single model. In conventional tunnels like the Langley Transonic Dynamics Tunnel, this parameter can only be satisfied at one flight condition of Mach number and altitude with a given model.

Finally, the panel report in reference 1 pointed out that additional capability may be required in the NTF to make it more useful for flutter testing. This includes provision for rapid tunnel shutdown, observation of the model during testing, and special support systems. Currently, there is no firm schedule to provide these features.

TUNNEL PRODUCTIVITY AND DATA QUALITY

The degree of interest by potential users of the NTF will depend upon tunnel productivity, the quality of the data obtained, and the cost to the user. Other papers in this conference will address how operating cost has driven the design of the NTF. The discussion to follow will emphasize productivity and data quality.

Tunnel Productivity

The NTF is designed to produce data at a relatively high rate. To achieve this goal, the tunnel control and data system is highly automated. The heart of this system is the data system complex shown in figure 8. It consists of four central processing units connected in a multi-point distributed network configuration. The data management and communication unit will contain user application programs for onsite data processing as well as capability for comparison with archival data. A communication system will provide a tie to the Langley central computer and also provide user access for pretest software development and debugging. This feature should have strong user appeal. The data acquisition system will provide 320 data channels for research measurements at rates up to 50,000 samples per second. A "quick look" data capability will be available during testing. The efficient and safe operation of the NTF will require extensive process monitoring. The process monitoring computer will record such measurements as tunnel pressure and stress, drive system temperatures and vibration, power consumption, and liquid nitrogen flow rates. The tunnel parameter control computer controls tunnel test conditions of Mach number, temperature, and pressure, as well as model attitude.

The NTF will impose severe requirements on instrumentation -- in some cases beyond the state of the art. The extensive research and technology program, outlined in figure 9, is currently underway to develop the required

technology. Balances are being designed to operate in the cryogenic environment up to the severe loadings indicated. A new electronic scanning pressure measurement system is being developed that is about 50 times faster than conventional mechanical scan. Provision will be made for over 1000 data channels on a pressure model and calibrations can be made during testing for improved accuracy. Flow visualization will be difficult in the NTF because of optical constraints in the test section and the cryogenic environment. No system will be available during initial operation, but the concepts listed in figure 9 are under development. Unquestionably, the most challenging part of the development program is the measurement of model deformation. The four optical techniques shown in figure 9 are under study. However, at this state of development, recommendations for other types of remote displacement measuring systems are also being sought.

Other development efforts underway to support the NTF are shown in figure 10. It will be necessary to design and develop a variety of specialized model support systems compatible with the high pressure, cryogenic environment. This includes special stings and dynamic stability rigs as well as cryogenic model conditioning chamber for functional checkout prior to tunnel installation. It should be pointed out here that NASA plans to develop and make available general instrumentation and support equipment required to exploit the testing capability of the NTF. The inventory of this equipment will grow during the initial years of operation. This approach will not prevent users from furnishing their own testing equipment as necessary or from providing special equipment as required.

The stringent pressure and temperature environment of the NTF, plus surface finish requirements, will stretch the state of the art in model design and fabrication. The goal of NASA's immediate research program is to actually fabricate two pathfinder models to demonstrate the technology and allow NTF model criteria to be available to users by mid-1981.

Many of the NTF experiments discussed earlier in this paper will require precursor testing in other facilities, particularly in the Langley 0.3-Meter Transonic Cryogenic Tunnel. Most of these tests will be two-dimensional in nature, but some three-dimensional testing will also be done in low Reynolds number facilities for later correlation in the NTF. NASA urges all potential users of NTF to participate in these experiments.

Flow Quality

The quality of the flow in the test section of the NTF is most important. The user community has stated that it should be at least equal to the best of the present NASA tunnels. The flow quality targets for the NTF at maximum Reynolds number are shown in figure 11. In order to achieve turbulence levels and flow uniformity to within 0.1 percent, a contraction ratio into the test section of 15 was selected with provision for up to four screens. Acoustic treatment is used to reduce sound pressure levels to less than 150 dB.

It will be extremely important to document the actual test section flow characteristics to a relatively high degree of precision. This is planned in the calibration period during the initial operation and detailed tunnel characteristics will be supplied to potential users as soon as possible.

USER CONSIDERATION

NTF Management

The NTF will be managed by the Langley Research Center (fig. 12). The commitment to be capable of producing 8000 data polars per year has been used to project dedicated manpower skill mix requirements. These requirements are for a two-shift operation with adequate staffing to support production/development testing. It is planned to use a combination of civil servants and support service contract staffing. In this case, overall management, technical guidance, and interfaces with users will be provided by civil servants. Support service contractors will be used for facility operational functions.

An operations branch under NTF management will be responsible for plans, scheduling and facility operation. A research support branch will be responsible for facility documentation, facility improvement, user consultation and independent research. User consultation is particularly important to insure efficient use of the NTF in concert with other facilities. A project support office will provide for direct interface with users and supply project engineers for the conduct of specific programs.

It is proposed that an oversight committee reporting to Langley Research Center will review the past year's operation to insure that the NTF is best serving the interests of all users. It is expected that it will be made up of members from NASA, DOD, universities and industry.

NTF Utilization

The expected utilization of the NTF, after initial calibration and documentation, is outlined in figure 13. Four types of programs involving different combinations of users are envisioned. The first is support of the regular research and technology programs funded from the offices in NASA Headquarters. The users will be NASA Centers, universities and industry. The second type of program involves DOD testing in support of vehicle development or advanced technology. It is expected that DOD will pay all costs of such tests and will assign personnel for tests or for extended periods of time as they see the need. The third type of testing would support industry proprietary programs. The funding and approval procedures for such tests will follow the current practice used in the NASA Unitary

Plan Wind Tunnel. A fourth type of use of the NTF is somewhat unique. In an effort to encourage maximum use by the scientific community, provision will be made under NASA funding for unsolicited research proposals from universities and industry. Requests for approval would be submitted directly to the NASA Office of Aeronautics and Space Technology (OAST).

CONCLUDING REMARKS

In conclusion, the following points should be stressed (fig. 14):

1. The NTF offers scientists and engineers the opportunity to increase the efficiency and performance of most types of aircraft, missiles, and space vehicles envisioned for at least the next 20 years.

2. Participation by the scientific community is not only desirable, it is mandatory. The NTF, coupled with other transonic facilities and high speed computers, provides an unprecedented opportunity for transonic research. Annual planning and reporting workshops will be held to stimulate programs and communicate results. Maximum use will also be made of existing mechanisms such as grants involving joint NASA/industry principal investigators, faculty fellowship programs, National Research Council fellowships, and NASA/industry research associate programs.

3. NASA is dedicated to having an NTF with user appeal, minimizing costs and maximizing productivity and data quality.

4. This conference will furnish much technical information on the design and operation of the NTF. Potential users are urged to start planning now for tests in the NTF and work with NASA on special needs. Where possible, users should participate in precursor experiments in order to gain experience in testing in cryogenic facilities.

REFERENCE

1. High Reynolds Number Research, NASA CP 2009, Oct. 1976.

● SPECIAL CAPABILITIES

● AREAS FOR RESEARCH AND DEVELOPMENT

● TUNNEL PRODUCTIVITY AND DATA QUALITY

● USER CONSIDERATIONS

Figure 1.- Use of NTF as a national testing facility.

● HIGH REYNOLDS NUMBER

● INDEPENDENT CONTROL OF:
 • MACH NUMBER (COMPRESSIBILITY EFFECTS)
 • REYNOLDS NUMBER (VISCOUS EFFECTS)
 • DYNAMIC PRESSURE (AEROELASTIC EFFECTS)

Figure 2.- Some unique capabilities of cryogenic tunnels.
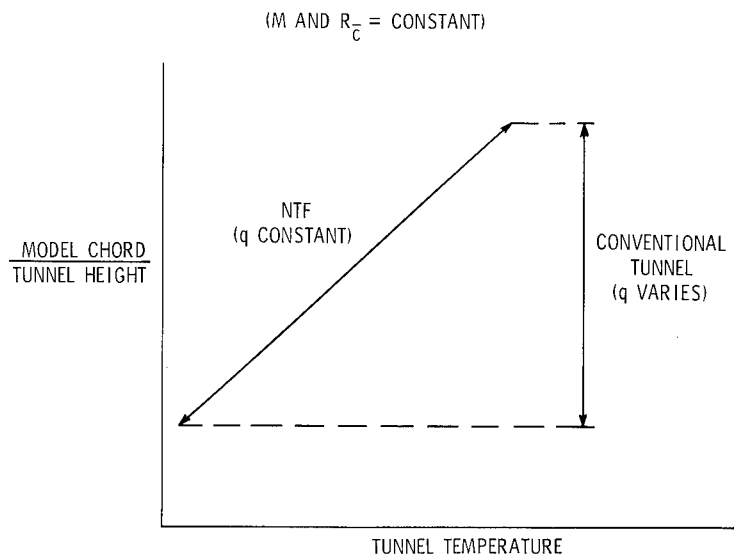
Figure 3.- Capability of NTF for wall interference research.

- SYSTEMS DEVELOPMENT AND EVALUATION
    - COMPONENT STUDIES
    - CONFIGURATION DEVELOPMENT
    - PRELIMINARY DESIGN ASSESSMENT
    - FINAL AERODYNAMIC DESIGN EVALUATION

- RESEARCH AND TECHNOLOGY
    - FLUID MECHANICS - AERODYNAMICS
    - PROPULSION AERODYNAMICS
    - DYNAMICS AND AEROLASTICITY

Figure 4.- Proposed programs for NTF.

- BASIC STUDIES
    - TURBULENT BOUNDARY LAYERS
    - SEPARATED FLOWS
    - VORTEX FLOWS

- SUPPORT OF COMPUTATIONAL AERODYNAMICS
    - EMPIRICAL INPUTS - TURBULENCE MODELING
    - THEORY VALIDATION

- WIND TUNNEL TEST TECHNIQUES
    - FIXED TRANSITION CORRELATIONS
    - AEROELASTIC EFFECTS
    - SUPPORT INTERFERENCE
    - WALL INTERFERENCE

Figure 5.- Fluid mechanics studies in NTF.

- AFTERBODY/JET DRAG

- INLET TRANSONIC DRAG

- CORRELATION OF WIND TUNNEL AND FLIGHT DATA

- PROPULSIVE LIFT

Figure 6.- Propulsion aerodynamics studies in NTF.

- CONTROL SURFACE UNSTEADY AERODYNAMICS

- BUFFET ONSET AND LOADS

- TRANSONIC UNSTEADY AERODYNAMICS

- FLUTTER

Figure 7.- Dynamics and aeroelasticity studies in NTF.

```
USER    ⎫          ┌─────────────────────────┐
        ⎬───────→  │   DATA MANAGEMENT       │
ACCESS  ⎭          │ AND COMMUNICATION UNIT   │
                   └─────────────────────────┘
```

┌──────────────┐   ┌──────────────┐   ┌──────────────────┐
│   DATA   │   │ PROCESS   │   │ TUNNEL PARAMETER │
│ ACQUISITION │   │ MONITORING   │   │ CONTROL COMPUTER │
│   SYSTEM   │   │ COMPUTER   │   │   │
└──────────────┘   └──────────────┘   └──────────────────┘
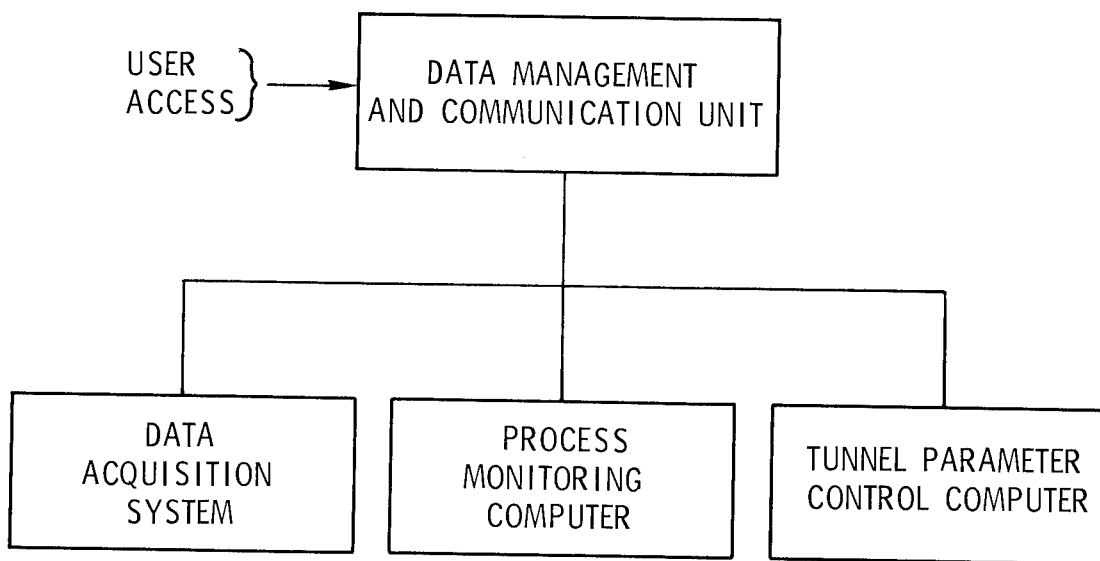
Figure 8.- NTF data system complex.

- MODEL BALANCE

    - CRYOGENIC ENVIRONMENT
    - FORCES TO $\pm$ 84.5 kN (19 500 lb)

- MODEL DEFORMATION MEASUREMENT

    - STEREO PHOTOGRAPHY
    - STEREO SCANNING PHOTOGRAMMETRY
    - MOIRÉ TOPOGRAPHY
    - MICROWAVE MODULATED LIGHT

- PRESSURE MEASUREMENT

    - ELECTRONIC SCANNING
    - 1024 CHANNELS
    - IN-SITU CALIBRATION

- FLOW VISUALIZATION

    - SCHLIEREN
    - SHADOWGRAPH
    - LASER VELOCIMETER

Figure 9.- NTF instrumentation development.

TEST SUPPORT EQUIPMENT
- SPECIAL STINGS
- SIDEWALL SUPPORT SYSTEMS
- DYNAMIC STABILITY RIG
- CRYOGENIC MODEL CONDITIONING CHAMBER

MODEL TECHNOLOGY
- MATERIALS
- FABRICATION TECH
- PRECURSOR MODELS

PRECURSOR EXPERIMENTS
- CURRENT TUNNELS
- 0.3 meter CRYO TUNNEL

Figure 10.- Other NTF development efforts.

- AT REYNOLDS NUMBER $= 120 \times 10^6$

  - TURBULENCE INTENSITY ± 0.1 %

  - FLOW UNIFORMITY ± 0.1 %

  - SOUND PRESSURE LEVEL < 150 dB

Figure 11.- NTF flow quality targets.
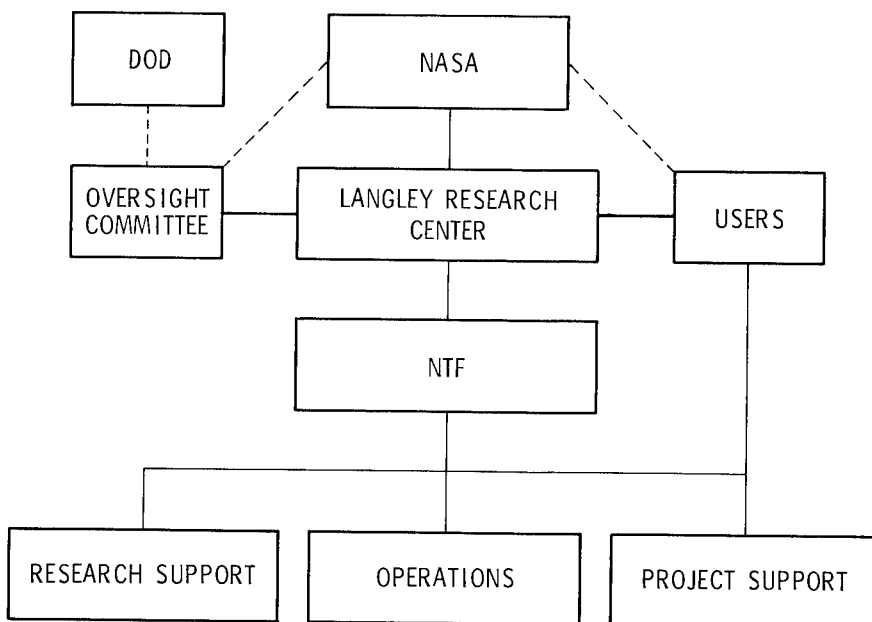
Figure 12.- NTF management.

USER	PROGRAM TYPE	FUNDING	APPROVAL PROCEDURE	PERCENT ALLOCATION
NASA CENTERS UNIVERSITIES INDUSTRY	RESEARCH	NASA	REGULAR NASA CYCLE	40
DOD INDUSTRY	DEVELOPMENT	DOD	REGULAR DOD CYCLE	40
INDUSTRY	PROPRIETARY	INDUSTRY	PROPOSAL TO LRC	15
UNIVERSITIES INDUSTRY	UNSOLICITED RESEARCH	NASA	NASA OAST	5

Figure 13.- NTF utilization.

- NTF OFFERS AN EXCITING TOOL FOR RESEARCH AND DEVELOPMENT

- PARTICIPATION BY THE ENTIRE SCIENTIFIC COMMUNITY MANDATORY

- EMPHASIS ON TUNNEL PRODUCTIVITY AND DATA QUALITY

- USERS SHOULD MAKE PLANS NOW

Figure 14.- Concluding remarks.

SESSION II - MECHANICAL/STRUCTURAL DESIGN

OVERVIEW OF STRUCTURAL AND MECHANICAL SESSION

Frank E. Mershon
Langley Research Center

The Langley 0.3-Meter Transonic Cryogenic Tunnel and the National Transonic Facility have been described previously in this conference. This session will show examples of how the temperature range of the tunnel gas, 78K to 353K (140°R to 635°R), affected the design and development of structural and mechanical components, and will provide a detailed description of four major developmental areas.

The 0.3-m Tunnel, when compared to the NTF structurally and mechanically, is a much simpler concept. The more severe requirements of size, productivity, quiet flow, pressure containment, and life span (see figure 1) made the NTF a greater challenge for the structural or mechanical designer. Therefore, the discussions in this session will be devoted primarily to the NTF. The major challenges of the 0.3-m Tunnel were attachments, seals, and insulation which were reported in ASCE Preprint 2239, April 22-26, 1974 (ref. 1).

Before turning to the cryogenic features and major developmental areas of the NTF, let me enumerate some key physical effects of the cryogenic requirements on structures and mechanical devices. First, as the temperature of the tunnel gas is changed, thermal stresses are induced in the structures and differential growth between adjacent structures occurs. The latter results in misalinement of mechanical elements and aerodynamic flow surfaces, and also results in relative motion between sealing surfaces.

Second, very cold temperatures affect material properties. For the metallic elements of the tunnel, the predominant concern is for loss of fracture toughness. For bonded structures, thermal shock and fatigue life under thermal stress cycles are critical concerns.

A third physical effect of note is the viscosity change in the tunnel gas over the temperature range. This directly affects the resistivity of bulk-absorber-type acoustic panels, and places a restraint on the type of panels used.

These physical effects are summarized in figure 2.

The tunnel shell provides the first example of design features dictated by cyrogenic requirements. Although insulated internally, it is conceivable that a failure of the insulation could expose the shell to cryogenic temperatures. Therefore, fracture toughness at low temperatures became one of the selection criteria for the shell material, and 304 stainless steel was selected.

There are turning vanes at each of the four corners of the tunnel. Langley wind tunnels generally have these vanes welded at top and bottom.

In the NTF, however, they are floating in guides at the bottom to allow for thermal contraction and expansion.

A close examination of the internal structures labelled "Contraction" and "High Speed Diffuser" on figure 3 will reveal tracks on which these devices are moved to allow sealing off of the test section area. The tracks are located at the top, the bottom, and at both sides. They are designed to allow radial growth, but to constrain tangential motion so that the structures remain centered when there is differential expansion between these tunnel elements and the shell.

The test section area contains many mechanical devices moved by electric or hydraulic actuators. To avoid designing and qualifying these actuators for cryogenic temperatures, they have been enclosed in insulated covers, and heater elements have been provided.

The nacelle area uses a similar approach, where the nacelle itself is insulated and heated to protect the bearings and lubrication system inside. Externally, the nacelle is supported on the aft end by two angled struts and a vertical strut, all made of Invar. The low coefficient of thermal expansion of this material makes it suitable for reducing thermal stresses and misalinements.

In addition, the nacelles are supported by Watts linkages. These are simple devices in concept (see figure 4) which provide for centering and relief of thermal stress.

Turning from these examples of design details, there are four major developmental areas which will be discussed in the following papers. The first deals with the control of NTF noise. There are two requirements to control noise. One is the requirement for quiet flow in the test section. The other is the requirement to control the noise environment external to the tunnel. To meet these requirements, there is acoustic treatment of the nacelle region upstream and downstream of the fan, which is the primary noise source. An extensive program was undertaken to develop panels capable of absorbing the noise and also capable of withstanding the tunnel environment. One result of this development was a change of the panel concept from that originally considered.

The second developmental area was the relief of thermal stress. To maintain productivity, the tunnel gas temperature must be changed frequently and rapidly. However, there are many large structures immersed in the stream, and these are thermally stressed by the change. By the use of finite element models and extensive structural and thermal analyses, the original design was improved to accommodate the required temperature changes.

The third paper deals with seal development. There are numerous seals in the NTF. By minimizing leakage, they serve to maintain flow quality and to reduce power loss. Large size, material availability and compatibility, and relative motion of the seal surfaces have all required developmental effort, an effort which is still in progress.

The final paper deals with fan disk development. Fan disk failure would be a catastrophic event. Flying debris, shock waves, and the release of very cold, inert gas present a very real hazard. As a consequence, much effort has been directed toward ensuring the integrity and safety of this component. Particular attention has been given to material selection, disk shape, manufacturing processes, and quality assurance. The result is a conservative, safe piece of equipment.

In summary, the design and development of structural and mechanical elements of cryogenic wind tunnels have required adaptations of conventional practice, ranging from simple solutions to time-consuming developmental efforts in the areas of design, materials development, manufacturing, and quality assurance.

REFERENCE

1. Wilson, John F.; Ware, George D.; and Ramsey, James W., Jr.: Pilot Cryo Tunnel: Attachments, Seals, and Insulation. Meeting Preprint 2239, American Soc. Civ. Eng., Apr. 1974.

- SIZE   NTF   – 60 m (200 ft)
                 0.3 m – 9 m (30 ft)

- PRESSURE   NTF   – 900 kPa (130 psia)
                 0.3 m – 500 kPa (70 psia)

- LIFE   NTF   – 50 yr
                 0.3 m – 50 hr

- PRODUCTIVITY   NTF   – 8000 polars/yr
                 0.3 m – NOT SPECIFIED

- QUIET FLOW   NTF   – SPECIFIED
                 0.3 m – NOT SPECIFIED

Figure 1.- Comparison of structural/mechanical design features.

TEMPERATURE RANGE 70 K (140° R) TO 353 K (635° R)

- CHANGING GAS TEMPERATURE
  - INDUCES STRESSES IN THE STRUCTURES
  - INDUCES DIFFERENTIAL GROWTH IN STRUCTURES
    - ALINEMENT MUST BE MAINTAINED
    - CHANGING GAPS MUST BE SEALED

- LOW TEMPERATURES AFFECT MATERIAL PROPERTIES
  - FRACTURE TOUGHNESS IN METALS
  - BONDLINE PROPERTIES IN BONDED STRUCTURES

- N_2 VISCOSITY CHANGE WITH TEMPERATURE AFFECTS RESISTIVITY
  OF ACOUSTIC TREATMENT

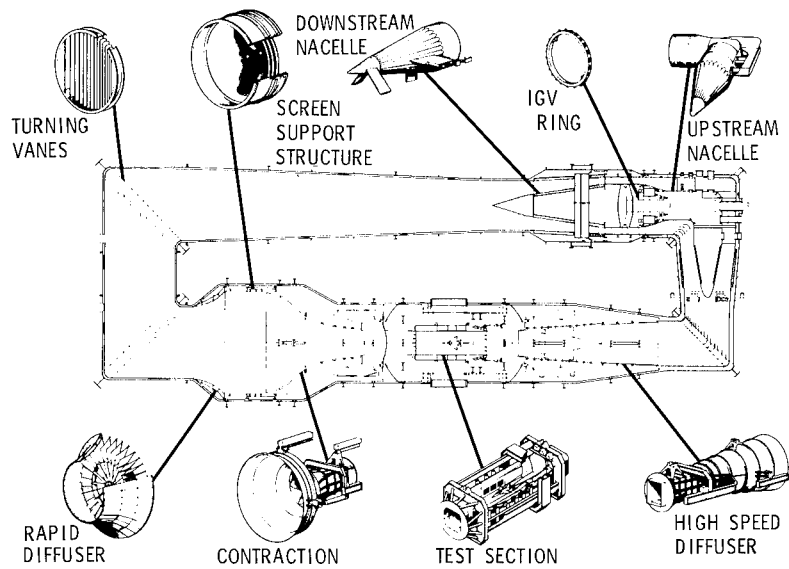Figure 2.- Summary of cryogenic effects on structures and mechanisms.

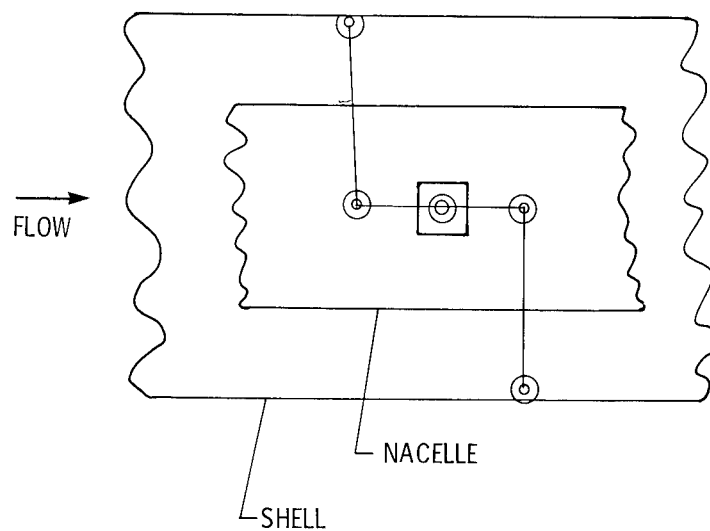Figure 3.- National Transonic Facility internal structures.

Figure 4.- Watts linkage.

DESIGN FOR THERMAL STRESS

James W. Ramsey, Jr.
Langley Research Center

SUMMARY

The large cryogenic wind tunnel structures inside the National Transonic Facility (NTF) were analyzed and designed for mechanical plus thermal stresses. The MITAS and SPAR computer programs were utilized to solve the large, forced convection (up to a 700 to 1 ratio) driven, thermal stress problem. To prevent overstressing, yielding, and fatiguing, structural criteria were developed. All requirements from the criteria imposed on these structures have been exceeded. An analysis and design procedure was developed with two large internal structures used to demonstrate this procedure. Several design approaches to reduce high thermal stresses are presented.

INTRODUCTION

The major problem encountered at Langley Research Center in the design of the large cryogenic wind tunnel structures shown in figure 1 is thermal stress. The major cause of thermal stress is forced convection. These structures must be capable of accommodating approximately 278K (500°R) range in temperature. The thermal stress is minimized in this range by proper conditioning through a programmed cooldown or warmup period. Once conditioning has been accomplished, operating temperature changes of large thermal excursions occur in essentially instantaneous time. The internal structures in figure 1 are exposed to GN_2 which is circulated throughout the NTF by the fan at speeds up to Mach 1.2 in the test section. Due to this circulation, different heat transfer rates exist between inside and outside surfaces of these structures. For example, the movable contraction section has vastly different heat flux coefficients. The inside surface was assumed to be high forced convection, whereas, the outside surface/beams were assumed to be natural or very low forced convection. This amounted to a 700 to 1 convection ratio; thus, a large, forced convection driven, thermal stress develops. Computer thermal profiles were generated on the Martin Interactive Thermal Analysis System (MITAS) and on the Structural Performance Analysis and Redesign (SPAR) programs. The thermal plus mechanical stresses were obtained from SPAR. The remaining sections of this paper will present (1) the criteria utilized to assure the structural integrity of these internal structures, (2) the analysis method for selected structures, and (3) the design approach to reduce the local thermal stress problem in several structures and configurations.

CRITERIA

In the NTF there are two types of forcing functions: (1) mechanical loads--aerodynamic induced pressure (173 kPa (≤25 psi) external), gravity,

actuator, and alignment; and (2) thermal loads--cryogenic cooldown and warmup and operating temperature changes. These loads impose high combined stresses on the internal structures. To prevent overstressing, yielding and fatiguing, structural criteria were developed.

Combined Stress

The total stress state in a structure consists of mechanical plus thermal stress. To prevent any yielding and permanent set or distortion, this total stress anywhere in the structures is to be below the tensile yield of the material used.

Conditioning Period

The cooldown and warmup of the structures are periods of time to "condition" the structures. These conditioning periods remove any residual change in temperature when cooling from room to desired test temperatures and when warming the structures up to "shop" environment from test conditions. The time required in cooling or warming while not exceeding yield in the structures is to be accomplished in one work shift, i.e. less than 8 hours.

Operating Temperature Change

Once conditioning of the structures has been accomplished, the tunnel is ready for data taking. The GN_2 fluid temperature may be changed rapidly to achieve the desired high Reynolds Number. This aerodynamic operation requires the structures to be able to absorb a rapid decrease or increase of the fluid temperature. To attain the "worst case for design purposes," an operating temperature change of at least $\pm39K$ ($\pm70^{o}R$) in 3 minutes must be allowed at Mach number (M=1.0) and full pressure (p=896 kPa (130 psia) absolute).

Life

A fatigue analysis must be performed on the internals and a corresponding nondestructive examination (NDE) program generated. By stressing the internal structures to the yield point numerous times, the life capability before re-examining by dye penetrant (PT), ultrasonic (UT), or radiographic (RT) examinations may not be adequate. Therefore, the requirement on all the internal structures is to provide at least 10 years of life before any NDE is required.

PROCEDURE

The overall procedure used to analyze and design the internal structures will be discussed.

Configuration

Size the structure such that all primary mechanical stresses determined from simple calculations and formulas (PR/t, Mc/I) are less than 1/4 the ultimate stress. This is the requirement from the ASME Boiler and Pressure Vessel Code - Section VIII, Div. 1 (Design by Rule). Computer models are generated to represent the structures and more exact detail principal stresses obtained. These are combined into an "equivalent intensity of stress" or "stress intensity." The stress intensity is defined as twice the maximum shear stress and is equal to the largest algebraic difference between any two of the three principal stresses ($\nabla_1 - \nabla_2$, $\nabla_2 - \nabla_3$, and $\nabla_3 - \nabla_1$). This is from ASME Section VIII, Div. 2 (Design by Analysis); moreover, the requirement is to be below 2/3 of yield. Since the stress state is completely defined by magnitudes and directions of the three principal stresses, the actual proximity to yielding must be determined by means of a strength theory. The theories most commonly used are the maximum stress (Section VIII, Div. 1) and the maximum shear (Section VIII, Div. 2). It is well known from tests that the maximum shear theory is better than the maximum stress theory for predicting yielding and fatigue failure--both project requirements. Thus, the more accurate code, Div. 2, is used to assure structural integrity.

Operating Temperature Change

Once the general configuration satisfies Section VIII, thermal stresses are caluclated. For ease of analyses, the change in temperature is input as a step forcing function of ±39K (±70°R) to MITAS or SPAR to obtain thermal profiles. Eventually stresses are obtained and combined with the mechanical stresses. The total structural stress intensity is then compared to yield.

Cooldown

The next step is to obtain the conditioning time required to cool the structure. The amount of GN_2 will be controlled and circulated at a slower speed and lower pressure not to exceed yield in the structures.

Life

Once all the above requirements have been satisfied, the peak local stress intensities are used to predict a safe number of cycles the structure is capable of absorbing. If these cycles exceed the expected number of cooldowns, warmups, and operating temperature changes in a typical 10-year period, the life requirement is met.

ANALYSIS METHOD

The contraction and downstream nacelle internal structures shown in figure 1 will be used to demonstrate the analysis approach to determine the

mechanical and thermal stresses. Most of the internal structures are to be fabricated from aluminum. The non-cryogenic operation of the NTF requires ≤ 353 K ($\leq 635^{o}$ R) temperature from the fan through the rapid diffuser--see figure 1. Cooling coils are mounted to the downstream end of the rapid diffuser to control the temperature to ≤ 339 K ($\leq 610^{o}$ R) from the coils to the fan. The 14 K (25° R) temperature rise is due to the heat of the fan. The major aluminum material used in industry for high yield in a welded state is 5083; however, its use is restricted to temperatures ≤ 339 K ($\leq 610^{o}$ R) to avoid stress corrosion in the material grain boundaries in a highly stressed state. An aluminum that is capable of exposures >339 K (>610° R) is 5454; however, its yield is 50 percent less. Consequently, the NTF operation and the cooling coil performance allow the contraction, test section, high speed diffuser, and upstream nacelle to be 5083; whereas, the downstream nacelle, shrouds, and rapid diffuser are required to be 5454.

Typical Temperature Gradient

The framing for the contraction structure shown in figure 1 will demonstrate the analysis approach to determine thermal stresses. A finite element model of this section was coded on SPAR. Mechanical stresses were generated, and allowable thermal stresses were scoped. A computer thermal profile (see figure 2) was obtained from another program, MITAS, using different heat transfer rates between inside and outside surfaces of the structure. Since there were uncertainties in these heat flux coefficients, worse cases were generated. The outside surface was assumed to be natural or very low forced convection with a coefficient 2.94 Watts/M^2K (1 x 10^{-6} BTU/(in.^{2}sec.^{o}R)). The inside surface was assumed to be forced convection with a 1764 Watts/M^2K (600 x 10^{-6} BTU/(in.^{2}sec. ^{o}R)). This thermal profile was then input to SPAR to obtain the total mechanical plus thermal stresses. A 4-hour cooldown satisfied the smallest time to condition the structure ready for data taking.

Thermal Forcing Function

The cooldown and operating temperature changes force the internal structure to develop high thermal stresses. These thermal forcing functions are shown in figure 3 as a plot of gas temperature with time. The time history of the temperature of the cooling of the fluid flowing past the contraction consists of two phases. The first phase is denoted the "structural conditioning" of the tunnel. In this phase, the fluid at room temperature is slowly cooled in about 3.7 hours to 117 K (210° R) by the addition of cryogenic nitrogen and then raised to a "hold" temperature. The fluid temperature is maintained for about 1 hour to allow the temperature of the contraction to become uniform in order to minimize any thermal stresses prior to data taking. The second phase is, for design purposes, a rapid decrease/increase of the fluid temperature with subsequent operation at a Mach number of one and full pressure to attain the desired test condition. Design calculations were carried out for instantaneous $\Delta T = -48$ K (-86° R), which was found to be the critical load due to a small residual stress in the structure at the end of the "conditioning" phase.

INTEGRATED STRUCTURAL ANALYSES

General

The downstream nacelle in figure 1 represents the most comprehensive region analyzed. This region was analyzed for mechanical plus thermal stresses and for dynamic interactions. It is composed of the following principle components: liner, internal rings, conical tip, main (horizontal) struts, secondary (vertical) struts, diagonal struts, acoustic rings, stringers and panels. The internal rings are structural load-carrying members. The struts provide the supports for the nacelle and are attached to the tunnel shell. The acoustic rings and stringers are used to attach the acoustic panels to the outer surface of the liner. The purpose of the acoustic panels is to alleviate flow-induced noise. Stator vanes are located at the large (upstream) end of the liner and are used to straighten the flow of the test fluid as it exits the fan.

Liner

The nacelle liner is a cylindrical-conical structure having a minimum diameter of 1.8 meters (6 feet), a maximum diameter of 4.6 meters (15 feet) and a length of 7.6 meters (25 feet). The wall is reinforced in a rectangular region where the horizontal strut penetrates the nacelle. The inside of the nacelle is stiffened by rings having rectangular cross sections.

Struts

The main strut has a hollow rectangular cross section. Since this main strut passes entirely through the nacelle, it is attached at each end to the tunnel shell. The attachment at the shell allows thermal expansion in the direction of the nacelle axis to minimize thermal stresses. Also, the attachment of the strut to the nacelle is accomplished by a slip joint which also minimizes thermal stress. The vertical strut penetrates the nacelle at the lower surface and is bolted to the main strut at the nacelle centerline. The diagonal struts penetrate the conical tip of the nacelle and are joined at the centerline. These struts are attached to the tunnel shell.

Miscellaneous Attachments

Acoustic panels are attached to the outer surface of the nacelle. Rings and stringers are attached to the outer wall in the indented region of the shell from the upstream end of the conical tip to the downstream end of the cylindrical liner portion of the nacelle. The structural rings and stringers

form a rectangular grid work which fills in the indented region to within 2.5 cm (1 inch) of the outer surface. The acoustic panels are attached to the rings and stringers and result in a smooth outer surface of the nacelle.

External Loads

Three types of loads are applied to the nacelle: thermal, pressure and torsional. A brief description of each type of load is given in this section.

Thermal Loads

The time history of the temperature of the transient cooling of the fluid flowing past the nacelle is shown in figure 3 and consists of two phases. The first phase is denoted the "conditioning" of the tunnel. In this phase the fluid, initially at room temperature, is slowly cooled in about 3.5 hours to 117 K (210° R) by the addition of cryogenic nitrogen and then raised to a "hold temperature" of 156 K (280° R). The fluid temperature is maintained at 156 K (280° R) for about one hour to allow the temperature of the nacelle to become uniform in order to minimize any thermal stresses prior to the next phase. The second phase is denoted the "research swing" and is either a rapid decrease or increase of the fluid temperature to attain the desired test condition for tunnel operations. Design calculations were carried out for $\Delta T = -49$ K (-88° R) which was found in preliminary analyses to be the critical load due to a small residual stress remaining in the structure at the end of the "conditioning" phase.

Pressure Load

Differential pressure loading on the nacelle due to the expansion of fluid flow creates a crushing load on the structure. The nacelle is vented at the larger end resulting in a zero differential pressure at that location. The maximum value of differential pressure, 124 kPa (18 psi), occurs at the nose of the nacelle.

Torsion Load

Stator vanes are located at the upstream (larger) end of the nacelle. The aerodynamic purpose of the vanes is to straighten the flow of the test fluid as it exits the fan thus producing parallel flow. Impingement of the flow on the vanes generates a twisting moment on the nacelle structure. The maximum magnitude of the moment, 16×10^5 Joule (14×10^6 in-lbf), was used as the design condition.

106

Detail Finite Element Models

The conical tip and a portion of acoustic panel region was coded on SPAR. The mechanical, pressure and torsional loads were applied and corresponding stresses obtained. Thermal profiles were generated on MITAS and then inputed to SPAR to obtain thermal stresses. The remaining portion of the downstream nacelle, portion of acoustic panel through horizontal strut to end of conical cylindrical liner, was modeled as 1/4 of the circumference on SPAR, figure 4. By this time the thermal profile software had been completed in SPAR. This allowed the use of one computer program to generate the total stress state, mechanical plus thermal. This saved considerable manpower, calendar time, and computer dollars.

The total downstream nacelle model was extended to include the exterior shell. The minimum natural frequency was obtained to address the dynamic requirement of >15 Hz to avoid resonance with the fan at peak speeds due to potential unbalance of the fan blades. This dynamic model is shown in figure 5. Rather than reduce weight, the increase in natural frequency was accomplished by increasing stiffness which also increases thermal stress. Thus, there is considerable interaction between the thermal stress and dynamic models.

Life

With the peak stresses from the finite element models of the contraction and downstream nacelle, a fatigue analysis was performed on the internal structures and a corresponding NDE program generated to assure this life. A fatigue (S-N) curve for the two aluminums, 5454 and 5083, in the welded state was generated. Using the Div. 2 factor of safety of 2.0 on stress and fatigue data of 5454 and 5083 Aluminum in the O condition (welded state), one curve was produced, figure 6. This curve is shown as a plot of stress intensity with years. Since the yield requirement of 83 MPa (12 ksi) will govern the structures fabricated from 5454, the 50-year life requirement is easily satisfied. The yield band on 5083 is from data and code allowables which show yield as a function of plate thickness. Since the thicknesses specified will provide yields from 103 to 117 MPa (15 to 17 ksi), the life from the structures fabricated from 5083 will be 15 to 45 years before any NDE is required. Since these structures are not "true" pressure vessels, minimum NDE requirements were specified - PT of root and final passes and RT of only critical regions.

DESIGN APPROACH TO REDUCE THERMAL STRESS

Introduction

Concepts to reduce high thermal stresses can be iterated with the analysis process (design by analyses). However, this is very time consuming. The best design approach is to prevent or absorb thermal change and then analyze to

confirm the design. The design approach to reduce the local thermal stress problem is as follows: (1) select appropriate material; (2) equalize heat transfer; and (3) modify configurations.

Material Selection

The important features of a material selection for the internal structures are shown in figure 7. Since the internals were designed after the supporting shell, three times the expected relative weight of any aluminum structure was used as the design load to the shell. This would permit a change of material at any time to steel. The yield, fatigue (for 50-year life), and developing ($E\alpha\Delta T$) stresses are used to scope the best material(s) to absorb high thermal stress with no permanent set and still have good life. The developing stress of 5454 and Nitronic 40 materials is very near the yield; moreover, they are both below the 50-year life stress. This does not leave any room for a local stress to be high, and it does not take advantage of the life stress. The developing stress of 5083 and 9% Ni materials is below the 50-year (life) fatigue stress which is below the yield stress. This allows a local stress to be developed to either the fatigue stress or the yield stress. The latter would result in a small penalty to the structures in life before reinspection of the welds. Since only 6% of the welds in the internals were affected, the life band of 15 to 45 years shown on figure 6 is certainly reasonable. Even today, it is not obvious that 9% Ni/Nitronic 40 structures would be cheaper than 5083/5454 structures. Our decision to fabricate with aluminum was based on cost comparisons and rapid material response to GN_2 (test) temperatures. What is clear is that the material that best absorbs a high mechanical stress in addition to the thermal stresses with no permanent set is 9% Nickel. An example of a configuration where the proper material selection of 9% Ni solved the high mechanical plus thermal stress problem with no extra cost is the arc sector strut in figure 8. The material assessment is shown in figure 9. The criteria for the arc sector is shown in the first column. The 27 minimum and 34 average Joules (20 to 25 ft-lb) Charpy V-notch (C_{VN}) energies are ASTM requirements and are implied in the ASME Section VIII, Div. 1 and Div. 2 codes.

The 304 stainless steel and nitronic steels did not appear to be viable because of yield. The A-286 material might have passed if tests could have solved welding problems. The 15-5-Ph-H1150M had the required yield and ultimate, but the technical literature reported lower Charpy impact energies than those required. In-house tests gave much lower results--4 Joules (3 ft-lb) minimum with an average of 11 Joules (8 ft-lb). The yields for these tests ranged from 590-670 MPa (85-95 ksi). Reheat treating of the material reduced the yield and increased the minimum C_{VN} to 11 Joules (8 ft-lb) with an average of 15 Joules (11 ft-lb). Reducing yields through further heat treatments and using different weld rods could enhance C_{VN}. However, the 9% Ni material met all requirements including the budget cost. In-house tests to provide the missing data for a backup material would have been quite expensive and difficult to define to fabricators in a fixed price procurement; consequently, the decision was made to rely on Charpy impact energies as the indicator of these materials' toughness and use 9% Ni for the strut.

Active Equalization of Heat Transfer

The highest thermal stress in the internals was the downstream nacelle skin-to-strut intersection. The finite element model in figure 4 was used to confirm that the downstream nacelle strut would cool uniformly through piping, figure 10. This piping introduces the test medium into a box encasing the structural strut inside the nacelle. This GN_2 sufficiently cools the strut such that the thermal stresses plus the corresponding mechanical stresses do not exceed the acceptable level of yield between the strut beam and the nacelle skin. The system would also prevent the skin from going "egg shape"due to difference in contraction between the beam and skin during cooldown. Differential pressure will force the flow into the box around the strut and exhaust it upstream through the bulkhead at the fan.

Configuration Changes

Reducing thermal stress by configuration changes can be illustrated by the movable contraction section, figure 11. One change is to eliminate corners and provide generous radii. Further design improvements are to increase thicknesses. The radius should be set as large as practical by the designer and the thickness increase determined by analyses. Another structural change is to decouple or isolate deep support beams from each other or liners, figures 11 and 12. The support beams, 0.13 meter (5 inch) flanges, and 0.10 meter (4 inch) flange on the movable and fixed contraction sections are typical examples of decoupling.

Examples of decoupling, isolating, and coating necessary to assure no yielding are found in the test section. The test section structure, shown in figure 13, requires all three of these methods. These methods are directed toward overall compatibility within the test section since the arc sector will govern how rapid the thermal transients may occur.

The plenum conditioning capability is accomplished through "plumbing." Once the gate valves are closed, the heating capability of 117 K to 294 K (210 to 530° R) is accomplished in 5.9 hours by dry air introduced to manifolds on each side of the test section. The manifolds contain holes which direct the dry air to the top of the plenum while the GN_2 is vented at the top of the test section. Once model work has been accomplished and the plenum is secured, bypass valves which open lines between the tunnel circuit and plenum are "throttled" to cool the entire mass from 217 K to 173 K (390 to 312° R) in 2.86 hours. The pressures on both sides of the gate valves are equalized at 173 K (312° R) and cooling terminates. The residual ΔT of -62 K (-112° R) will be eliminated by opening the gate valve with natural convection and/or forced convection (fan induced flow) bringing the plenum to approximately the same temperature as the rest of the circuit.

In this conditioning process, substantial thermal stresses are generated as a result of significantly different thermal inertias of interconnecting

structural members. Figure 13 shows a detail finite element SPAR model of the entire plenum. This model generates the total, thermal coupled with full aerodynamic and model induced, stress. The stresses in any of the components must not exceed yield.

Figure 14 indicates methods that were utilized to minimize thermal stresses before any analyses were performed. These methods were isolating and decoupling the critical structural components. Isolation serves as a blockage mechanism to prohibit the large thermal gradients. Decoupling will allow remaining relative differential growth to take place without inducing additional stress. Therefore, the finite element model is used to verify the design, i.e. to investigate and evaluate the remaining mechanical plus thermal stresses. To reduce any high stresses to acceptable levels, insulation can be added as shown in figure 15. Insulating the members with lower thermal inertias (support frame vs. 0.13 meter (5 inch) flange) will force the temperature differential between members to acceptable levels.

CONCLUDING REMARKS

The major problem in the design of large cryogenic wind tunnel structures is typical in any large, transient, thermal environment. Our experience is based on the analysis and design of the NTF internal structures.

The design must:

- Adhere to nationally recognized codes
- Select appropriate materials
- Establish a sound, conservative stress criteria
- Select structural configurations with inherent low stress constraints
- Execute state-of-the-art structural analysis

The fabrication must:

- Adhere to nationally recognized code requirements
- Plan and execute a quality control program

The checkout must:

- Adhere to restrictions imposed by analyses
- Adjust analyses to test results

The operations must:

- Adhere to recertification guides
- Provide an operating plan consistent with the facility design constraints
- Maintain an operating log of cyclic data for application to the recertification plan

110

The minimum requirements described in the criteria section of this paper have all been exceeded. The mechanical plus thermal stresses are all below yield on stress intensity. The cooldown time can be accomplished in less than 4.7 hours. The warmup time can be achieved in less than 5.9 hours.

The operating temperature change of ±48 K (±86° R) instantaneous change is ±50 K (±90° R) in 3 minutes at design Mach (M=1.0) number and full pressure (896 kPa, abs) (p=130 psia). For an average Mach number of 0.5 and a peak pressure of 896 kPa (130 psia) or an average pressure of 345 kPa (50 psia) and a nominal Mach number of 0.8, the "research swing" capability of ±48 K (±86° R) instantaneous change translates into a ±67 K (±120° R) possibility. This is due to reduction in forced convection and thermal stress and less pressure and mechanical stress.

The life provided by the internals before recertification is greater than 15 years on the structures fabricated from 5083 and greater than 50 years on structures fabricated from 5454. A summary of the requirements and capability of the internal structures shown in figure 1 is given in Figure 16. The structures fabricated from 5454 are the shrouds, downstream nacelle, and rapid diffuser. Those constructed from 5083 are the contraction, test section, high speed diffuser, and the upstream nacelle.
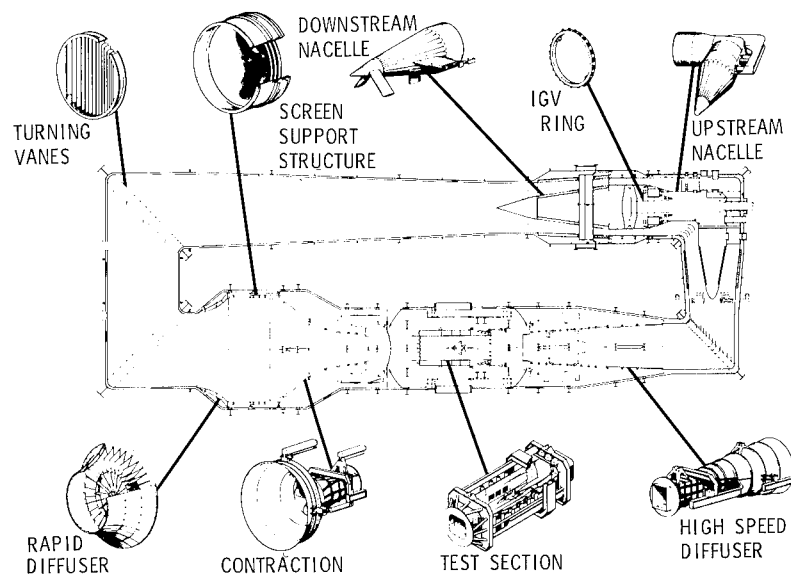
Figure 1.- National Transonic Facility internal structures.
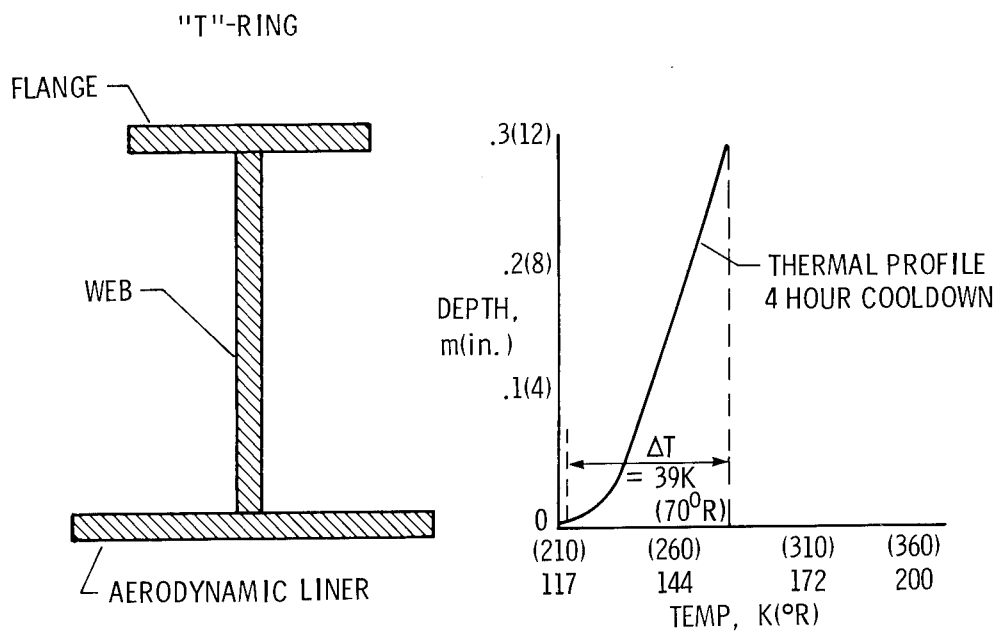
Figure 2.- Typical temperature gradient in contraction framing.

GAS TEMP.
K(°R)

294(530)

117(210)

@ m = 0.1
p = 207 kPa
(30 psia)

AVAILABLE FOR
DATA TAKING

-39°(-70°) TEMP CHANGE
@ m = 1.0
p = 896 kPa(130 psia)

STRUCTURAL
CONDITIONING

DATA TAKING
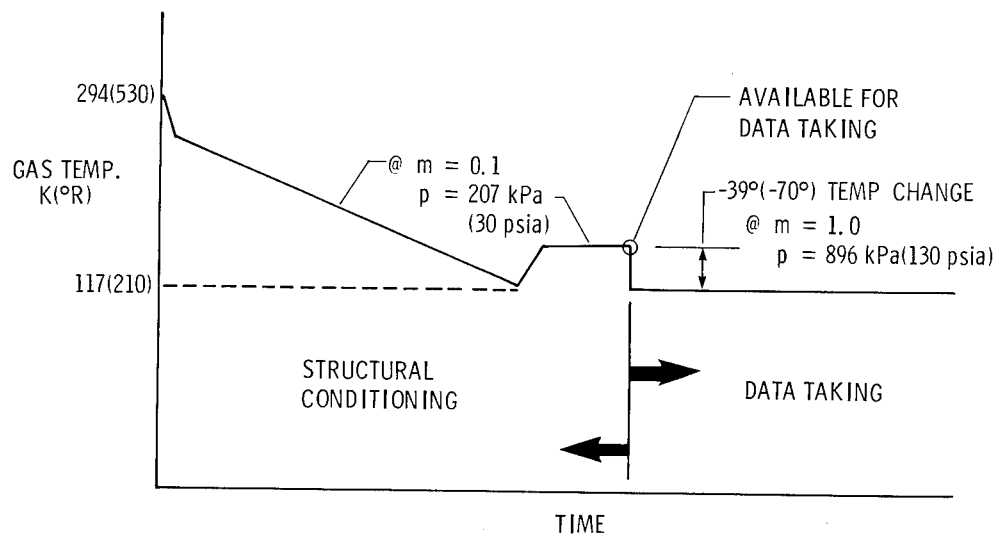
TIME

Figure 3.- Thermal forcing function cooldown and operating
temperature change.

DOWNSTREAM NACELLE
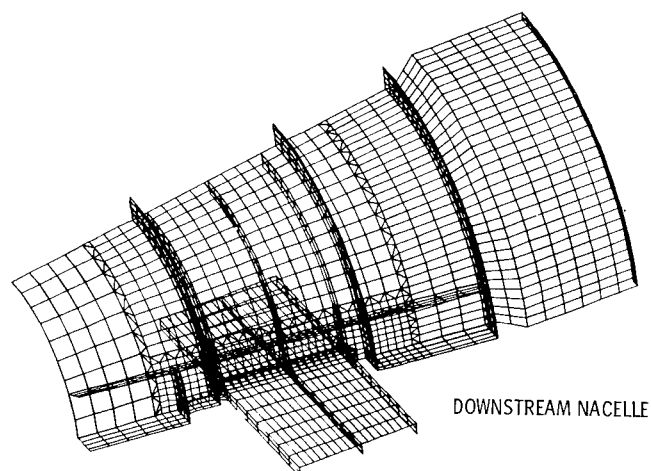
THERMAL – 2300 DOF, 2000 TIME STEPS
STRUCTURAL – 13000 DOF, 3 LOAD CASES
SAVES – MANPOWER, TIME, COMPUTER COSTS

Figure 4.- SPAR integrated thermal-structural analysis key factor
in NTF design.

DYNAMIC MODEL
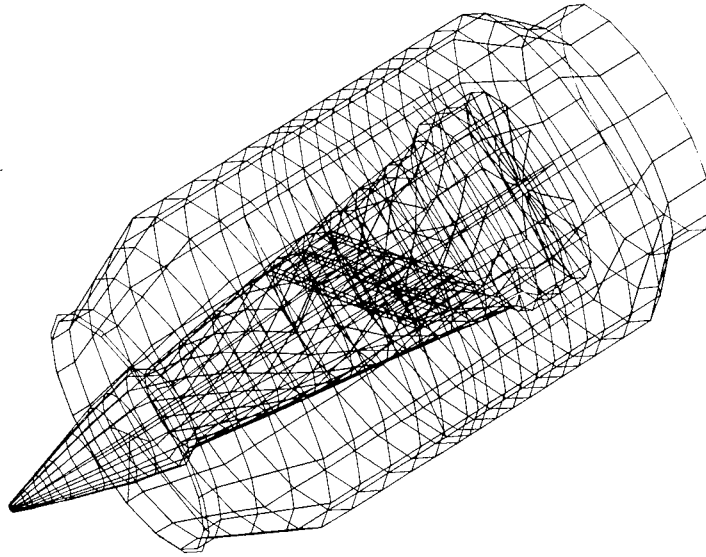
Figure 5.- Downstream nacelle and external shell.
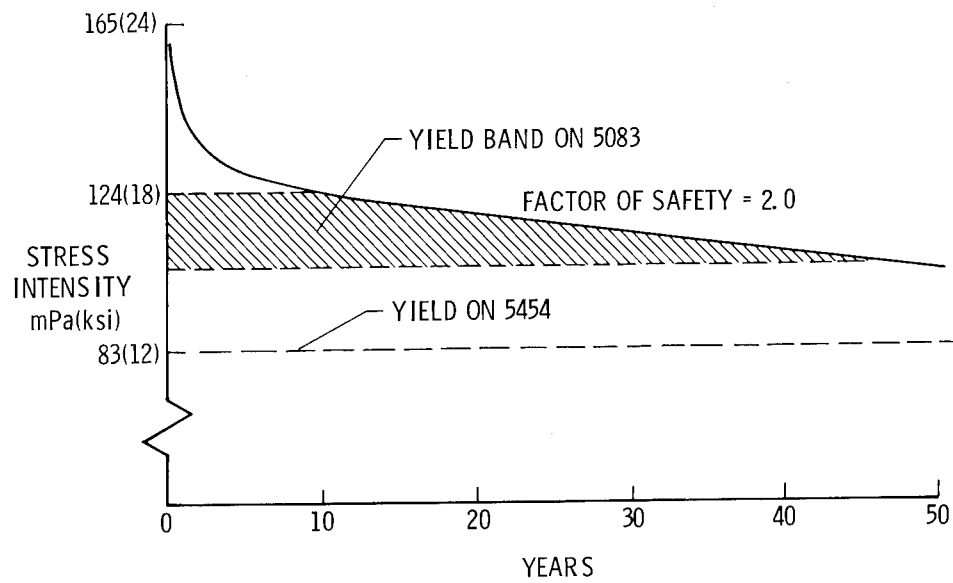
Figure 6.- 5454 and 5083 aluminum.

	5454-0 ALUM.	5083-0 ALUM.	9% Ni	NITRONIC 40
RELATIVE WEIGHT	1	1	3	3
YIELD STRESS mPa(ksi)	83(12)	103-124(15-18)	362(52.5)	345(50)
FATIGUE STRESS kPa(ksi)	97(14)	97(14)	276(40)	>379(55)
EαΔT STRESS mPa(ksi) ΔT =	78(11.3) 47 K(85°R)	78(11.3) 47 K(85°R)	251(36.4) 128 K(230°R)	355(51.5) 139 K(250°R)

Figure 7.- Internal structures, material selection.
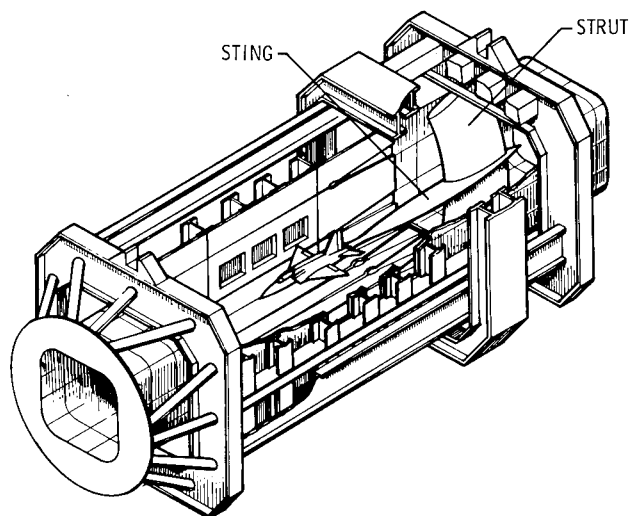
Figure 8.- Test section.

	CRITERIA	304 ST. STL.	NITRONIC 40	A-286	15-5PH -H1150M	9% Ni
YIELD mPa(ksi)	517(75)	207(30)	345(50)	586(85)min	517(75)min	517(75)
ULTIMATE mPa(ksi)	793(115)	517(75)	621(90)	896(130)min	793(115)min	793(115)
CHARPY J(ft-lb)	27(20)min	68(50)	88(65)	68(50)	20(15)min; 27(20)avg	27(20)min
(V-NOTCH)	34(25)avg				4-11(3-8)	34(25)avg
COATING REQ'D	-	NO	NO	NO	NO	YES
WELDABLE	-	YES	YES	NO	YES	YES
COST	BUDGET	>>	>>	>	=	<

Figure 9.- Arc sector, material assessment.
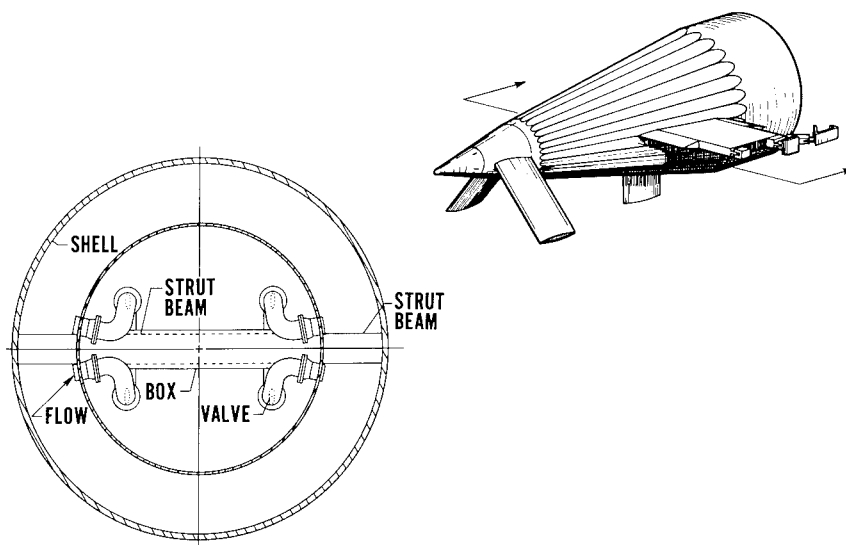
Figure 10.- Downstream nacelle strut cooling piping.
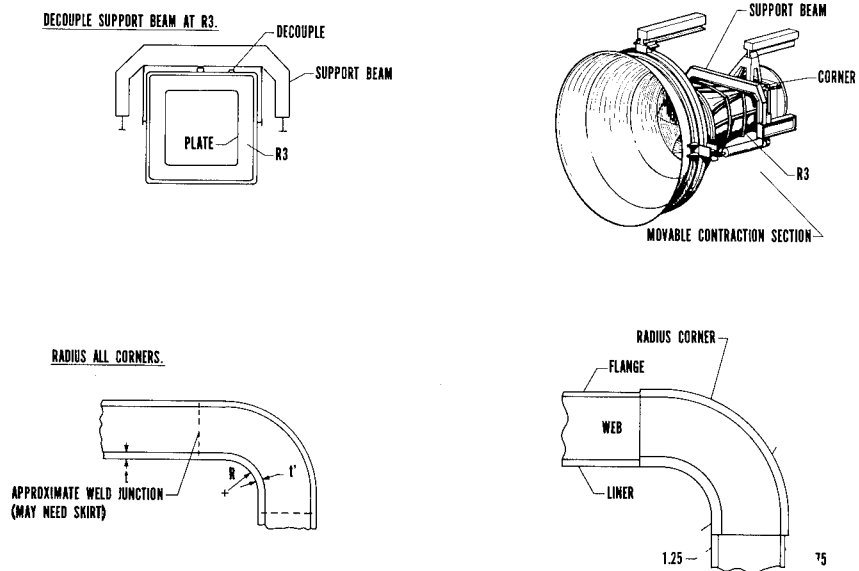
Figure 11.- Examples of configuration changes.
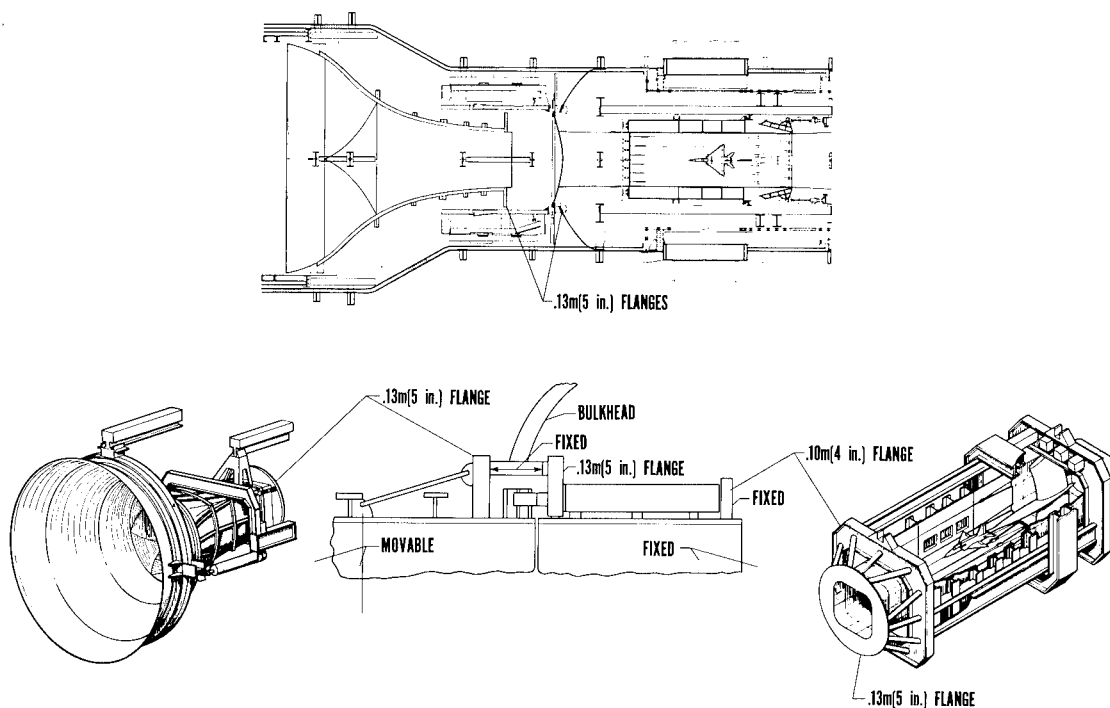
Figure 12.- Movable and fixed contraction sections.
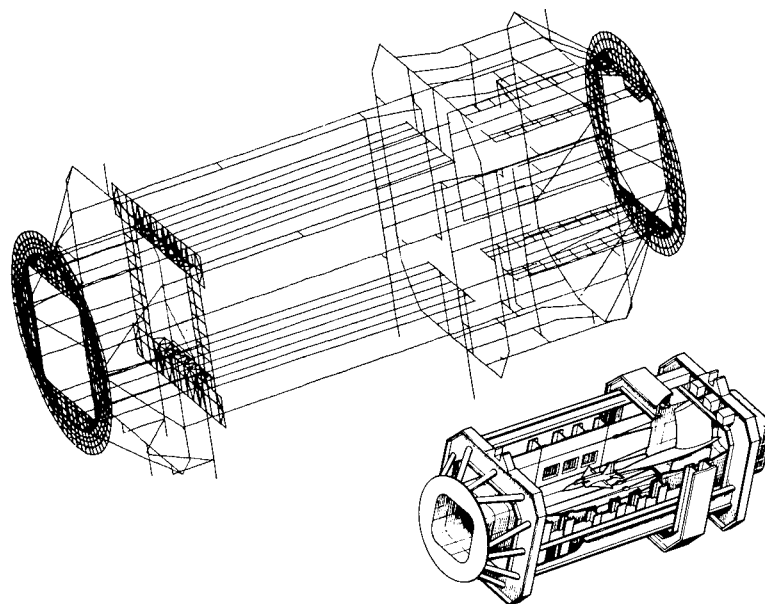
Figure 13.- Test section.
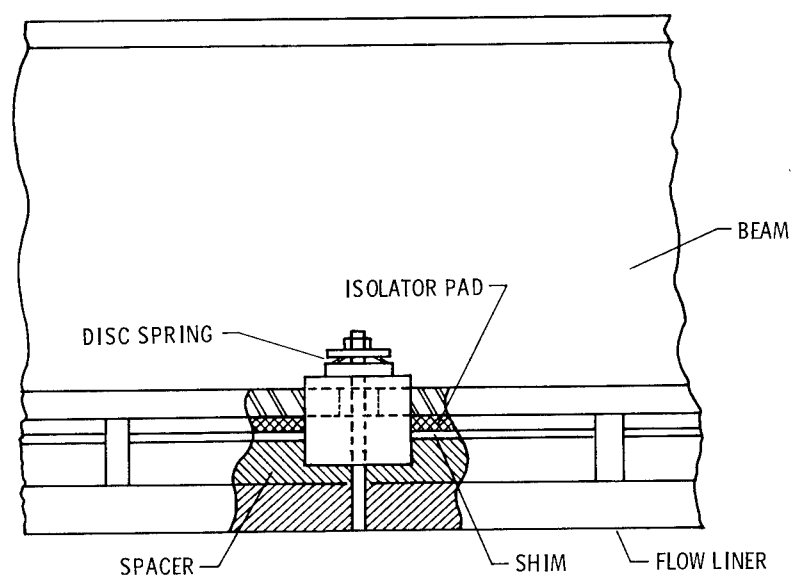
Figure 14.- Typical decoupling of large beams, test section.
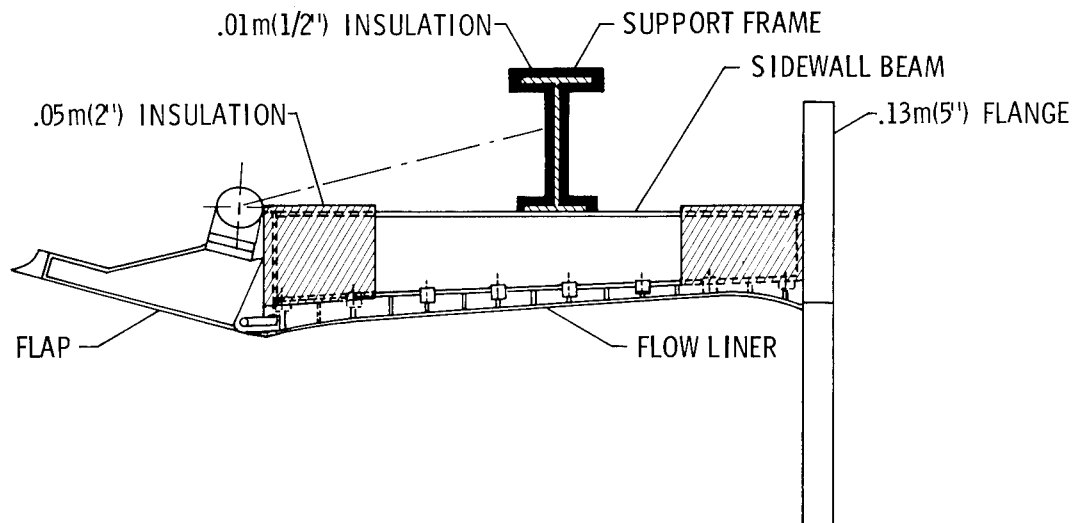
Figure 15.- Typical coating on test section beams.

ITEM	REQUIREMENTS	CAPABILITY
MECH + THERMAL STRESSES	<YIELD	<YIELD ON STRESS INTENSITY
COOLDOWN TIME	<8 hrs.	<4.7 hrs.
WARMUP TIME	<8 hrs.	<5.9 hrs.
OPERATING TEMPERATURE CHANGE	±39 K(70°R) IN 3 min @ m = 1.0, p = 896 kPa(130 psia)	±50 K(90°R) IN 3 min (±48 K(86°R) STEP) @ m = 1.0, p = 896 kPa(130 psia)
LIFE (FATIGUE)	>10 YEARS BEFORE RECERTIFICATION	>15 YEARS ON 5083 >50 YEARS ON 5454 BEFORE RECERTIFICATION

Figure 16.- Summary.

NOISE ATTENUATION IN A PRESSURIZED,

CRYOGENIC ENVIRONMENT

William S. Lassiter
Langley Research Center

SUMMARY

Analyses were performed which showed that a dual resonator attenuation lining was more effective than a bulk absorber lining in attenuating drive fan noise levels over a broad range of temperatures and pressures in the National Transonic Facility. Tests at ambient and cryogenic temperatures showed that the adhesive material used to bond the resonator system together retained shear, tensile, and fatigue properties at cryogenic temperatures. An attenuation test resulted in good agreement between experiment and theory in determining the attenuation of a prototype dual resonator panel.

INTRODUCTION

Transonic wind tunnels are known to be large noise producers. The two major noise sources are usually the test section and diffuser area and the drive fan. Methods for predicting test section and diffuser noise are not maturely developed. Design methods such as smoothing of surfaces and prevention of lips or cracks were employed in the National Transonic Facility (NTF) design in an effort to minimize test section and diffuser noise. Fan noise, however, can be more accurately predicted by using existing semi-empirical methods. The need for a noise analysis of the NTF drive fan arrived from the requirement of restricting the induced turbulence level in the test section and the sound pressure level at a residential trailer park located 137 m from the NTF. A turbulence level of less than 150 dB in the test section and a sound pressure level of 66 dBA or less at the trailer park were developed as criteria. It was desired to maintain the noise level in the test section due to the drive fan 8-10 dB below the test section criterion, such that it would not add to any test section/diffuser generated noise level. The trailer park criterion was based on 66 dBA being the maximum level at the trailer park produced by an existing NASA facility, the 16 Foot Transonic Tunnel.

An analysis based on a semi-empirical fan model was made of the NTF drive fan. Comparing the results of the analysis with the test section criterion indicated a need for attenuating the acoustic power produced by the fan. Conceptual designs of a bulk absorber system and an all-metallic resonator system along the upstream and downstream nacelles and associated walls were generated. The analysis resulted in a dual cavity all-metallic resonator being the most feasible and economic approach.

Final design of 335 dual cavity aluminum-honeycomb-sandwich flat panels was performed. The panels cover a total flow area of about 213.7 m^2 downstream and 111.5 m^2 upstream of the drive fan. The honeycomb core is bonded to two perforated thin sheets and a backing plate by a B. F. Goodrich modified epoxy adhesive. Immersion cycling of a full-size prototype panel into LN$_2$ indicated no thermal stress failures. Fatigue tests simulating the cold temperature and loads in excess of the acoustic environment were carried out with coupons and no failures or degradation detected. A full-size panel was exposed to acoustic power levels in excess of calculated drive fan levels for up to 40 hours and no degradation in the panel was detected by visual observation. Tensile tests on bonded test coupons exposed to ambient and cryogenic conditions showed no degradation in bond strength. Attenuation measurements of a full-size panel section in a flow impedance tube showed agreement with analytically determined attenuation.

DRIVE FAN ACOUSTIC POWER

The acoustic power generated by the NTF drive fan was calculated using a semi-empirical model (reference 1) with the aid of the Boeing Wichita Co. in Wichita, Kansas. The semi-empirical model is expressed as

$$P_a = K \dot{m} c^2 \left(\frac{\Delta T_f}{T_i}\right)^2 \qquad (1)$$

where K is an experimentally determined constant, $\dot{m}$ is the mass flow rate, c is the speed of sound, and $\Delta T_f/T_i$ is the ratio of the drive fan stagnation temperature rise to the inlet stagnation temperature. This analysis includes upstream and downstream radiation of broadband noise generated by the single stage fan, upstream and downstream radiation of rotor-stator interaction tones, and upstream radiation of inlet flow distortion tones. Figure 1 shows the predicted worst case sound pressure level in the test section due to the drive fan alone, assuming no attenuation in the flow circuit. The overall test section level exceeds the test section target criterion of less than 150 dB. The target criterion at the residential trailer park located 137 m from the NTF site is also violated by this noise level. The trailer park is in a very noisy location, being 25 to 50 m from a stockcar race track and less than a kilometer from the Langley Air Force Base, home of several F-15 squadrons. The excessive acoustic levels at this trailer park and in the tunnel test section brought about the need for a system for attenuating the drive fan acoustic power.

122

FAN ATTENUATION SYSTEM

Two approaches for attenuating the NTF drive fan noise were studied, a bulk absorber lining and a metallic resonator. Figure 2 shows the NTF circuit with the shadowed area upstream and downstream of the fan as the area selected for the acoustic lining, about 325.2 m^2 surface area adjacent to the tunnel flow path. The approach of placing the lining as close to the fan noise as feasible was employed. The upstream area on the nose cone and adjacent wall was selected because of installation feasibility, rather than an area closer to the fan.

Bulk Absorber Concept

A bulk absorber lining of known resistivity (flow resistance per unit depth) at ambient temperature was initially chosen as the lining concept. Extrapolation of the resistivity to cryogenic and high pressure conditions was necessary due to a lack of data at these conditions. The extrapolation was based on viscosity dependence on temperature and the perfect gas law,

$$R_1 (T, P) = R_1 (T_0, P_0) (T/T_0)^{.85} \tag{2}$$

and

$$\rho c (T, P) = \rho c (T_0, P_0) \frac{P}{P_0} \left(\frac{T_0}{T}\right)^{1/2} \tag{3}$$

resulting in a normalized resistance of

$$\frac{R}{\rho c} (T, P) = \frac{R}{\rho c} (T_0, P_0) \left(\frac{T}{T_0}\right)^{1.35} \left(\frac{P_0}{P}\right) \tag{4}$$

where ρ is the density, T the temperature, P the pressure, R_1 the resistivity of the material, and R the flow resistance of the material. The subscript o indicates ambient conditions (STP).

A conceptual design of the lining was developed for the operating condition shown in figure 1 by using the above flow resistance in impedance math models which were input to computerized acoustic performance prediction programs developed for aircraft engine nacelles by the Boeing Wichita Co. These programs calculate duct attenuation as a function of wall lining

impedance, duct geometry, and aerothermodynamic environment. The models were extrapolated to cryogenic conditions. The conceptual design resulting from the analysis consisted of a segmented bulk absorber lining composed of segments with different resistivities as shown in table I. The high upstream and downstream resistivities of 13.29×10^5 kg/m^3-s and 44.29×10^5 kg/m^3-s, respectively, were required by the high pressure and cold temperatures. Three segments were required upstream and downstream of the fan. The segment with highest resistivity was for broadband attenuation of the noise. The other segments were tuned to the blade passage frequency and varied in resistivity due to the variable duct height. Figure 3 shows the attenuation of the segmented lining. Due to the conceptual status of the design when this analysis was performed, the total lining area in table I is more than the actual lining area shown in figure 2. The attenuation of the segmented bulk absorber lining shown in table I was significant, reducing the test section sound pressure level from 155 dB to about 140 dB. Specific materials having such high resistivities were not identified. More commonly used bulk absorbers have resistivities ranging from 1000 to several hundred thousand kg/m^3-s. Subsequent analysis of other operating conditions in the tunnel showed that the acoustic performance of this segmented lining was very sensitive to the operating pressure and temperature. For example, for the case of a higher temperature of 283°K, a somewhat lower pressure of 7.445×10^5 N/m^2 and Mach 0.8 the overall test section sound pressure level was reduced from 152 dB to only 148 dB, a drastic reduction in attenuation compared to the colder case considered. Due to non-availability of materials with the required resistivities and the pressure and temperature dependence of bulk absorbers, the bulk absorber concept was abandoned.

Resonator Concept

The alternate concept of resonator linings for attenuating the NTF drive fan power was explored. A dual resonator concept (two cavities) was selected in the investigation of resonator concepts because of the broader acoustic bandwidth over which attenuation was achieved compared with a single cavity. Figure 4 shows a schematic of the dual resonator. The concept consists of two honeycomb core cavities separated and capped by perforated sheet. The open areas of the perforate sheets (OA_1 and OA_2) and the cavity depths are the important parameters affecting the attenuation. Several depth combinations of the cavities for the upstream lining were considered in attempting to meet the test section and trailer park target criteria. The acoustic impedance of these lining configurations was calculated using impedance math models based on perforated sheet material parameters and aerothermodynamic conditions. These impedances were used as input to computing the attenuation by computerized acoustic performance prediction programs developed for aircraft engine nacelles by the Boeing Wichita Co. These impedance and acoustic performance prediction models were extrapolated to cryogenic conditions. The configuration giving the best overall performance for the operating conditions shown in figure 1 resulted in upstream cavity depths of 3.3 cm and 11.7 cm, and downstream depths of 6.4 cm and 19.1 cm. Sound pressure levels of 71.7 dBA and

141.5 dB at the trailer park and test section, respectively, resulted for the worst case operation condition shown in figure 1. Levels resulting from analysis of other operational conditions were less than these. Thus, the dual resonator concept was very effective over the broad NTF operational range of temperature and pressure. The far field criterion of 66 dBA at the trailer park was not satisfied but minimum transmission loss of the tunnel shell and no transmission loss due to the closed cell thermal insulation inside the tunnel were assumed. Upon operation of the NTF, measurements of the noise at the trailer park will be made and if the target criterion is exceeded retrofit measures will be considered, such as erecting a thin metal enclosure about the portion of the tunnel not enclosed by the building.

FAN ATTENUATION SYSTEM DESIGN

The analysis of the dual resonator concept showed it to sufficiently attenuate the NTF drive fan noise. An all-aluminum system was desirable from the standpoint of cost, material availability, and cryogenic capability. The depth and dual cavity geometry led to considering attaching the perforate sheet, honeycomb, and backing plate with a structural adhesive, rather than by welding or mechanical attachments. The adhesive must be capable of operating at cryogenic temperatures. It also must reticulate, or migrate to the honeycomb cell edges, before bonding in order to prevent blockage of the perforate sheet open area. A candidate adhesive that had been used in the aircraft industry and for which strength data was available from 218°K to 449.7°K was a B. F. Goodrich Plastilock 729-3 modified epoxy (reference 2). An extensive test program was carried out at Langley Research Center that determined the optimum reticulation and bonding conditions for bonding .95 cm hexagonal aluminum honeycomb core to aluminum perforate sheet and backing plate. Figure 5 shows a sheet of PL729-3 successfully reticulated on a piece of honeycomb core. Figure 6 shows the honeycomb-perforate sheet combination bonded with PL729-3. The resulting fillet bond is desirable in that it minimizes blockage and creates a large surface bond area.

Figure 7 shows a prototype acoustic panel for the NTF. Three hundred and thirty-five flat panels will be placed in the areas shown in figure 2 creating ducts with 24-sided inner and outer polygons. Little effects on the aerodynamic flow and the higher costs of fabricating panels with curvative led to the flat panel-polygonal geometry. The NTF panels are trapezoidal in shape to fit the egg-crate like support cavities fabricated on the nacelles and surrounding shroud areas. Upstream and downstream panels are 16.5 and 26.7 cm deep, respectively. The honeycomb core is .95 cm hexagonal 5052 aluminum honeycomb, 67.28 kg/m^3. Perforate sheet is .08 cm thick 5052 aluminum. Backing plates are 2024-T351 and 7075-T6 aluminum. Springy-like hangers are shown on the sides and end of the panel in figure 7. The middle-side hangers have holes drilled in them to allow fixing of those locations by bolting them to the support cavities inside the tunnel. The end-side hangers have slots to allow for thermal expansion and contraction of the panels during operational swings in the tunnel. An edge support sheet is riveted along the sides of each panel

to prevent peeling of the outer perforate sheet, in case of adhesive failure at that joint. An .08 cm shim is placed under the edge support sheet to allow for thermal expansion and contraction. Mechanical bolts extend through the thickness of each panel as a safety measure to prevent dislodging of the perforate sheet, honeycomb or backing plate in case of adhesive failure.

TESTING

Coupon Strength Tests

A series of tests were carried out in order to support the calculations in the design of the panels and to test the strength of the structural adhesive bond at cryogenic temperatures, where no data exist.

A concern for the structural integrity of the PL729-3 adhesive at cryogenic temperatures led to lap shear and flatwise tensile tests of coupon samples at ambient and cryogenic temperatures. The sample configurations and results of the tests are shown in figure 8. The average load at failure for five lap shear tests at 116.3°K was 1.125×10^4 N, which was about 15% lower than the average load at failure for five tests at ambient temperature. This could be due to degradation in shear properties and/or statistical scatter. These results were considered very encouraging and showed no large degradation in shear strength of the adhesive at cryogenic temperatures.

Flatwise tensile tests of 5.1 cm x 5.1 cm x 1.59 cm thick specimens of Flexcore aluminum honeycomb bonded with the 729-3 adhesive to .16 cm thick 6061-T6 aluminum sheet were carried out at ambient temperature and 77°K. Prior to each test each specimen was subjected to 20 thermal cycles from ambient to 77°K. The results of three tests at each temperature showed no difference in the tensile strength of the epoxy. The average load to failure for the cryogenic tests was 1.107×10^4 N.

Coupon Fatigue Tests

As a result of concern of the fatigue characteristics of the PL729-3 adhesive at cryogenic temperatures, honeycomb coupons were tested in tension under combined dynamic loading and ambient and cryogenic temperature. Figure 9 shows a schematic of the test configuration and results at ambient and cryogenic temperatures. A sample consisted of aluminum honeycomb core bonded to aluminum perforate sheet with PL729-3 adhesive. The sample was placed in a servo-hydraulic loader and cycled to failure at ambient and cryogenic temperatures under one-half the static failure load.

Thermal Shock Test

A test was devised as shown in figure 10 to determine if a full-size panel could withstand extreme thermal shock. A prototype panel was subjected to an extreme thermal shock condition by dipping the top side of the panel into liquid nitrogen (LN_2) in a tray until the temperature of that face reached 77°K, then ejecting the LN_2 and heating the top side of the panel to 366.3°K by quartz heaters in the tray. Two hundred cycles of these thermal shock conditions were applied to the panel. A severe thermal gradient of at least 433°K existed throughout the thickness of the panel during each cycle. The NTF cooldown and warmup sequence generates a much less severe thermal shock condition in the panels since it requires 5 hours for cooldown and a slow warmup. The results of these tests show a great durability of the panel to extreme temperature changes.

Sonic Fatigue Test

A full-size panel was tested in the Thermo-Acoustic Fatigue Apparatus Facility at Langley Research Center which simulated the maximum expected noise levels of the NTF. Figure 11 shows a photograph of the facility and mounting of the panel in the test section by a sidewall mounting system. The panel was mounted in a grazing incidence orientation with respect to the noise propagation in the test section.

The sonic fatigue tests were performed in two phases. The first phase consisted of subjecting the panel to a series of 0.5-1.25 hour tests at 155 dB overall sound pressure level for a cumulative time of 10 hours. The second phase of testing consisted of subjecting the panel to a level of 158 dB overall sound pressure level for a cumulative time of 30 hours. Figure 12 shows the spectra for this latter phase of testing, the spectral shape of which is near that of the first phase. The panel survived both phases of sonic testing without any visual degradation. It is noted in figure 12 that the noise spectrum generated by the facility is very near that anticipated for the NTF. The levels generated at higher frequencies (> 1 kHz) were slightly greater, thus subjecting the panel to even worse conditions than expected in the NTF. This system test showed that the panel can withstand a severe noise and fatigue environment.

Attenuation Verification

A 5.1 cm x 40.6 cm section of a 26.7 cm deep test panel was placed in an aluminum holder and attached to the test section of the Grazing Flow Impedance Tube at Langley Research Center, as shown in the schematic of figure 13. The panel section was attached to the flow tube test section such that noise propagating down the tube was incident on the panel section in a grazing manner, typical of the situation in the NTF. The electromagnetic drivers generated noise levels of 115-125 dB below 2 kHz and from 95-115 dB between 2-5 kHz.

A traversing microphone positioned above the panel section measured the sound pressure levels at the leading and trailing edges of the panel section, the difference of the two being the attenuation of the panel section. The results of the experiment are shown in figure 14 in which attenuation, shown by the solid curve and increasing in the negative direction, is plotted versus frequency of the noise generated. The diamonds are values of attenuation calculated by a finite element attenuation model (reference 3). The agreement between theory and experiment is good at the troughs of the attenuation experimental curve (areas of least attenuation) and not very good at the attenuation peaks (areas of maximum attenuation). The difference is attributable to noise leakage at the edges of the panel section and suggests the presence of extended reaction effects (reference 4). Overall, the agreement is considered good and indicates that the panel is a strong attenuator, as predicted by theory.

CONCLUDING REMARKS

The following conclusions were arrived at in the effort of controlling drive fan noise in the NTF:

1. A dual resonator concept was selected to attenuate drive fan noise inside the NTF. It was shown through analysis that this concept was very effective over a broad range of pressures and temperatures.

2. Attenuation of the dual resonator concept was shown to experimentally agree with theoretical predictions.

3. A prototype of the dual resonator concept was shown through extensive testing to withstand severe noise fatigue and thermal shock conditions.

4. A reticulating structural adhesive bonding the dual resonator system together was shown to retain shear and tensile properties at cryogenic temperatures.

REFERENCES

1. Heidmann, M. F.: Interim Prediction Method for Fan and Compressor Source Noise. NASA TM X-71763, Lewis Research Center, Cleveland, Ohio, June 1975.

2. Weber, C. D.; Gross, M. E.; and Austin, H. J.: Controlled Flow Structural Adhesives for Film Reticulation. Presented at 7th National SAMPE Technical Conference, Albuquerque, New Mexico, October 14-16, 1975, and reproduced from Materials Review 1975, Vol. 7, National SAMPE Technical Conference Series.

3. Abrahamson, A. L.: A Finite Element Algorithm for Sound Propagation in Axisymmetric Ducts Containing Compressible Mean Flow. NASA CR-145209, June 1977.

4. Lester, H. C.; and Parrott, T. L.: Application of Finite Element Methodology for Computing Grazing Incidence Wave Structure in an Impedance Tube: Comparision with Experiment. AIAA Paper 79-0664, AIAA 5th Aeroacoustics Conference, Seattle, Washington, March 12-14, 1979.

TABLE I. – ACOUSTIC LINING BULK ABSORBER RESISTIVITIES REQUIRED FOR
WORST DRIVE FAN NOISE CONDITIONS

ABSORBER RESISTIVITIES, 10^5 kg/m^3-s

Location	Lining Area, m^2	R_1 (T, P)	R_1 (T$_o$, P$_o$)
Upstream	30	2	4.43
Upstream	28.14	4	8.86
Upstream	41.9	6	13.29
Downstream	169.17	20	44.29
Downstream	73.86	0.6	1.33
Downstream	114.82	1	2.21
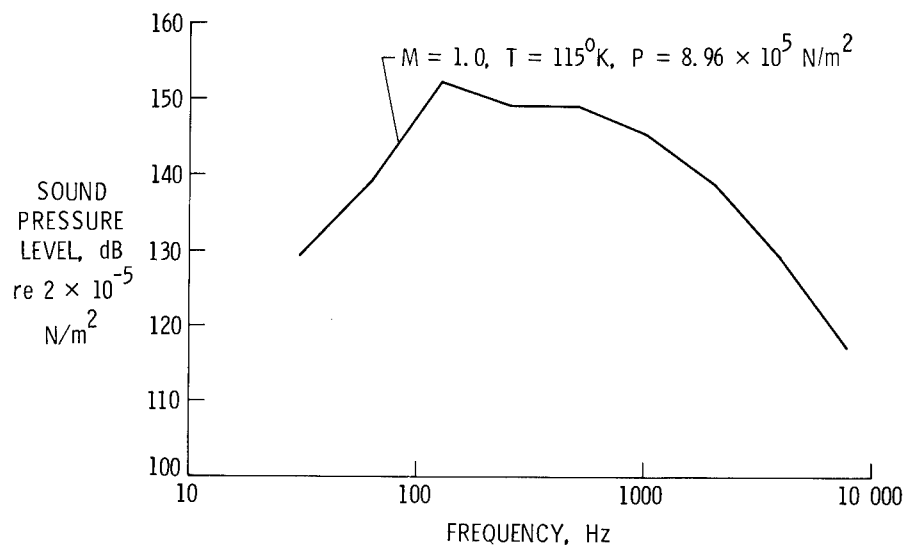
Figure 1.- Worst case NTF drive fan noise levels in the test section.
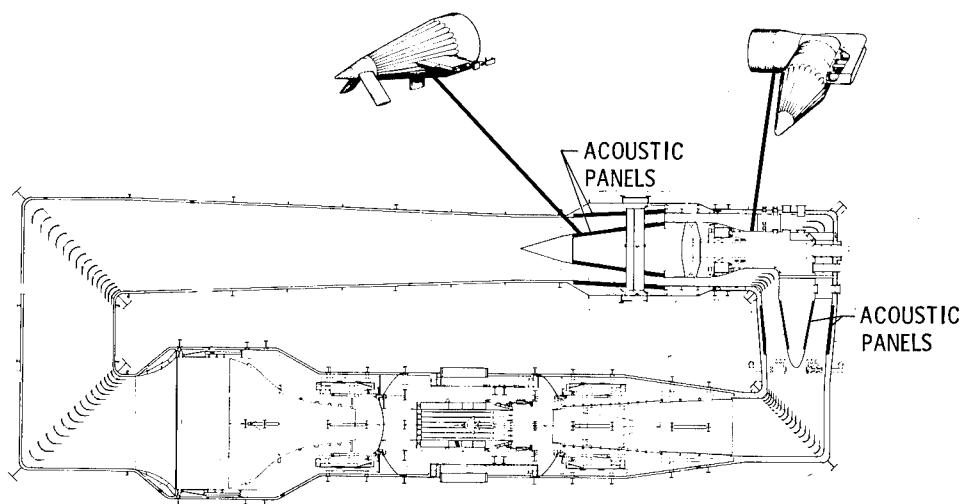
Figure 2.- NTF circuit flow showing location of acoustic panels.
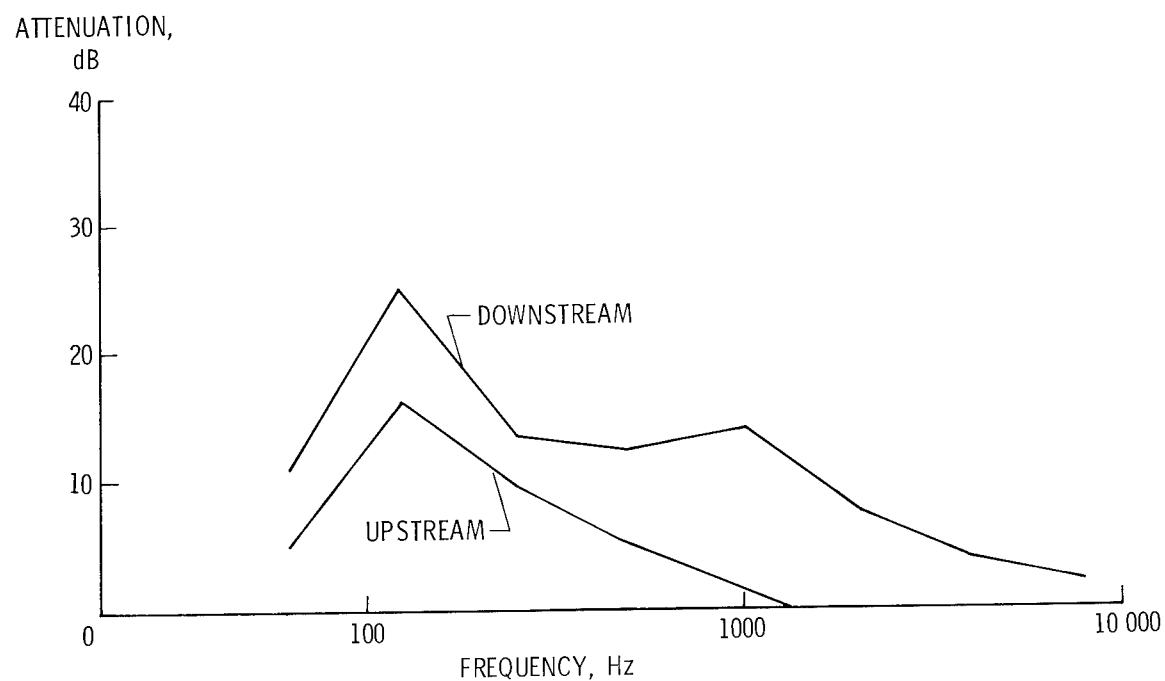
ATTENUATION,
dB

Figure 3.- Attenuation of bulk absorber segmented lining.
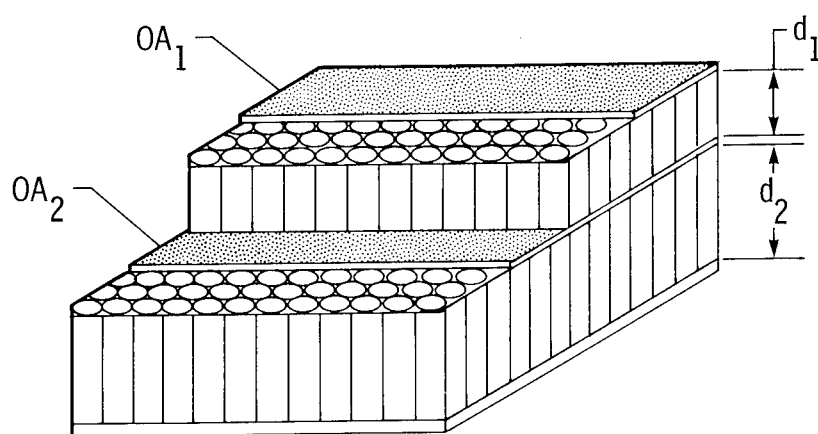
Figure 4.- Dual resonator concept.
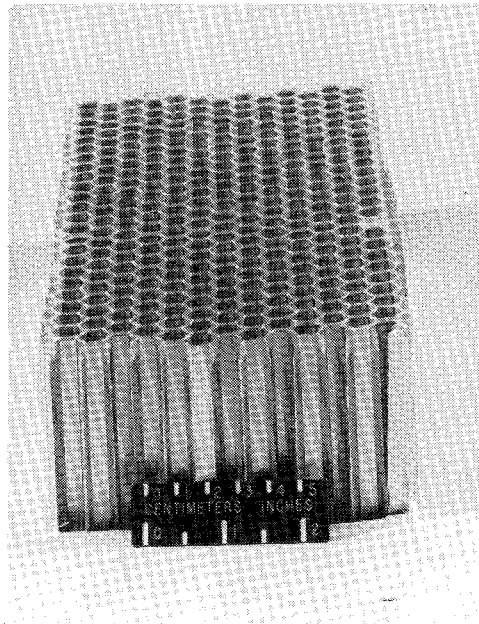
Figure 5.- Successful reticulation of B. F. Goodrich PL729-3 adhesive on 0.95 cm hexagonal aluminum honeycomb.
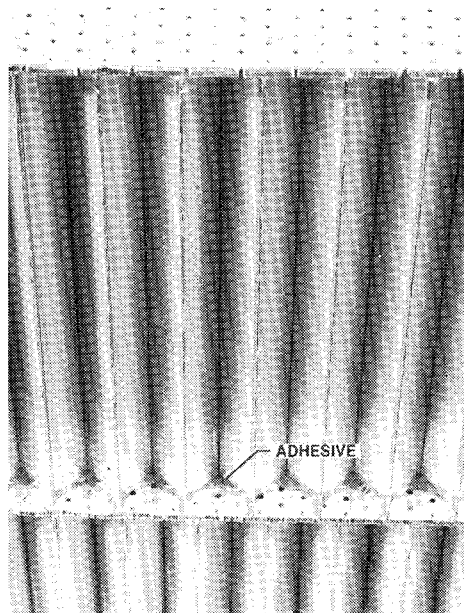
Figure 6.- Aluminum perforate sheet bonded to 0.95 cm hexagonal aluminum honeycomb with B. F. Goodrich PL729-3 adhesive.
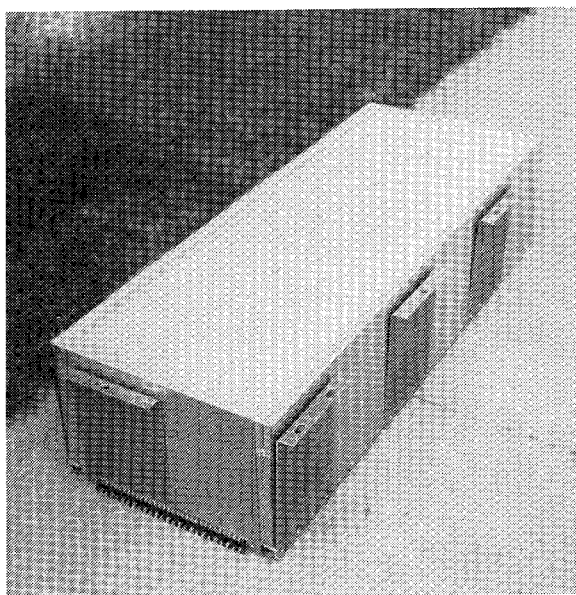
Figure 7.- Prototype NTF acoustic panel.

LAP SHEAR   FLATWISE TENSILE

STRESS AT FAILURE, N/m^2

● AMBIENT 2×10^7 4.14×10^6

● CRYO 1.72×10^7 $4.14 \times 10^6 +$

Figure 8.- Adhesive structural tests at ambient and cryogenic temperature.

CYCLIC LOAD

.064 m
(2.5 in.)

LOAD ADAPTER

CYCLIC LOAD

CYCLES TO FAILURE
AT 1/2 STATIC FAILURE LOAD

AMBIENT 7.7×10^4

CRYO 48×10^4
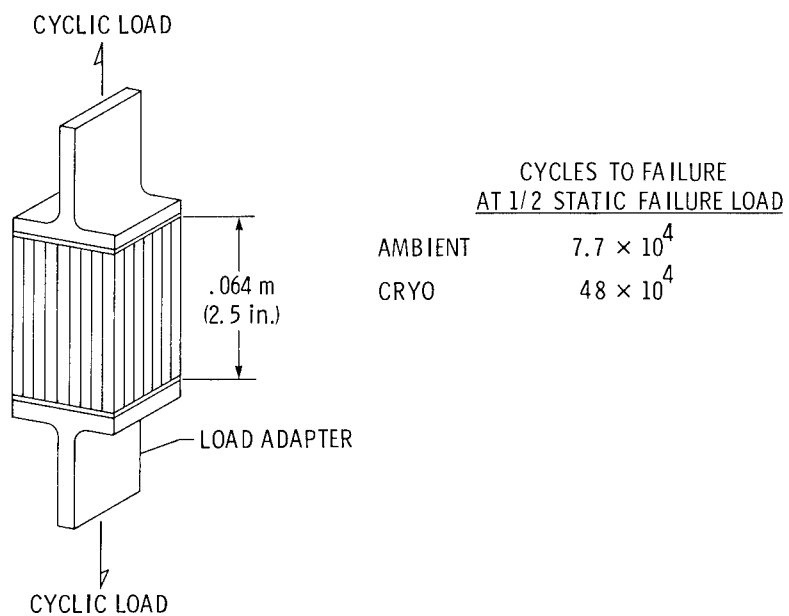
Figure 9.- Fatigue test of bonded samples at ambient and cryogenic conditions.

PANEL

LN2

TRAY

Figure 10.- Thermal shock test of prototype model.
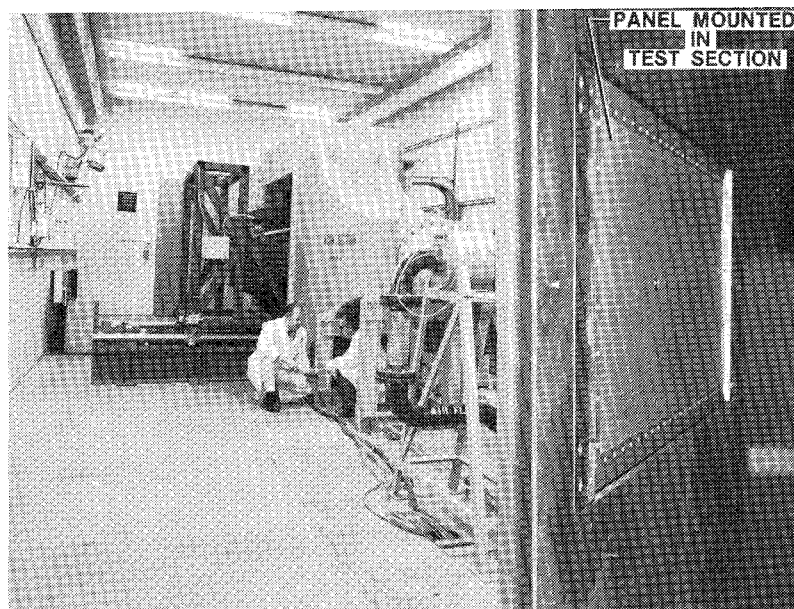
Figure 11.- Thermo-Acoustic Fatigue Apparatus Facility and mounting of prototype acoustic panel.
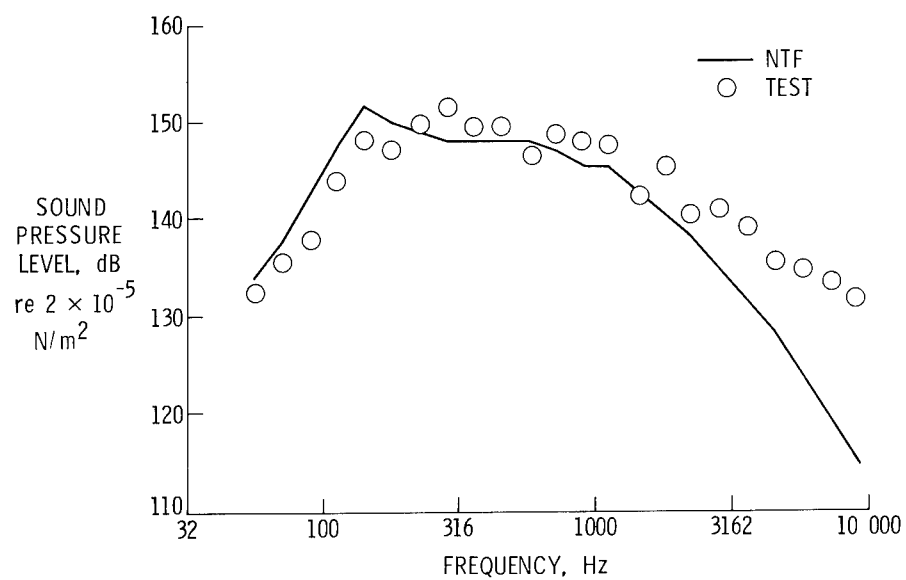
Figure 12.- Simulation of NTF noise levels in Thermo-Acoustic Fatigue Apparatus Facility.
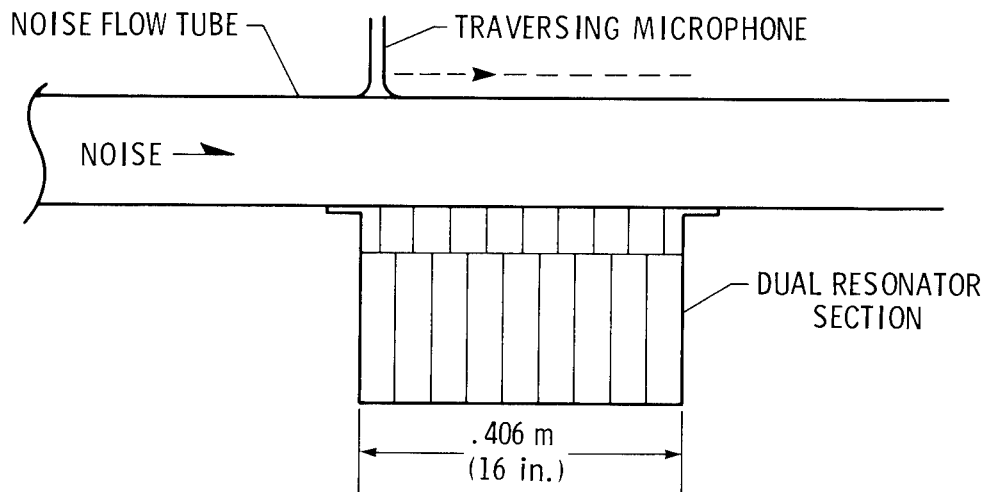
Figure 13.- Attenuation test of acoustic panel section in Flow Impedance Tube.
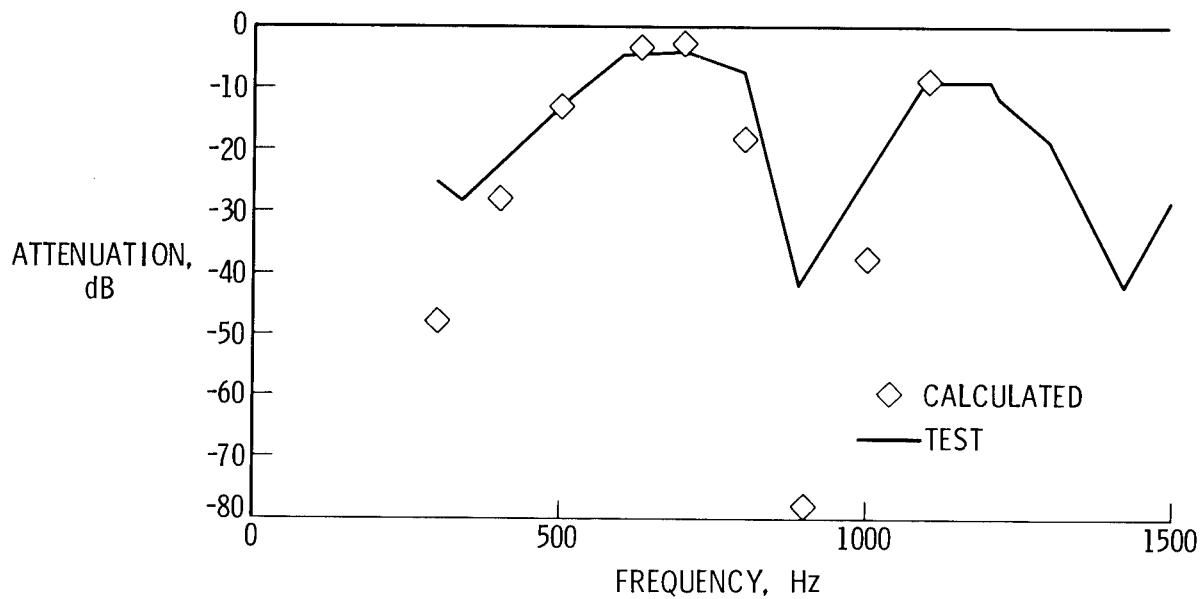
Figure 14.- Attenuation of a 26.7 cm deep section of acoustic panel.

STATUS REPORT ON DEVELOPMENT OF LARGE SEALS

FOR CRYOGENIC APPLICATIONS

Sammie D. Joplin
Langley Research Center

SUMMARY

The development program for large seals to be used in the cryogenic environment of the National Transonic Facility (NTF) has established that a "U" shape cross section seal made from a polymer material is best suited to meet the design criteria and fabrication requirements. Several parameters have been identified that influence seal performance including surface finish, spring and pressure activation, seal fit in the groove, and treatments to the sealing surface with polymer tapes. The seals have also demonstrated the capability of sealing a 0.16 cm (0.064 in.) gap between sealing surfaces. Tests are in progress to establish the seal performance with lubricants, with bonded joints, and for a radial installation. Tests will also be made to establish that the seals will seat at cryogenic temperatures and will seal variable gaps during a thermal cycle.

INTRODUCTION

The factors considered in the choice of the correct seals for the many complex sealing problems existing in the National Transonic Facility (NTF) are presented. The basic approach to the design has been to identify the seal parameters where technology is adequate to meet the NTF design criteria and use existing data and design techniques in the selection of the seals. In those areas where current technology was not adequate the selection of the correct parameter has been supported by analysis and development testing. The status of this selection process is presented along with the test results to date.

FUNCTIONS OF SEALS IN THE NTF

In order to discuss the factors considered in the selection of seals for NTF, it is first necessary to understand their three functions. The first function is to prevent undesirable recirculation of the tunnel fluid in areas between the shell and flow surfaces of the internal components shown in figure 1: the movable contraction, fixed contraction, test section, and high speed diffuser. The requirement to prevent this recirculation is illustrated in figure 2 which shows a schematic of the NTF contraction section. The des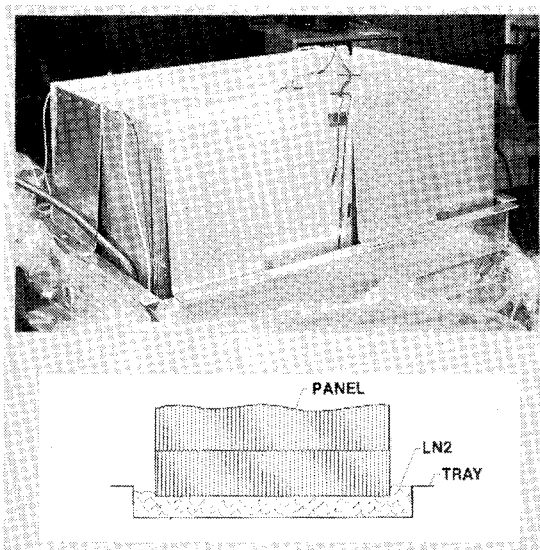ign in this section requires a gap between the movable section and the fixed section as indicated in figure 2. In order to prevent flow through this gap that may cause disturbances in the test section and/or require additional power, seals are

provided at all openings around the wall of the movable section and the tunnel shell. Secondly, the nacelle area (see figure 1) seals are used to prevent the low temperature gaseous nitrogen from flowing into the areas containing drive equipment that would be damaged by the cryogenic temperature. Finally, seals are provided in the isolation valves at each end of the test section (figure 1) to control the leakage during model changes.

BASIC DESIGN CONSIDERATIONS

The NTF Environment

The critical environmental factors for the NTF seals are the following: the large size and varied shape, figure 3; the large temperature range 97 K to 294 K (-320° F to $+150^\circ$ F); variable pressure 0 to 895.7 kPa (130 psia); reversible pressure requirements; compatibility of seals to the fluid; structural materials; seal spring material; the requirement to seal gaps that vary due to thermal contraction and expansion; and to break and reseat seals at cryogenic temperatures. Some of these requirements have been addressed in previous designs; others represent new challenges. The basic approach was to design the seal carrier and sealing surfaces according to current design practice. When this was not possible, a test program was developed that focuses on the area of departure from past practice in order to select the correct seal parameter. The factors in seal design are identified and grouped into those within current technology, those requiring an extension in current technology, and those requiring a departure from current technology, figure 4.

Current Technology

Existing data and designs were reviewed and selections of the following factors were based on past design practices: material, seal type and cross section details, seal groove design, and spring activated seals.

A review of current cryogenic seal applications indicated that the principal materials used are metals and polymers. Metal cryogenic seals are made from several metals including the 300 series stainless steels, Inconel, aluminum and copper. From a fabrication point of view these metal seals were attractive for the large sizes and varied shapes required for NTF (figure 3) since (1) they are typically formed from tubes and (2) the joints are welded. Metal seals are suitable for a wide range of temperatures and pressures and make the compatibility of material easy to resolve. There is also a wide range of coatings available including silver and fluorocarbon resins. However, metal seals were not selected for use in the NTF because they are not recommended in applications requiring repeated cycles and because there is insufficient data on the suitability of a metal seal to close a gap that varies in size due to thermal cycling.

Cryogenic seals of various polymers are common and provide good performance when the materials are matched properly to the environment and to fabrication

requirements. Based on existing data and manufacturers' experience, three materials were selected for development testing: polytetrafluoroethylene (TFE), tetrafluoroethylene-hexafluoropropylene copolymer (FEP), and ultrahigh molecular weight polyethylene (UHMWPE). Fabrication of the large seals emerged as a critical parameter since previous experience has been with relatively small circular seals (1.2 m (4 ft) or less in diameter). Fabrication of the smaller seals is by machine cutting a continuous circle from a billet of annealed material. Annealing during the machining is used to obtain dimensional accuracy. These materials (TFE, FEP, and UHMWPE) have been used successfully over a wide range of pressures in static seal applications. With the addition of additives to enhance particular properties the so-called "filled" polymers have been used successfully in numerous dynamic applications. Considerable attention has been given in the technical literature to an analysis of the leak rate, particularly for mechanical face seals, but no test data or analytical methods were found to predict the performance of seals in the environment of the NTF. Therefore, a development test program is underway to measure the leak rate of these polymer seals and in particular to establish their performance versus hardware and environmental variables. Of particular interest is the materials' ability to reseat at cryogenic temperature and to seal during a cryogenic cycle when the gap varies due to the thermal contraction and expansion of the NTF structure.

Numerous seal cross sections have been used to meet different sealing requirements. Some of these are illustrated in figure 5. Based on the NTF requirement that the seals be capable of sealing a variable gap, the "U" shape cross section was chosen. Its principal features are: (1) the sides of the seal can remain relatively thin and therefore flexible while spanning a large width, (2) the "U" offers a pressure activation feature as illustrated in figure 6, (3) and the "U" allows for use of a spring to activate the seal (figure 6) to improve performance and to accommodate pressure reversals.

The NTF seals included in this development are basically static seals. Sealing of rotational or linear motion is not required in the normal sense of dynamic seals. However, there is a requirement to seal in the presence of axial and radial motion caused by thermal expansion and contraction as illustrated in figure 7.

Extension of Current Technology

The following group of factors in seal design requires a departure from past design practice in order to meet the NTF requirements: surface finish, material for sealing surface, and seal retainers. These factors are summarized in figure 8. Past experience in seal design and testing indicates that surface finish has a significant influence on leak rate; i.e. the better surface finishes provide the most satisfactory sealing surface. However, these surface finishes depend on the size, material, shape of the part, and the machine tool and production process available. The high quality surface finish normally recommended for the NTF environment was not selected due to the cost associated with providing this finish on large NTF parts. The surface finish selected for NTF was 0.8 μm RMS (32 μin. RMS).

The material for the sealing surfaces was chosen for structural design considerations due to the cryogenic environment. Tests have been completed to verify that the material and surface finish will provide a satisfactory sealing surface.

For the NTF seals, retainers are required to keep the seals in place during the remote positioning of the movable contraction and the high speed diffuser (figure 1). This is a slight departure from existing designs where seal retainers are utilized as an aid during installation and/or to keep the seal in place under pressure.

Departures from Current Technology

The final group of factors in seal design are areas of major departure from past design practice: sealing variable gaps; seating seals at cryogenic temperatures; fabricating large seals using bonded joints; and requiring the seal material to remain elastic at cryogenic temperature. These factors are summarized in figure 9.

The current practice in sealing gaps would be to eliminate them through mechanical design and allow "a few thousandths" lift-off in the case of a flange due to pressure. In the NTF, structural design considerations require gaps between adjacent tunnel sections that vary from 0 to 0.23 cm (0.090 in.) to prevent overstressing the structure due to the thermal cycle.

Another major departure is the requirement that the NTF seals be capable of reseating at cryogenic temperatures. This is due to moving the contraction and high speed diffuser to seal off the test section with gate valves, figure 1, to allow access to the test model without purging the entire tunnel circuit.

The fabrication of large seals from polymers requires bonded joints because: (1) the size of some of the NTF seals is much larger than available sizes (figure 10); (2) the fabrication ability and/or experience to extrude large cross section shapes of suitable quality are inadequate; and (3) the NTF requirement to install the seals in the field (figure 10).

The final major departure from past practice is the requirement that the seal material must elongate approximately 1% at cryogenic temperatures. Normal design practices would be to allow clearance in the seal groove and to use a compatible material for the seal carrier and sealing surface to prevent restricting contraction of the seal. In the NTF, selection of materials was made from overriding structural considerations. The resulting difference in material contraction from room temperature to 97 K (175° R) is illustrated in figure 11. The NTF seal carriers and sealing surfaces are made of three different materials: Invar, aluminum, and 300 series stainless steel. The spring used to activate the seals is made of 302 stainless steel. The seal material will be either FEP, TFE, or UHMWPE. The effect of the different coefficients of linear thermal expansion for the large 4.3 m (14 ft.) diameter seal is shown in figure 11. One example of the problem with these different materials is that the 302 stainless steel spring will contract by 4.1 cm

(1.6 in.) in circumferential length while the seal cover of TFE will contract 27.7 cm (10.9 in.). This means that the seal cover will become loaded as it contracts around the spring. In small seals this problem can be eliminated by providing radial clearance between the base of the seal cover and the spring; whereas, in large seals, this solution becomes impractical. A similar set of circumstances exists for radial seals. The only practical solution is to require the seal material to exhibit elastic properties at the cryogenic temperatures.

Results

The previous evaluation of current design practice for the NTF seals has resulted in several areas where existing data and analysis techniques were not sufficient to design the seals. These areas have been identified as test requirements and a test program is underway to evaluate alternative designs.

One of the fundamental requirements was to develop a method to fabricate the large seals in segments and still achieve adequate structural strength and elongation in the joints. Figure 12 illustrates two types of joints that were tested. The results at 294 K (530° R) and 97 K (175° R) are presented in figures 13 and 14. The scarf joint performed better than the lap joint; moreover, at cryogenic temperatures the scarf joint performed as well as a test specimen without a joint. The method of joining is described in the appendix. Performance tests, using the test apparatus illustrated in figure 15, are planned to evaluate the leak rate of seals with a scarf joint and without a joint. This fixture is capable of testing either one or two seals at the pressures and temperatures required by the NTF.

In order to summarize the test data, one of the test seals is designated the "baseline" for comparison of test parameters. The baseline seal performance and test parameters are described in figure 16. The terms "gap" and "fit in gland" are used to describe two test parameters. The "gap" is the standoff that exists between the two sealing surfaces, figure 17. The fit is either "loose" or "tight" based on the relationship of the seal to the inside surface of the groove, figure 17.

The baseline seal performance is plotted in figure 18 and shows the measured leak rate at a chamber temperature of 294 K (530°R). The three curves represent 3 test cycles for 2 different seal installations. No attempt has been made to isolate the parameter(s) contributing to the variation of leak rate for the 3 tests since satisfactory seal performance was achieved. The pressure activation design feature of the "U" cross section seals is responsible for the reduction in leak rate as the pressure is increased.

The results of testing to date is summarized in figure 19. The "baseline" seal leak rate of 262 cc/min. (16 cu in/min.) at ambient temperature is equated to unity for comparison with other test data. The seal performance for the different test variables is listed. For example, the baseline seal leak rate at cryogenic temperature is 33 times the leak rate of the baseline seal at ambient temperature. The results are being used to identify additional tests and to evaluate the seal design.

CONCLUDING REMARKS

The development status of large seals that will be used in the cryogenic environment of the National Transonic Facility (NTF) can be summarized as follows:

- Seals with a "U" shape cross section have been selected since the performance can be improved by use of both spring and pressure activation.

- The large seals can be fabricated segments from a polymer material and the segments assembled using bonded joints.

- Either polytetrafluoroethylene (TFE) or tetrafluoroethylene-hexafluoropropylene (FEP) will satisfy the design requirements of leak rate and elongation at cryogenic temperatures.

- The polymer materials that were tested experienced little or no permanent shrinkage due to thermal cycling.

- The seal design will utilize a tight fit in the seal groove to improve the performance.

- Sealing surfaces with 0.8 μm RMS (32 μ in. RMS) finish have provided acceptable performance.

- Treatment of the sealing surfaces with FEP or TFE adhesive backed tapes or lubricants has the potential of improving performance.

- Static "gaps" up to 0.16 cm (0.064 in.) can be sealed by the "U" cross section spring activated seal.

The current test program in progress is designed to establish seal performance and design requirements in these areas:

- Ability to seat at cryogenic temperatures
- Effect of lubricants on performance
- Ability to seal variable gaps
- Performance of radial seals
- Performance of bonded joints

APPENDIX

NTF SEAL BONDED JOINT

Material

1. TFE or FEP Seal
2. TFE Pressure Sensitive Tape
3. Freon Cleaning Agent, manufactured by E. I. duPont de Nemours & Company, Inc.
4. Tetra-Etch manufactured by W. L. Gore & Associates, Inc.
5. Methyl Ethyl Ketone (MEK)
6. Detergent
7. EA 934 Structural Adhesive, manufactured by Hysol Division, The Dexter Corporation
8. Bonding Fixture

Bonding Procedure

1. Clean area to be bonded with MEK and then Freon.
2. Mask around areas to be bonded with TFE tape. All areas to be bonded must be free of masking.
3. Clean bonding area again with a lint free wiper dampened with Freon.
4. Etch per manufacturer's procedure.
5. Clean all surfaces in contact with etchant using each of the following: (a) MEK, (b) Freon, (c) Detergent, (d) Running Water, (e) Freon. Remove masking.
6. Protect etched surface from contamination and keep undisturbed for one (1) hour minimum before bonding.
7. Mix EA 934 adhesive as per manufacturer's instruction. Apply enough mixed adhesive to all etched faying surfaces to ensure fill out of bond line with a minimum amount of squeeze out.
8. Assemble and clamp in bonding fixture. Cure at room temperature overnight or a minimum of 16 hours. Remove from fixture and clean up.
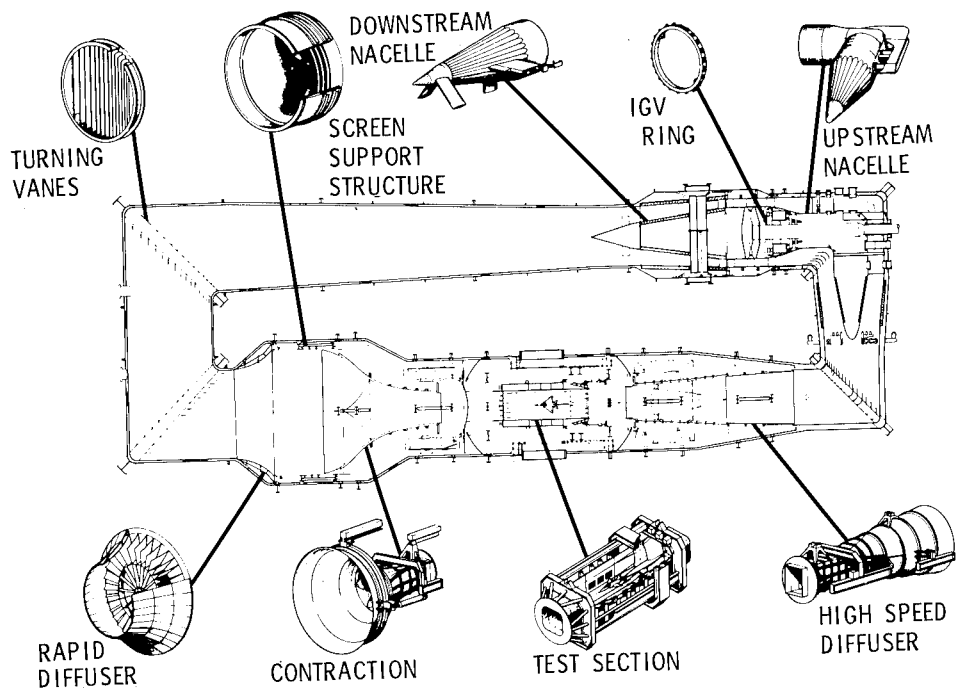
Figure 1.- Internal structures of National Transonic Facility.
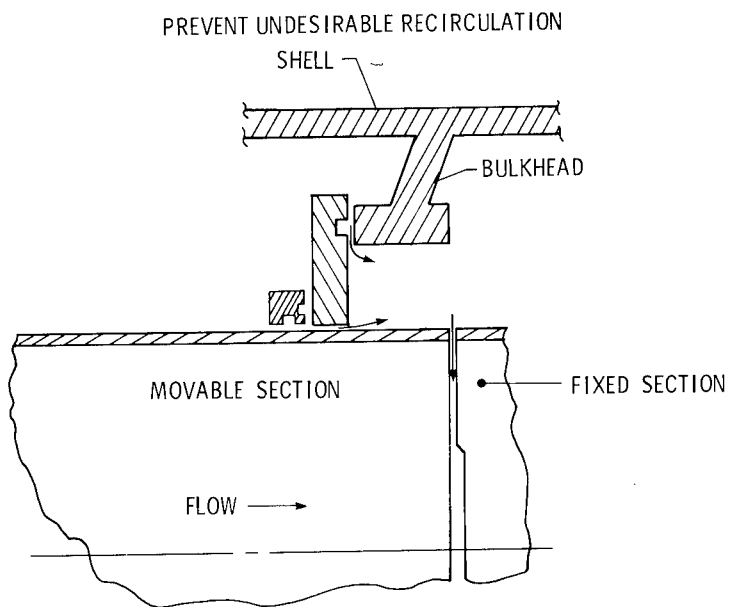
Figure 2.- Function of seals at
contraction section.
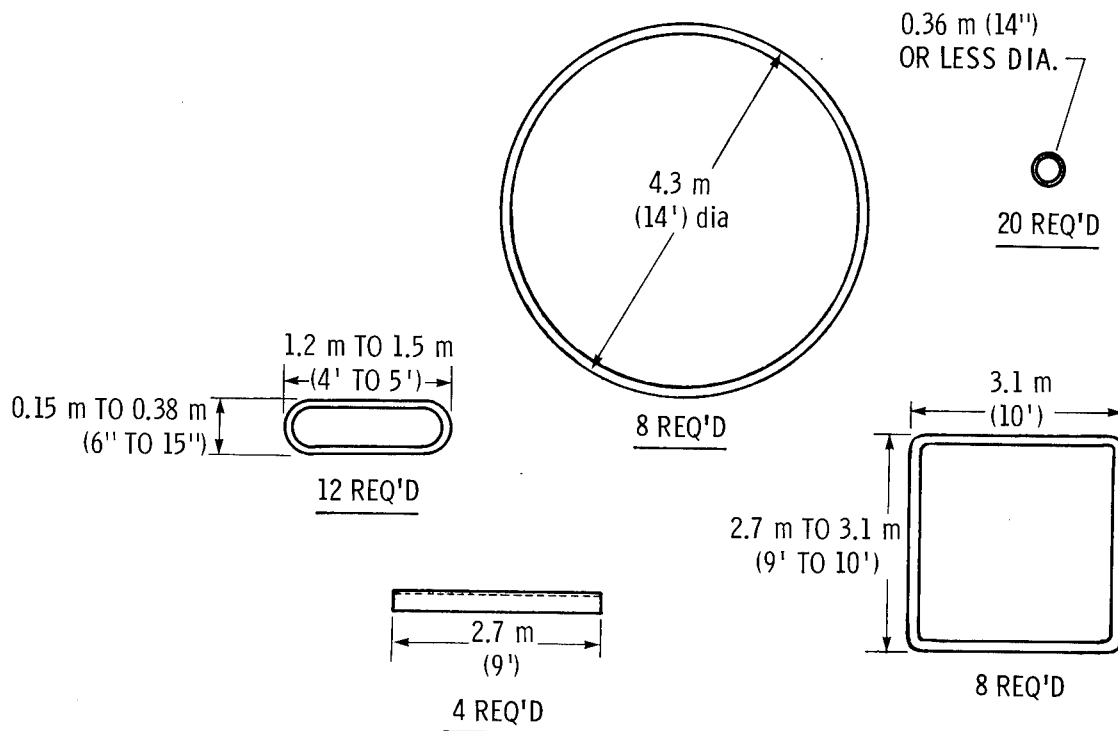
Figure 3.- Size and shape of NTF seals.

- AREAS WHERE CURRENT TECHNOLOGY IS ADEQUATE
  (1) MATERIAL
  (2) SEAL TYPE/CROSS SECTION DETAILS
  (3) SEAL GROOVE DESIGN
  (4) SPRING ACTIVATED

- AREAS REQUIRING SLIGHT DEPARTURE FROM PAST PRACTICE
  (1) SURFACE FINISH VS. FLUID
  (2) MATERIAL FOR SEALING SURFACES
  (3) SEAL RETAINERS

- AREAS REQUIRING MAJOR DEPARTURE FROM PAST PRACTICE
  (1) VARIABLE GAPS DUE TO THERMAL CONTRACTION
  (2) UNSEATING AND RESEATING SEALS AT CRYOGENIC TEMPERATURES
  (3) SEALS WITH BONDED JOINTS
  (4) DESIGN REQUIRES SEAL ELONGATION AT CRYOGENIC TEMPERATURES

Figure 4.- Factors in seal design.
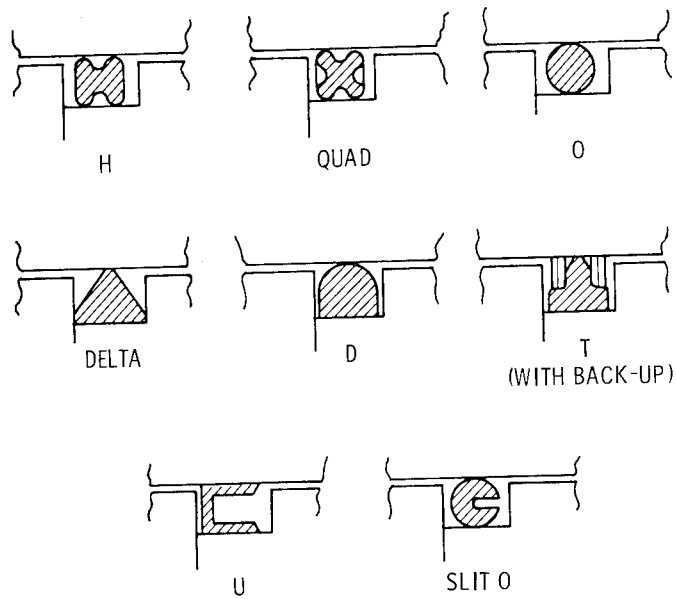
Figure 5.- Typical seal cross sections.

PRESSURE ACTIVATED   SPRING ACTIVATED
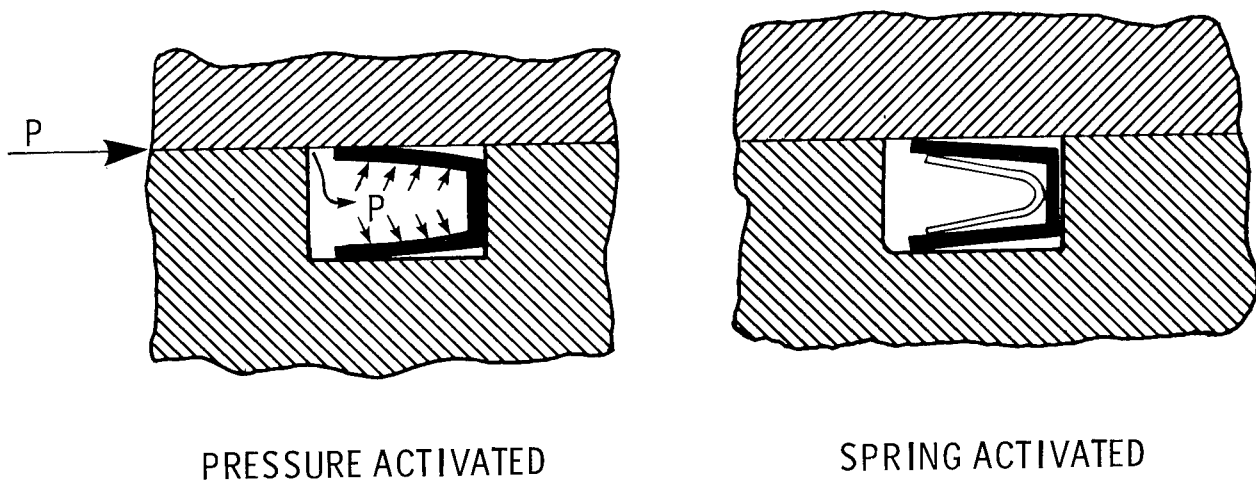
Figure 6.- "U" seal.
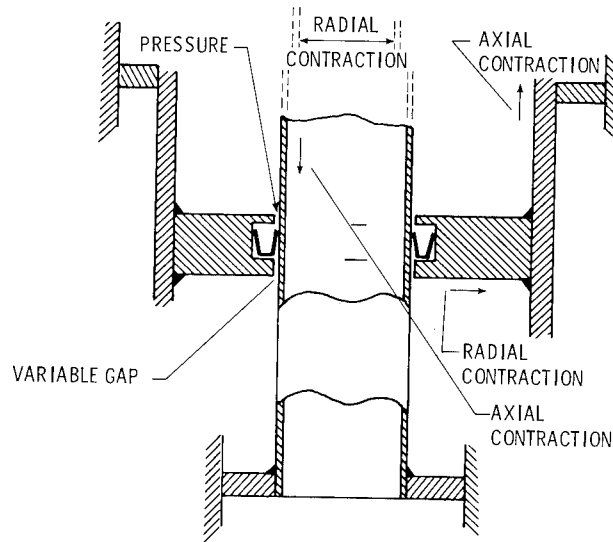
Figure 7.- Illustration of variable gap
due to thermal contraction.

AREA	USED IN PAST DESIGNS	NTF DESIGN	PARAMETERS INFLUENCING SELECTION
SURFACE FINISH	RANGE 0.3 TO 0.8 µm RMS (12 TO 32 µin. RMS) - 0.4 µm RMS (16 µin. RMS) RECOMMENDED	32 RMS	COST TO PROVIDE FOR LARGE SURFACE AREA
MATERIAL FOR SEALING SURFACE	HARDENED STEEL- CHROME OR NICKEL PLATED IS RECOMMENDED	ALUMINUM ALLOYS STAINLESS STEEL INVAR	STRUCTURAL DESIGN CONSIDERATION DUE TO CRYOGENIC ENVIRONMENT
SEAL RETAINERS	KEEPS SEALS IN GROOVES DURING INSTALLATION	KEEP SEALS IN GROOVES DURING REMOTE REPOSITIONING OF SEALING SURFACES	OPERATIONAL REQUIREMENTS

Figure 8.- Departures from past design practice.

AREA	USED IN PAST DESIGNS	NTF DESIGN	PARAMETERS INFLUENCING SELECTION
VARIABLE GAPS	"A FEW THOUSANDTHS" LIFT OFF OF FLANGE DUE TO PRESSURE	0.00 cm (0.000') TO 0.23 cm (0.090')	STRUCTURAL DESIGN CONSIDERATION DUE TO CRYOGENIC ENVIRONMENT
RESEATING SEALS @ CRYOGENIC TEMPERATURE	INITIAL SEATING @ AMBIENT TEMPERATURE	RESEATING REQUIRED SEVERAL TIMES EACH DAY	OPERATIONAL REQUIREMENTS TO CHANGE SEATING SURFACES @ CRYOGENIC TEMPERATURE
SEALS WITH BONDED JOINTS	LITERATURE INDICATES TFE & FEP CAN BE BONDED OR WELDED; NO KNOWN DATA ON TYPE OF JOINT OR PROPERTIES	BONDED JOINT	INSTALLATION REQUIRES A FIELD JOINT IN SEVERAL LOCATIONS SIZES OF TFE AND FEP STOCK REQUIRE THE SEAL TO BE IN SEGMENTS
SEAL ELONGATION	RADIAL CLEARANCE BETWEEN SPRING & SEAL/GLAND. SPRING DESIGN TO MECHANICALLY ACCOMMODATE SHRINKAGE OF SEAL COVER	SPRING DESIGN SEAL ELONGATION RADIAL CLEARANCE	RADIAL CLEARANCES IS NOT EFFECTIVE ON LARGE DIAMETER SEALS.

Figure 9.- Major departures from past design practice.

A-A

SPLIT SEAL & SEAL-CARRIER

4.3 m
(14' dia)

A   A

1.2 m × 1.2 m
(4' × 4') - STOCK
SHEET SIZE

MATERIAL AVAILABILITY

INSTALLATION REQUIREMENTS
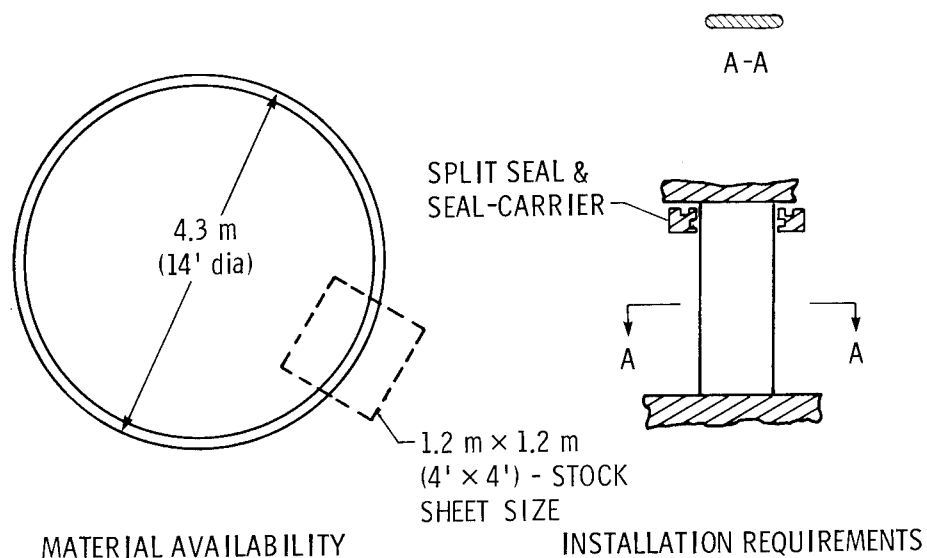
Figure 10.- Bonded joints.

NTF PARTS	MATERIAL	COEFFICIENT OF THERMAL EXPANSION	CONTRACTION FOR A 4.3m (14') DIAMETER SEAL 297 K TO 97 K (535 °R TO 175 °R)
SEAL CARRIERS	INVAR	7.2×10^{-7} m/m/°C $(1.3 \times 10^{-6}$ in./in./°F)	0.61 centimeters (0.24 inches)
SEALING SURFACES	ALUMINUM	6.1×10^{-6} m/m/°C $(10.9 \times 10^{-6}$ in./in.°F)	5.3 centimeters (2.1 inches)
SPRINGS	300 SERIES ST. STL.	4.5×10^{-6} m/m/°C $(8.1 \times 10^{-6}$ in./in./°F)	4.1 centimeters (1.6 inches)
SEALS	FEP	2.4×10^{-5} m/m/°C $(42.9 \times 10^{-6}$ in./in./°F)	21.1 centimeters (8.3 inches)
	TFE	3.1×10^{-5} m/m/°C) $(56.3 \times 10^{-6}$ in./in./°F)	27.7 centimeters (10.9 inches)

Figure 11.- Contraction of materials.

TEST SPECIMEN WITH SCARF JOINT

TYPICAL CROSS SECTION

LAP JOINT
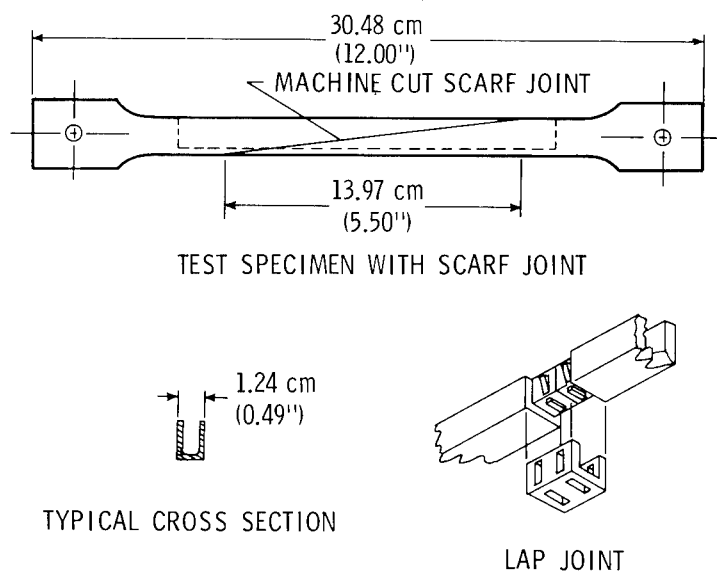
Figure 12.- Two types of seal joints tested
for strength and elongation.
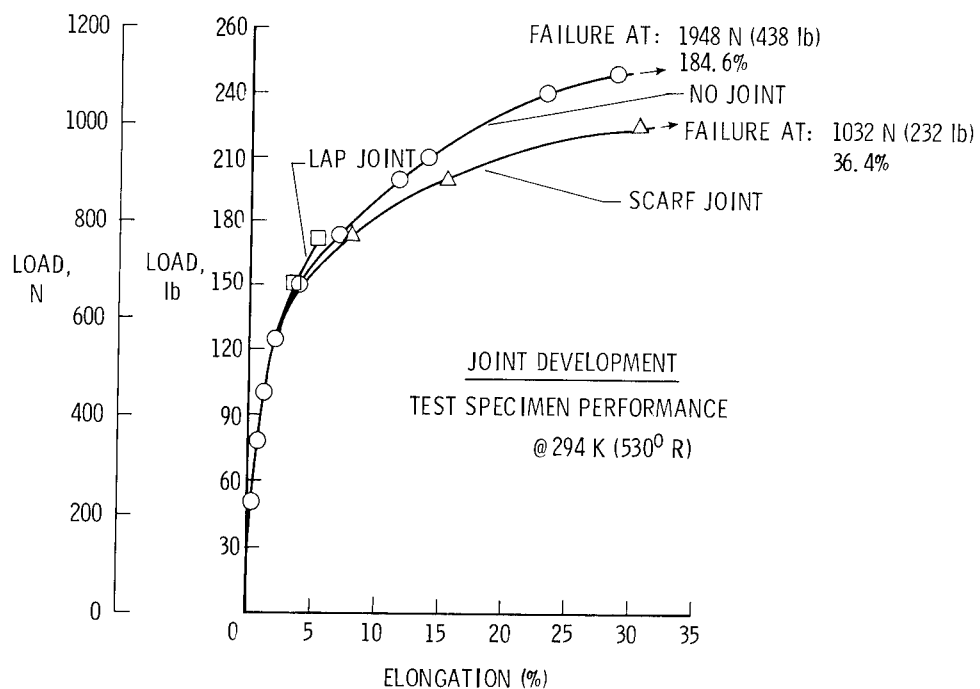
Figure 13.- Strength and elongation test at ambient temperature.
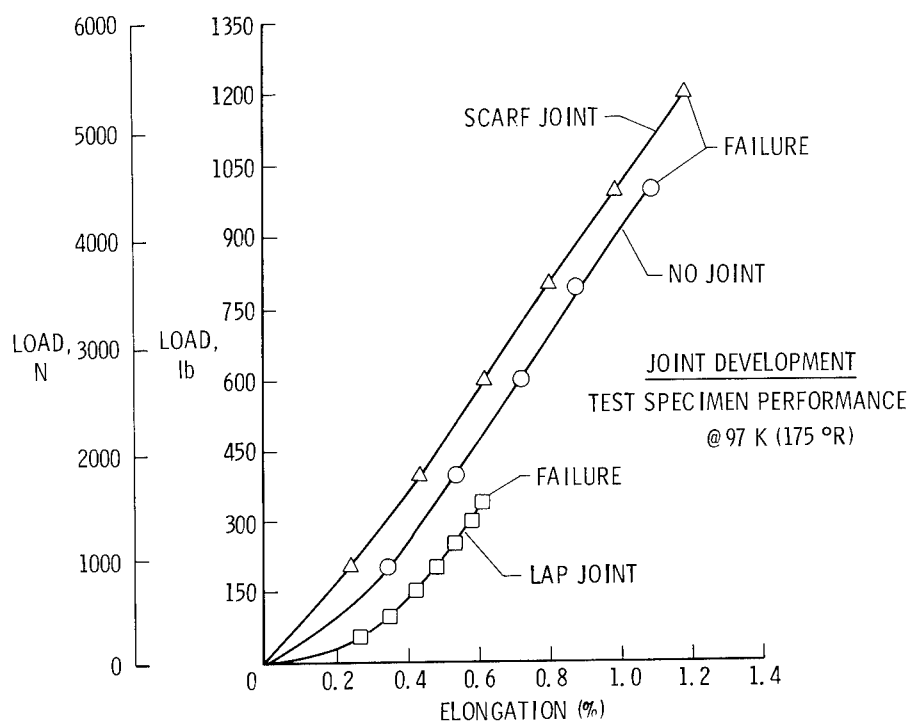
Figure 14.- Strength and elongation test at
cryogenic temperature.
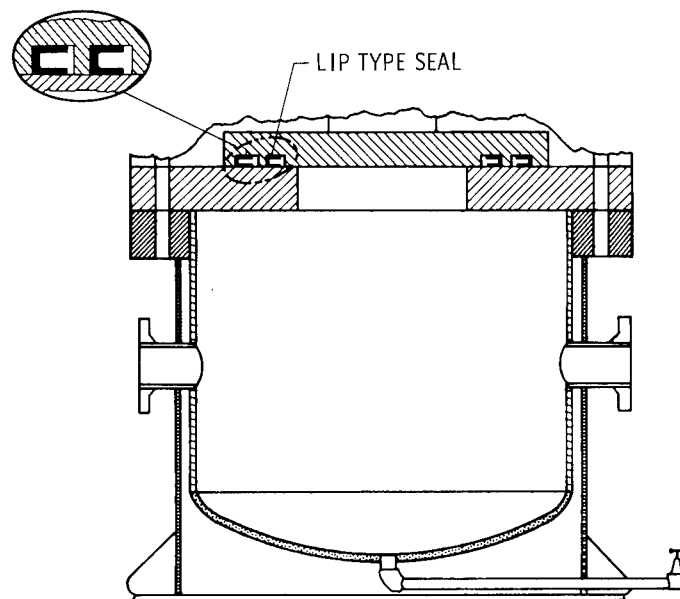
Figure 15.- Leak test apparatus for face-type seals.

SEAL						
TYPE	MATERIAL	SPRING	GAP (LIFT OFF)	FIT IN GLAND	DIAMETER	CROSS SECTION
U-RING	TFE	7000 N/m (40 lb/in.) (OF CIRCUM-FERENCE)	NONE	LOOSE	73.5 cm (28.92 in.)	1.3 cm (0.5 in.)

HARDWARE		
SEALING SURFACE	FINISH	LUBRICATION
STAINLESS STEEL	0.8 μm RMS (32 μin. RMS)	NONE

ENVIRONMENT	
TEMPERATURE	PRESSURE
AMBIENT	690 kPa (100 psig)

CRITERIA
MAXIMUM LEAK RATE cc/min (cu in./min)
16 390 (1000)

PERFORMANCE
MEASURED LEAK RATE cc/min (cu in./min)
262 (16)

Figure 16.- Performance and test parameters of
baseline test seal.
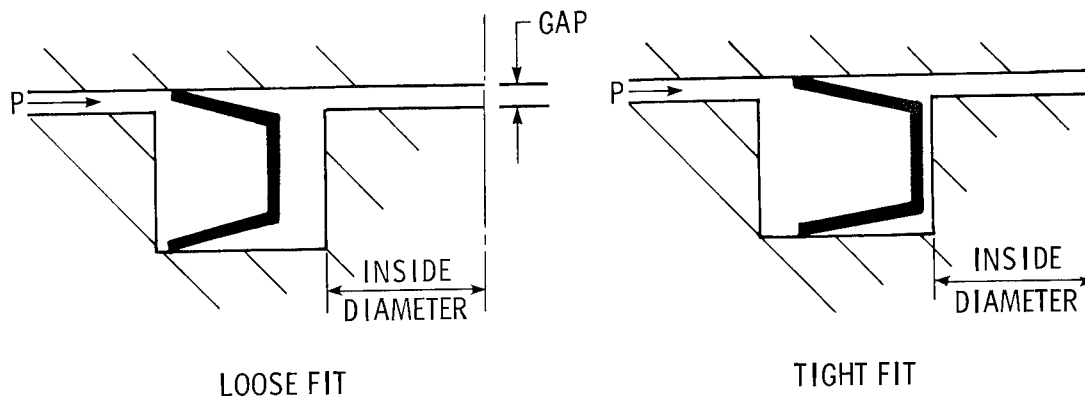
Figure 17.- Illustration of gap and fit.

CURVE NO.	PRESS. CYCLE NO.	INSTALLATION NO.
1	1ST	1ST
2	2ND	1ST
3	1ST	2ND
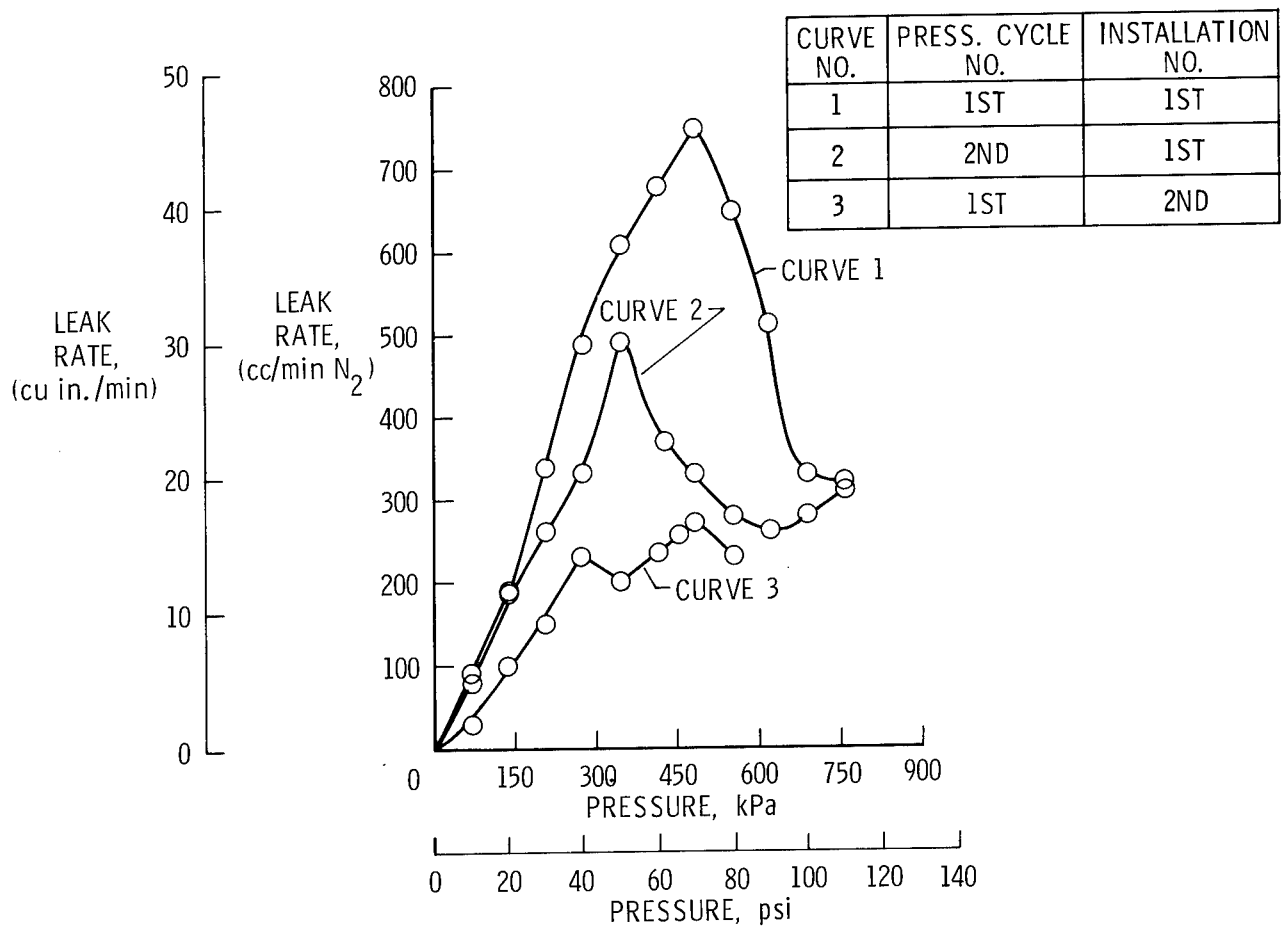
Figure 18.- Performance of baseline seal.

TEST VARIABLES	LEAK RATE (cc/min)	
	AMBIENT	CRYOGENIC
BASELINE	1.0	33.0
VARIABLES:		
FEP	1.0	23.0
17500 N/m (100 lb/in.) SPRING/NEW CROSS SECTION	0.4	2.0
TAPE ON SEALING SURFACE:		
TYPE I	0.7	1.0
TYPE II	1.5	1.9
TIGHT FIT	0.3	9.8
GAPS:		
0.05 cm (0.020")	1.2	16.0
0.09 cm (0.036")	0.7	8.5
0.16 cm (0.064")	1.4	44.0
PRESSURE kPa (psi)		
138 (20)	0.6	7.3
276 (40)	1.2	11.5
414 (60)	1.4	16.0
552 (80)	1.1	28.5

Figure 19.- Summary of seal performance versus hardware
and environment variables.

DESIGN OF COMPRESSOR FAN DISKS FOR LARGE

CRYOGENIC WIND TUNNELS

Robert T. Wingate
Langley Research Center

SUMMARY

A number of general practical design considerations in the design of a large fan disk for a transient cryogenic environment arose out of the National Transonic Facility (NTF) fan disk design studies. Highlights of these considerations including design philosophy and factors influencing the geometry or external profile are discussed. Specific features of the NTF fan disk design are also presented as an example of a compromise design resulting from tradeoffs between these competing factors.

INTRODUCTION

Pressurized cryogenic wind tunnels can be designed to operate over a broad evelope of Mach and Reynolds numbers by varying the compressor fan speed in conjunction with the tunnel temperature and static pressure (ref. 1). Test programs which traverse the operating envelope subject the tunnel to a changing thermal environment. This cold, thermally transient mode of operation makes the mechanical design of cryogenic wind tunnels considerably more complicated than that of more conventional wind tunnels.

The purpose of this paper is to highlight some of the practical design considerations for one critical component of a large cryogenic wind tunnel — the compressor fan disk. The information presented herein resulted from design of the fan disk for the National Transonic Facility (NTF) shown in figure 1.

Basic design and analysis methods for compressor or turbine disks are well documented (e.g. refs. 2 and 3). In a new application, such as a cryogenic wind tunnel, practical limitations can overshadow, or at least temper, a purely analytical design approach. The NTF will be the first large cryogenic wind tunnel and the experience gained in its design should prove useful in future designs.

This paper presents some of the design philosophy and tradeoffs which must be considered in designing a disk which is properly stressed, yet practical to fabricate. A number of factors including safety, thermal stresses, manufacturing limitations, and non-destructive examination methods are shown to be significant design considerations in selection of materials and profile

geometry. The NTF disk was built from 9% Nickel steel and some of the pertinent fabrication data are presented as an illustrative example of a cryogenic disk design.

DESIGN PHILOSOPHY

Rupture of a fan disk in a large pressurized cryogenic wind tunnel could be catastrophic to adjacent personnel and property. A large fan disk rotating at a high speeds contains considerable kinetic energy. A disk burst could rupture the pressure vessel and release a large volume of pressurized cryogenic nitrogen (the gas medium for cryo tunnels). Upon release, cold nitrogen gas can displace air and suffocate personnel while high overpressure can blow out windows and structurally damage adjacent buildings. Since it is difficult, if not impossible, to design a pressure vessel to contain a large disk burst, extreme care must be taken in design and operation to eliminate this as a credible mode of failure. Consequently, the following design philosophy is recommended:

(1) Design for a forging and not a casting.

(2) Select a high strength material with good fracture toughness at cryogenic temperatures.

(3) Select a conservative design stress.

(4) Perform thorough stress, vibration, fatigue, and fracture mechanics analyses.

(5) Design to accommodate a flaw large enough to be easily detected by non-destructive examination (NDE).

(6) Perform NDE to insure actual flaws do not exceed design size.

(7) Test samples of actual material to verify "as built" mechanical properties.

(8) Spin test to maximum expected in-service speed.

(9) Develop a fracture control plan and perform periodic in-service inspections.

Amplification of these design considerations is discussed in the following.

Forgings or Castings

The recommendation of forgings over castings stems from the susceptibility of castings to inclusions, voids, and cooling cracks. These imperfections can be more closely controlled in forgings. Rotating parts are subject

158

to cyclic loads and castings, because of their imperfections, are much more likely to fail in fatigue.

Cryogenic Materials

Charpy V-notch impact strength is a simple, easily obtained discriminator for screening candidate metals for "cryogenic" applications. A criterion that the Charpy V-notch shall not be less than 34 J at service temperature is given in Supplementary Requirement S9 of ASTM A-522, "Forged or Rolled 9 Percent Nickel Alloy Steel Flanges, Fittings, Valves, and Parts for Low Temperature Service." This same criterion is a useful rule-of-thumb for selection of any cryogenic material. Ultimately the selection of a metal for cryogenic service should be based on its fatigue and fracture toughness properties. Experience has indicated, however, that metals which meet the stated impact strength criterion generally have acceptable fatigue and fracture toughness properties.

High tensile strength is another desirable characteristic of cryogenic fan disk materials. Unfortunately, most high strength metals ($\sigma_y > 689$ MN/m^2) will not meet the impact toughness criteria. Aluminums have good toughness, but low strength. Austenitic stainless steels, although expensive, also have good toughness and are available in a higher range of strengths.

Typical mechanical properties of some candidate "cryogenic" steels are shown in table 1. Of this list, only 304 stainless (the lowest strength steel) has been widely manufactured in large sizes. This lack of experience in forging and heat treating other cryogenic steels makes most potential vendors reluctant to undertake manufacture of a large disk with guaranteed mechanical properties. A metallurgical development program is, thus, a likely precursor to the manufacture of any large "cryogenic" disk.

Design Stress

The most important factor in preventing a disk burst, or other type of failure, is limiting the magnitude of the design stresses. The most catastrophic disk bursts result from high tangential stresses induced by centrifugal force. This type of failure results when a high tangential stress point on the disk yields and transfers the load to the remaining portions of the disk. This process continues until the entire disk has yielded and reached ultimate strength. At this point any increase in tangential stress will cause the disk to burst or fracture along a diametrical plane.

The burst speed is defined as the speed at which the average tangential stress becomes equal to a factor k times the ultimate tensile strength σ_u of the material. The factor k has been found to range from .75 to 1.0 depending on the notch sensitivity of the material. The burst margin, which is

defined as the ratio of the burst speed N_B to the design speed N_D, is given in reference 3 as

$$\text{Burst Margin} = \frac{N_B}{N_D} = \sqrt{\frac{.75\ \sigma_u}{\sigma_{avg}}} \qquad (1)$$

where σ_{avg} is the average tangential stress in the disk at design speed and the factor k has been taken conservatively to be .75.

Typical design burst margins are 1.3 for aircraft jet engines and 1.9 for large steam turbines. Disk bursts are not uncommon in jet engines but are rare in steam turbines. Consequently, the recommended design burst margin for cryogenic tunnel disks is in the range of 2-3.

Radial disk burst in which the disk fractures along a circumferential plane due to high radial stresses can also occur. The best means for avoiding this mode of failure is to keep the radial stresses below the average tangential stress and well below the ultimate stress.

The burst margin criteria can normally be met by adhering to the following design criterion on stress:

$$\sigma_D = \text{minimum } [2/3\ \sigma_y,\ 1/3\ \sigma_u] \qquad (2)$$

where σ_D is the design stress, σ_y is the yield stress, and σ_u is the ultimate stress. The design stress σ_D is a peak combined stress which includes stress concentrations and thermal stresses.

By limiting the peak stress to the value of equation (2), it is seen from equation (1) that the burst margin is greater than 1.5 assuming that the average stress is equal to the design stress. In practice the average stress is generally less than 1/2 the peak stress so burst margins greater than 2.1 (in the recommended range) typically result from the criterion of equation (2).

Since most steels have an endurance limit (σ_e) greater than $1/2\ \sigma_u$, the criterion of equation (2) also yields

$$\sigma_D < 2/3 \, \sigma_e$$

which indicates a high cyclic life design.

Allowable Flaw Size

The allowable flaw size in a disk is second in importance only to design stress is designing for long life. Selection of the allowable flaw size cannot be made strictly from a fracture mechanics analysis without considering the resolution ability of ultrasonic testing to detect an imbedded flaw in the material. The allowable flaw should be large enough that an imbedded flaw 1/2 to 1/4 the allowable size can be detected. This allows a large margin of error in inspecting the disk for manufacturing flaws.

The detectable flaw size is sensitive to material and heat treatment because of grain and other microstructure characteristics. This detectable size is best established by ultrasonically testing a specimen of the required depth having calibrated flaws machined into the back surface as shown in figure 2. It is important that the through-the-depth heat treatment be representative of the disk.

After establishing a tentative allowable flaw size from NDE requirements, it should be evaluated by a fracture mechanics analysis. This is to insure that an allowable flaw in the worst possible location (shortest time to failure) would grow to the surface before growing to critical size. This is analogous to the leak before failure condition in pressure vessels. It should also take a "reasonable" interval of time for the crack to become critical after appearing at the surfaces. If these conditions are not met a different material or design should be chosen.

Non-Destructive Examination

A surface NDE method such as dye penetrant or magnetic particle should be combined with ultrasonic testing to insure that all disk flaws are initially below the allowable flaw size. Because of the criticality of this operation and its susceptibility to operator error or interpretation, these tests should be performed under strict quality control conditions and in accordance with accepted standards.

Mechanical Property Tests

Mechanical property tests of the disk in the "as-built" condition are recommended to verify design stress and life predictions. The test specimens should be removed from prolongations in the critical stress regions, where possible.

161

Three types of tests are useful - tensile strength, impact strength, and fracture toughness. The first two are normally done as part of the forging acceptance criteria. Specimen sizes and methods of performing the tests are given in applicable ASTM or other standards. Fracture toughness tests are not normally done by manufacturers because of the complexity of the testing and the size and number of specimens required. Also, because of the relatively wide variation in fracture toughness data with slight changes in heat treatment, manufacturers are reluctant to guarantee fracture toughness properties.

Spin Test

A spin test to maximum expected in-service speed provides the designer with added confidence that nothing gross has been overlooked in design or NDE. A requirement to spin the disk above the expected speed does not necessarily increase the confidence in the disk design. In fact it may decrease it. A crack that was an acceptable size before an overspeed test may grow to an unacceptable size during the test and lead to a decreased life.

Fracture Control Plan

Periodic in-service NDE of a disk for surface cracks allows simple detection of a flawed disk, which can be removed from service before a catastrophic failure. The inspection interval should be somewhat shorter than the interval between the appearance of crack at the surface and its growth to failure. This approach has been used successfully in the steam turbine industry for a number of years to prevent disk burst failures.

DESIGN GEOMETRY

Many factors in addition to centrifugal and bending stresses must be considered when designing a disk profile for cryogenic operations. Thermal stresses, manufacturing processes, materials, and non-destructive testing all play an important role.

Thermal Environment

In a cryogenic wind tunnel, the compressor fan blades run in a cryogenic environment and the drive shaft runs in a warm environment — at least in the support bearing region and at the connection to the drive motor (see figure 3-a). A fundamental question in designing the disk is where to make the transition from the cold blades to the warm shaft (i.e. where to take this large thermal gradient). The basic options are

1. Run the disk and shaft warm and take the thermal gradient in the rim of the disk (figure 3-b).

2. Run the disk cold and take the thermal gradient in the shaft (figure 3-c).

Option 1 has the disadvantage of requiring a complex dynamic seal in a high velocity region. Also, high tangential tensile stresses can potentially develop in the rim because the rim tries to contract and the warm center portion of the disk holds the rim back. The main advantage of option 1 is that, outside the disk rim region, thermal stresses are not a design consideration.

Option 2 has the disadvantage that thermal stresses must be considered in the disk design, the shaft design, and the shaft/disk interface. The advantage is that the dynamic seal is in a much lower velocity region and not sensitive to axial motions of the shaft.

The option 2 configuration was selected for the NTF because a venting requirement prevented sealing the disk near the outer rim.

Thermal Stresses

If the disk is housed in a transient cryogenic environment, as in option 2 above, a radial thermal gradient will develop and induce thermal stresses. For example, if a spinning disk is subjected to a cooldown transient environment, the rim region convectively cools much faster than the center portion because of the higher tangential velocity. As the rim region cools, it tries to contract, but is restrained by the warmer center portion. Tensile thermal stresses, thereby, develop in the rim region and compressive thermal stresses in the center region (see figure 4-a). The disadvantage of this stress situation is that the thermal stresses are additive to the centrifugal stresses in the high stress region near the rim where the blades are attached. Stress concentrations in this area can amplify the basic stresses by a factor of 2-3.

Further variations in the radial thermal gradient are caused by the local thickness (or thermal mass) variations. Thick regions have more thermal mass and are slower to cool than thin regions. Hence, added thickness near the center of the disk aggravates the center thermal stresses by further slowing down the cooling rate. Conversely, added thickness near the rim tends to alleviate the rim thermal stresses by slowing down cooling rate.

The designer will find that by judicious choice of local thickness variations, thermal stresses can be developed to partially offset centrifugal stresses. For example, if near the rim, the thickness is flared from thin to thick (see figure 4-b), compressive tangential thermal stresses can be developed in the outer rim to offset the tensile tangential stress due to spin. This is because the thin region cools faster than the thick rim, tries to contract, and is restrained by the warmer rim. The additional thickness also lowers the centrifugal stress in the rim due to the blades. The increased stresses in the thin region of the disk present no problem since they occur away from the stress concentrations of the blade attachment.

The full spectrum of heatup as well as cooldown cases must be investigated to find the best compromise between thermal and centrifugal stresses. In general, it is best to avoid large variation in thickness anywhere, especially near the center.

Heat Treatment

Attainment of proper heat treatment is strongly influenced by the disk geometry. Thick sections undergo nonuniform cooling during quenching or air cooling and tend to have through-the-thickness variations in properties. There is a lack of manufacturer experience in heat treating cryogenic steels in thick (> .13 m) sections so the thickness profile must be selected to be compatible with the proposed heat treatment. In general, the thinner the disk, the better.

Nonuniform cooling during heat treatment also can leave residual thermal stresses locked in the forging. These thermal stresses are additive to in-service stresses and can cause warpage of the forging during finish machining. Stress relieving of forged parts before machining is recommended to minimize these undesirable effects.

Forging Size

The size of a disk forging is directly limited by the size and capacity of forging presses. The distance between the posts on a forging press limits the maximum diameter of the disk. Also, the tonnage of the press and the stiffness of the steel limit the diameter of forging which can be worked by the press.

Most domestic forging presses will accommodate a maximum diameter of about 3.66 m. Somewhat larger presses are available off-shore, particularly in Japan. The manufacturing site is then a necessary consideration when selecting the disk geometry.

Center Hole in Disk

From a disk stress analysis, the tangential stress near the center of a solid disk can be shown to be smaller than the corresponding stress in a disk with a center hole. In fact, if a pin-hole is placed in the center of a solid disk, the tangential stress increases by a factor of two. All things being equal, it would appear that it is desirable to have a solid disk.

In upset forgings, the material at the center of the disk is not worked as much as the surrounding metal. The very center of the disk is, consequently, subject to inclusions and inferior mechanical properties. To eliminate this inferior material in a high stress region, it may be desirable to put a small bore hole in the disk. The addition of a bore hole also allows better heat

164

treatment of the bore region and potential access to the interior of the shaft, if it is hollow.

Shaft/Disk Interface

If the shaft-disk interface is subject to thermal transients, the attachment geometry must be carefully designed to eliminate large thermal stresses. In particular, the conventional tapered shrink-fit method for mounting a shaft to a disk (figure 5-a) is likely to be untenable. A face mounted design (figure 5-b) is much more tolerant to thermal stresses. Whatever method is chosen, the differential centrifugal and thermal growth between the disk and shaft must be minimized to prevent large stresses.

Non-Destructive Examination

Non-destructive examination methods can dictate the size and shape requirements for a rough disk forging. To perform ultrasonic testing, the rough disk forging must first be machined to a smooth constant thickness disk for proper reflection of ultrasonic sound waves. To extract test specimens, this disk must contain excess material or prolongations as shown on figure 6 for the NTF fan disk. Both of these requirements necessitate a larger forging than that required for the basic, finish-machined disk.

APPLICATIONS TO NTF DISK DESIGN

The NTF disk fan design is the result of many design iterations and tradeoffs between the practical considerations discussed earlier. Some of the significant features of the NTF disk are presented in the following.

Material

The NTF disk material was selected to by 9% Nickel steel based on the favorable results of a research program conducted by The Japan Steel Works, Ltd. on forging 9% Nickel in heavy sections (ref. 4 and 5). Japan Steel found that by lowering trace element contents, adding a small amount of molybdenum, and adjusting the heat treatment cooling rates, forgings up to .4 meters thick could be manufactured with good uniform properties through the thickness. Considering that current ASTM specifications for 9% Nickel limit thickness to .13 meters, Japan Steel made a quantum jump in the state-of-the-art for manufacturing 9% Nickel steel in heavy sections.

Configuration

The NTF fan disk (shown in figure 1) is a face-mounted design, which is bolted to a flange on the drive shaft. The bore of the shaft fits over

a shear lip on the disk with a slight interference fit. All torque is transmitted through the attachment bolts and all transverse shear is transmitted through the shear lip. Twenty-five fan blades are each attached around the rim of the disk by a single pin clevis joint. The disk is 3.96 meters in diameter and has a relatively thin uniform thickness profile. A maximum thickness of .25 meters occurs at the shear lip while both the bore and the rim are .2 meters thick.

A photograph of the fan disk configuration as it was machined for ultrasonic inspection is shown on figure 7. This forging was manufactured by Japan Steel under subcontract to General Electric, the NTF drive system contractor. Note the smooth, flat sides. Upon completion of ultrasonic testing, mechanical property test specimens were removed from the rim and bore regions. The disk was then machined to the final configuration shown in figure 8.

The NTF drive shaft shown in figure 9 was also forged from 9% Nickel steel for thermal compatibility with the fan disk. Induction heaters were used to heat the shaft flange region during mating with the disk. The complete mated configuration is shown in figure 10.

As-Built Properties

A comparison between the design and the as-built values is shown in table 2 for several of the more significant design quantities. Since the NTF disk is a fracture controlled design it is of particular significance that both the fracture toughness and the initial flaw size indicate a design life far in excess of that based on the design values. The remaining quantities in the table also show the as-built values to be conservative. Consequently, the NTF fan disk is seen to be an overall ultra-conservative design capable of a long, safe life.

CONCLUDING REMARKS

The design of a large cryogenic disk has been shown to be influenced by many practical considerations which are not necessarily obvious at the outset. Chief among these considerations are materials and manufacturing techniques. Potential thermal stress problems were also discussed along with means for minimizing or avoiding them.

The metallurgical research performed to manufacture the NTF disk has advanced the state-of-the-art in forging 9% Nickel steel in heavy sections. Manufacture of a large fan disk from other cryogenic steels would require a similar research program.

The NTF disk design was shown to be ultra-conservative and capable of a long, safe life.

166

REFERENCES

1. Kilgore, Robert A.: Evolution of the Cryogenic Wind Tunnel and Experience With the Langley 0.3-Meter Transonic Cryogenic Tunnel. Cryogenic Technology, NASA CP-2122, 1980. (Paper 1 of this compilation.)

2. Stodola, A. (L. C. Lowenstein, trans.): Steam and Gas Turbines. Vols. I and II, McGraw-Hill Book Co., Inc., 1927.

3. Sawyer, John W., ed.: Sawyer's Gas Turbine Engineering Handbook, Vol. I, Second ed., Gas Turbine Publications, Inc., 1972.

4. Staff of The Japan Steel Works, Ltd.: Report of Progress of the Investigation for Heavy Section 9% Nickel Steel. PL76-12-324 through 327, The Japan Steel Works, Ltd., Research Laboratory, Muroran, Japan, December 4, 1976.

5. Staff of The Japan Steel Works, Ltd.: Report of Progress of the Study for Heavy Section 9% Nickel Steel (2nd Report), PL77-3-351 through 353, The Japan Steel Works, Ltd., Research Laboratory, Muroran, Japan, April 15, 1977.

TABLE 1. - CANDIDATE CRYOGENIC STEELS
BASED ON IMPACT STRENGTH

STEEL	TENSILE STRENGTH, 294°K		CHARPY V-NOTCH, J AT 78°K
	σ_y, MN/m^2	σ_u, MN/m^2	
17-4 PH (H1150M)	724	931	34
15-5 PH (H1150M)	517	862	34
304N	345	621	79
304	207	483	84
A286	586	896	77
Nitronic 40	345	621	88
9% Ni	517	689	34

TABLE 2. – COMPARISON OF "AS-BUILT" VERSUS DESIGN VALUES
FOR THE NTF FAN DISK

QUANTITY	DESIGN/SPEC. VALUE	AS-BUILT VALUE
Tensile Ultimate Strength at Room Temp.	$689 \ MN/m^2$	$792 \ MN/m^2$
Fracture Toughness at 78°K	$93.4 \ MN/m^{3/2}$	$178 \ MN/m^{3/2}$
Peak Stress	$228 \ MN/m^2$	$214 \ MN/m^2$
Burst Margin	> 2	3
Max. Flaw Size	$.02 \ m$	$<< .005 \ m$
Charpy V-Notch at 78°K	$34 \ J$	$106 \ J$

169
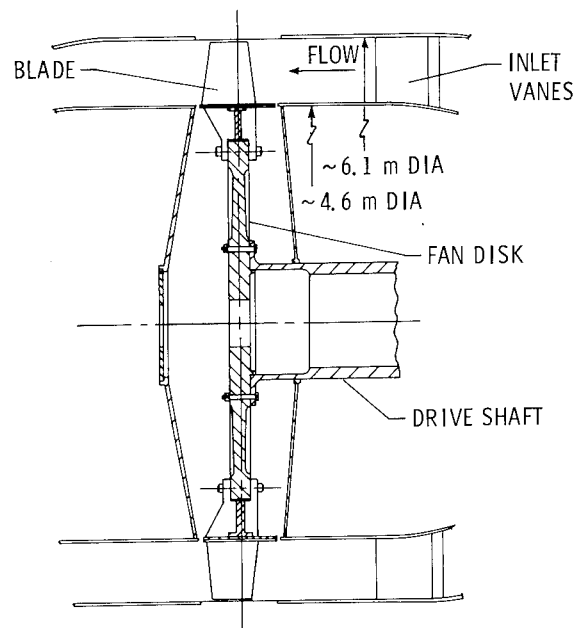
Figure 1.- Cross section of NTF fan region.
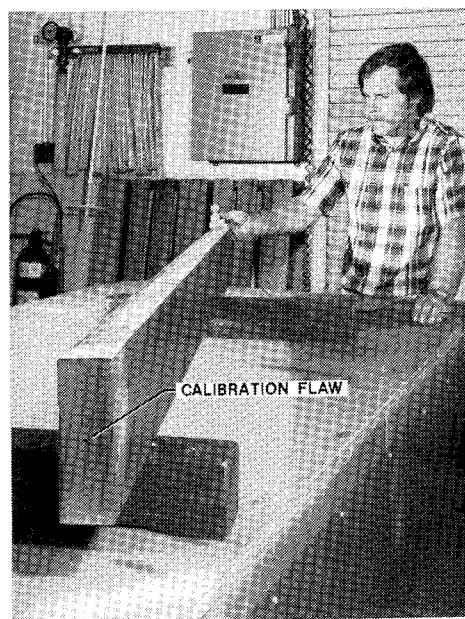
Figure 2.- Determination of detectable flaw size.

COMPRESSOR BLADES**

CRYOGENIC FLOW

DRIVE* MOTOR

BEARINGS*
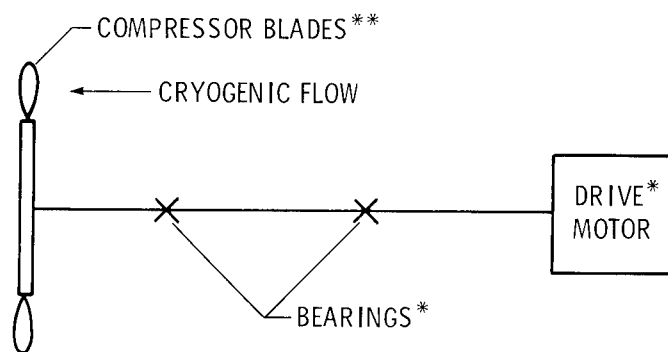
*MUST BE WARM FOR LUBRICATION

**MUST BE COLD BECAUSE OF CRYOGENIC FLOW

(a) Compressor drive thermal constraints.

TUNNEL WALL

CRYOGENIC FLOW

DYNAMIC SEAL*

DRIVE MOTOR

INTERNAL NACELLE

HEATED AREA
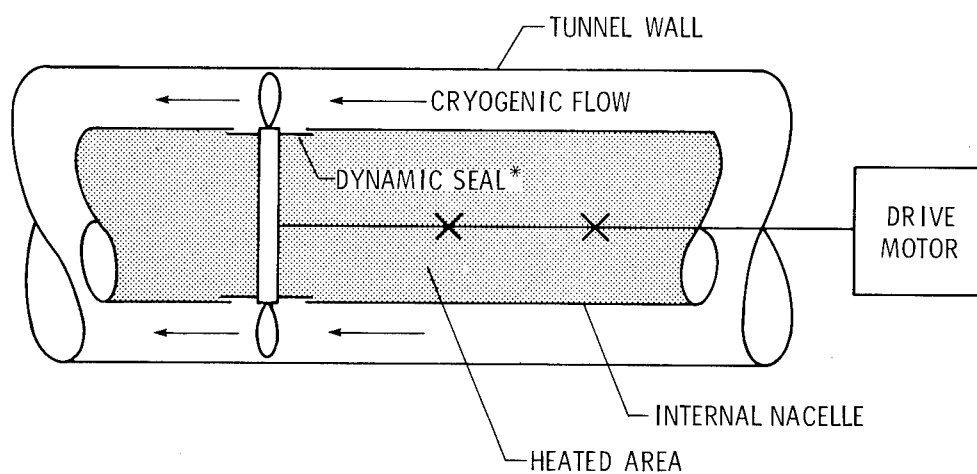
*TO PREVENT HEAT LOSS

(b) Thermal gradient in disk.

Figure 3.- Fan drive system thermal environment.
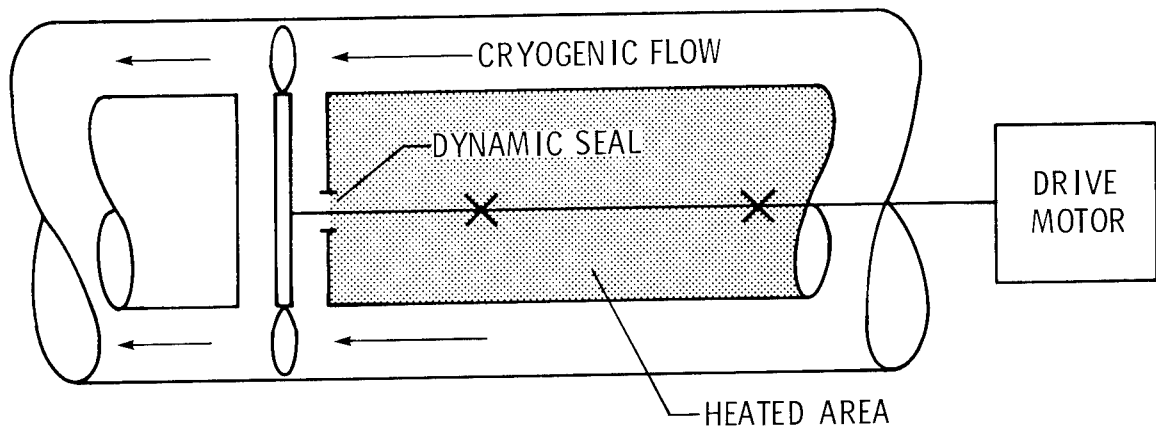
(c) Thermal gradient in drive shaft.

Figure 3.- Concluded.
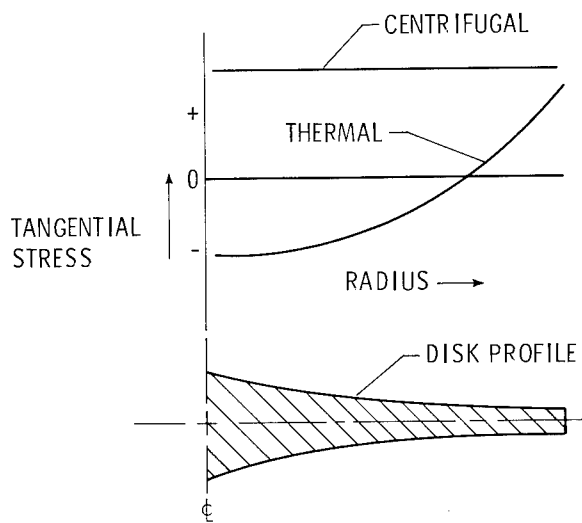
(a) Decreasing thickness profile.
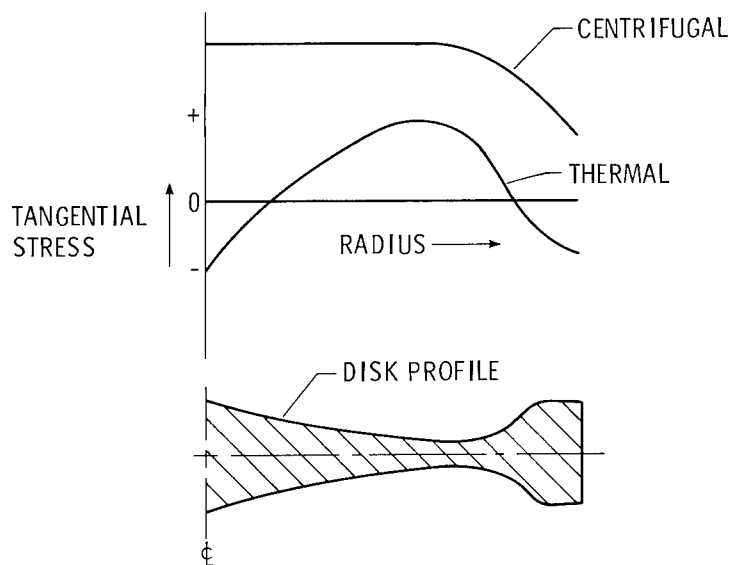
(b) Flared rim profile.

Figure 4.- Effect of thickness profile on thermal cooldown stress in a spinning disk.
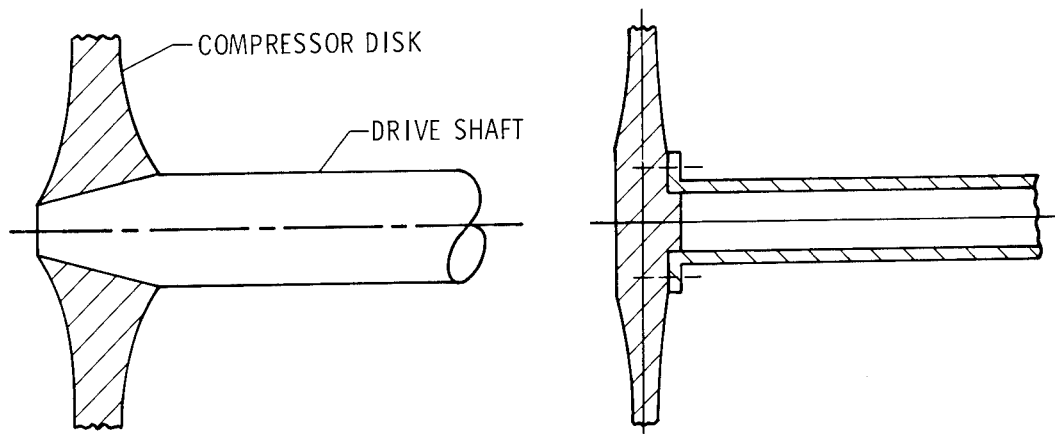
(a) Tapered shrink fit disk attachment.   (b) Face mounted disk attachment.

Figure 5.- Shaft-disk attachment methods.

*CLEARANCES FOR ULTRASONIC INSPECTION
AND TEST SPECIMEN REMOVAL
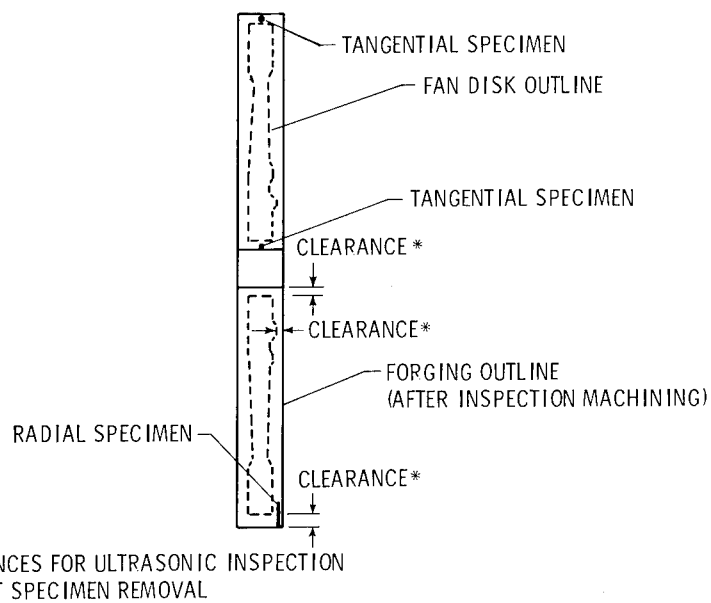
Figure 6.- Forging allowance for ultrasonic inspection and test specimens.

174
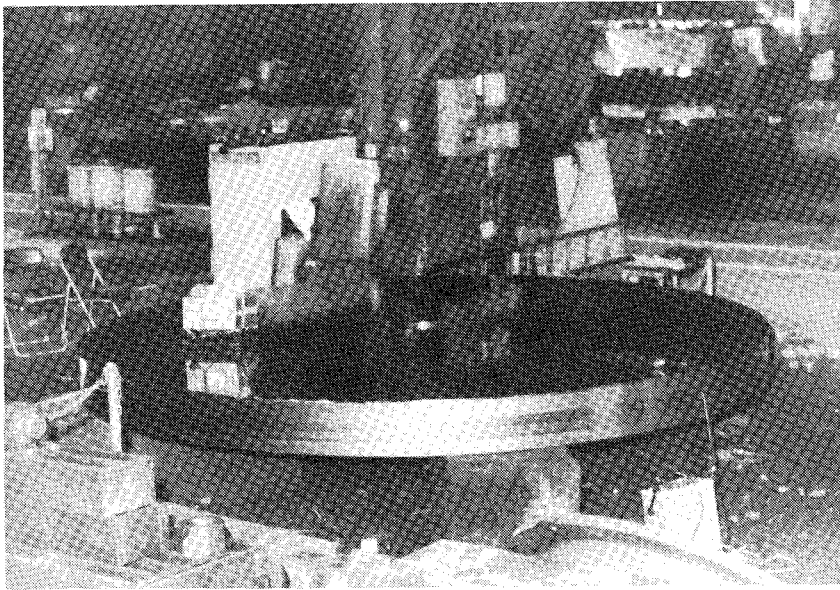
Figure 7.- NTF fan disk machined for ultrasonic inspection.
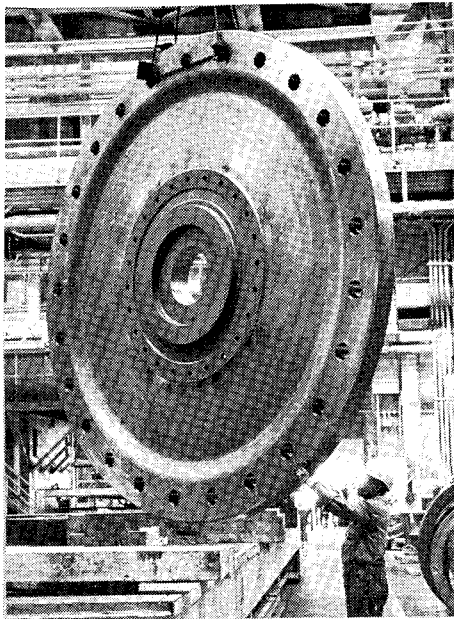
Figure 8.- NTF fan disk.

175
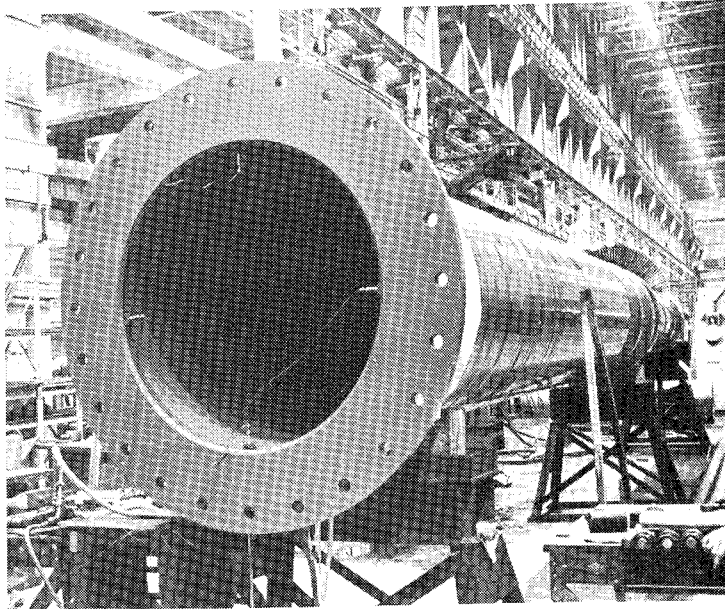
Figure 9.- NTF drive shaft.
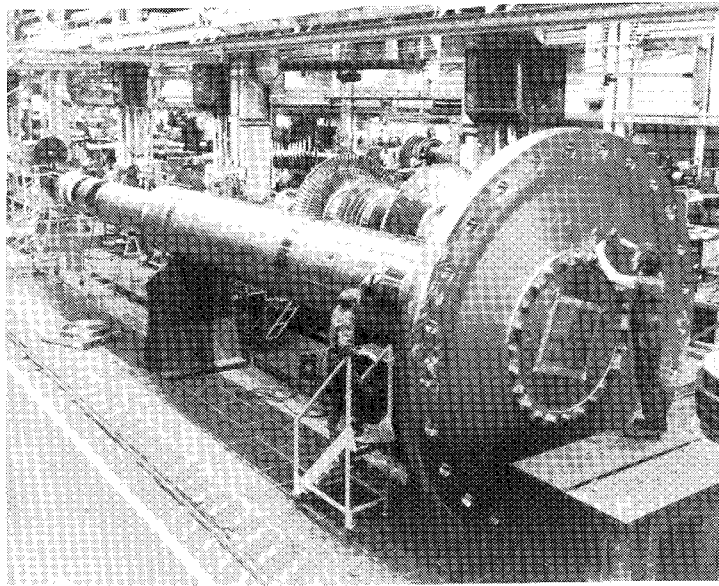
Figure 10.- NTF fan disk mounted on drive shaft.

SESSION III - SYSTEMS DESIGN

SYSTEMS DESIGN SESSION

Walter E. Bruce, Jr.
Langley Research Center

OVERVIEW

The previous paper by Mr. R. R. Howell entitled "Overview of Engineering Design and Operating Capabilities of the National Transonic Facility" presented an overview of the various systems of the tunnel and described the basic operations of each. In this session, the focus will be on the systems designed to control fluids and energy which are affected by the cryogenic test gas and/or the cryogenic operation of the tunnel. There are six papers to be presented in this session as indicated in figure 1.

Cold gaseous nitrogen will be contained within the tunnel circuit for long periods (see fig. 2). These periods consist of the time the tunnel is operating and a time for model configuration change or other pre- and post-test work and will be approximately 3400 hours per year (20 weeks per year). With the tunnel surface area of 2900 square meters, there is an appreciable annual energy transfer to the nitrogen. To provide for an energy efficient thermal system capable of withstanding the NTF environment, a development program was undertaken to define an acceptable design. This development work, along with the final design configuration, is presented in the paper by Dr. N. D. Watson and Mr. D. E. Williams.

For the operation of the tunnel in the cryogenic mode, temperature is maintained by injection of liquid nitrogen into the tunnel to offset the heat addition of the fan (see fig. 3). To maintain mass equilibrium, nitrogen gas is vented through two control valves through a muffler and into a vertical stack where it is mixed with ambient air, and the mixture is discharged to the atmosphere. The exhaust system is designed to vent nitrogen gas at rates up to 544 kg/sec for normal operation and up to 907 kg/sec for short time fail-safe operation. This nitrogen must be discharged into the atmosphere in a safe manner so as not to generate fogging at ground level, an oxygen deficient environment, and excessive noise. The design approach selected to satisfy the requirements and the performance predictions are presented in the paper by Dr. G. W. Ivey.

When operating in the air mode, the thermal energy input by the fan is removed by a water cooled heat exchanger located on the downstream end of the rapid diffuser. The basic element of the cooling coil is an elliptical tube with rectangular fins (see fig. 4). These elements are stacked four deep in the direction of flow and side-to-side to span the

tunnel diameter. For operating in the cryogenic mode, the water is evacuated and isolated from the cooling coil, and the coil structure is allowed to adjust to the flowing gas temperature. The low temperature and the temperature cycling caused concern regarding the service life of tube joint bonds and fin to tube bonds. It initially appeared that the elliptical tube would have to be fabricated in short lengths and jointed in order to span the tunnel diameter. The tube joint work performed along with the fin to tube bond work are presented in the paper by Dr. J. D. Buckley and Mr. Paul G. Sandefur.

For the NTF, the prime cost driver is liquid nitrogen, and in order to be energy efficient, the tunnel transient time associated with obtaining set points and recovering from model upsets must be minimized. Figure 5 shows operating cost as a function of dwell time and illustrates the necessity to minimize operating time. The ordinate reflects the cost of tunnel fill and cooldown, obtaining initial test conditions and obtaining angle of attack. The abscissa represents dwell time (at an angle of attack) required to stabilize the test medium to within desired error band and acquire test data. The shaded band width is the envelope that encompasses curves for various types of research test configurations selected to perform an operating cost and time analysis. The slope of the curve (approximately \$130 per second per polar) represents a substantial operation cost. From the controls standpoint, goals for the rate of changing test conditions have been established (see fig. 6) aimed at providing energy efficient operations. Two parameters, $\Delta\alpha$ and ΔM, are time dependent and two, ΔP and ΔT, are not necessarily time dependent. An automatic multivariable control system is being provided to afford energy efficient operation, and a math model study is underway to study the process characteristics and define control laws. The work in these two areas are presented in the papers by Mr. J. A. Osborn and Dr. C. E. Kirby.

In the area of electrical systems, three cryogenic problems were encountered (see fig. 7). There are many electrical actuators inside the tunnel, such as the ones that move the diffuser inlet and test section walls. The problems resulting from the low temperature environment were overcome by providing an enclosure around the actuators with a controlled thermal environment. For electrical connectors located inside the tunnel, only one type could be located which was rated for the cryogenic temperature of the NTF and it was very expensive. Due to the number of connectors inside the NTF and the potential savings if a low cost connector could be certified, a test program was undertaken to explore the feasibility of using a standard low cost unit. The results of this test program are presented in the paper by Mr. E. L. Kelsey. Also, for signal and power cables, a test program was performed to screen various types of conductor insulation. A brief description of the tests and the results from the program are included in the paper.

180
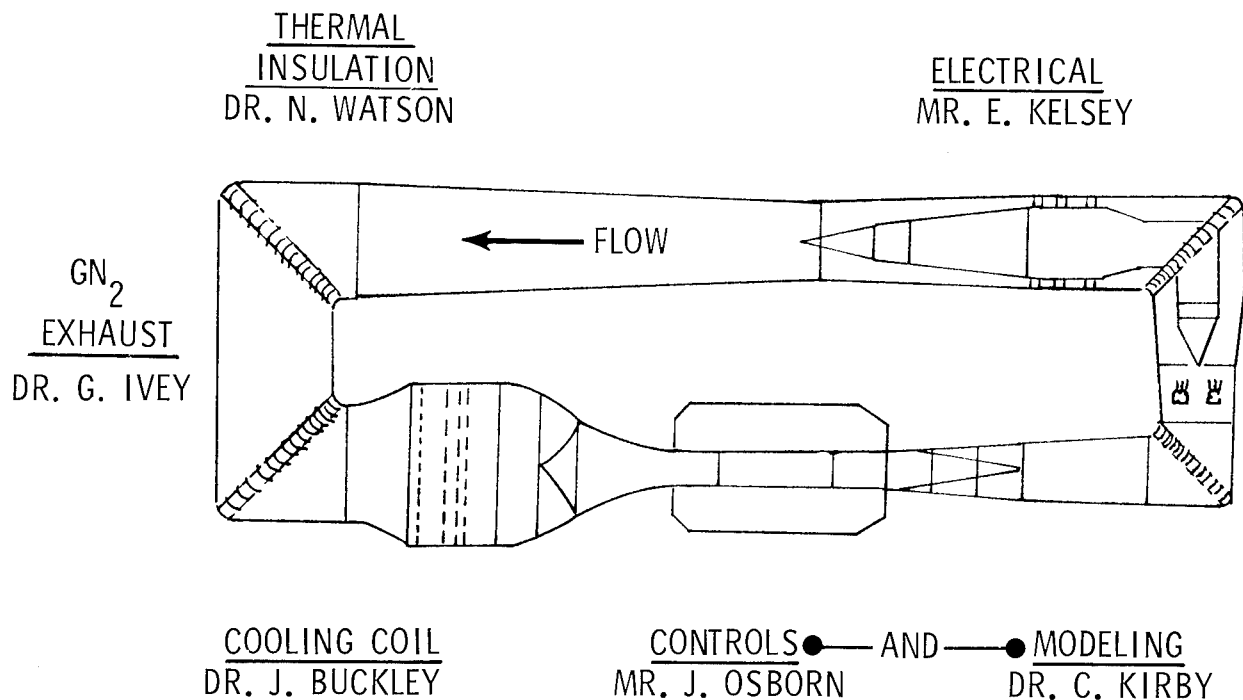
Figure 1.- Systems influenced by cryogenic test environment.

- GN$_2$ CHARGE TIME LARGE

    - OPERATING

    - IDLE

- INSULATION SURFACE AREA LARGE

- TOTAL ENERGY LOSS THROUGH WALL CAN BE APPRECIABLE

Figure 2.- Factors influencing shell insulation concept.
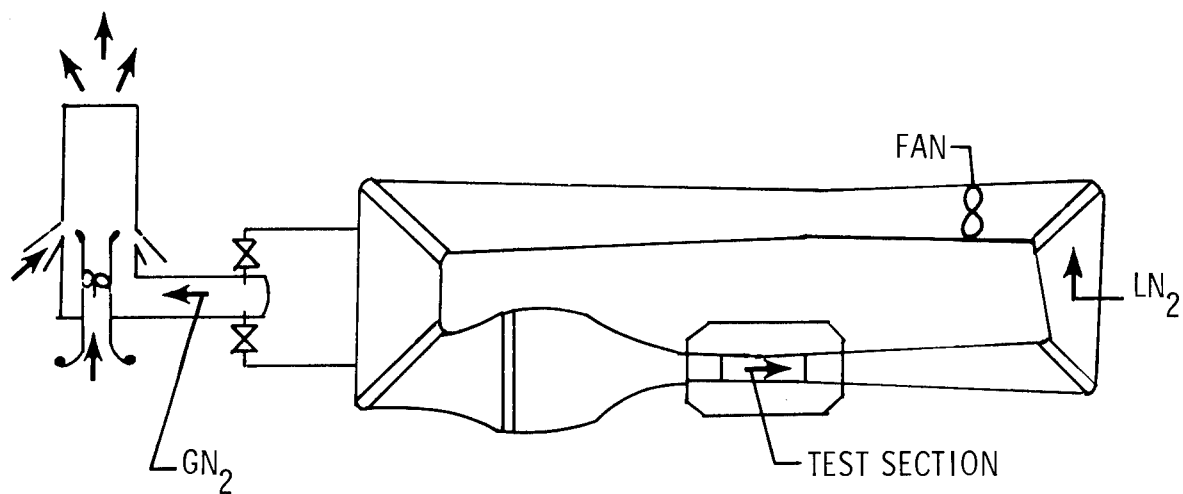
Figure 3.- Schematic showing GN_2 venting system.
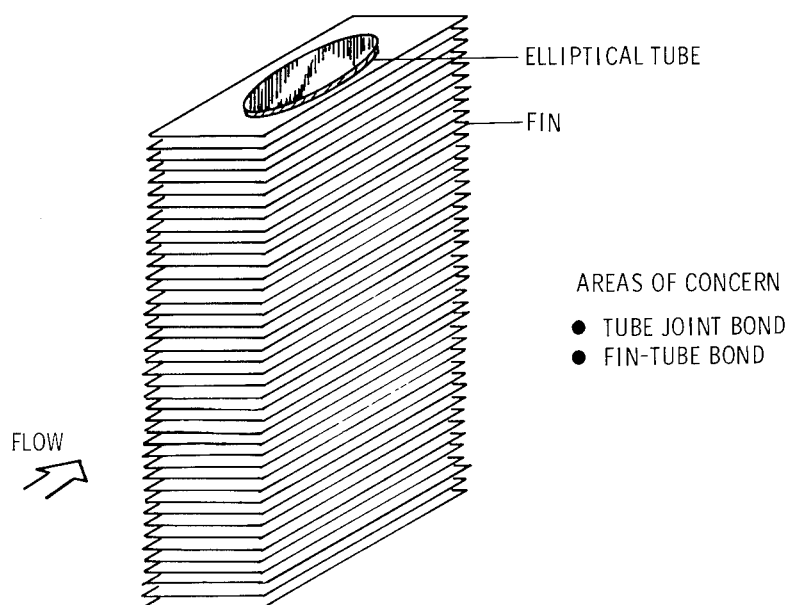
Figure 4.- Sketch of elliptical fin-tube used in cooling coil.
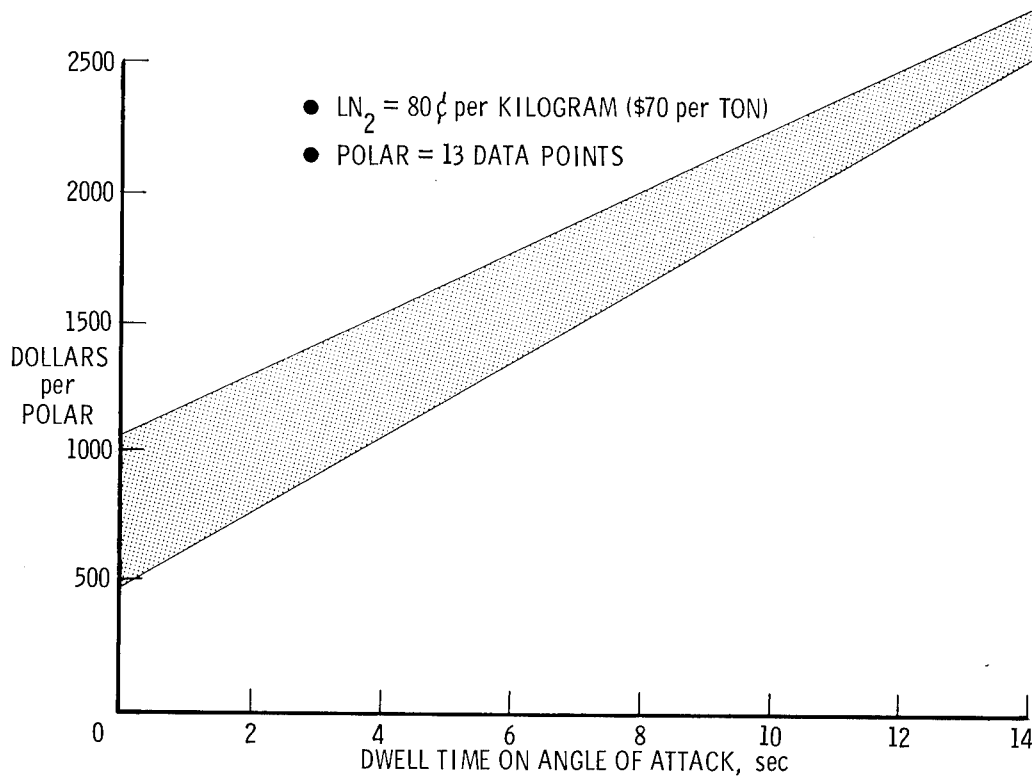
Figure 5.— Summary curve indicating cost of data versus time necessary
for data gathering.

- FOR $\Delta\alpha$ = 0.07 rad (4°) – BE ON SET POINT IN 3 SECONDS

- FOR ΔM = 0.2 – BE ON SET POINT IN 7 SECONDS

- FOR ΔP = 0.69 bar (10 psi) ⎫
                            ⎬ PERFORMS WITH MINIMUM CONSUMPTION OF
- FOR ΔT = 56 K (100 °R) ⎭   ENERGY

Figure 6.— Goals for changing test conditions.
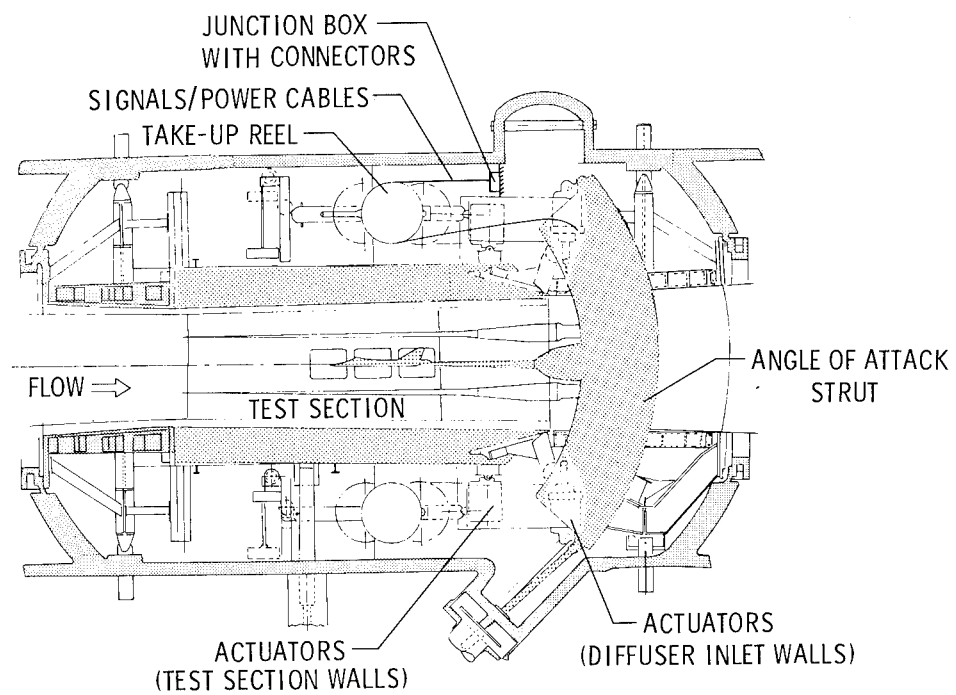
Figure 7.- Electrical systems in the plenum.

DEVELOPMENT OF AN INTERNAL THERMAL

INSULATION SYSTEM FOR THE NATIONAL TRANSONIC FACILITY

Nathan D. Watson and Dave E. Williams
Langley Research Center

SUMMARY

This paper presents the results of a design effort that provided a cost effective and reliable insulation system for the pressure shell of the National Transonic Facility (NTF). Critical factors affecting the choice of internal insulation instead of an external insulation system are discussed. Design criteria established for the internal insulation system are presented.

Factors affecting the selection of a closed cell foam insulation over a fibrous insulation are also discussed. The test apparatus used to produce data on the performance of the fibrous and closed cell insulation systems at high pressures and cryogenic temperatures is described. Experimental data from these tests indicating degraded performance of a proposed fibrous insulation system at these conditions led to a search for a suitable closed cell foam insulation. The subsequent development of the foam insulation system is discussed and the resulting design is explained. Results from the thermal and structural analyses of this design and the thermal insulation verification tests are presented and discussed. Finally, results and conclusions are drawn based on the design, analyses, and tests performed.

INTRODUCTION

The NTF wind tunnel utilizes cryogenic nitrogen gas at relatively high pressures to achieve high Reynolds numbers in the transonic flow regime without significantly increasing the tunnel dynamic pressure. The cryogenic temperatures are maintained inside the tunnel by injecting prescribed amounts of liquid nitrogen (LN_2) into the flow stream to balance the heat loads generated by the compressor, the stored energy in the internal components of the tunnel, and the parasitic heat gain from the ambient environment. A typical run of the wind tunnel will involve a continual injection of LN_2 and continual exhausting of the gaseous nitrogen in varying amounts. An efficient thermal insulation system is desirable in order to minimize the heat gain from the ambient environment. Early in the design program a goal of allowing only 3.165×10^5 J/sec (300 Btu/sec) for 3716 m^2 (40,000 ft^2) of surface area total heat leak from the ambient air to the inside of the tunnel was established.

The design of the NTF thermal insulation system was a challenge if only from the fact that it is the first large size cryogenic wind tunnel ever to be built. Standard design practice for insulation systems had to be modified and enhanced in order to meet the unique requirements of a low temperature wind tunnel. Design trade-offs such as whether the insulation should be internal or external to the tunnel pressure shell, of using a fibrous or a foam type insulation, and the method of attaching the insulation system to the tunnel shell had to be considered. Existing data on the performance of the insulation materials in an environment of high pressure, cyrogenic temperature, and/ or large temperature differentials was insufficient to make an engineering judgment of which material would be suitable for application to the NTF. Therefore, an insulation materials performance testing program was conducted for the NTF environment. This required the design and fabrication of a test apparatus to determine the effective conductivity of the materials.

Special attention was given to the attachment of the insulation system to the tunnel shell because of both the possibility of severe thermal stresses that could occur as a result of the large temperature differences across the thickness of the insulation and the installation problems presented in installing large amounts of insulation to the complex structure of a wind tunnel.

This paper presents and discusses the tradeoffs, analyses, and testing conducted during the design phase. It represents the culmination of a successful effort to provide a cost effective and reliable thermal insulation system for the NTF.

INTERNAL VERSUS EXTERNAL INSULATION

Initial studies of the type of thermal insulation system, internal or external, which would be best for the proposed NTF Cryogenic Facility leaned heavily in favor of an external insulation system. The benign external environment, the low initial installation cost, the ease of installation, and the ease of performing periodic inspections were all good reasons to go with an external insulation system. Also, no previous data base could be found to provide insight into the problems of developing an internal insulation system for the severe predicted environments in this facility or how such a system could be expected to perform in these environments.

After careful deliberation on the results of several studies to help provide more insight into these concerns, two overriding factors emerged in favor of developing an internal insulation system. The first was that in the absence of internal insulation, large thermal gradients would produce unacceptably large thermal stresses in the reinforcing rings of the tunnel pressure shell, thus severely limiting the useful fatigue life of the tunnel shell using the then proposed 9 percent nickel steel. This was particularly true in the corners. The second overriding factor was the unacceptably high cost of nitrogen to change the temperature of the several million kilograms of steel when it was necessary to change the working gas temperature and the

186

possible negative effects on the boundary layer due to the thermal lag of the large mass of steel in the tunnel shell. This would greatly increase the user cost over the whole operating lifetime of the cryogenic tunnel facility.

These factors were considered to be of sufficient magnitude to force abandonment of the relative design simplicity and lower initial cost of an external insulation system and to proceed with the development of an internal thermal insulation system.

DESIGN CRITERIA AND DESIGN ENVIRONMENT FOR AN INTERNAL INSULATION SYSTEM

The internal NTF tunnel conditions to which the insulation system will be subjected are severe and are characterized by having several different environments superimposed for a given run condition. In addition to cryogenic temperatures, these include high pressure, vibration, acoustic noise, and pressure gradients generated by the tunnel flow. The basic design environments are presented in Table 1. Based on these design environments and a desired thermal performance, a set of design requirements for the insulation system was generated. These design criteria are presented in Table 2.

In addition to this general criteria, specific criteria depending on the location within the tunnel must also be addressed. For example, the insulation system must serve as the aerodynamic flow liner over approximately 50 percent of the tunnel, as shown in Figure 1. This insulation system liner must be structurally capable of withstanding the local aerodynamic forces in these areas. Dynamic forces resulting from vibration of the fan drive system and aerodynamic induced vibration must also be considered in the design.

One of the more difficult design criteria to achieve was the flammability requirement. This requirement was that the insulation material be self extinguishing at 8.96×10^5 N/m^2 (130 psia) and still have the strength to withstand the structural loads at the high pressure since the addition of a flame retardant caused wide variations in the mechanical properties. It was also difficult to obtain the proper balance between the coefficient of thermal expansion, Young's modulus, and Poisson's ratio in order to keep the thermal stresses within acceptable limits. In addition to the above criteria, the necessity of bonding the closed cell insulation to the tunnel shell to eliminate convection at the combined condition of cryogenic temperatures and high pressures required a large test program to identify candidate cryogenic adhesives which would be acceptable for this application. Only one of the many adhesives which were tested proved to be acceptable. This was Crest 391, a polyurethane based adhesive, which remained slightly visco elastic down to cryogenic temperature. Finally, the geometry of the shell and aerodynamic lines prohibited the thickness of the insulation from being more than about 0.165 m (6.5 inches). This restriction dictated the maximum allowable thermal conductivity to maintain the heat loss to the design point of 3.165×10^5 J/sec (300 Btu/sec).

A PROPOSED FIBROUS INSULATION DESIGN CONCEPT

An initial conceptual engineering design using a fibrous insulation was generated by the FluiDyne Engineering Corporation as a part of the overall NTF tunnel system design. This design is shown in Figure 2. It utilized a corrugated aluminum structural liner which was bolted to the tunnel shell through thermal insulator blocks and a series of circumferential "T" rings which were spaced about 1.22 m (4 foot) on centers. This mechanically retained aluminum liner system held the slightly compressed fibrous insulation in contact with the tunnel shell.

An in-house NASA Langley literature search did not reveal any available test data to permit an evaluation of the thermal performance of a fibrous insulation system at the tunnel test conditions of cryogenic temperatures and high pressures. A test facility to measure the effective thermal performance of the proposed insulation system for the static, or non-flow condition, was designed and fabricated. This facility was essentially a slightly modified guarded hotplate thermal conductivity measuring apparatus, enclosed in a pressure vessel. A picture of this fixture is shown in Figure 3. The desired pressure in the facility was maintained by a pressure regulated gaseous nitrogen supply. Cooling of the facility was accomplished by pumping liquid nitrogen through a series of copper tubes attached to the cold boundary plate. The hot plate and ring guard heaters and the rear guard heater were powered by attached electrical resistance heaters. This test setup is shown schematically in Figures 4 and 5. Other equipment included 3 power supplies, a digital volt meter, a digital ohm meter and a Honeywell recorder and controller.

To obtain a typical data point, the specimen was installed in the test setup as shown in Figure 5 and the pressure vessel was purged with GN_2 to remove entrapped air and moisture. The specimen was cooled to the desired test temperature by flowing LN_2 through the cold plate assembly. Power was applied to three of the heaters in the heater assembly to maintain the heater assembly near $294^{\circ}K$ ($70^{\circ}F$) during the cooling process. When the temperature of the cold plate stabilized the GN_2 pressure on the test specimen was adjusted to the desired test condition.

The power on the three heaters, the primary heaters, the ring guard heater, and the guard heater was adjusted until all three heaters were at the desired temperature. All conditions were maintained until the heater assembly was stabilized. Stabilization of the heater assembly was defined as when the temperature of all three heaters stabilizing within ± 0.56 $^{\circ}K$ ($\pm 1^{\circ}F$) for 4 (four) consecutive readings taken at 30 minute intervals with no power change on the primary heater. Power on the primary heater was monitored by a digital volt meter and an ohm meter.

The effective conductivity (K) of the specimen was calculated by:

$$K = \frac{QL}{A \Delta t}$$

Q = Primary Heater Power (watts)

L = specimen thickness m (in.)

A = primary heater area m^2 (ft^2)

Δt = primary heater temp minus cold wall temp ^OK (^OF)

Using this facility, numerous thermal conductivity tests were performed on several candidate fibrous materials with various densities, under varying conditions of temperature and pressure.

RESULTS OF FIBROUS INSULATION PERFORMANCE AT CRYOGENIC TEMPERATURE AND HIGH PRESSURE

These thermal conductivity measurements showed that for the effective heat loss for either a combination of cryogenic temperature and atmospheric pressure or high pressures and relatively warm temperature, the thermal performance of the fibrous materials agreed with the manufacturers' data. However, when the more common tunnel static hold conditions of cryogenic temperature and high pressure were simulated the effective thermal conductivity increased exponentially when the heater was below the insulation and decreased slightly when the heater was above the insulation. These two cases simulated the top and bottom of the tunnel shell. These results showed that even for the static condition the effective thermal conductivity was unacceptably high.

Attempts were made to decrease this loss by increasing the flow resistance. This was done by adding perforated sheets of aluminum foil between the layers of fibrous insulation and also by using fibrous insulation made from smaller fibers. This helped decrease the magnitude but the heat loss was still unacceptably high.

The effective thermal conductivity versus temperature and pressure for a commercially available fibrous insulation with a perforated aluminum foil is shown in Figure 6. The thermal conductivity of nitrogen gas is also given for reference. The conductivity of N_2 gas remains essentially unchanged for the maximum tunnel run pressure of 8.96×10^5 N/m^2 (130 psia) but does increase for very high pressure. Also, the effective thermal conductivity versus temperature and pressure for another commercially available denser fibrous insulation is shown in Figure 7.

Flow resistance measurements were made on candidate insulation materials in an attempt to better understand the relationship between the flow resistance and effective thermal conductivity. The results of the flow resistance tests are shown in Figure 8. However, from the thermal conductivity test it

was apparent that the convection could not be totally eliminated and that it would be virtually impossible to define for all possible conditions.

These results show that for the combined conditions of cryogenic temperatures and high pressures the convective component of heat transfer becomes the dominant factor for an insulation that can breathe. These results also show that the magnitude of the convective heat transfer varies as a function of geometric location (top or bottom of tunnel).

The limit to which the insulation flow resistance could be increased without exceeding the structural capability of the aluminum liner retainer was limited by the tunnel quick venting requirement of $\frac{dp}{dt} = 8.27 \times 10^4$ N/m^2 sec (12 psi/sec). Decompression tests using the same facility were performed by venting the pressurized chamber through a quick acting valve and an orifice designed to provide the depressurization rate of 8.27×10^4 N/m^2 sec (12 psi/sec). Results of these tests indicated that the structural limit might be approached before the flow resistance required to reduce the heat loss to an acceptable value could be reached. Considerable testing would have had to be done to verify an acceptable liner strength at the required flow resistance.

One additional test, using a mock-up of a section of the tunnel shell with the "T" rings, fibrous insulation, and aluminum liner plate was performed. This was a 1.22 m (4 ft.) by 1.22 m (4 ft.) section which was inverted over a container of liquid nitrogen. The heat loss was measured at atmospheric pressure. Then this apparatus was placed in the LaRC high pressure autoclave and raised to 8.96×10^5 N/m^2 (130 psia). Absolute values of heat loss were not obtained from this test but the difference between the heat loss at atmospheric pressure and cryogenic temperatures and the heat loss at cryogenic temperature and 8.96×10^5 N/m^2 (130 psia) agreed in magnitude with the results from the previously described guarded hot plate facility. Another result from this test was that at the high pressure and cryogenic temperature condition, the "T" rings functioned as cooling fins and increased the heat loss by a factor of 4 or 5.

Moisture condensation in the fibrous insulation during cool-down was a concern. Also, should the fibrous insulation become saturated with water, drying it would restrict the tunnel operation. The possibility of trapping liquid oxygen condensed out of the air on the initial cool-down in the fibrous insulation and creating a potentially explosive hazard was also a serious concern.

To complete the data base on the fibrous insulation system, an acoustic test was run on a mock-up of a representative sample of the tunnel shell and insulation system. This was instrumented throughout the thickness of the material with thermocouples and subjected to 160 dB for 10 minutes in the 2.44 m (8 ft.) Thermal Structural Tunnel. The test set-up is shown in Figure 9, the test levels in Figure 10, and the test results in Figure 11. The test results show that considerable heat is generated within the layers of fibrous

insulation as a result of dissipating the incident acoustic energy. No valid means of evaluating this effect on the fibrous insulation over a long life span, on the order of 20 years, could be found.

When the results of the previously discussed tests on the fibrous insulation system were evaluated, it was apparent that this system could not be expected to function as required for this application. Also the thermal performance varied as a function of geometrical location in the tunnel, as a function of tunnel run condition, and as a function of compactness which would vary as a function of geometry and operating time. This result was obviously applicable to any insulation system that had porosity and was exposed to these environments.

These variations were virtually impossible to predict for all the possible conditions. The result of the variable insulation effectiveness was that a highly variable and unpredictable thermal stress profile would be experienced in the tunnel shell. This raised serious questions about the fatigue life of the shell.

The basic conclusion reached as a result of the previously discussed tests on the fibrous insulation system was that the convective component of heat transfer to the tunnel shell had to be eliminated from an internal insulation system design for the combined environment of cryogenic temperature and high pressure. This conclusion led to the initiation of a design of a closed cell foam insulation system.

DEVELOPMENT OF A CLOSED CELL FOAM INTERNAL INSULATION SYSTEM

As a result of the experience gained from the environmental testing on the fibrous insulation concept, some additional performance criteria were added to the original criteria given in Table 2. These additional criteria are:

a. The insulation system shall be closed cell and shall be bonded to the internal NTF pressure shell to prevent convective thermal "shorts" to the shell.

b. The thermal conductivity of the insulation material shall remain essentially constant at all tunnel operating conditions.

c. The insulation material shall have a factor of safety of

$$F.S. = \frac{\text{Compressive Yield Stress}}{\text{Working Compressive Stress}} > 2.0$$

In order to decrease the heat loss through the mechanical attachments to the shell of the structural part of the insulation system, a new retention system was designed. The current mechanical retention system, which evolved through several design iterations, is shown in Figures 12 through 15. This

system consists of .01 m (0.375 inch) thick 5454 - 0 aluminum liner plate, broken on one end and in the center, "T" shaped structural longerons of fiberglass impregnated with a polyester filler, a fiberglass polyester retainer cap strip and two sets of 304 stainless steel clevis type attachment links which are drilled on one side and drilled and tapped on the opposite side.

This assembly is bolted to the tunnel shell, through the clevis links, to .076 m by .076 m by .016 m (3 inch by 3 inch by 5/8 inch) 304 stainless steel tabs welded to the pressure shell. These tabs are located in 24 lines equally spaced along the tunnel flow direction and are spaced approximately 0.61 m (2 feet) on center. The larger diameter sections of the shell have 32 and 40 equally spaced rows of these tabs. Tabs in the tunnel section between the exit of the high speed diffuser and the entrance of the fan shroud region are gusset re-enforced to carry the additional loading from the deeper structural "T" sections required to maintain the aerodynamic flow lines in this tunnel section (See Figure 14). The "T" sections range in length from 1.22 to 1.83 m (4 to 6 feet), are fixed on one end and are free to expand on the other to allow for thermal expansion and contraction. The fiberglass-polyester structural members are made by a commerically available pultrusion process in which the fiberglass is fed continuously into a die, impregnated with the polyester resin, run through a heat dryer, and cut to the desired length as it comes out of the dryer. This mechanical retention system will accommodate any type of foam insulation system.

The closed cell foam insulation is bonded to the tunnel shell in the configuration shown in Figure 12. The insulation consists of one piece of insulation, .076 m (3 inches) thick, bonded to the shell with Crest 391 re-enforced with fiberglass. A second layer of insulation .076 m (3 inches) thick is bonded to the first and then a third layer of .038 m (1.5 inch) thick insulation is bonded to this layer with the same fiberglass re-enforced Crest adhesive. Finally, the entire outside is covered with this same fiberglass/ adhesive cover. The Crest provides an excellent bond to both the shell and to the insulation material. All joints will be completely filled with the adhesive to prevent thermal "shorts" to the shell.

The insulation is made up of prefabricated blocks for each section of the tunnel, then cut as shown in Figure 15. Tolerances are accounted for by on-site measurements. Only one saw cut is necessary on one of the prefabricated block pieces in order to have a close fit. The turning vane areas of the tunnel and other difficult geometric areas are to be cut and fitted on site.

The upstream nacelle is also insulated internally using the same closed cell foam and fiberglass with Crest 391 adhesive. This configuration, shown in Figure 16, is mechanically retained to the internal nacelle shell by welded stud and threaded fiberglass rod and large flat washers with nuts and cotter pins.

Using the insulation system design criteria, a set of performance criteria was established. These criteria are outlined in Table 3 along with the appropriate ASTM test that was used to verify that the proposed insulation materials met the desired performance parameter.

To create an interest in supplying a closed cell foam with the desired properties, a request for bids to supply the NTF insulation material was initiated. Tests on laboratory produced samples from three different companies proved to be successful. The General Electric Company, Thermal Systems Programs, Tacoma, Washington was selected to supply the NTF closed cell cryogenic insulation material. The material properties of the G.E. foam material obtained from the results of the specified tests are given in Table 4. This data shows that the material meets or exceeds all of the physical properties requirements. The material is a proprietary formula of modified polyurethane material. A simulated 1.22 m by 1.22 m (4 foot by 4 foot) section of the tunnel shell with the foam insulation and liner structure system to be used in the tunnel was constructed to run thermal and pressure cycle tests on the insulation system. This panel is shown in Figure 17 and the cold cycle test setup is shown in Figure 18.

The panel was inverted over a container of liquid nitrogen, insulated around the sides and thermal cycled 5 times. The thermocouple locations and test results for a typical cycle are shown in Figures 19 through 23. The tunnel shell remains within about 8.33^oK (15^oF) of the outside ambient temperature which is well within the required 22.22^oK (40^oF) of outside ambient. Conduction through the mechanical attachments was also very low and produced no local cold spots on the shell.

The panel was then placed under a radiant heating facility and heated to 355^oK (+180^oF) for 5 cycles. Results of a typical hot cycle are shown in Figure 24. Finally the entire panel was placed in the high pressure autoclave facility and run through the pressure cycles shown in Table 5.

Post test inspection of the test panel revealed no problems with the survivability of the system and showed that the thermal effectiveness met all the design criteria.

The fiberglass/Crest 391 bond system was chosen by conducting an extensive literature survey and an adhesive test program. Since the thermal performance of the insulation system depended on a bonded system which would withstand the environments and maintain bond integrity, an effort was initiated to either identify and test possible cryogenic adhesives and/or develop one that would be suitable for this application. Many other candidate adhesives were reviewed but all of them were rejected either on the basis of literature data or after LN_2 immersion screening tests and in some cases after more extensive testing.

Crest 391 is a two part polyurethane based adhesive mixture manufactured by Crest Products located in Santa Ana, California. It remains slightly visco-elastic down to liquid nitrogen temperature of 77^oK (-320^oF). This characteristic was demonstrated by performing a cryogenic flex test on a fiberglass specimen impregnated with Crest adhesive. The specimen was immersed in a liquid nitrogen bath and cycled 5000 cycles with no degradation. This test fixture is shown in Figure 25. Other bond tests included foam to re-enforced fiberglass polyester assembly tests at cryogenic temperature, foam to stainless steel assembly tests at cryogenic temperature, tensile

193

shear tests at various temperatures, and foam insulation compatibility bond tests.

Parametric tests of bond strength as a function of cure temperature and cure time were also performed on the Crest adhesive. The results of these tests are shown in Figure 26.

INSULATION SYSTEM ANALYSES

The analysis of the insulation material bonded inplace with Crest adhesive required a finite element math model in order to gain insight into the stresses in the insulation material. Due to the non-homogenity of this system, predicted stresses from the finite element model could not be taken as absolute values but the analysis did provide insight into the relative values of the stresses throughout the thickness and at the boundaries. A NASTRAN finite element math model of a low density bonded system was used to predict a stress profile produced by a linear temperature profile through the thickness of $105^\circ K$ to $294^\circ K$ ($-270^\circ F$ to $70^\circ F$) and a 7.92×10^5 N/m^2 (115 psig) pressure loading. The resulting stresses predicted some locally high stresses which exceeded the material allowables. However when the test panel of this system was tested to these loads using an even lower strength material no failure occurred. From these results it can be concluded that the finite element predictions are conservative. This analysis was repeated for the current system using the GE material. Figure 27 shows the coordinate system and boundary and loading conditions. The predicted stresses are given in Table 6. Stresses at the shell foam boundary are given in Table 7 for the combined shell thermal and pressure loadings. These results show factors of safety much greater than the required factor of 2 for the insulation material system.

The stress analysis of the other structural elements in the system was performed using conventional references and standard stress equations. No finite element model was required. A 1556 N (350 pound) load was used in the most critical direction and the resulting stresses calculated. Figures 28 and 29 give the geometry of shallow and deep shell attachment structure and the predicted stresses with a 1556 N (350 pound) load applied as shown. The stress allowable on the 304 stainless steel components to give the required factor of safety of 4 is 1.38×10^8 N/m^2 (20,000 psi) while on the fiberglass parts it is 5.52×10^7 N/m^2 (8000 psi). Figures 30 through 33 give the geometry, loads, and predicted stresses for both the deep and shallow link sections. Figure 34 shows the geometry, worst case load conditions, and predicted stresses and natural frequencies of the 5454-0 aluminum liner panels. Figure 35 gives the venting calculations for the volume between the top of the insulation material and the aluminum liner panels using the required 8.27×10^4 N/m^2 sec (12 psi/sec) as the maximum tunnel pressure time rate of change. The cap strip worst case loadings and predicted stresses are given in Figure 36. Figure 37 shows the results of the calculations to

194

determine the allowable effective conductivity of the insulation system.

All components of the insulation system support structure meet the requirement for factors of safety of 4 based on the predicted stresses for worst case loading conditions and the allowables for the materials.

RESULTS AND CONCLUSIONS

An internal bonded closed cell foam thermal insulation system which meets or exceeds all of the design criteria has been successfully developed, analyzed, and tested for the NTF Cryogenic Facility. The thermal effectiveness of this system remains essentially constant for all tunnel operating pressures and cryogenic temperatures. Calculated structural margins show factors of safety of at least 4 in all cases for the structural components and greater than 2 for the closed cell insulation material.

Porous or fibrous insulation for the tunnel operating conditions of cryogenic temperatures and high pressures is unacceptable because of the exponential increase in the effective thermal conductivity due to the sharp increase in the convective component of heat transfer at these operating conditions. Even sharper increases in the convective component of heat transfer occurs when the tunnel is running. These increases vary as a function of geometry, tunnel flow condition, and material compactness in a virtually unpredictable fashion, when looking at the whole tunnel.

Additional concerns with a fibrous system such as water absorption, possible liquid oxygen entrapment, and effects of the acoustic environment over longer periods of times would severely restrict tunnel operations.

TABLE 1.- DESIGN ENVIRONMENTS

- TEMPERATURE
- PRESSURE
- RAPID DEPRESSURIZATION
- VIBRATION
- ACOUSTIC
- FLOW VELOCITY

77 K TO 352 K (-320^0F TO 175^0F)

0 TO 8.95×10^5 N/m^2 (0 TO 130 psia)

8.27×10^4 N/m^2 sec (12 psi/sec)

15 Hz IN FAN REGION

OSPL 150-155 dB

<76.2 m/sec (<250 FPS)

TABLE 2.- DESIGN CRITERIA

1. LOCATION - THE INSULATION AND LINEAR SYSTEM SHALL BE LOCATED INTERNAL TO THE PRESSURE SHELL.

2. GEOMETRY - IN GENERAL, THE INSULATION AND LINEAR SYSTEM SHALL CONFORM TO THE GEOMETRY OF THE PRESSURE SHELL AND TO THE GEOMETRY OF THE AERODYNAMIC LINES IN THE AREA WHERE IT FUNCTIONS AS THE FLOW SURFACE. CIRCULAR CROSS SECTION MAY BE APPROXIMATED BY MULTISIDED POLYGONS.

3. THICKNESS - THE INSULATION SHALL HAVE A NOMINAL THICKNESS OF 0.15 METER (6.0 INCHES).

4. HEAT GAIN - THE TOTAL HEAT GAIN THROUGH THE PRESSURE SHELL INSULATION SHALL NOT EXCEED 3.165×10^5 J/s $\left[300 \text{ btu/sec} \left(27 \text{ btu/ft}^2 - \text{hr. BASED ON } 40,000 \text{ ft}^2 \right) \right]$. FOR INTERNAL GAS TEMPERATURE 77^0 K $(-320^0$ F) AN EXTERNAL AMBIENT TEMPERATURE OF 311^0 K $(100^0$ F).

5. RETENTION - THE INSULATION SHALL BE MECHANICALLY RETAINED TO THE PRESSURE SHELL.

6. FLAMMABILITY - THE INSULATION AND LINER SYSTEM MATERIALS SHALL BE SELF-EXTINGUISHING AT 8.96×10^5 N/m^2 (130 psia AIR).

7. TOXICITY - THE INSULATION AND LINER SYSTEM MATERIALS SHALL BE NON-TOXIC.

8. DESIGN LIFE - THE INSULATION AND LINER SHALL BE DESIGNED FOR A MAXIMUM EFFECTIVE LIFE, WITH NO DEGRADATION, CONSISTENT WITH THE CALCULATED PRESSURE SHELL RECERTIFICATION PERIOD.

9. CHEMICAL STABILITY - THE INSULATION AND LINER SYSTEM MATERIALS SHALL NOT POSSESS ANY TENDENCY TO DETERIORATE OR UNDERGO ANY CHEMICAL DECOMPOSITION RESULTING FROM EXPOSURE TO HYDRAULIC FLUID AND THE VARIETY OF SOLVENTS AND LUBRICANTS COMMONLY USED IN WIND TUNNEL ACTIVITIES.

10. PARTICULATE CONTAMINATION - THE INSULATION AND LINER SYSTEM SHALL NOT PRODUCE PARTICULATE CONTAMINATION IN THE TUNNEL FLOW SYSTEM.

11. REMOVAL/REPLACEMENT - THE INSULATION AND LINER SYSTEM SHALL BE DESIGNED TO MINIMIZE THE DIFFICULTY OF SHELL INSPECTION OF INSULATION MATERIAL REPLACEMENT WITHIN THE REQUIREMENTS.

12. LINER AND STRUCTURAL ATTACHMENTS SHALL HAVE FACTORS OF SAFETY OF

$$F. S. = \frac{\text{ULTIMATE STRESS}}{\text{WORKING STRESS}} > 4.0.$$

197

TABLE 3.- CLOSED CELL FOAM - CRITERIA AND TEST METHODS

TEST IDENTIFICATION & REQUIREMENT	TEST METHOD
FLAMMABILITY (ATM) REQUIREMENT: < 0.254 METER (10 INCHES) FLAME TRAVEL, NO GLOW AFTER 10 min., NO SPARKING, SPUTTERING, OR DRIPPING	D3104
LN$_2$ COMPATIBILITY REQUIREMENT: NO VISIBLE DAMAGE OR DEGRADATION	PARA. 3.6.2 (RFP)
CHEMICAL RESISTANCE REQUIREMENT: DIMENSIONAL CHANGE < 2%	D543
THERMAL CONDUCTIVITY REQUIREMENT: 0.0056 J/sec-m K AT 339 K (0.39 btu-in/hr ft^2 ^{0} F AT 150^0 F)	C518
THERMAL DEGRADATION REQUIREMENT: NO PERMANENT PHYSICAL OR CHEMICAL CHANGE	D2126

TEST IDENTIFICATION & REQUIREMENT	TEST METHOD
COMPRESSIVE STRENGTH REQUIREMENTS: 294 K (70^0 F) TO 77 K (-320^0 F), 1.79 $\times$ 10^6 N/m^2 (260 psi) 294 K (70^0 F) TO 352 K (175^0 F), 1.28 $\times$ 10^6 N/m^2 (185 psi)	D1621

TEST IDENTIFICATION & REQUIREMENT	TEST METHOD
THERMAL STRESS FACTOR REQUIREMENT: > 1.05	PARA. 3.6.8 (RFP)
DENSITY REQUIREMENT: > 224 kg/m^3 (14.0 lb/ft^3)	D1622
WATER ABSORPTION REQUIREMENT: < 10% BY wt.	D2842
CHAR YEILD REQUIREMENT: > 35% BY wt.	PARA. 3.6.11

TEST IDENTIFICATION & REQUIREMENT	TEST METHOD
TENSILE STRENGTH REQUIREMENTS: 294 K (70^0 F) TO 77 K (-320^0 F) 1.79 $\times$ 10^6 N/m^2 (260 psi) 294 K (70^0 F) TO 352 K (175^0 F), 1.28 $\times$ 10^6 N/m^2 (185 psi)	D1623

TABLE 4.– CLOSED CELL FOAM – CRITERIA AND TEST RESULTS

TEST IDENTIFICATION & REQUIREMENT	TEST METHOD	TEST RESULTS	
FLAMMABILITY (ATM) REQUIREMENT: < 0.254 METER (10 INCHES) FLAME TRAVEL, NO GLOW AFTER 10 min., NO SPARKING, SPUTTERING, OR DRIPPING	D3104	AVERAGE TIME TO EXTINGUISHMENT FOR 6 SPECIMENS AVERAGE WEIGHT PERCENT RETAINED FOR 6 SPECIMENS AVERAGE FLAME HEIGHT FOR 6 SPECIMENS COMMENT: NO FLAME OR GLOW COMBUSTION AND NO SPARKING, SPUTTERING OR DRIPPING OF FLAMING PARTICLES OCCURED AFTER EXTINGUISHMENT.	11.3 sec 97.4 0.203 m (8.0 in)
LN$_2$ COMPATIBILITY REQUIREMENT: NO VISIBLE DAMAGE OR DEGRADATION	PARA 3.6.2 (RFP)	THREE SPECIMENS OF SIZE 1.5 × 11.5 × 2.5 in. WERE IMMERSED IN LN$_2$ FOR 5 MINUTES FROM A ROOM TEMPERATURE CONDITION. THEN THEY WERE RETRIEVED AND STORED AT ROOM TEMPERATURE FOR 1 HR. THIS PROCESS WAS REPEATED 10 TIMES.	THERE WAS NO VISIBLE DAMAGE OR DEGRADATION
CHEMICAL RESISTANCE REQUIREMENT: DIMENSIONAL CHANGE < 2%	D543	MAXIMUM DIMENSIONAL CHANGE FOR DISTILLED WATER MAXIMUM DIMENSIONAL CHANGE FOR HYDRAULIC OIL MAXIMUM DIMENSIONAL CHANGE FOR LUBE OIL COMMENT: NO EVIDENCE OF TACKINESS, CRACKING OR SOLUBILITY.	1.32 .38 .75
THERMAL CONDUCTIVITY REQUIREMENT: 0.0056 J/sm K AT 339 K (0.39 btu-in/hr ft^2 °F AT 150° F).	C518	TWO SPECIMENS 0.203 m (8 in.) DIAMETER × 0.0127 m (0.5 in.) THICK PLACED IN THE GUARDED HOT PLATE APPARATUS AT 339 K (150° F) MEAN TEMPERATURE. THE RESULTING K-FACTOR IS LISTED.	0.0054 J/sec K (0.374 btu-in/hr ft^2 °F)
THERMAL DEGRADATION REQUIREMENT: NO PERMANENT PHYSICAL OR CHEMICAL CHANGE	D2126	MAXIMUM DIMENSIONAL CHANGE OF THREE SPECIMENS MAXIMUM WEIGHT CHANGE OF THREE SPECIMENS COMMENT: POST TEST CHECK OF COMPRESSIVE AND TENSILE STRENGTH AND MODULES SHOWED NO DEGRADATION AT 355 K (180° F). NO SIGNIFICANT PHYSICAL OR CHEMICAL CHANGES WERE OBSERVED.	0.25% 0.8%

TEST IDENTIFICATION & REQUIREMENT	TEST METHOD		TEST RESULTS			
COMPRESSIVE STRENGTH REQUIREMENTS: 294 K (70° F) TO 77 K (-320° F) 1.79 × 10^6 N/m^2 (260 psi) 294 K (70° F) TO 352 K (175° F), 1.28 × 10^6 N/m^2 (185 psi)	D1621	SPECIMEN	YIELD STRENGTH ⊥ TO RISE 294 K (75° F) 355 K (180° F)		YIELD STRENGTH ‖ TO RISE 355 K (180 °F)	
		#1	2.72 × 10^6 (394)	2.42 × 10^6 (351)	3.03 × 10^6 (439)	
		#2	2.78 × 10^6 (404)	2.16 × 10^6 (314)	2.70 × 10^6 (391)	
		#3	4.43 × 10^6 (643)	2.96 × 10^6 (430)	2.70 × 10^6 (392)	N/m^2 (psi)
		#4	4.01 × 10^6 (582)	2.99 × 10^6 (433)	-	
		AVERAGES:	3.49 × 10^6 (506)	2.63 × 10^6 (382)	2.81 × 10^6 (407)	
		STANDARD DEVIATION:	8.7 × 10^5 (126)	4.1 × 10^5 (59)	1.9 × 10^5 (28)	
		SPECIMEN	MODULUS ⊥ TO RISE		MODULUS ‖ TO RISE	
		#1	5.8 × 10^7 (8411)	5.71 × 10^7 (8284)	7.8 × 10^7 (11309)	
		#2	6.1 × 10^7 (8789)	5.73 × 10^7 (8308)	7.43 × 10^7 (10780)	N/m^2 (psi)
		#3	8.7 × 10^7 (12681)	7.33 × 10^7 (10637)	6.77 × 10^7 (9826)	
		#4	9.5 × 10^7 (13718)	6.93 × 10^7 (10050)	-	
		AVERAGES:	7.5 × 10^7 (10900)	6.43 × 10^7 (9320)	7.33 × 10^7 (10638)	
		STANDARD DEVIATION:	1.85 × 10^7 (2694)	8.32 × 10^6 (1206)	5.18 × 10^6 (752)	

199

TABLE 4.- CONCLUDED

TEST IDENTIFICATION & REQUIREMENT	TEST METHOD	TEST RESULTS					
TENSILE STRENGTH REQUIREMENTS: 294 K (70°) TO 77 K (-320° F) 1.79×10^6 N/m² (260 psi) 294 K (70° F) TO 352 K (175° F), 1.28×10^6 N/m² (185 psi)	D1623	SPECIMEN	YIELD 297 K (75°F)	STRENGTH ⊥ 77 K (-320°F)	TO RISE 355 K (180°F)	YIELD STRENGTH ‖ TO RISE 355 K (180°F)	N/m² (psi)
		#1	2.03×10^6 (295)	1.77×10^6 (257)	1.74×10^6 (252)	2.82×10^6 (410)	
		#2	2.41×10^6 (350)	1.83×10^6 (265)	1.97×10^6 (285)	2.47×10^6 (359)	
		#3	2.84×10^6 (412)	2.39×10^6 (346)	2.32×10^6 (336)	2.54×10^6 (368)	
		#4	3.12×10^6 (452)	2.79×10^6 (405)	2.19×10^6 (318)		
		AVERAGES:	2.6×10^6 (377)	2.19×10^6 (318)	2.05×10^6 (298)	2.61×10^6 (379)	
		STANDARD DEVIATION:	0.47×10^6 (69)	0.49×10^6 (71)	0.26×10^6 (37)	1.86×10^5 (27)	
		SPECIMEN	MODULUS ⊥		TO RISE	MODULUS ‖ TO RISE	
		#1	1.02×10^8 (14738)	1.23×10^8 (17837)	8.28×10^7 (12005)	1.24×10^8 (17920)	N/m² (psi)
		#2	8.64×10^7 (12536)	1.13×10^8 (16390)	7.66×10^7 (11113)	1.03×10^8 (14951)	
		#3	1.16×10^8 (16757)	-	9.79×10^7 (14192)	1.04×10^8 (15027)	
		#4	1.03×10^8 (14907)	1.33×10^8 (19306)	9.86×10^7 (14300)	1.17×10^8 (16972)	
		AVERAGE:	1.02×10^8 (14734)	1.23×10^8 (17844)	8.9×10^7 (12902)	1.12×10^8 (16218)	
		STANDARD DEVIATION:	1.19×10^7 (1728)	1.01×10^7 (1458)	1.1×10^7 (1594)	1.01×10^7 (1470)	

TEST IDENTIFICATION & REQUIREMENT	TEST METHOD	CERTIFIED DATA	
THERMAL STRESS FACTOR REQUIREMENT: > 1.05	PARA. 3.6.8 (RFP)	$\alpha_1 = 1.57 \times 10^{-5}$ m/m/K (2.82×10^{-5} in/in °F) $E_1 = 1.02 \times 10^8$ N/m² (14734 psi) $\sigma = 2.6 \times 10^6$ N/m² (377 psi) $\alpha_2 = 8.89 \times 10^{-6}$ m/m/K (1.60×10^{-5} in/in °F) $E_2 = 1.23 \times 10^8$ N/m² (17840 psi) $\mu = 0.32$	1.8
DENSITY REQUIREMENT: > 224 kg/m³ (14.0 lb/ft³)	D1622	AVERAGE OF 5 SPECIMENS	245 kg/m³ (15.3 pcf)
WATER ABSORPTION REQUIREMENT: < 10% BY wt.	D2842	AVERAGE WATER ABSORBED OF THREE SPECIMENS IN VOLUME PERCENT (9.1 MAXIMUM)	9.1%
CHAR YIELD REQUIREMENT: > 35% BY wt.	PARA. 3.6.11	273 K (0°C) - 00% 573 K (300°C) - 80% 873 K (600°C) - 35.4% 373 K (100°C) - 100% 623 K (350°C) - 55% 107 K (800°C) - 32.5% 473 K (200°C) - 99% 773 K (500°C) - 41%	35.4% @ 873 K (600°C)

TABLE 5.- PRESSURIZATION-DEPRESSURIZATION TIME HISTORY

CYCLE	SOAK TIME @ 1.1×10^6 N/m^2 (145 psig)	MAX. VENT RATE
1	4 hr 10 min	0.034×10^6 N/m^2/sec (5 psi/sec)
2	20 hrs	0.034×10^6 N/m^2/sec (5 psi/sec)
3	UNKNOWN	PRESSURE LEAKED DOWN TO 0.41×10^6 N/m^2 (45 psig) SLOWLY
4	46 hrs 20 min	0.034×10^6 N/m^2 (5 psi/sec)

NOTE: TEST CONDUCTED BETWEEN COLD & HOT CYCLE

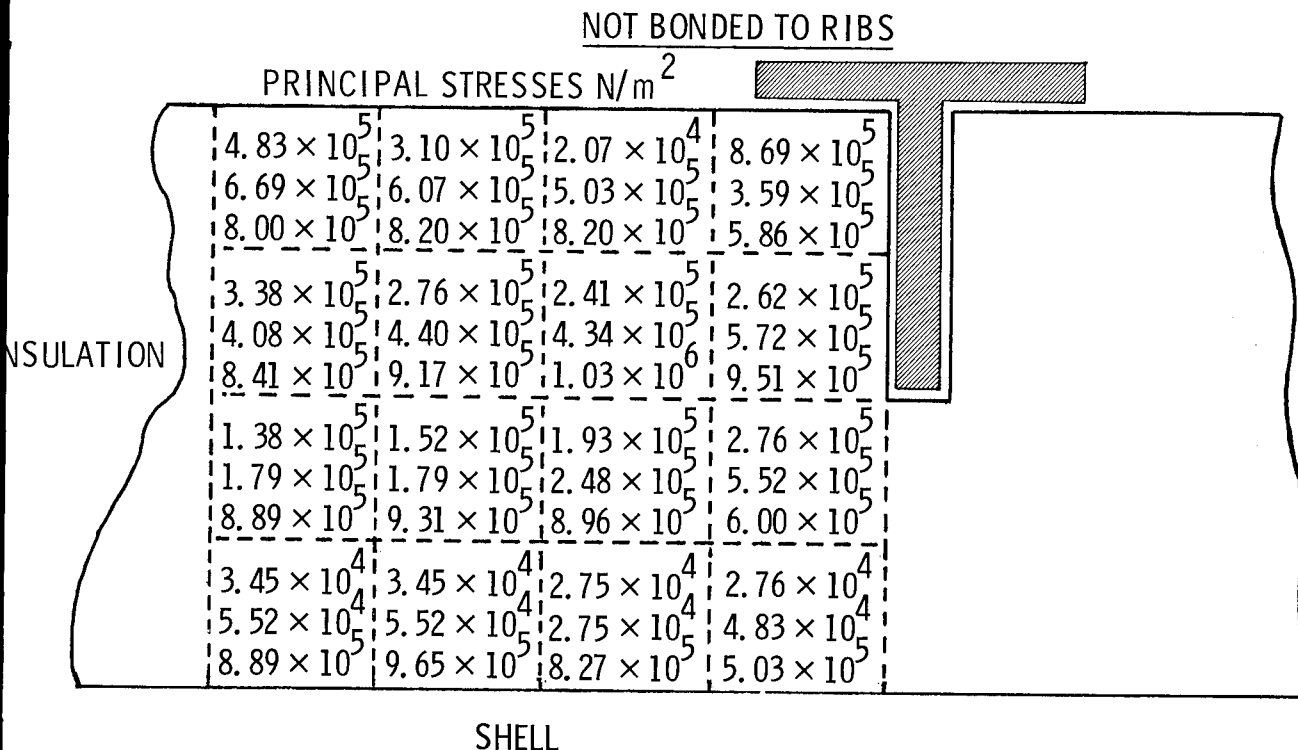TABLE 6.- RESULTS: LOCATION – NEAR CORNER AT X = 0, Z = 0.45m (18 in.)

NOT BONDED TO RIBS

PRINCIPAL STRESSES N/m^2

4.83×10^5	3.10×10^5	2.07×10^4	8.69×10^5
6.69×10^5	6.07×10^5	5.03×10^5	3.59×10^5
8.00×10^5	8.20×10^5	8.20×10^5	5.86×10^5
3.38×10^5	2.76×10^5	2.41×10^5	2.62×10^5
4.08×10^5	4.40×10^5	4.34×10^5	5.72×10^5
8.41×10^5	9.17×10^5	1.03×10^6	9.51×10^5
1.38×10^5	1.52×10^5	1.93×10^5	2.76×10^5
1.79×10^5	1.79×10^5	2.48×10^5	5.52×10^5
8.89×10^5	9.31×10^5	8.96×10^5	6.00×10^5
3.45×10^4	3.45×10^4	2.75×10^4	2.76×10^4
5.52×10^4	5.52×10^4	2.75×10^4	4.83×10^4
8.89×10^5	9.65×10^5	8.27×10^5	5.03×10^5

INSULATION

SHELL

TABLE 7.- SUMMARY

DELTA STRESS IN FOAM INSULATION DUE TO SHELL PRESSURE
GROWTH AT 1.63×10^8 N/m^2 (23,700 psi)

Δ STRESS FOAM = 9.38×10^4 (13.6 psi) TENSION

DELTA STRESS IN FOAM INSULATION DUE TO THERMAL
EXPANSION AT SHELL

Δ STRESS $\quad = 7.58 \times 10^4$ N/m^2 (11 psi) <u>TENSION AND COMPRESSION</u>

SUPERIMPOSED WORST CASE STRESSES IN FOAM AT SHELL
FOAM BOUNDARY

MAX. STRESS = 9.65×10^5 (140) + 7.58×10^4 (11) - 9.34×10^4 (13.6) =
9.47×10^5 N/m^2 (137.4 psi) <u>COMPRESSION</u>

INSULATION NOT
EXPOSED
TO FLOW

INSULATION NOT EXPOSED TO FLOW

TOTAL INSULATION SURFACE AREA $= 3902\,\text{m}^2$ (42 000 ft^2)
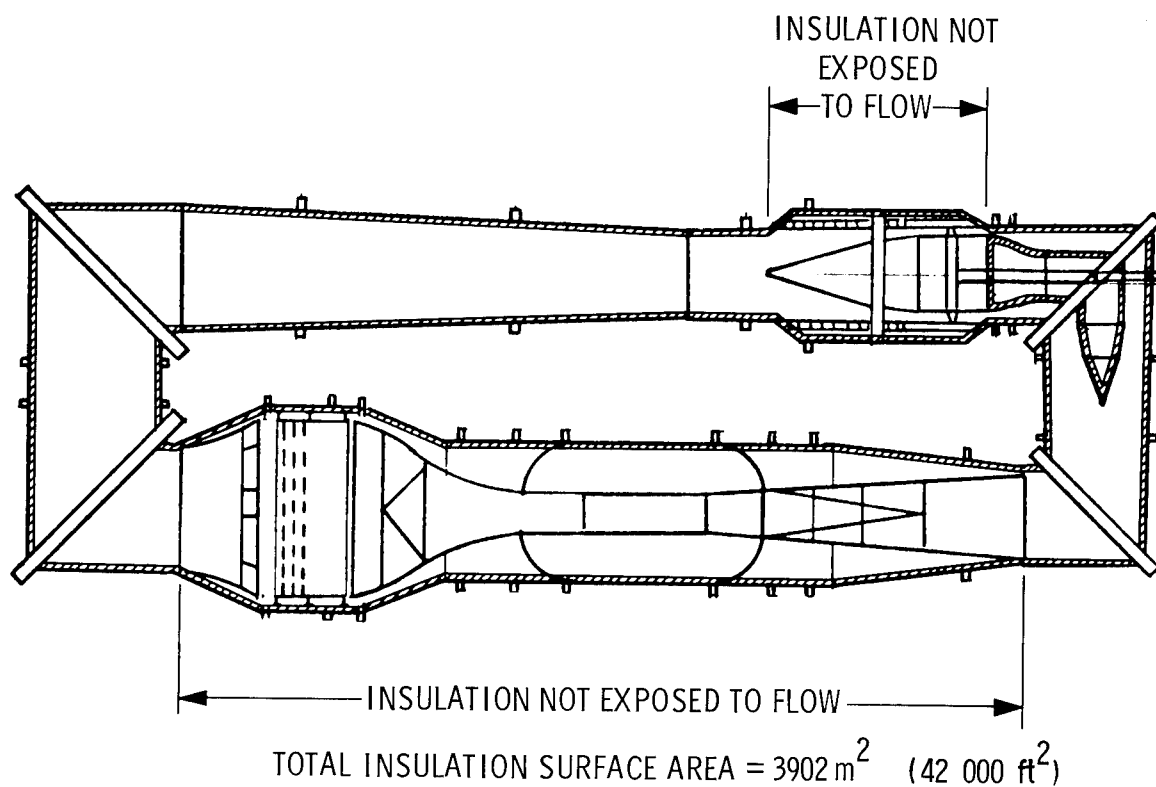
Figure 1.- National Transonic Facility insulation and liner system.

CORRUGATED ALUMINUM LINER
FLOW
A
THERMAL ISOLATOR
PERFORATED ALUMINUM FOIL
FIBROUS INSULATION
.025 m
(1 in.)
TYPICAL
SECTION AA
A
SIDE VIEW
STEEL SHELL
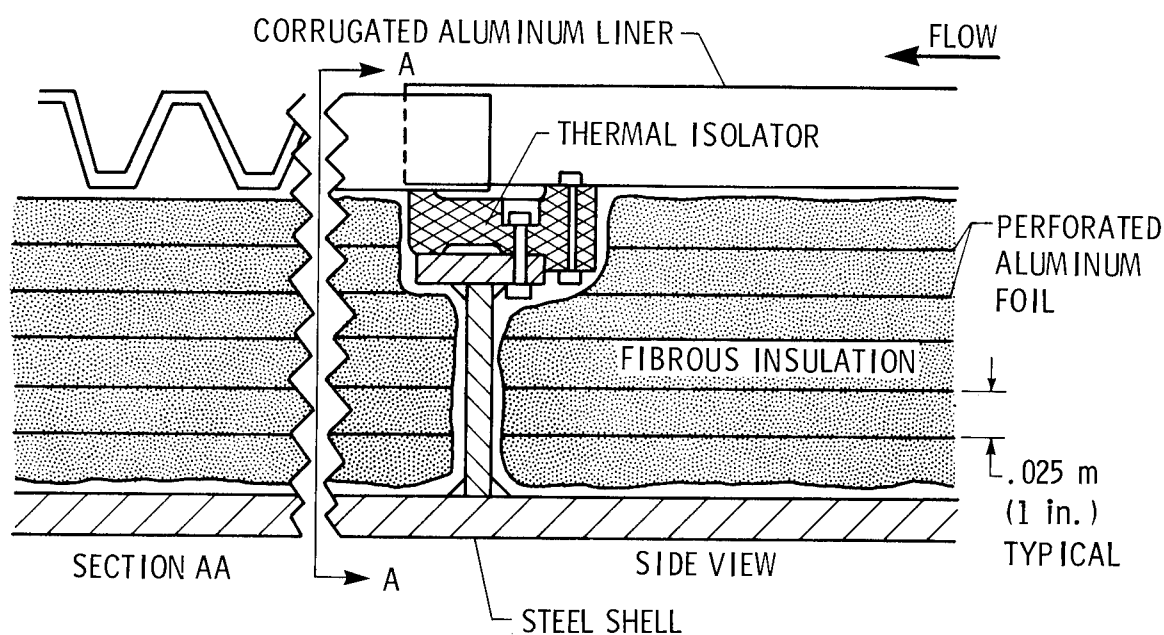
Figure 2.- Internal insulation liner concept.

203
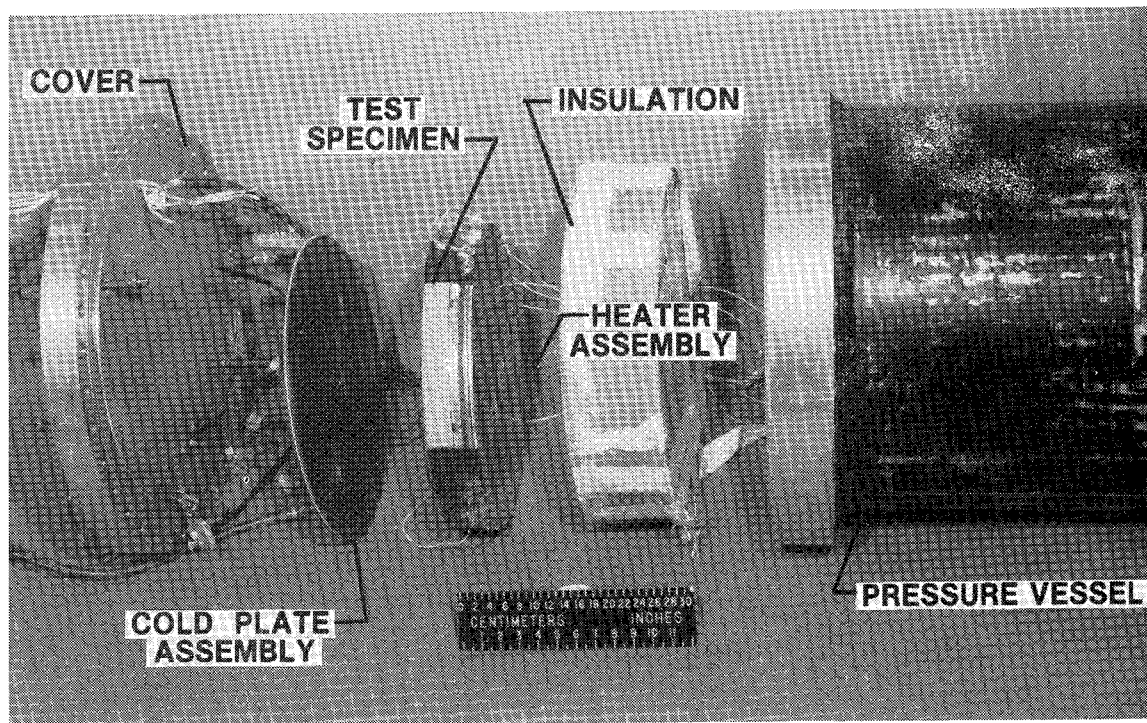
Figure 3.- Thermal conductivity test facility.
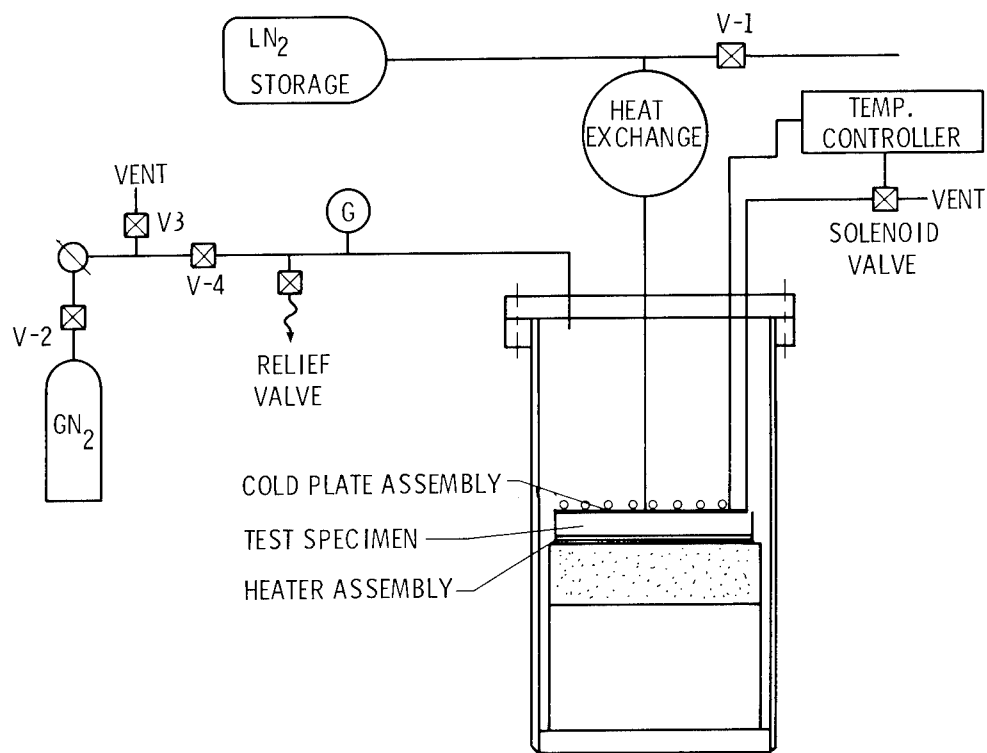
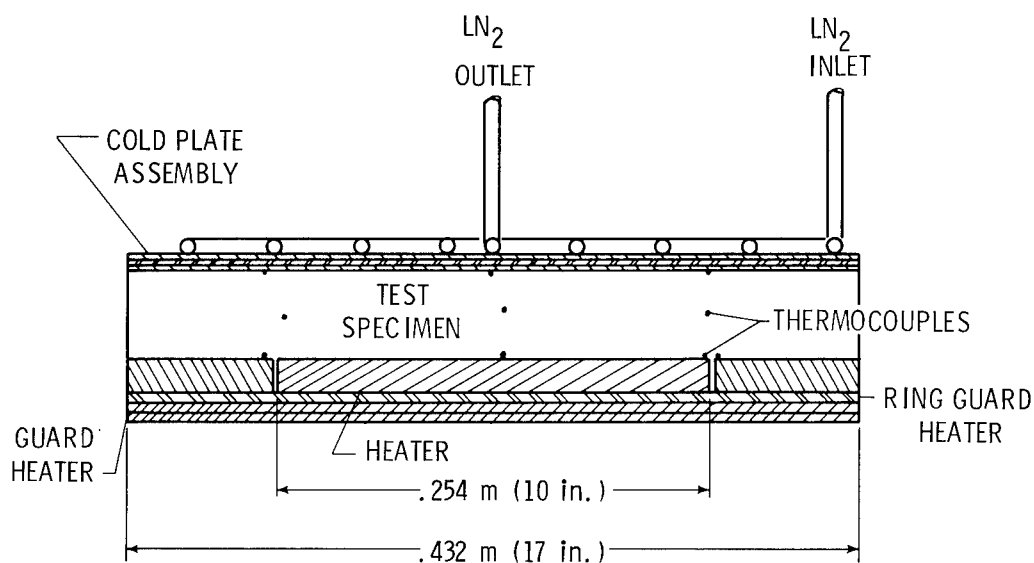Figure 4.- Thermal conductivity test configuration.

LN$_2$
OUTLET

LN$_2$
INLET

COLD PLATE
ASSEMBLY

TEST
SPECIMEN

THERMOCOUPLES

RING GUARD
HEATER

GUARD
HEATER

HEATER

.254 m (10 in.)

.432 m (17 in.)

Figure 5.- Guarded hot plate test set-up.

$K\left(\dfrac{J}{sec,\,m\,K}\right)$ $K\left(\dfrac{Btu-in.}{hr-ft^2\,{}^{o}F}\right)$

.0086   .6

.0072   .5

.0057   .4

.0043   .3

.0029   .2

.0014   .1

$\triangle$ 1.01×10^5 N/m^2 (0 psig)
$\bigcirc$ 2.96×10^5 N/m^2 (28 psig)   UPRIGHT
$\square$ 5.86×10^5 N/m^2 (70 psig)
$\diamond$ 8.96×10^5 N/m^2 (115 psig)

$\blacktriangle$ 1.01×10^5 N/m^2 (0 psig)
$\blacksquare$ 5.86×10^5 N/m^2 (70 psig)   INVERTED
$\blacklozenge$ 8.96×10^5 N/m^2 (115 psig)

$\triangleright$ MANUFACTURER'S DATA (1 atm PRESSURE)
BOUNDARY T$_2$ = 300 K (80°F)

N$_2$ GAS CONDUCTIVITY

-300   -200   -100   0   100   200

BOUNDARY TEMPERTURE T, ^{o}F

89   144   200   255   311   366
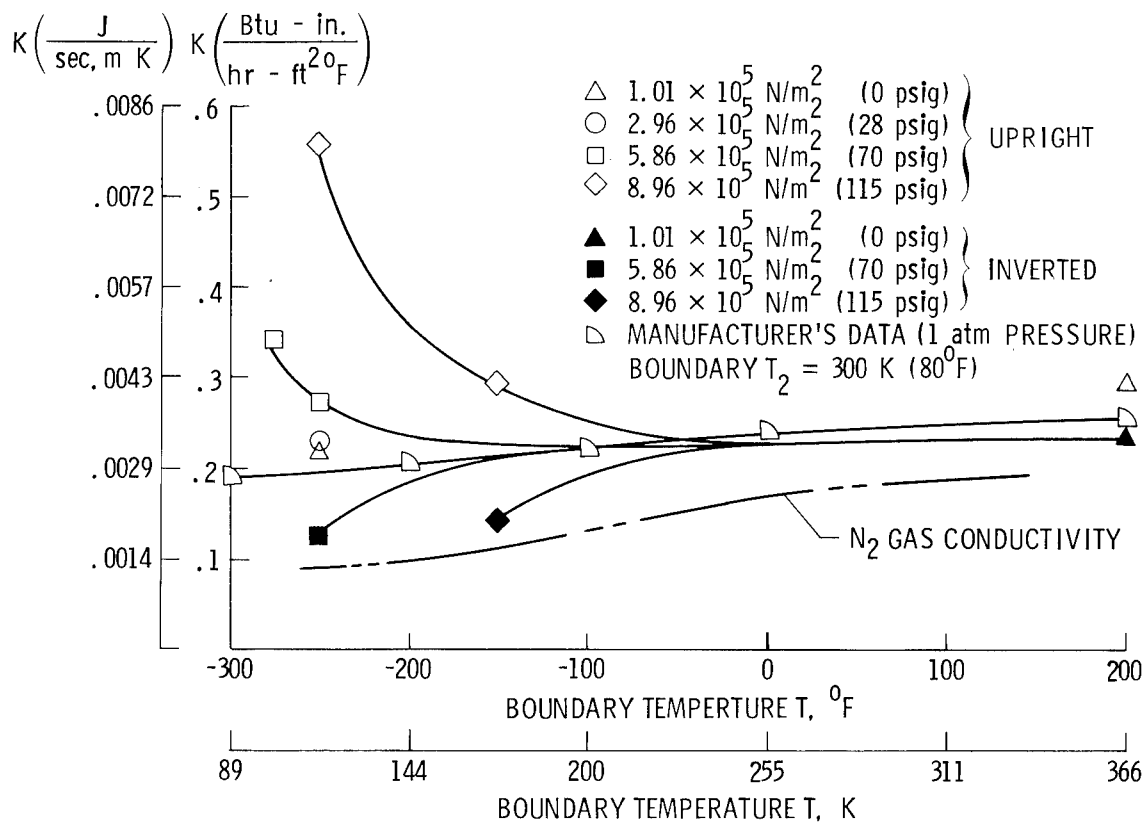
BOUNDARY TEMPERATURE T, K

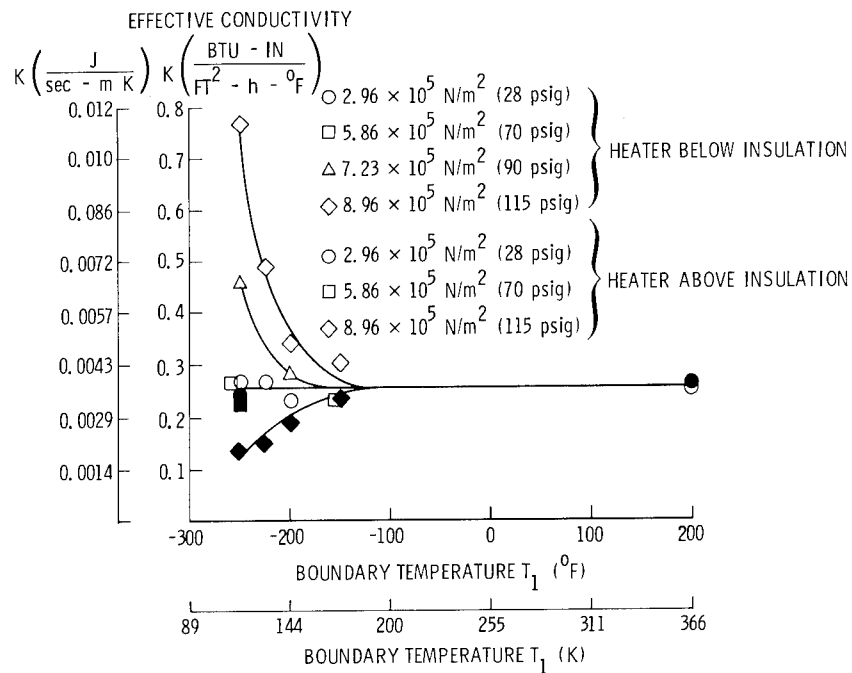Figure 6.- Effective thermal conductivity of temp-mat/alum
flow blockers.

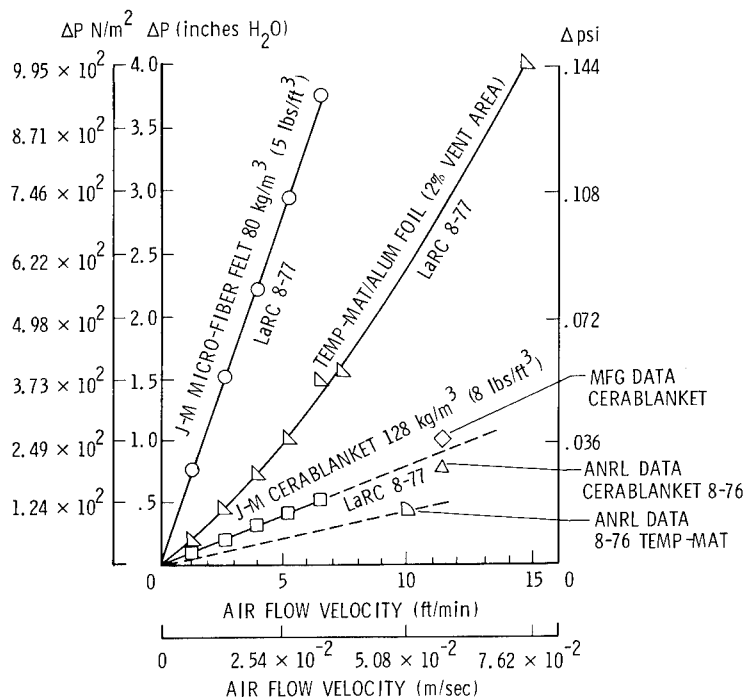Figure 7. J-M Cerablanket 128 kg/m^3 (8 lb/ft^3).
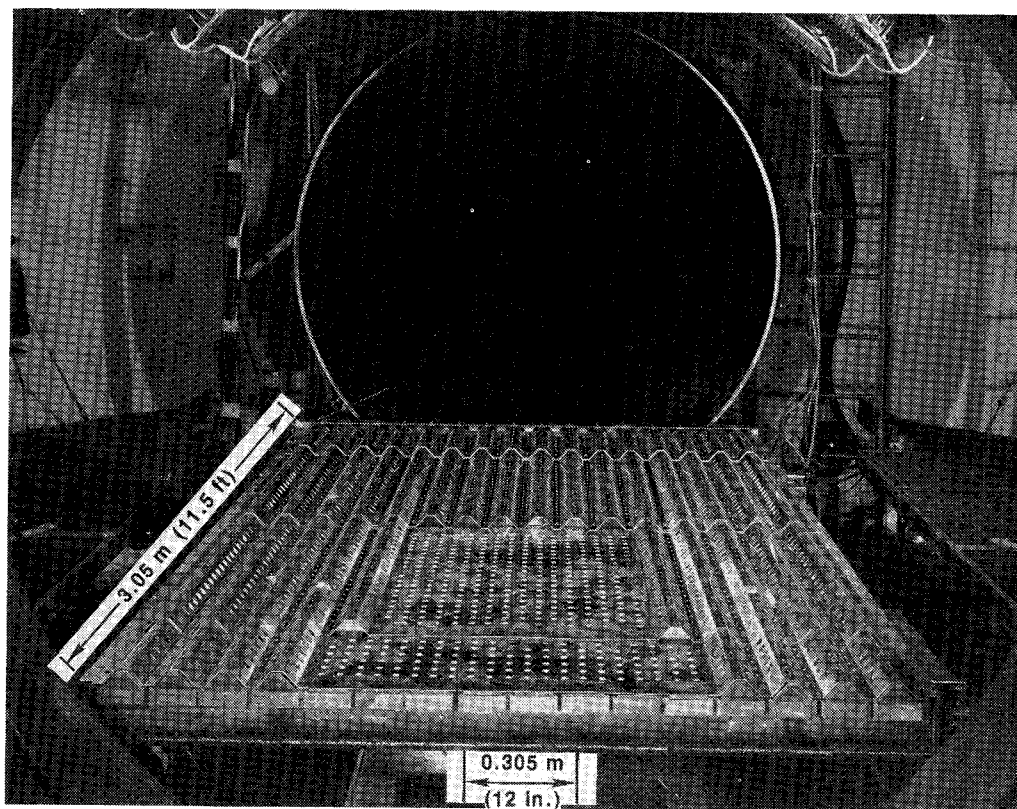

Figure 8.- Flow resistance tests.

Figure 9.- Acoustic test configuration.

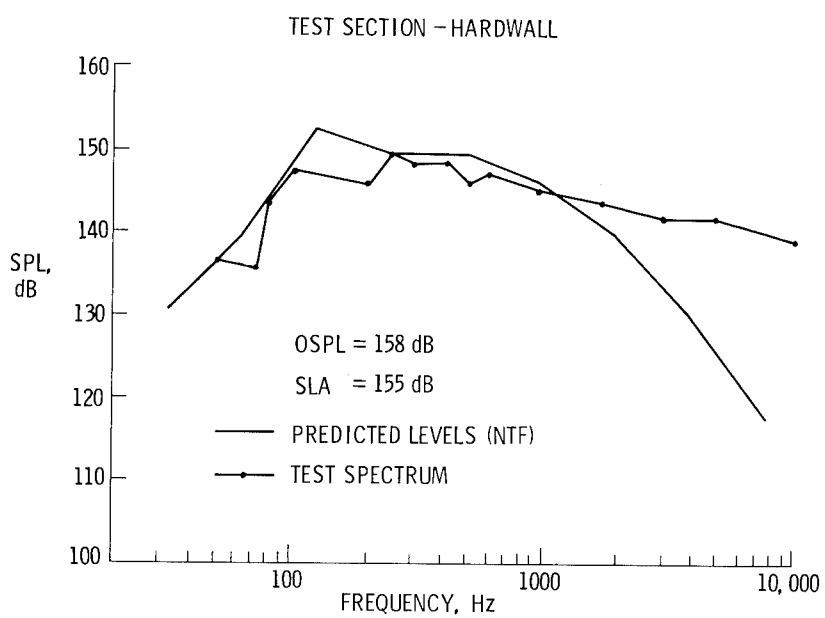Figure 10.- NTF drive fan noise levels.

TEMPERATURE K
TEMPERATURE °F
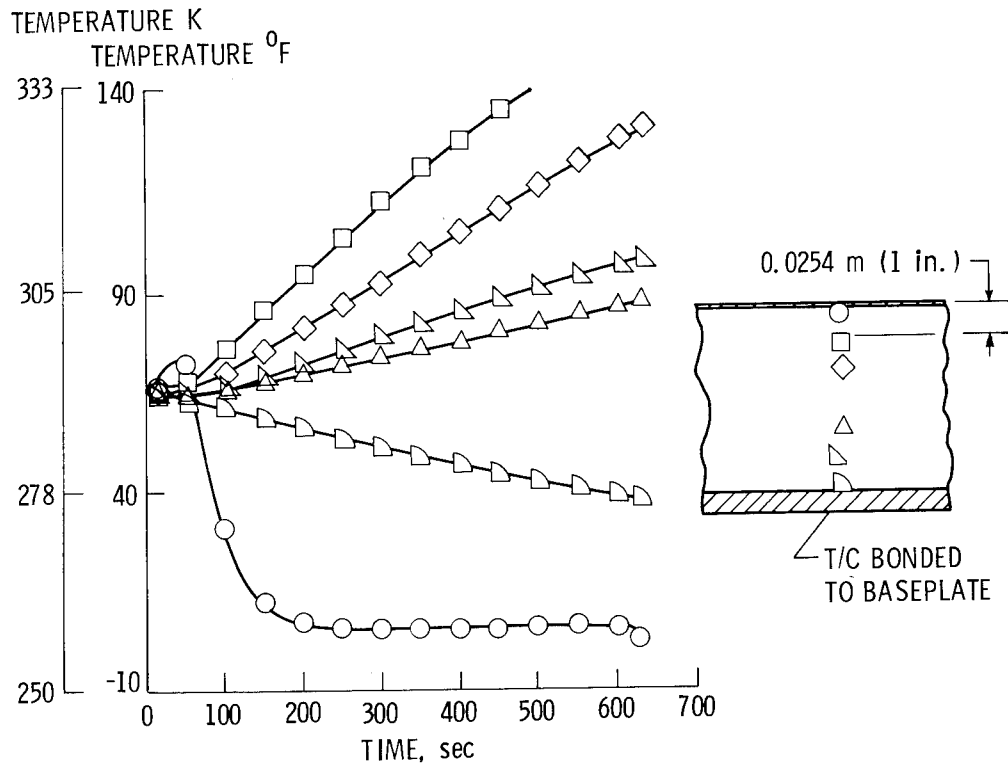
333 — 140

305 — 90

278 — 40

250 — -10

TIME, sec
0 100 200 300 400 500 600 700

0.0254 m (1 in.)

T/C BONDED
TO BASEPLATE

Figure 11.- Acoustic test on fibrous insulation system
(temp-mat).

FIBERGLASS AND
CREST ADHESIVE

ALUMINUM
LINER

POLYESTER/GLASS
PULTRUSION RIB &
CAP STRIP

CROSS SECTION THROUGH INSULATION
(LOOKING AXIALLY)

CAP STRIP

PULTRUSION
RIB

LINK

SHELL TAB

DETAIL OF LINER ATTACHMENT
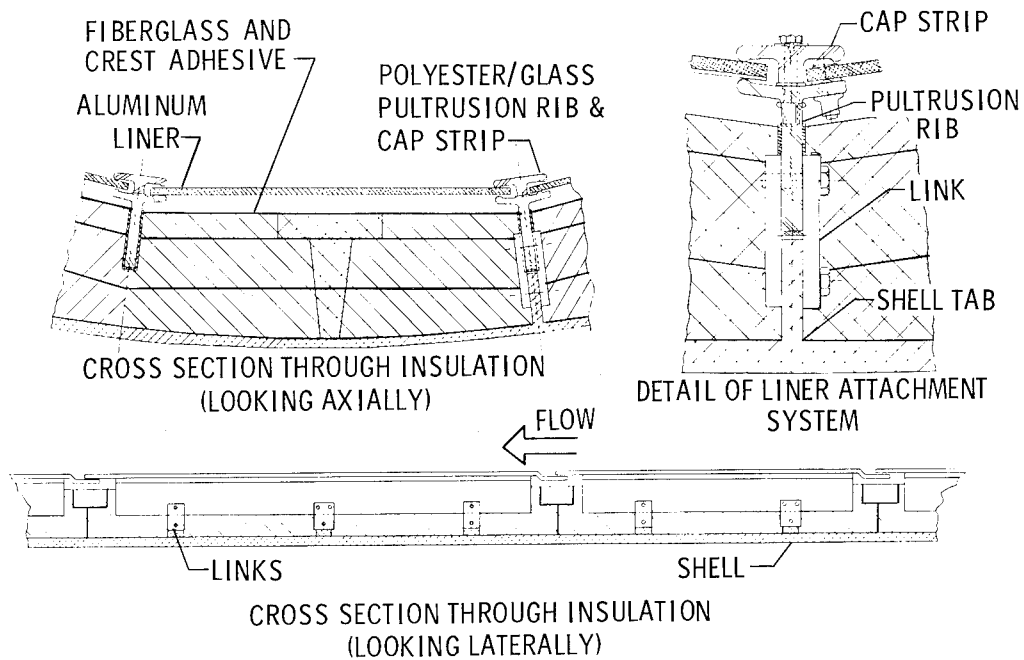SYSTEM

FLOW

LINKS

SHELL

CROSS SECTION THROUGH INSULATION
(LOOKING LATERALLY)

Figure 12.- Insulation and liner system configuration.
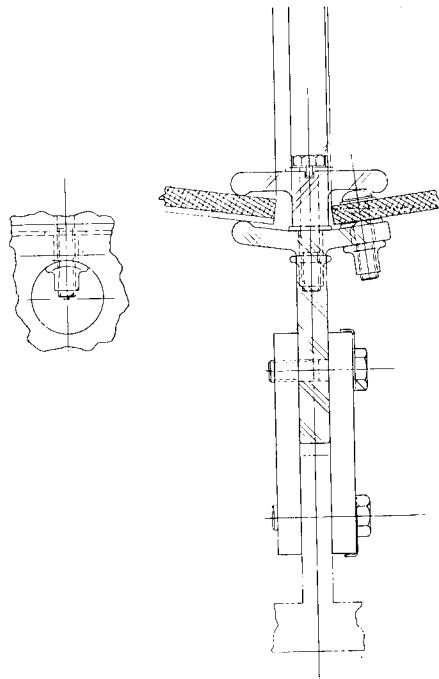
Figure 13.- Detail of liner attachment system.

ALUMINUM LINER

POLYESTER/GLASS PULTRUSION RIB & CAP STRIP

FIBERGLASS AND CREST ADHESIVE

CROSS SECTION THROUGH INSULATION (LOOKING AXIALLY)

CAP STRIP

PULTRUSION RIB

LINK

SHELL TAB

DETAIL OF LINER ATTACHMENT SYSTEM

LINKS

SHELL

CROSS SECTION THROUGH INSULATION

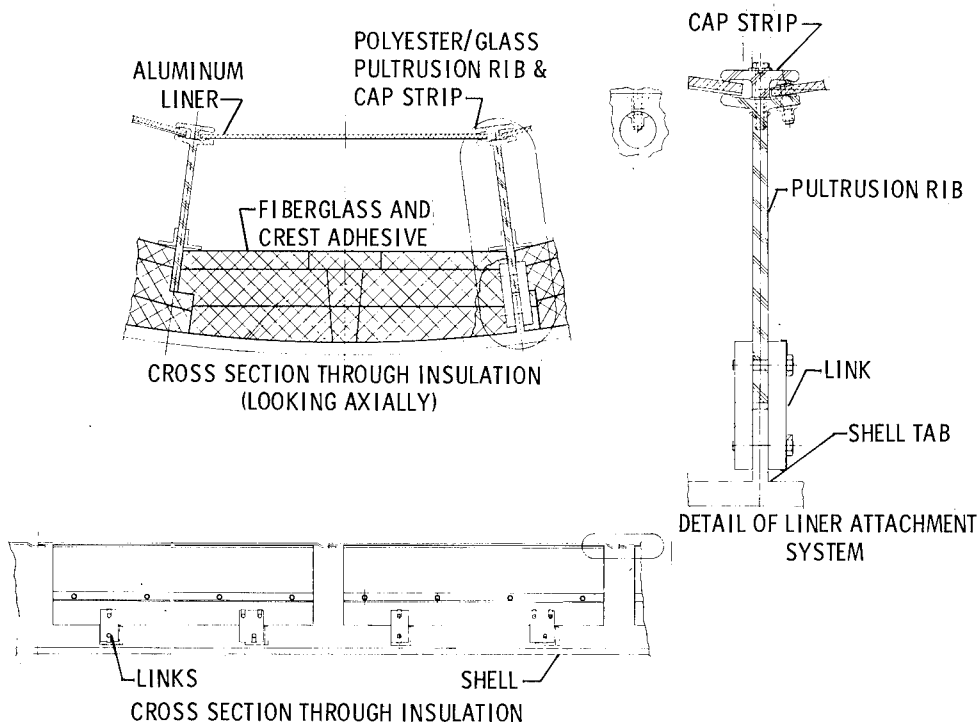Figure 14.- Basic insulation and liner system configuration (deep section).
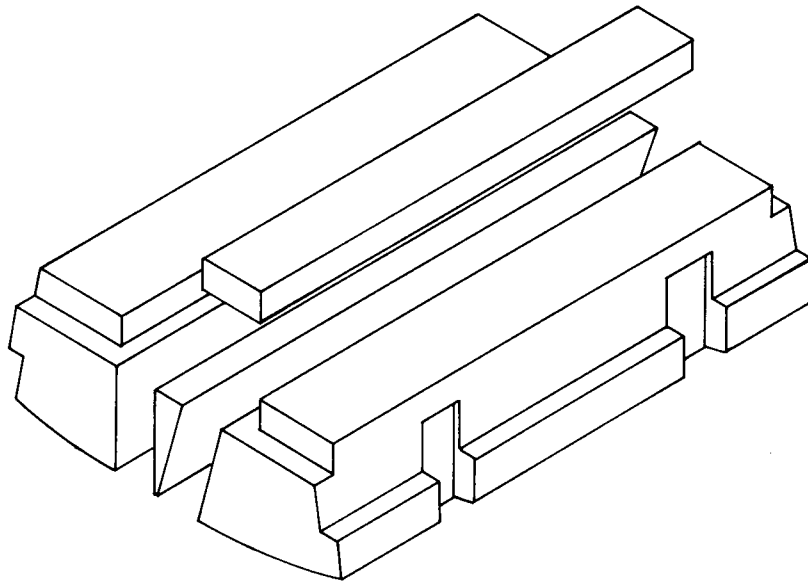
Figure 15.- NTF insulation block configuration.

THREADED ROD 0.013 m (1/2 in.) DIA.
WITH RETAINER WASHER

INSULATION SYSTEM
(12 SIDED POLYGON)

5 LAYERS OF
INSULATION &
CREST/FIBERGLASS
ADHESIVE

NACELLE SKIN

WELD STUD

NACELLE
SKIN

DETAIL OF INSULATION
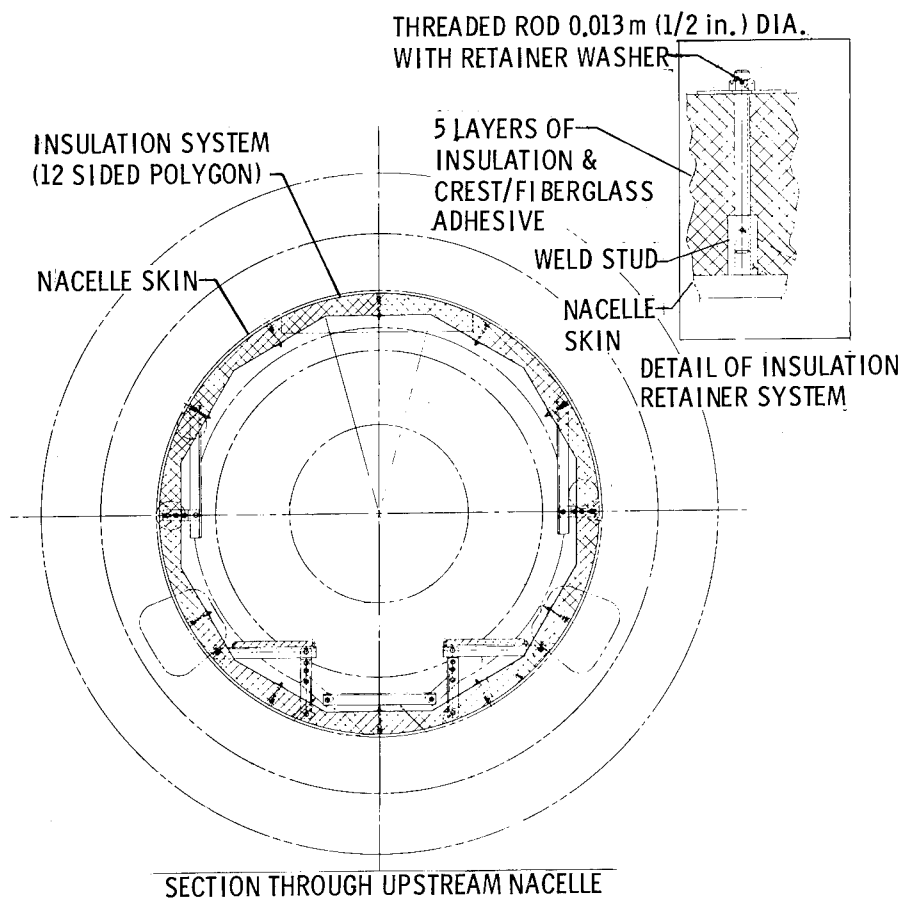RETAINER SYSTEM

SECTION THROUGH UPSTREAM NACELLE

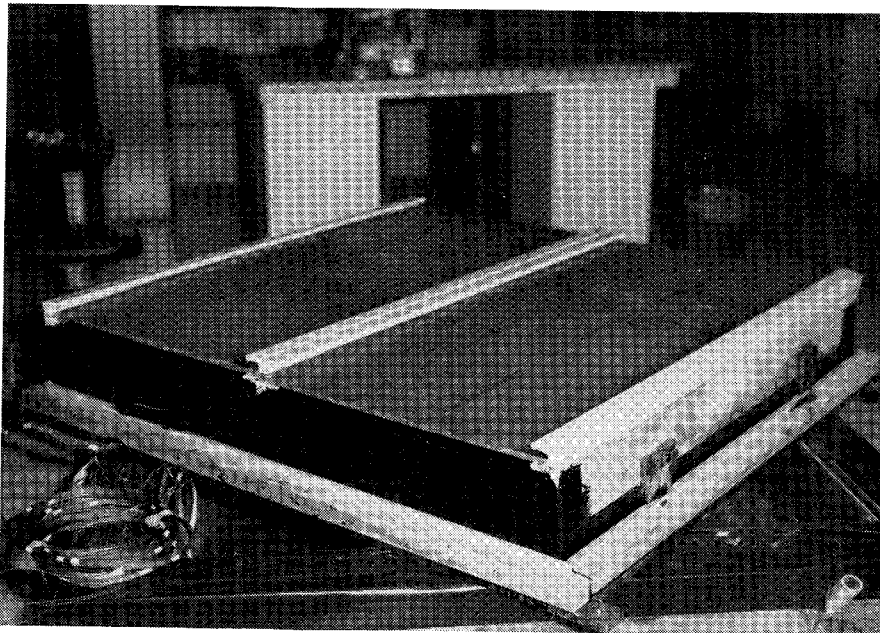Figure 16.- Upstream nacelle insulation system.

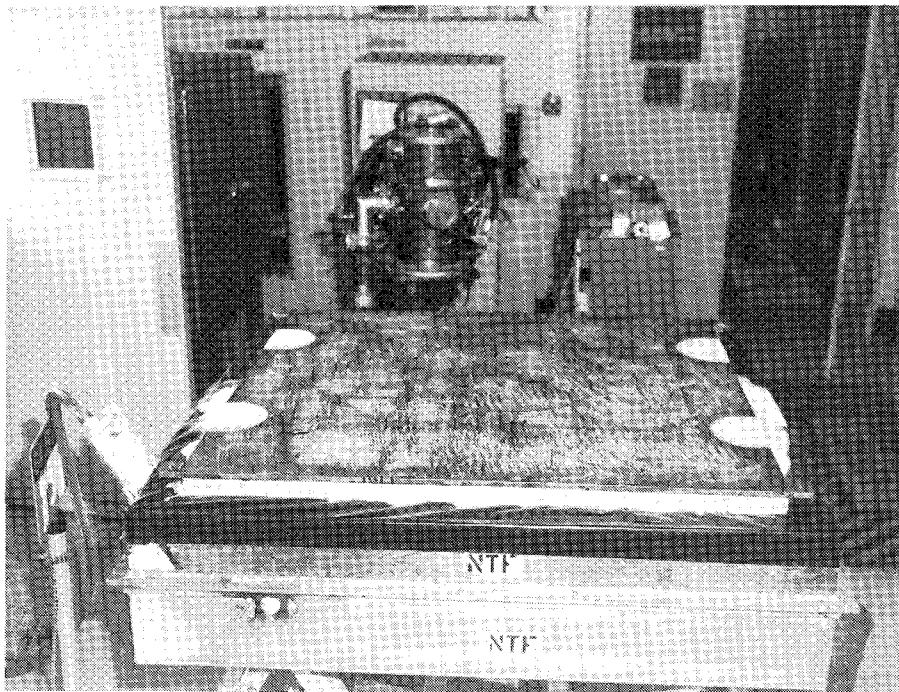Figure 17.- 1.22-m (4 foot) insulation test panel.

Figure 18.- 1.22-m (4 foot) insulation test panel - cold
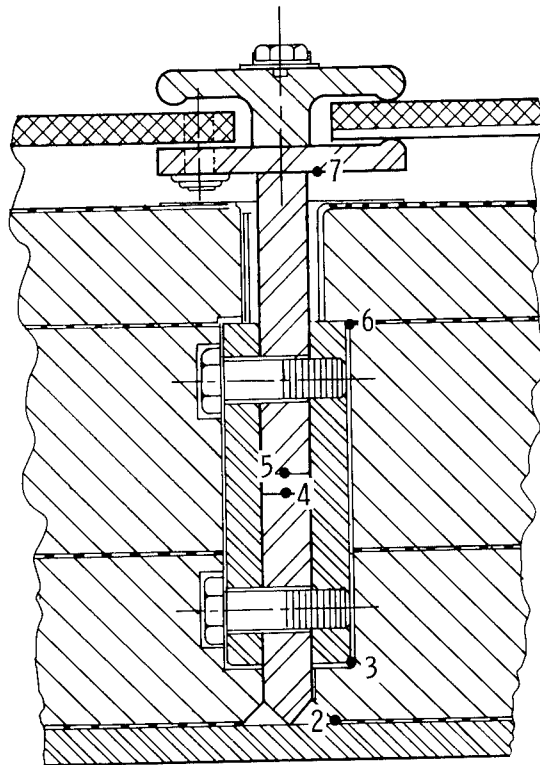cycle test.

211

Figure 19.- 1.22-m (4 foot) test panel thermocouple location
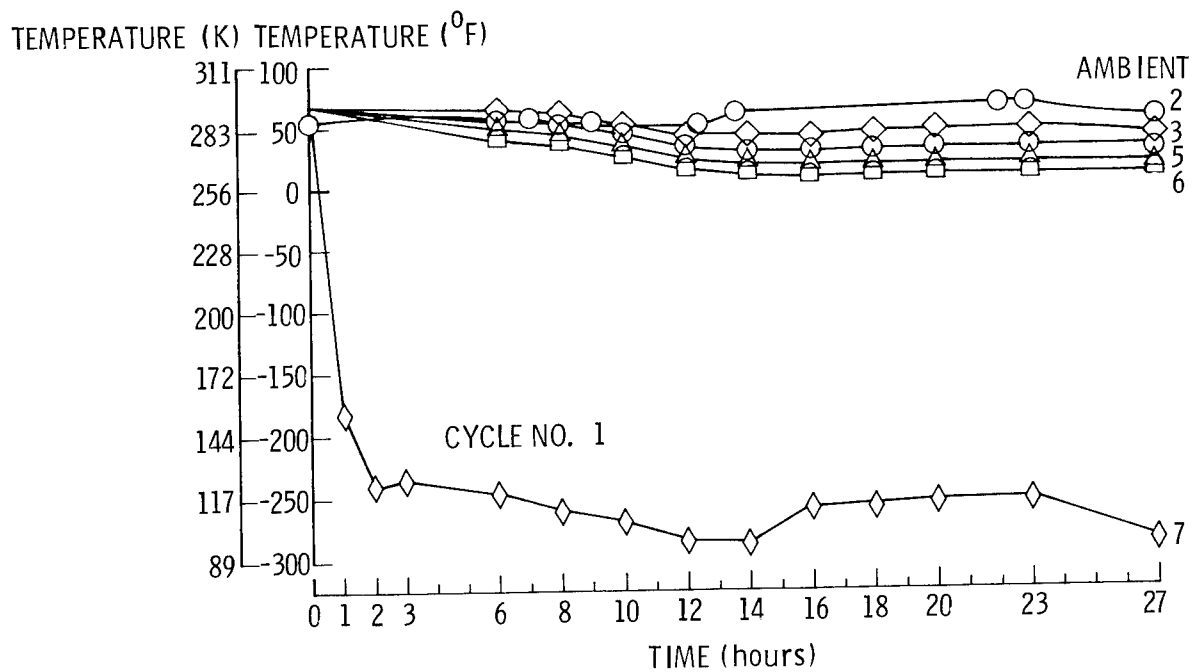(at tab and link).

Figure 20.- 1.22-m (4 foot) test panel cold cycle test results.
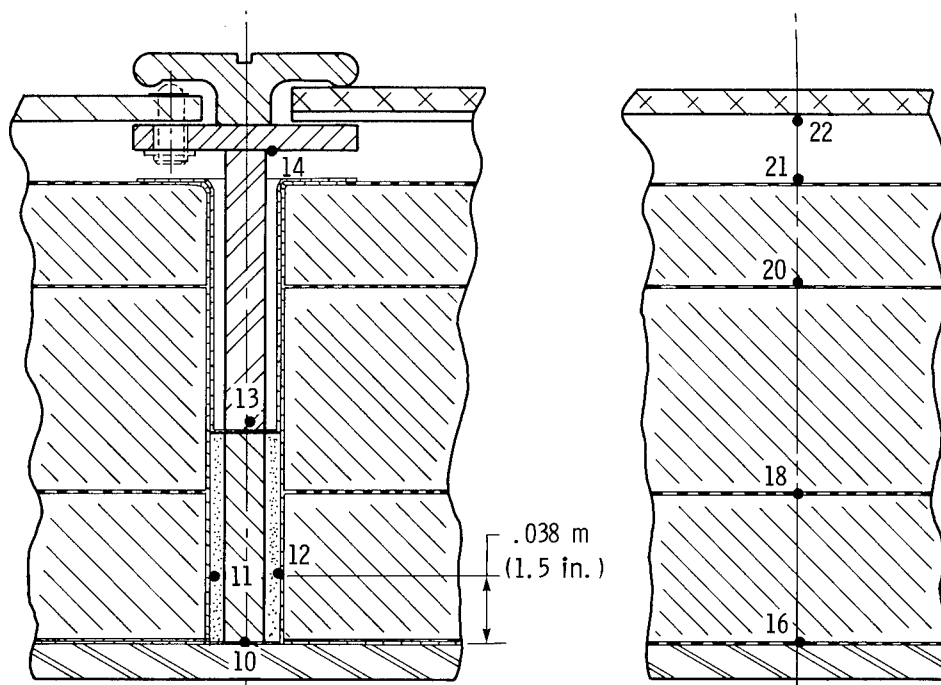
Figure 21.- 1.22-m (4 foot) test panel thermocouple locations.
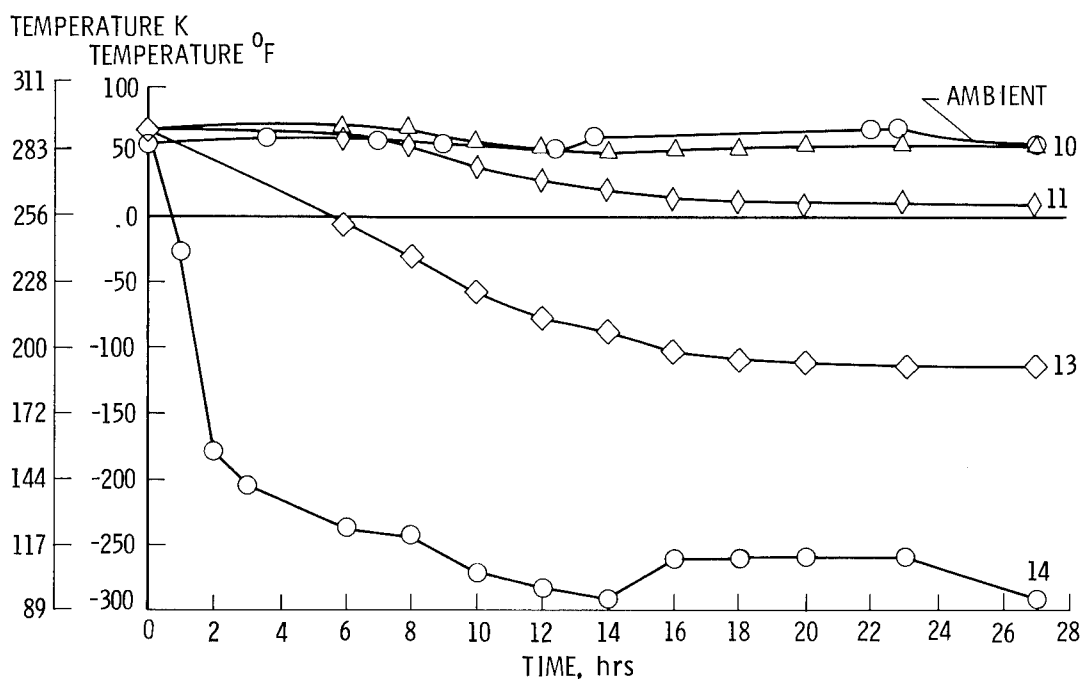
Figure 22.- Cold cycle test results for 1.22-m (4 foot) test panel.

TEMPERATURE (K) TEMPERATURE (^{0}F)

AMBIENT

CYCLE NO. 1

16

18

20

21

22

TIME (hours)
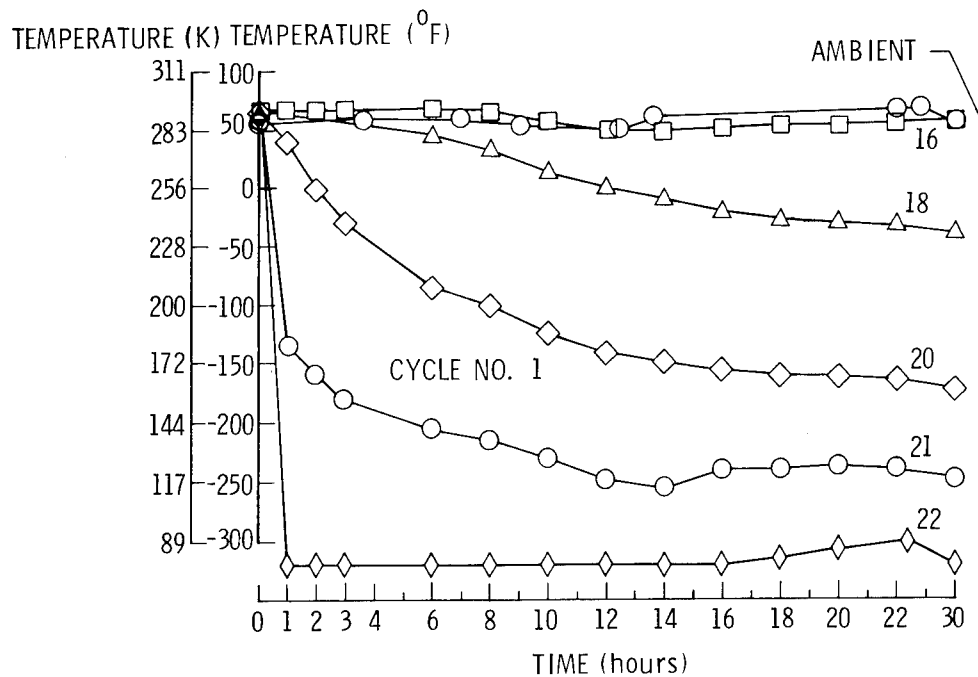
Figure 23.- 1.22-m (4 foot) test panel cold cycle test results.

☐ T/C – 16
△ T/C – 18
◇ T/C – 20
○ T/C – 21
◊ T/C – 22

TEMPERATURE K
TEMPERATURE (^{0}F)

TIME, hours

Figure 24.- 1.22-m (4 foot) test panel for hot cycle test results.

214

Figure 25.- Fatigue test cycle machine - instron driven.
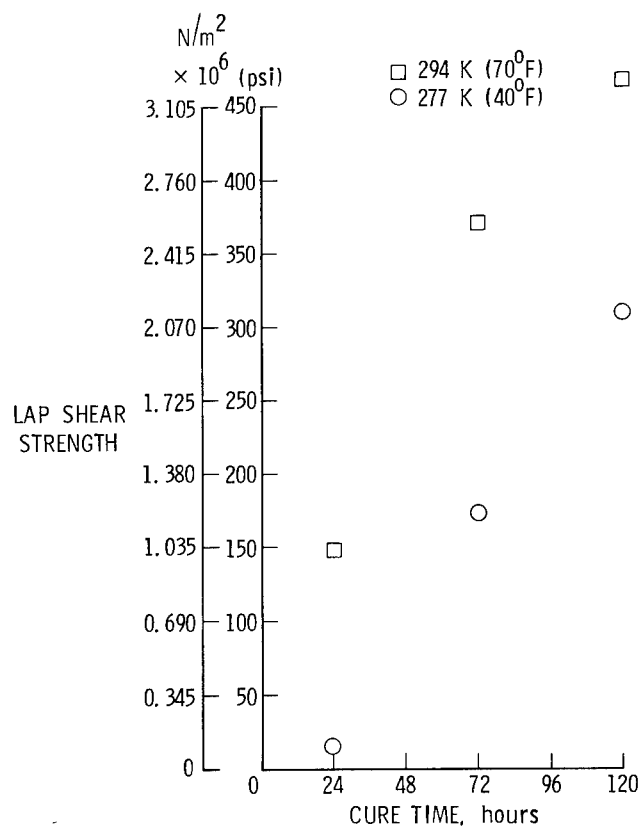
Figure 26.- Crest 391 strength versus cure time.

NASTRAN MODEL – BOUNDARY CONDITIONS

X DEFL. = 0   Z DEFL. = 0

.167 m
(6.6 in.)

.3 m
(12 in.)

.45 m
(18 in.)

X DEFL. = 0

Z DEFL. = 0

LOADS
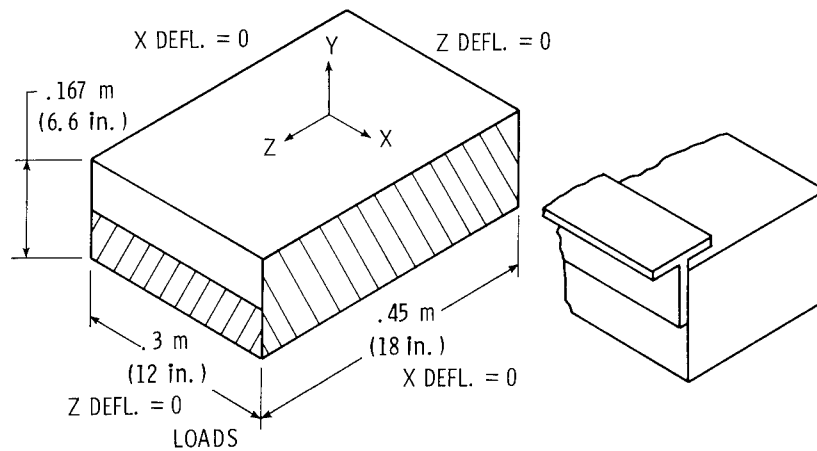
SUBCASE 1: TEMPERATURE LOADING
            LINEAR PROFILE – 106 K TO 294 K (-270°F TO 70°F)

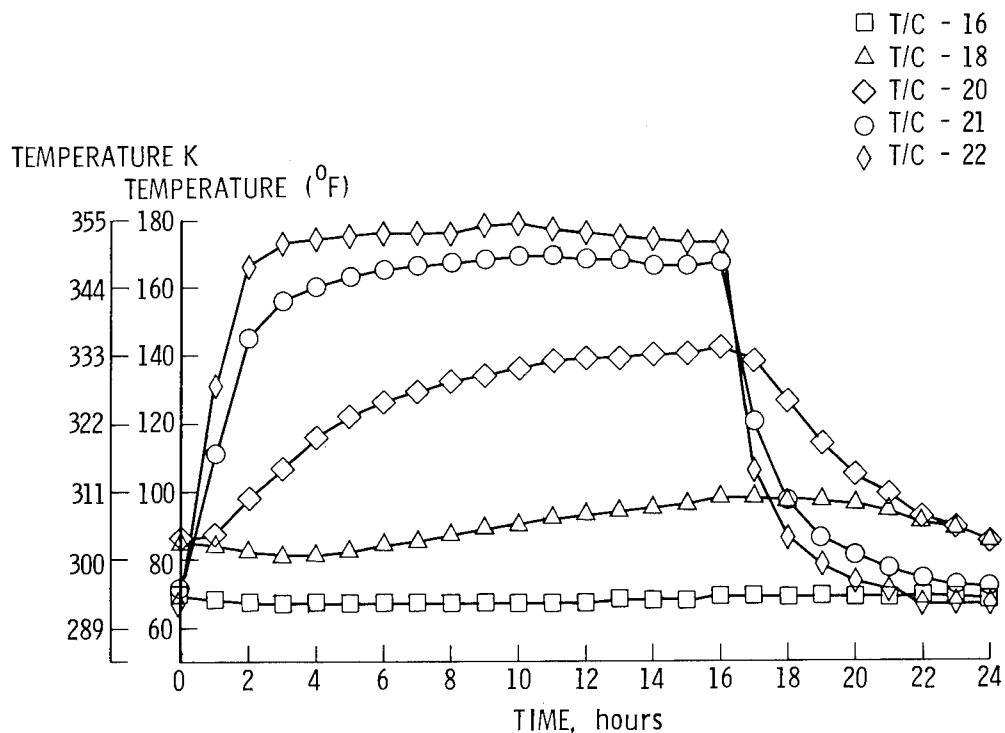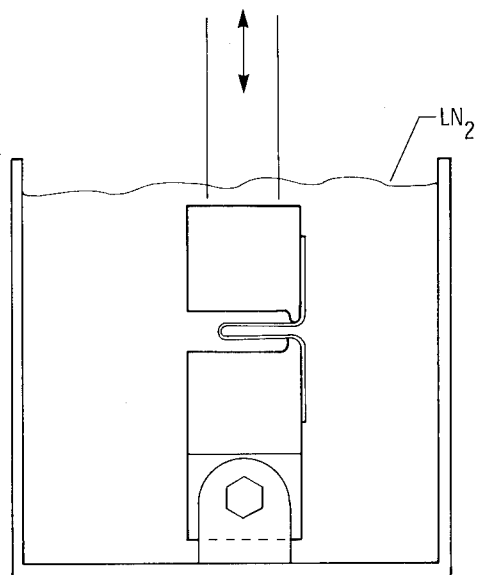SUBCASE 2: TEMPERATURE LOADINGS 8.96 × 10^5 N/m^2
            PRESSURE

Figure 27.- Closed cell.

1556 N (350 lbs)

0.241 m (9.5")

0.019 m (.75")

0.076 m
(3.0")

0.016 m (0.62")

0.019 m (.75")

0.038 m (1.50")

LOCATION NO.	STRESS N/m^2 (psi)	TYPE/ELEMENT	
1	4.92 × 10^7 (7168)	BENDING	PULTRUSION
2	4.19 × 10^7 (6080)	TENSION	BOLT
3	1.04 × 10^8 (15150)	BENDING	LINK
4	4.14 × 10^7 (6010)	TENSION	BOLT
5	1.17 × 10^8 (17020)	BENDING	TAB WELD
6	4.14 × 10^7 (6000)	BEARING	PULTRUSION FOR X = 0.002 m (.096") FOR PARABOLIC BEARING DISTRIBUTION
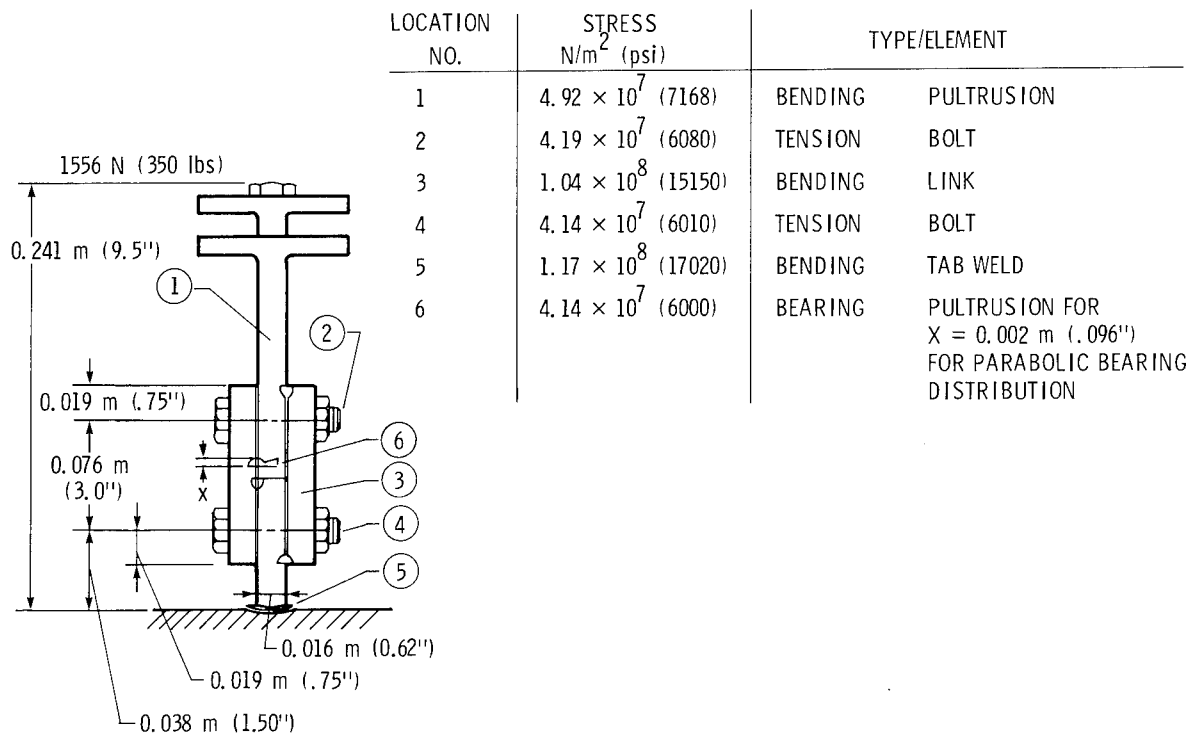
Figure 28.- Stress analysis summary – standard section.

216

1556 N (350 lbs)

LOCATION NO.	STRESS N/m^2	(psi)	TYPE/ELEMENT	
1	5.56×10^7	(8060)	BENDING	PULTRUSION
2	1.25×10^8	(18100)	TENSION	BOLT
3	1.06×10^8	(15440)	BENDING	LINK
4	1.03×10^8	(14950)	BENDING	LINK
5	1.01×10^8	(14655)	TENSION	BOLT
6	3.56×10^7	(5080)	BENDING	TAB WELD
7	4.14×10^7	(6000)	BEARING	PULTRUSION FOR X = 0.005 m (.204") FOR PARABOLIC BEARING DISTRIBUTION

0.0254 m (1.0")
0.45 m (17.75")
0.083 m (3.25")
0.038 m (1.5")
0.016 m (.62")
0.0254 m (1.0")

Figure 29.- Stress analysis summary - deep section.

1334 N (300 lbs)

0.19 m (7.5")

F = 1334 N (300 lbs)

R_1 = 417 N (93.75 lbs)

R_2 = -417 N (-93.75 lbs)

Figure 30.- Stress analysis summary, tab reaction - standard section.

$$F_{MAX} = \sqrt{(1455 + 208)^2 + (667)^2} = 1792 \text{ N (403 lbs)}$$

BOLT SHEAR STRESS

$$\tau = \frac{1792}{2(1.26 \times 10^{-4})} = 7.09 \times 10^6 \text{ N/m}^2 \text{ (1026 psi)}$$

RIB BEARING STRESS

$$\sigma_B = \frac{1792}{(1.5875 \times 10^{-2})(1.27 \times 10^{-2})} = 8.88 \times 10^6 \text{ N/m}^2 \text{ (1290 psi)}$$
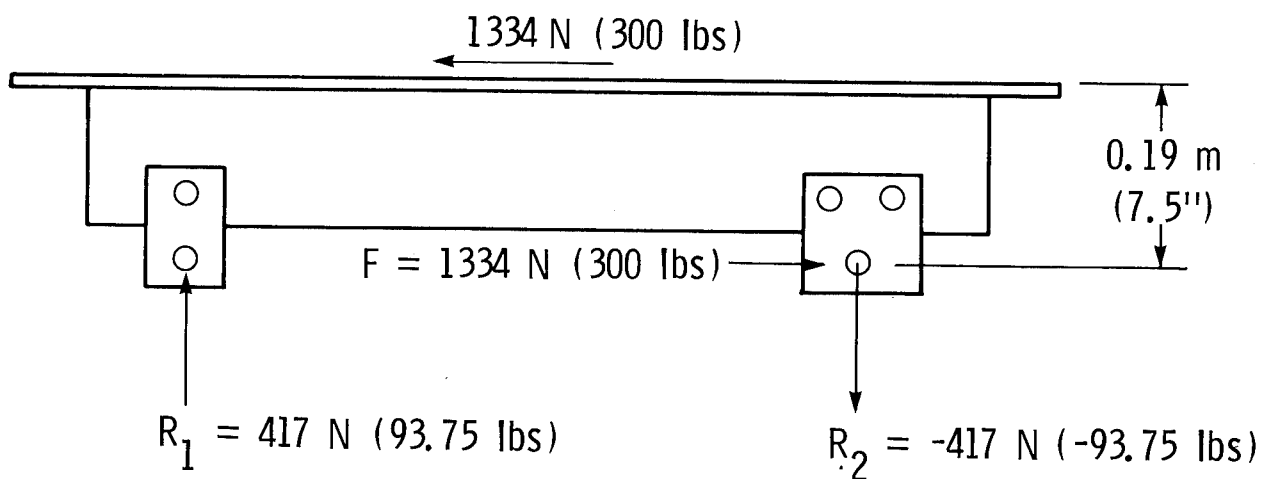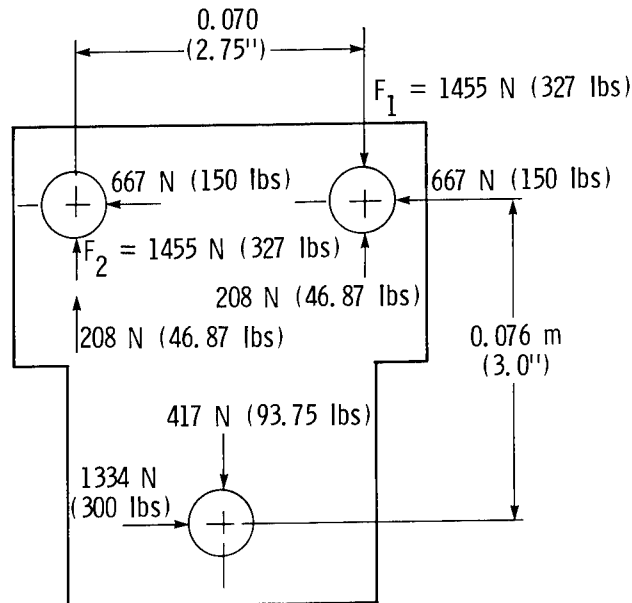
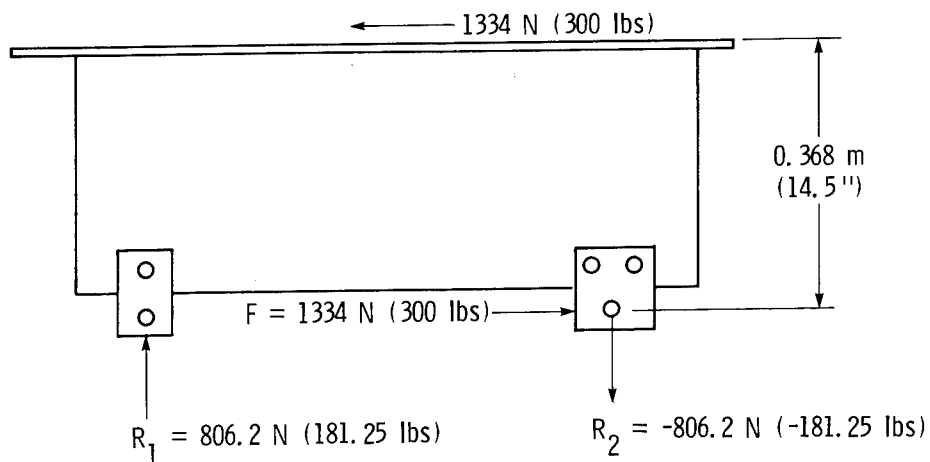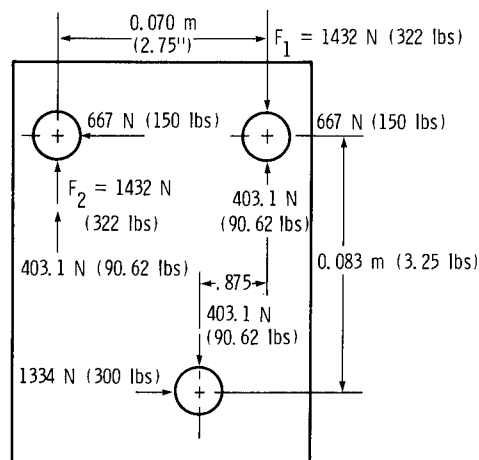Figure 31.- Stress analysis summary, fixed link - standard section.

Figure 32.- Stress analysis summary, tab reactions - deep section.

$$F_{MAX} = \sqrt{(1432 + 403.1)^2 + (667)^2} = 1952 \text{ N } (439 \text{ lbs})$$
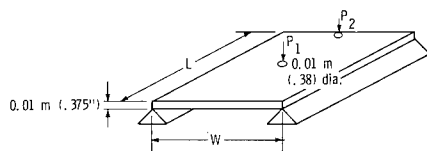
BOLT SHEAR STRESS

$$\tau = \frac{1952}{2(1.26 \times 10^{-4})} = 7.7 \times 10^6 \text{ N/m}^2 \ (1120 \text{ psi})$$

RIB BEARING STRESS

$$\sigma_B = \frac{1952}{(1.5875 \times 10^{-2})(1.27 \times 10^{-2})} = 9.7 \times 10^6 \text{ N/m}^2 \ (1405 \text{ psi})$$

Figure 33.- Stress analysis summary, fixed link – deep section.

MATERIAL: 5054-0 ALUM. $\sigma_{ALLOWABLE} = 6.55 \times 10^{10}$ N/m^2 (9500 psi)

TUNNEL AREA	L	W	$P_1 = 1334$ N CENTERAL LOAD		$P_2 = 1334$ EDGE LOAD	1.915×10^3 N/m^2 DISTRIBUTED LOAD	NATURAL FREQUENCY
			σ, N/m^2	$\bar{Y}$, m	σ, N/m^2	σ, N/m^2	W_1 Hz
LE-944859 SHORT CYL	1.22 m	.61 m	2.90×10^7	-2.60×10^{-3}	5.80×10^7	6.19×10^6	59.5
LE-944861 CORNER # 3	1.22 m	.91 m	3.10×10^7	-6.45×10^{-3}	6.21×10^7	1.39×10^7	26.4
LE-944863 CORNER # 4	1.22 m	.66 m	2.93×10^7	-3.18×10^{-3}	5.86×10^7	7.25×10^6	50.7
LE-944864 SETTLING CHAMBER	1.22 m	.86 m	3.07×10^7	-5.69×10^{-3}	6.15×10^7	1.25×10^7	29.6
LE-944866 GATE VALVE AREA	1.22 m	.99 m	3.17×10^7	-7.72×10^{-3}	6.33×10^7	1.62×10^7	22.5
LE-944877 CORNER # 1	1.22 m	.56 m	2.90×10^7	-2.26×10^{-3}	5.80×10^7	5.67×10^6	70.8
LE-944880 CORNER # 2	1.22 m	.71 m	2.96×10^7	-3.73×10^{-3}	5.92×10^7	8.46×10^6	43.7

Figure 34.- Stress analysis summary – aluminum liner panel.

$$AREA = \sqrt{\frac{v^2 \left(\frac{dp}{dt}\right)^2}{2g \, PC_D^2 \, \Delta P \, RT}}$$

TUNNEL PRESSURE $(P) = 9.653 \times 10^5$ N/m^2

DEPRESSURIZATION RATE $\left(\frac{dp}{dt}\right) = 8.27 \times 10^4$ N/m^2/sec

TUNNEL GAS TEMP $(T) = 353^0$ K

ACCEPTABLE $\Delta P = 1.915 \times 10^3$ N/m^2

ORIFICE COEFFICIENT $(C_D) = 0.85$

GRAVITATIONAL CONSTANT $(g) = 6.673 \times 10^{-11}$ N m^2/kg^2

GAS CONSTANT $(R) = 8.31 \times 10^3$ J/k mole ^{0}K

TUNNEL AREA	VOLUME m^3	AREA REQD m^2/PANEL	PANEL P CAPABILITY/N/m^2
SHORT CYLINDER	2.35×10^{-2}	1.18×10^{-4}	2.03×10^4
CORNER # 3	2.35×10^{-2}	1.18×10^{-4}	9.03×10^3
CORNER # 4	2.35×10^{-2}	1.18×10^{-4}	1.73×10^4
SETTLING CHAMBER	2.35×10^{-2}	1.18×10^{-4}	1.01×10^4
GATE VALVE AREA	2.35×10^{-2}	1.18×10^{-4}	7.72×10^3
CORNER # 1	2.12×10^{-1}	1.07×10^{-3}	2.21×10^4
CORNER # 2	2.12×10^{-1}	1.07×10^{-3}	1.48×10^4
ACCESS DOOR POCKET	1.27×10^1	6.38×10^{-2}	ACTUAL VENT AREA = 1.08×10^{-1}
ACCESS DOOR COMPARTS	1.70×10^{-1}	8.5×10^{-4}	ACTUAL VENT AREA = 1.14×10^{-3}

Figure 35.- Stress analysis summary - venting requirements.
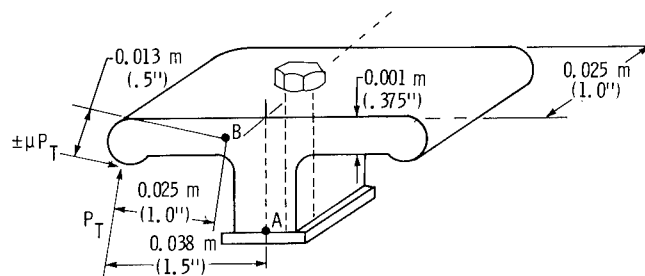
BENDING STRESS AT POINT "B"

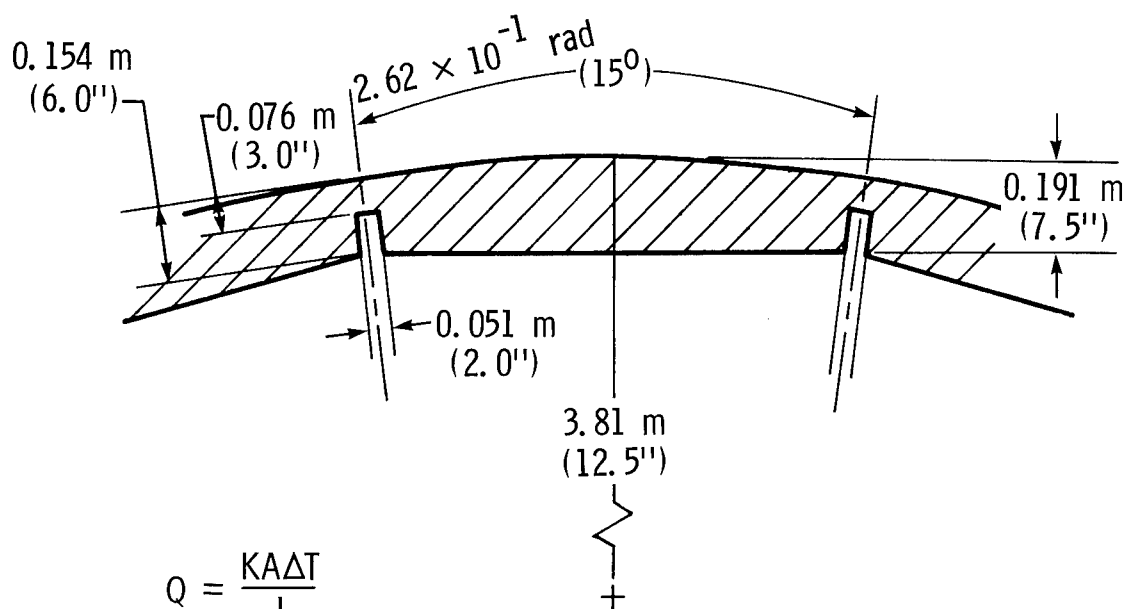$P_T = P_S + P_{\Delta P}$, $P_{SPRING} = 445$ N (100 lbs), $P_{\Delta P} = 267$ N (60 lbs), $\mu = .3$

$\sigma = 5.41 \times 10^7$ N/m^2 (7850 psi)

LOAD (P) REQUIRED TO CAUSE SEPARATION AT POINT "A"

BOLT PRESTRESSED TO 70% A-638 ALLOWABLE 3.52×10^8 N/m^2 (51000 psi)

$P = 13.88$ N (312 lbs)

Figure 36.- Stress analysis summary - cap strip stress.

$$Q = \frac{KA\Delta T}{L}$$

$A_{TOTAL} = 3.90 \times 10^3 \text{ m}^2 \ (42000 \text{ ft}^2)$

$A_1 = (.051)(24) \ 1.52 \times 10^2 = 1.86 \times 10^2 \text{ m}^2 \ (2000 \text{ ft}^2)$

$A_2 = 3.90 \times 10^3 - 1.86 \times 10^2 = 3.716 \times 10^3 \ (40000 \text{ ft}^2)$

$Q_{ALLOW} = 3.165 \times 10^5 \text{ J/S} \ (300 \text{ btu})/\text{sec}$

$$3.165 \times 10^5 = \frac{(K)(3.716 \times 10^3)(217)}{.1524} + \frac{(K)(1.86 \times 10^2)(217)}{.0762}$$

$K = .0054 \text{ J/Sm K} \left(.377 \ \dfrac{\text{RTU} - \text{IN}}{\text{ft}^2 - \text{HR} - {}^\circ\text{F}} \right)$

Figure 37.- Allowable thermal conductivity for closed cell
insulation material.

CONNECTORS AND WIRING FOR CRYOGENIC TEMPERATURES

Eugene L. Kelsey and Robert D. Turner
Langley Research Center

SUMMARY

Electrical connectors and wiring insulation exposed to cyclic cryogenic thermal environment are subject to cyclic stresses which can lead to cracking and failure of these components. This paper describes a series of tests which were implemented to qualify connectors and wiring for the transient thermal environment of the National Transonic Facility at NASA's Langley Research Center. The MS-A (MIL-C-5015) connector with diallyl phthalate (DAP) inserts and Tefzel insulated wire was found to be acceptable.

INTRODUCTION

The National Transonic Facility (NTF) will require between 1000 and 1500 electrical connectors and over 9000 meters (30,000 feet) of wire and cable in the internal working systems and controls. These components will be subjected to the full range of pressure and temperature on a cyclic basis for a period of ten or more years. The large temperature range of this facility, from 353 K (+175°F) to 89 K (-300°F), imposes rigid requirements on materials and operations. A product search for connectors qualified for the NTF environment produced only one manufacturer and the cost of these connectors was prohibitive.

Of the wire and cable insulation materials in current use, none was found to be cited for use at liquid nitrogen (LN$_2$) temperatures and nothing was known of their ability to withstand flexing and bending in a cryogenic environment.

A limited test program was instigated to tentatively qualify a type or types of wire and cable insulation and a less expensive family of "off-the-shelf" connectors. Time was limited so tests were designed to be quick and simple and as a result the tests were generally much more extreme than actual expected conditions.

The Military Standard (MS) connector series was selected for testing since it is readily available, rugged, and inexpensive. In addition, some LN$_2$ cryogenic experience was found. The tests generally consisted of cyclic hot and cold soak with fast transition times.

Thirty-six different samples of wire and cable were tested to determine the longitudinal shrinkage of the insulator and its flexing or bending

characteristics. These tests consisted of cyclic hot and cold soak to determine shrinkage, followed by cyclic flex of some samples around a 15.24 cm (6 inch) pulley.

A detailed description of the test programs and their results are presented in the following sections.

TEST SPECIMENS

Connectors

Connectors and wiring for use within the internal space of the NTF circuit are accessible and could be replaced should failures occur during the design life. However, failure could result in operational shut-down and cause increased operational costs. To minimize such failures, components must be selected or designed for a minimum ten year life. This can be characterized by approximately 1000 temperature cycles for the purpose of qualification testing. A temperature cycle is defined as starting at room ambient, rising to 353 K (175°F) back to room ambient, lowering to 89 K (-300°F) and returning to room ambient. All tests were designed to include 1000 temperature cycles. Since one cycle during actual tunnel operation will require at least eight hours, from one to three years would be required for real-time qualification testing. Since this was not practical, much faster cycle times were used which resulted in more severe thermal shock.

When the Langley 0.3-Meter Transonic Cryogenic Tunnel went into operation at Langley Research Center (LaRC) in 1973, a small number of electrical connectors of various types were used in the cold regions, none of which were recommended for use at cryogenic (LN$_2$) temperatures. One type was the Military Standard (MS), type A. The majority of the MS units were subjected to several hundred thermal cycles from room temperature to 83 K (-310°F) with no evidence of failure.

For the last 17 years, Langley Research Center has operated a Thermal-Vacuum Chamber 2.44 meters (8 feet) in diameter and 4.51 meters (15 feet) in length. During this period, the interior components have been subjected to temperatures as low as 89 K (-300°F) and as high as 589 K (+600°F). Three MS-A connector sets are among these internal components. A recent inspection and test (dye penetrant) revealed no detectable deterioration of any of these connectors.

The first specification for the MS connector series, MIL-C-5015, was written in 1949. For many years it served as the standard electrical connector for aircraft, ground vehicles, and ground support equipment. From three prime and several smaller manufacturers, the MS series offers 15 different shell sizes, provisions for wire sizes from 22 AWG to 0 AWG, pin configurations from 1 to 104 contacts, insert (contact insulation and spacing) materials of molded plastic, neoprene rubber and ceramics, and styles that

224

include hermetic seals, panel mounts, bulkhead feedthroughs, firewall, etc. A cut-away view of one set of the MS-A is shown in figure 1.

The insert material can either be a molding compound, mineral filled diallyl phthalate (DAP) or Neoprene rubber (resilient). Only the DAP insert, however, can be removed easily for re-clocking.

The thermal shock specification taken from MIL-C-5015-A is abbreviated in Table I. The instruction, between the temperatures listed in the table, is to "lower immediately". Note that the highest temperature is acceptable for the NTF environment but the low temperature extreme of the NTF represents a drastic differential.

Because of the experience with the MS-A connectors in cryogenic applications, their availability, and their low cost, they were selected as connector test specimens.

Wire and Cable

While there was a known requirement for some of the internal cables to be flexed on a radius of approximately 60 cm (2 feet), the only other require-ment was that all wire, insulation and conductors perform in an acceptable manner.

Some early experimentation with large temperature changes identified several potential problems. Most types of insulation material were observed to shrink back from the ends of the conductor or shield material exposing bare conductors as much as 1.3 cm (0.5 inches) and some specimens cracked open leaving conductors or shields exposed. Therefore, the wire and cable test program was designed to determine the most favorable insulation material in terms of minimal longitudinal shrinkage with temperature change and flexing capability at cryogenic temperatures. No insulation cracks or breakage could be tolerated. The four-conductor shielded configuration was selected as being most typical for use throughout the tunnel circuit (fig. 2). Some samples of single conductors were tested and will be included in later comments.

TEST APPARATUS

Thermal Cycle Tests

The test apparatus that was constructed for thermal cycle tests is shown in figure 3. It consisted of an upper compartment or oven, capable of temperatures in excess of 367 K ($+200^{o}$F); a transition area, maintained at room ambient temperature; and a lower tank, heavily insulated, to contain an adjustable quantity of LN_2. A specimen tray, supported by steel cables at the four corners, could be raised or lowered into the three temperature spaces. The controls provided manual or automatic cycling, with adjustable soak time and LN_2 level. The type of thermal cycle, hot to room ambient,

cold to room ambient or both, could be preset. The LN_2 level could be adjusted so that the specimen tray was as close as .64 cm (0.25 inches) or totally immersed.

Cyclic Bend Tests

Another machine was fabricated for cyclic bend test of wire and cable as shown in figure 4. This configuration made it possible to flex wire or cable on a 15.24 cm (6-inch) diameter pulley system after being placed in a cryogenic environment. During flexing, the test article was not visible, being inside the LN_2 container.

TEST PROCEDURES AND RESULTS

Connector Tests

Immersion tests.- A sample group of ten, seven-pin MS-A connectors, five MS3106-A-16S-1P and five MS3102-A-16S-1S, not mated, were subjected to 1,000 full range thermal cycles. Each cycle transitioned from room ambient to 353 K (+175°F) to room ambient to 78 K (-320°F) and returned to room ambient. The 78 K (-320°F) was attained by total immersion of the specimens in the LN_2. Total cycle time was 13 minutes and the transition time between temperature levels was 30 seconds. No intermediate inspection of the specimens was performed. After completion of 1,000 full cycles, the specimens were removed and inspected under a microscope (69X) and subjected to a dye penetrant test which revealed numerous cracks in the DAP insert. Each crack (fig. 5) started at a contact (pin or socket) hole but in no case was the insert completely severed and megger tests revealed no apparent deterioration of the insulating character. If the cracking of the insert can be deemed as failure--all connectors failed. However, if these specimens had been installed in a system, there would have been no discernible problem.

Separate hot-cold cycles.- This test series was designed to determine whether the high or low temperatures were the cause of the insert failure. Six connector pairs (twelve units), two four pin sets, two seven pin sets and two twenty-four pin sets were subjected to 1,000 hot cycles (room ambient to 353 K (175°F)). No failures of any kind could be detected. The same set of specimens were then cycled from room ambient to 83 K (-310°F) without immersion in LN_2. Inspection was scheduled at intervals of approximately 50 cycles. The first cracks occurred after 300 cycles on 2 of the 24 pin inserts and the test was stopped for a more detailed evaluation.

Installed configuration test.- Keeping temperature extremes and transient times as previously stated, eight sets of connectors were wired with approximately 20.3 cm (8 in.) of sixteen AWG wire per contact, mated together with backshells and neoprene rubber boots installed. Four sets were wrapped with insulating tape. An additional two sets with resilient inserts were included.

226

All connectors were subjected to 1,000 room ambient to 83 K (-310°F) cycles. Inspection after each 100 cycles was performed. The resilient inserts developed cracks after 300 cycles but DAP inserts passed the 1,000 cycle mark with no electrical deterioration and only microscopic cracks on two connector halves.

Wire and Cable Tests

Thermal cycle tests.- Thirty-six cables, constructed with combinations of shields and insulating materials, were tested. The summary (table II) lists 10 cables by as many manufacturers. Each was subjected to 1000 thermal cycles. Those that showed signs of shrinking, separation, or any severe deterioration were judged to have "failed". Only the last four on the list "passed". The ninth on the list was marginal in that its outer jacket was a TFE Teflon wrap with a covering of extruded FEP teflon. This outer cover shrank, but the inner cover did not. The tenth cable was in doubt in that there were two specimens; one shrank, the other did not. From the cable's manufacturer, we learned that the specimens were different in that Tefzel can be specially mixed for minimum temperature shrinkage; one of our specimens proved to be the special mix, the other was not. As a result, both the ninth and tenth were included with the seventh and eighth for cold flex testing.

Cold flex tests.- Each of the four cables was subject to 1000 cold-flex cycles; only the last two (table II) passed without damage. The Tefzel cable actually was cold-flexed 20,000 cycles without failing.

DISCUSSION OF RESULTS

Connectors

The transition time from one temperature region to another for any test was one minute or less. For the first two test series, the connector halves were not mated and consequently the face of the insert material was subjected to large thermal shock (Δt). From thermocouple readings taken during the tests, the temperature difference between the face of the connector insert to a point in the geometric center was measured to be in excess of 194 K (350°F). The resulting thermal shock stress was calculated to be 6.7 x 10^7 N/m^2 (9730 psi). The ultimate stress for DAP is given by a band from 3.45 x 10^7 N/m^2 (5000 psi) to 6.0 x 10^7 N/m^2 (8700 psi). The experienced stress in the material was well in excess of even the highest ultimate stress. While it is possible that the coefficient of thermal expansion could decrease by as much as a factor of 0.5, the stress developed by stress concentrations around the holes (pin and socket) could increase by as much as a factor of four. Figure 6 shows thermal stress developed in DAP as a function of thermal shock. The cross-hatched region depicts the ultimate stress band. The operating region of the tests are noted for reference. Also note that the maximum thermal shock expected in the NTF during operations is about 67 K (120°F) which results in thermal stress far below the DAP ultimate.

227

It was also determined during the first two test series that while the Δt from the geometric center to the exposed face of the insert reached 194 K (350°F), from the center to the side of the insert (between the insert and side area, directly under the aluminum shell) only reached 125 K (225°F). The aluminum shell obviously served to decrease heat flow rate and therefore thermal shock. It was based on this realization that the final test series was conducted with all connectors in the mated configuration, wired, with clamps and boots installed. This served to decrease the thermal shock and decrease effective internal stresses. Only minor cracking occurred during the final test and only on the rear face of the insert. It is reasonable to state that all tests conducted were severe, in terms of thermal shock, due to the rapid transition from one temperature region to another. This fast transition resulted in cool-down and warm-up times on the order of ten to fifteen minutes compared to one hour in the 0.3 meter tunnel and four hours planned in the NTF.

Wire and Cable Insulation

Some shrinkage was experienced on all samples tested. On three samples however, the shrinkage was no greater than 0.25 cm (0.1 inch). These were TFE Teflon, Kapton and Tefzel. For applications that do not require bending or flexing at cryogenic temperatures any of these three materials are acceptable. For cryogenic flexing, the shield material, braided copper or aluminum foil did not seem to be a significant factor. For single conductor, TFE has excellent properties but no multi-conductor cable could be located using TFE for the outer jacket insulator. Kapton is acceptable from a shrinkage viewpoint but splits readily when flexed. Multi-conductor cable using Tefzel can be readily obtained and has acceptable shrinkage and excellent cryogenic flex properties.

CONCLUSIONS

Connectors

In the mated configuration, wired, with back shell clamps and standard cable boots, the MS-A connector with DAP insert material is considered qualified for operation in the NTF and for cryogenic applications where temperature gradients do not exceed 367 K (200°F) per minute.

Wire and Cable Insulation

The cryogenic suitability of the four most commonly used insulation materials can be summarized as follows:

```
FEP Teflon  - High shrinkage rate in both hot and cold
TFE Teflon  - Little to no shrinkage - good flex qualities
Kapton      - Subject to tearing during cold-flex - low shrinkage
Tefzel      - low shrink mix - low shrinkage, excellent flex qualities
```

TABLE I.- MS-A CONNECTORS

THERMAL SHOCK SPECIFICATION FROM MIL-C-5015

" . . . EXPOSED TO AT LEAST 5 CYCLES . . . "

TEMPERATURE	SOAK TIME (MINUTES)
358 K (+185^{0}F)	30 (MINIMUM)
218 K (-67^{0}F)	30 (MINIMUM)
293 K (+68^{0}F)	2 (MAXIMUM)

TABLE II.- CABLE TYPES

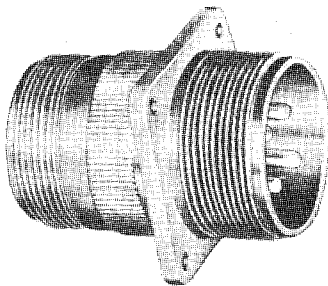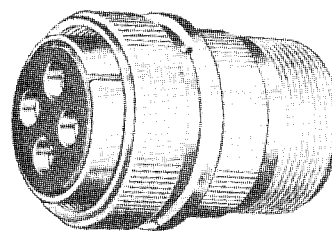|	JACKET	CONDUCTOR INSULATOR	TESTS THERMAL CYCLE	COLD FLEX
1.	FEP	FEP	F	
2.	SILICONE RUBBER	SILICONE RUBBER	F	
3.	FELTED ASBESTOS	FELTED ASBESTOS	F	
4.	GLASS BRAID	SILICONE RUBBER	F	
5.	FEP	TFE	F	
6.	TFE WRAP	TFE WRAP	F	
7.	TFE WRAP	TFE EXTRUDED	P	F
8.	KAPTON WRAP	KAPTON WRAP	P	F
9.	FEP EXT/TFE WRAP	TFE EXT.	?	P
10.	TEFZEL	TEFZEL	P	P

F - FAILED
P - PASSED
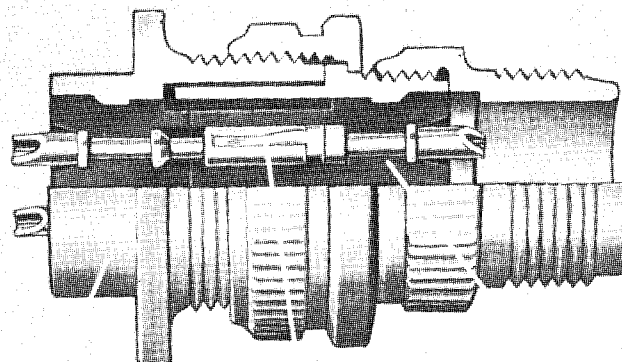
SHELL   CONTACTS   INSERT

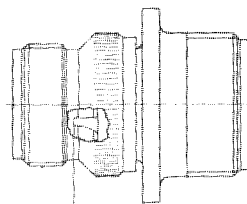MS3100 A WALL-MOUNTING RECEPTACLE   MS3106A STRAIGHT PLUG

Figure 1.- MS-A electrical connectors.

JACKET   SHIELD   INSULATION   CONDUCTOR
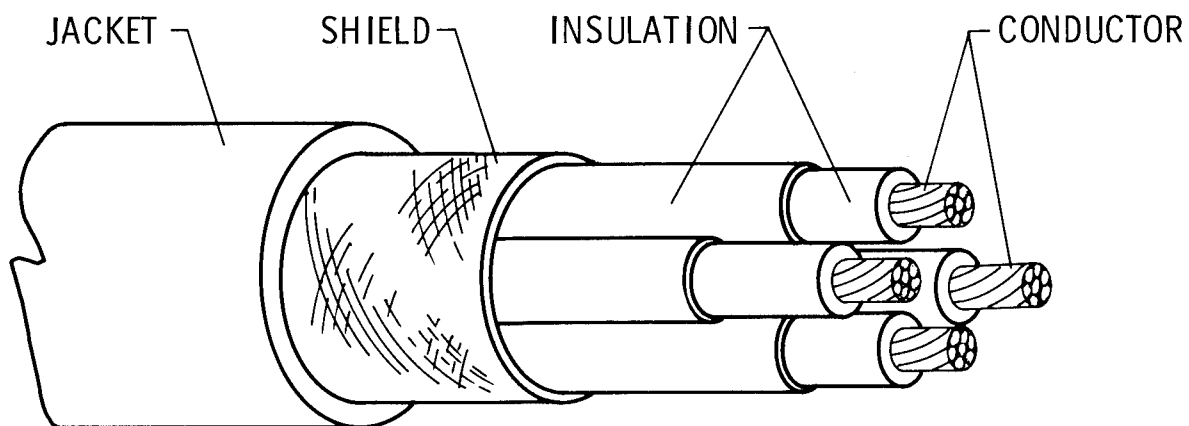
Figure 2.- Sample cable - 4-conductor shielded.

231
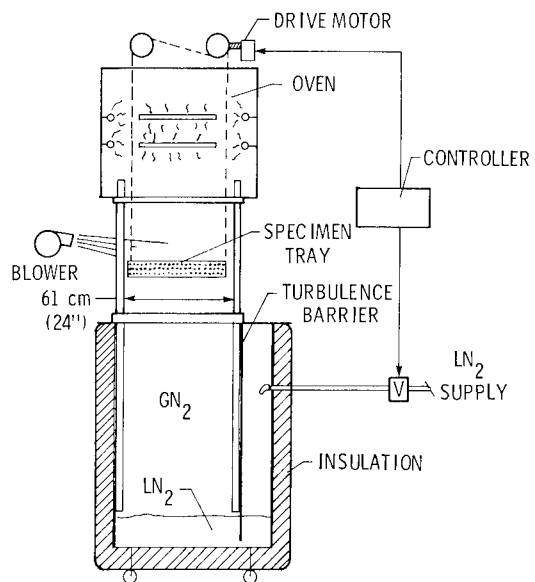
Figure 3.- Thermal cycle apparatus.

Figure 4.- Cyclic band test apparatus.

TYPICAL CRACK PATTERN
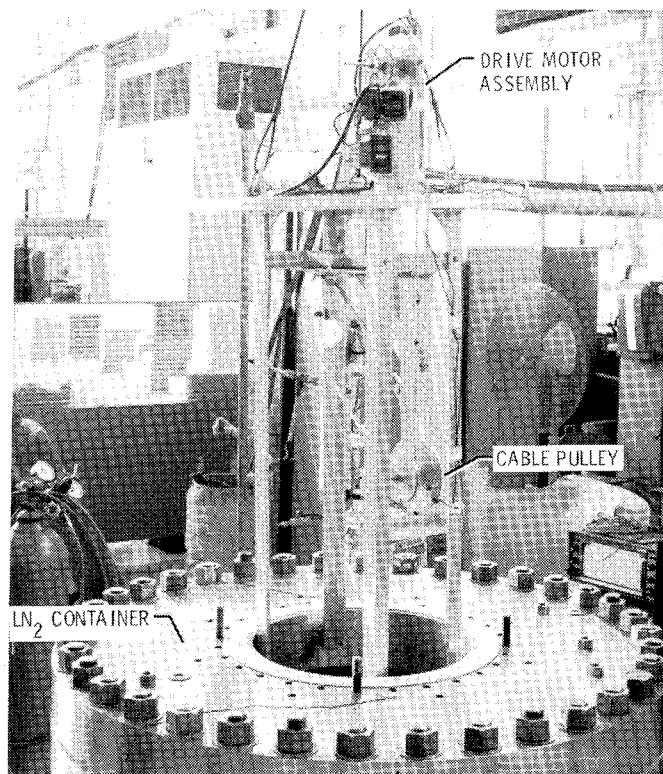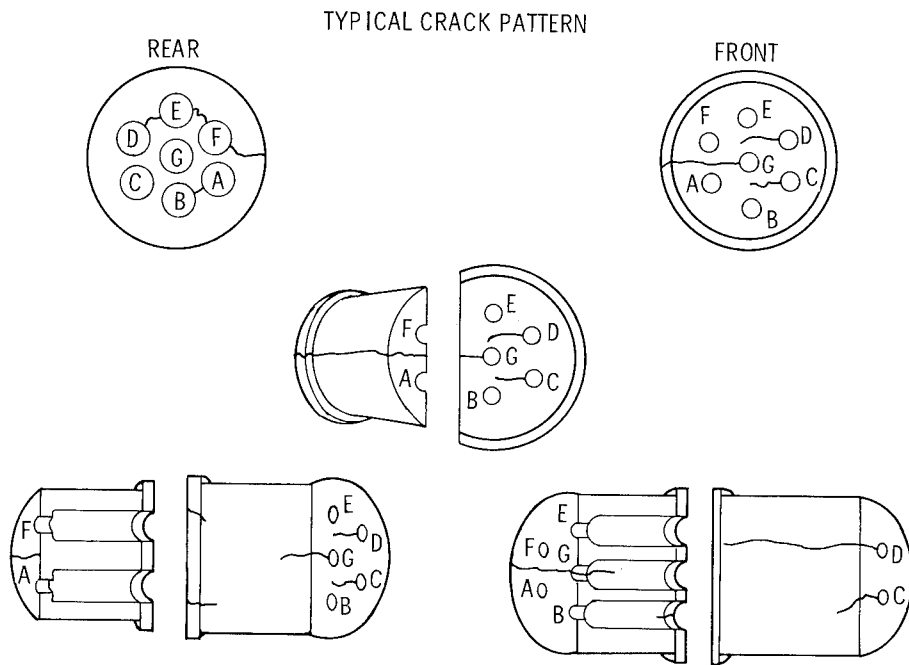
REAR   FRONT

Figure 5.- MS-A connector insert.
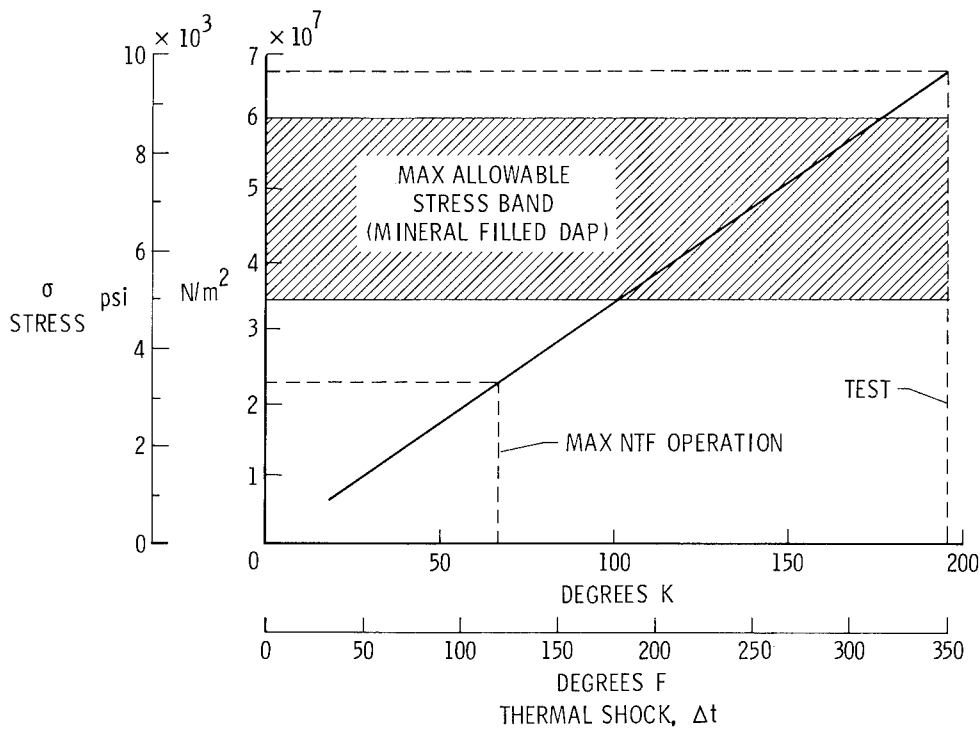

THERMAL SHOCK, Δt

Figure 6.- Thermal shock stress.

STATUS OF MATHEMATICAL MODELING OF NATIONAL

TRANSONIC FACILITY FLUID DYNAMIC PROCESSES

Cecil E. Kirby
Langley Research Center

SUMMARY

The theoretical basis of the four different approaches being used for mathematical modeling of the National Transonic Facility (NTF) are summarized in this paper along with results of limited experimental verification tests. Qualitative discussions are presented on the fan and plenum/slotted-wall test section performance and cross coupling effects between temperature, pressure and Mach number. Calculated results from the computer model for commanded changes in set points are also presented.

INTRODUCTION

Dynamic modeling of transonic closed circuit wind tunnels has never before been attempted to the degree required by the NTF. In the past such tunnels have been operated as steady-state devices with little concern being given to minimizing the time required to change to new data gathering points. As a result very little information was available at the beginning of the NTF mathematical modeling program. This is particularly true for the plenum-slotted-wall test section. Very little understanding exists as to the transient behavior of this section of the tunnel.

The primary objective of a math model is to assist in the design of the control system. If the model can provide a qualitative understanding of the process and the interactions of the parameters involved this information can be used to establish the requirements for hardware for the control system and the range of flexibility required of the hardware. If details of the time relationships of the various interactions can be obtained the model can be used for a more detailed definition of the controls hardware such as determining specific gain settings within the selected range of flexibility for a given loop. Accurate time constants for the processes are also required if the model is to be used as a basis for optimal control system design.

MODELING

There are four slightly different models being used in the NTF program. All use one dimensional analysis. This obviously introduces some errors since the real process is three dimensional. Further discussion of this is given later in this paper. All four of the models use the same basic equations for conservation of mass, momentum and energy and an equation of state. The tunnel

circuit is described in four different ways. One is a lumped parameter model divided into 15 discrete volumes plus the fan and plenum/test section as shown in Figure 1. For a lumped parameter model the basic equations are written in ordinary differential equation form. The set of basic equations is solved simultaneously for each instant of time in each discrete volume. The advantage of a lumped parameter model over the distributed parameter model (described later) is reduced computational time on the computer. A second version of the lumped parameter model uses only two volumes plus the fan and plenum/test section as shown in Figure 2. The third model is a modification of the 15 volume version with the equations written in integral form rather than ordinary differential equation form. This makes it more compatible with optimal control development methods. The fourth model is a distributed parameter type with the basic equations written in partial differential equation form using time and axial distance around the tunnel circuit as the independent variables. In this case, the area variation around the tunnel circuit is described continuously. This type model has the potential for high accuracy but requires longer run times on the computer.

The relationship between the various models for NTF development is shown in Figure 3. The four models are represented on the four horizontal rows of boxes. The lower row is the experimental verification part of the overall modeling effort. The upper three are different analytical models of the NTF, each of which is directly devoted to development of the NTF controls.

The fifteen volume lumped parameter model is being used for the basic control design. This basic controls design will be used for start-up of the NTF. It is also being used as the basis for the optimal controls model. The term "strawman" designates the initial set of optimal control strategy which will result from the optimal model. This terminology is being used since the state-of-the-art of theoretical modeling of wind tunnels is not sufficiently developed to provide a model with sufficiently accurate timewise behavior. After the start-up of the NTF the model will be updated using data from the real tunnel and the optimal control strategy will then be finalized.

The distributed parameter model in the top row will be used beyond the NTF for further research in wind tunnel modeling techniques. It is also a candidate for the on-site computer model to be used prior to a tunnel run to determine the liquid nitrogen consumption of any proposed research program prior to its initiation, and it will be used to analytically test the "strawman" optimal controls.

The experimental part of the modeling program shown on the bottom row consists of two types of tests. The plenum dynamics tests were performed to obtain a basic understanding of how a plenum-slotted-wall test section functions. The Langley 0.3-Meter Transonic Cryogenic Tunnel response tests were primarily performed for the development of its own control system design, and secondarily to provide qualitative information on the behavior of cryogenic tunnels. The experiments will be discussed in more detail later.

236

FACTORS CONSIDERED IN TUNNEL MODELING

Factors which should be considered fall into three categories. Each of these categories is summarized here and addressed in more detail in the next three sections. First; the pressure rise across the fan must be described as a function of pressure, temperature and Mach number and this must be matched to the pressure loss distribution around the tunnel circuit.

Second; cross coupling effects are also present in a cryogenic tunnel to a much greater extent than in a conventional tunnel. Liquid nitrogen injection is the basic temperature control mechanism and gaseous nitrogen venting the pressure control mechanism. These are related and in sometimes an unanticipated manner. For example, one might think that increasing the mass flow rate of liquid nitrogen into the tunnel would cause the pressure to rise. However, the cooling effect of the evaporation process dominates the mass addition effect in many cases and the pressure decreases. This process is also affected by the heat exchange between the flowing gas and the exposed wall metal. Heat transfer effects appear to be more significant in smaller tunnels where the heat transfer coefficients tend to be greater. This is, of course, also affected by the weight ratio of exposed metal and gas and the distribution of the metal around the tunnel circuit.

Another unusual phenomenon occurs during liquid nitrogen flow rate changes. The sudden change in cooling effect generates a temperature front which tends to propagate around the circuit at stream velocities. The one dimensional model predicts these fronts but has no mechanism for damping them out. Realistically there are at least two effects which do tend to damp these fronts. One is diffusion and the other path length differences around the inside of the tunnel circuit as opposed to the outside of the tunnel circuit. The differences in path length would tend to distort a temperature front. Even though these fronts have not been verified experimentally there is a strong intuitive feeling that they will be generated and will continue to exist over the short distance from the injector location to the fan on the NTF. This is of concern because the pressure ratio across the fan would be affected by temperature and this would cause the Mach number in the test section to change. When trying to maintain a Mach number accuracy of $\pm$ .002 such effects may be significant.

The third factor which must be considered is the dynamics of the filling and emptying of the plenum during Mach number changes in the tunnel.

FAN/INLET GUIDE VANES CONSIDERATIONS

The fan description is based on a simplified approach using conventional vector diagrams of gas flow through the inlet guide vanes, rotor and stator. Standard isentropic equations are used with variable efficiency. Correction factors from an existing LaRC experimentally verified three dimensional fan

design computer program are applied to the simplified equations. The simplified fan is then exercised over the entire envelope of operation of the NTF and the correction factors are changed at each point to obtain agreement with the three dimensional fan performance.

Pressure losses are assumed to be proportional to the local dynamic pressure. Coefficients are assigned to each section of the tunnel based on the NTF design distribution at a Mach number equal to unity. The same coefficients are used for other Mach numbers, changing only as the local dynamic pressure changes.

CROSS COUPLING EFFECTS

Figure 4 shows experimental results from response tests for the 0.3 meter cryotunnel. Two sets of curves of temperature, pressure and Mach number show the response to a liquid nitrogen flow rate change of about three seconds duration. The left set of curves, where the initial temperature is about 190 K (340° R), shows a decrease in pressure when the liquid nitrogen flow rate is suddenly increased. The curves on the right, where the initial temperature is about 260 K (470° R), show a pressure increase for the same type liquid nitrogen flow rate change. The increase in pressure is attributed to heat exchange with the wall metal. Similar effects were indicated in the calculated results.

On both sets of curves there is a hump in the Mach number curve during the liquid nitrogen pulse. This is due to the effect of the temperature decrease on the fan compression ratio. Figure 5 shows calculated results from the model using 0.3 meter tunnel geometry in which a similar "hump" is evident. Notice that the scales on the curves of Figures 4 and 5 are different so that direct comparisons are not possible but the trends are similar.

The temperature curve in Figure 5 clearly shows the temperature fronts mentioned previously. The spacing between the fronts is the circuit time for the 0.3 meter cryotunnel. The decreasing amplitude of the fronts on each succeeding circuit is due to heat transfer effects. The rate of decrease in amplitude is not as rapid when the model is set up for the larger size of the NTF.

PLENUM/SLOTTED-WALL TEST SECTION DYNAMICS

The initial plenum configuration used in all models and the one still being used in the two volume model is shown in Figure 6. In this configuration the plenum is connected to the test section through only one orifice. The result of this is that the filling and emptying of the plenum causes its pressure to lag behind that of the test section during Mach number changes. In effect the test section "drives" the plenum. With this approach it is difficult to obtain agreement between models and experimental data over the entire range of operation with only one orifice size.

238

The plenum configuration of Figure 7 referred to as the dual flow path plenum is currently being used in the 15 volume model and the distributed parameter model. It allows for three components of flow into the plenum, Q_t, for supersonic flow, Q_b, for boundary layer growth and Q_{dm}, for drag changes such as an angle of attack change of a model in the test section. Flow from the plenum reenters the mainstream at the aft end of the plenum/test section. This approach also allows for the existence of a shock wave in the diffuser entrance region for the transition from supersonic to subsonic flow when required. The significant factor in this configuration is that the plenum pressure follows the test section pressure closely so that the plenum "drives" the test section pressure.

Experiments have been performed in the LaRC 8 Foot Transonic Pressure Tunnel which is similar in size to the NTF and has a plenum-slotted-wall test section. Figure 8 shows the results of such a test and the calculated results with the computer model set up for the 8 Foot Transonic Pressure Tunnel geometry. The trend of the curves are similar even though the time constants differ by a factor of almost two. This is the worst case condition of all data from this tunnel. Agreement with experimental data was better at other Mach numbers. For this first-of-its-kind effort such agreement is considered as acceptable.

Other tests were performed in the LaRC Diffuser Flow Apparatus. This system is a one fifth scale model of the NTF test section leg. The purpose of these tests was not to determine time constants for the plenum but to gain a better understanding of how a plenum works.

In these tests a rotating paddle type mechanism was installed in the test section so that the paddles could be oriented parallel to the flow and suddenly rotated ninety degrees to introduce an area change disturbance into the test section. During these tests pressures were measured in the plenum in the test section, and across the wall of the test section as shown in Figure 9. Figure 10 shows the results of the experiment when the paddle type disturbers were rotated ninety degrees at time equals zero. Notice that the plenum pressure and test section pressure designated 3 and 4 on the Figure follow each other very closely and the pressure differential curve designated number 5 did not vary during the disturbed part of the test of about thirteen seconds. This type behavior agrees with the dual flow path plenum configuration. The dual flow path plenum description assumes that the plenum/test section performance is controlled from the downstream or diffuser end of the test section. When the downstream pressure is decreased, exit flow from the plenum increases and the test section responds to the resulting decreased pressure in the plenum. Similarly when the downstream pressure is increased, exit flow from the plenum decreases, causing the plenum pressure to rise. The test section pressure also rises since the decreased plenum exit flow reduces the slot flow into the plenum. Therefore, in the dual flow path plenum description the suction side of the fan is the controlling factor. It should be pointed out, however, that when a disturbance was introduced upstream of the test section, the plenum pressure did lag the test section pressure. When the plenum pressure lags the test section pressure the tunnel is behaving more like the single orifice configuration. For this description the assumption is

that pressure changes coming into the test section from upstream force the flow through the slots to increase or decrease so that the test section "drives" the plenum pressure changes. This is essentially opposite from the behavior of the dual flow path description where plenum pressure is controlled from the downstream end.

Since conflicting results were obtained from the plenum tests, no definite conclusions can be drawn as to how a plenum really behaves.

TYPICAL RESPONSE CURVES

Figures 11, 12, and 13 show calculated results from the computer model for commanded changes in temperature, pressure and Mach number. The parallel dotted lines represent the required error band established for the NTF. A commanded decrease in temperature from 167 K (300^0 R) to 150 K (270^0 R) can be achieved in about 12 seconds. A commanded decrease in pressure from 524 kPa (76 psia) to 490 kPa (71 psia) can be completed in about 9 seconds. A commanded decrease in Mach number from 0.8 to 0.7 can be accomplished in about 7 seconds. In each case the performance of the actuator dynamics is included and the control loops are active and using the preliminary set of controls laws developed with the 15 volume lumped parameter model.

CONCLUDING REMARKS

Figure 14 shows the status of the modeling effort. Completed elements are shown shaded. All four models are operational and are being exercised. A basic set of controls has been designed. An improved understanding of the process interactions has been achieved and limited experimental data shows qualitative agreement with the models. The existence of temperature fronts has not been verified but the preliminary control laws are designed to handle temperature fronts predicted by the theoretical models as a precautionary measure. If they do not exist to the degree expected this part of the control system will remain inactive. Further measurements are planned at start-up to update the models for use in optimal controls development.
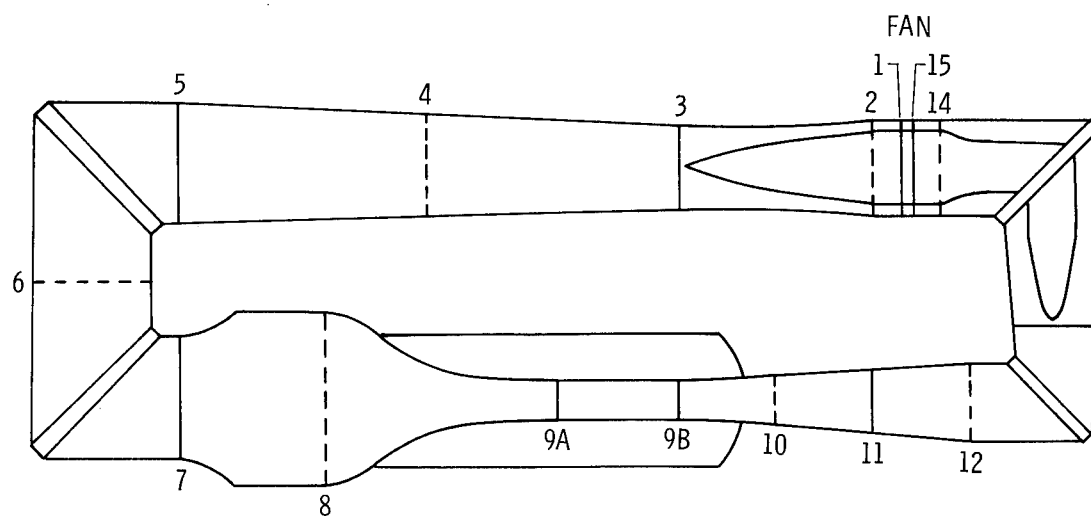
240

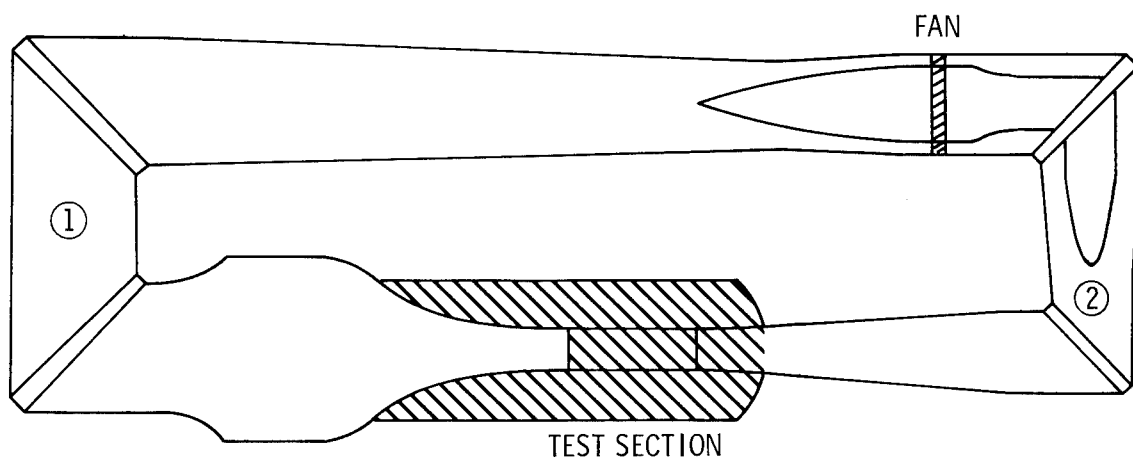Figure 1.- Fifteen volume lumped parameter model.

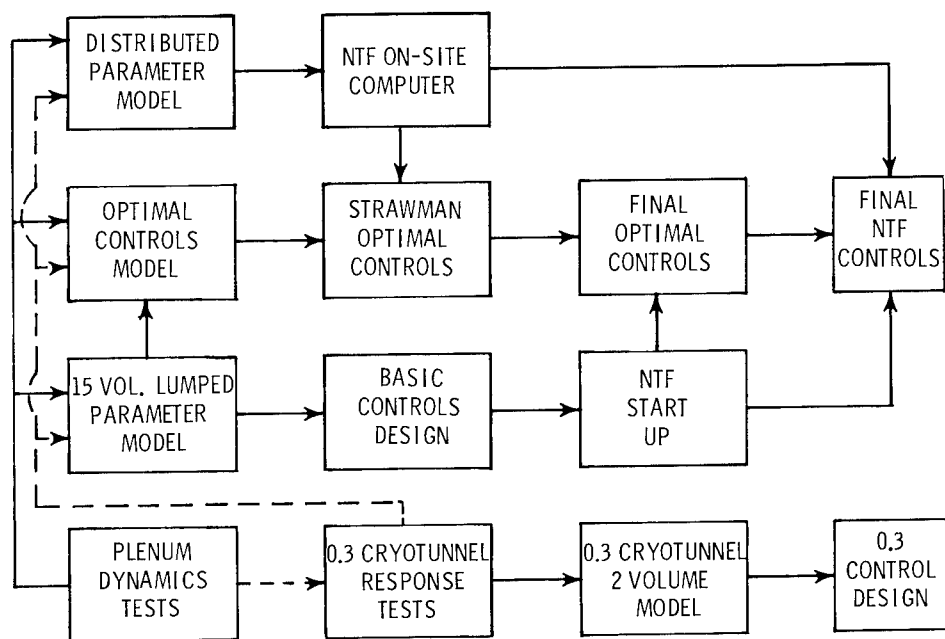Figure 2.- Two volume lumped parameter model.
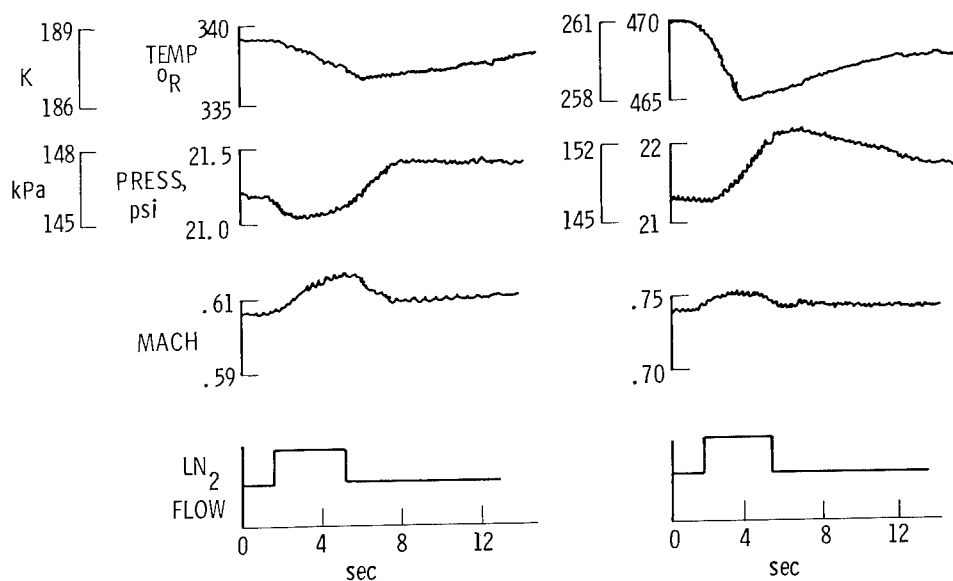
Figure 3.- Overall math model approach.

Figure 4.- Response to change of liquid nitrogen flow,
0.3-m experimental results.

242
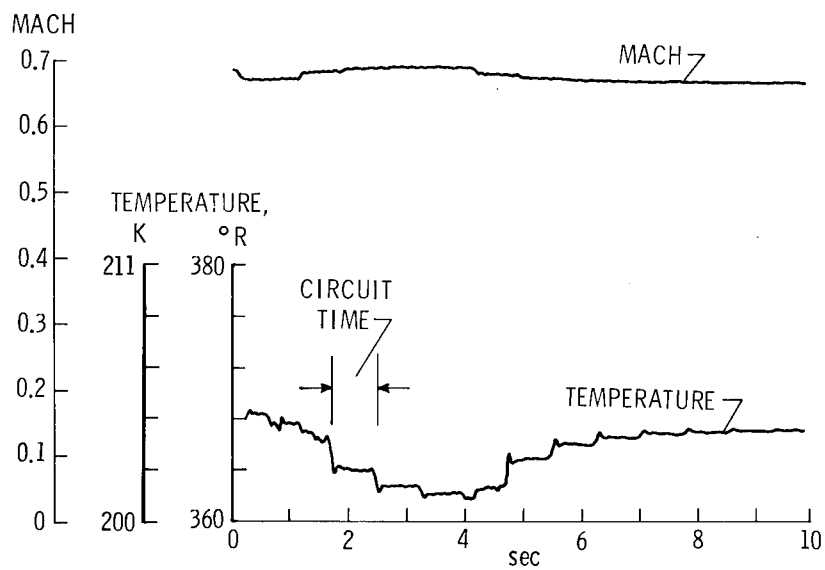
Figure 5.- Response to change of liquid nitrogen flow,
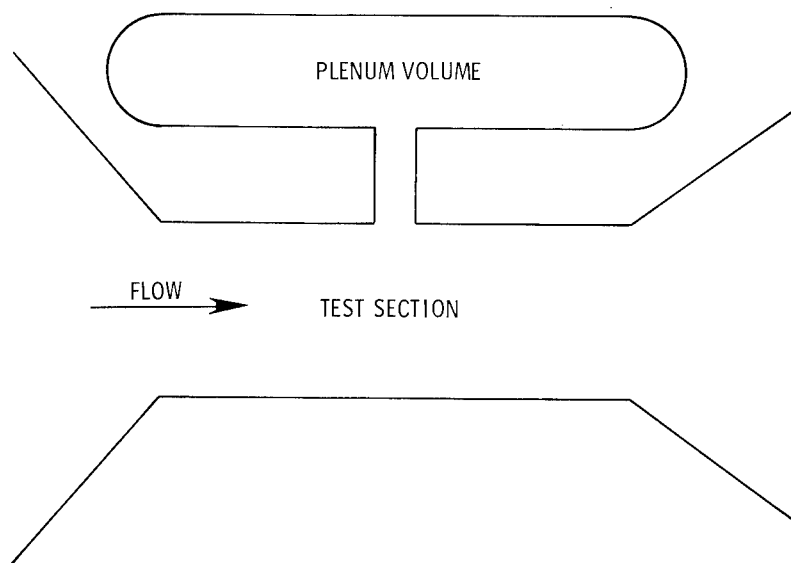calculated results.
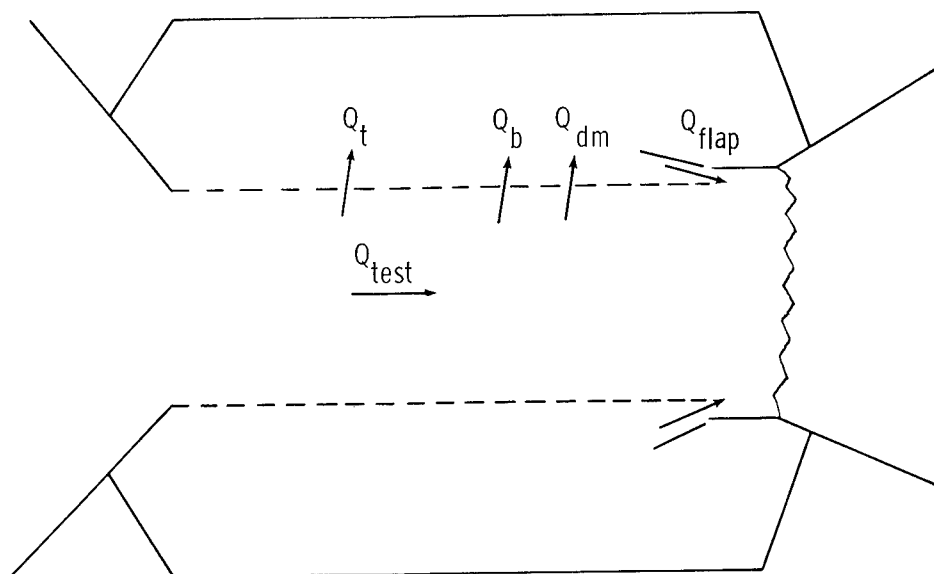

Figure 6.- Initial plenum configuration.

Figure 7.- Fifteen volume plenum configuration.
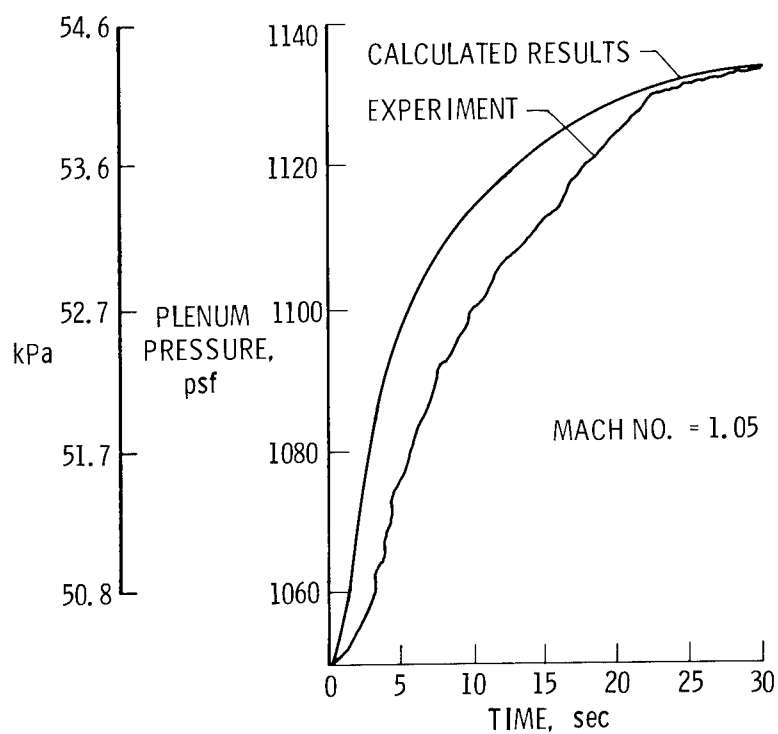
Figure 8.- Plenum response to test section blockage,
8 foot transonic pressure tunnel.
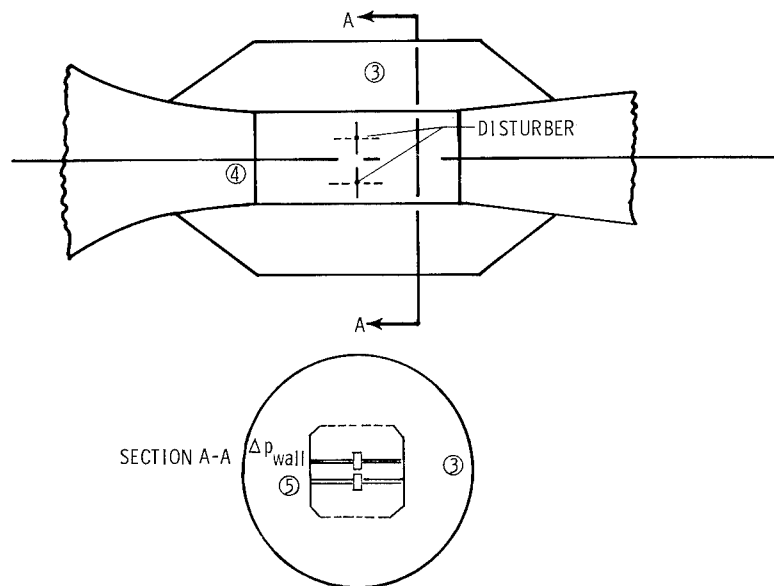
Figure 9.- Schematic of instrumentation.

$M \approx 0.80, \quad \Delta M \approx 0.04$
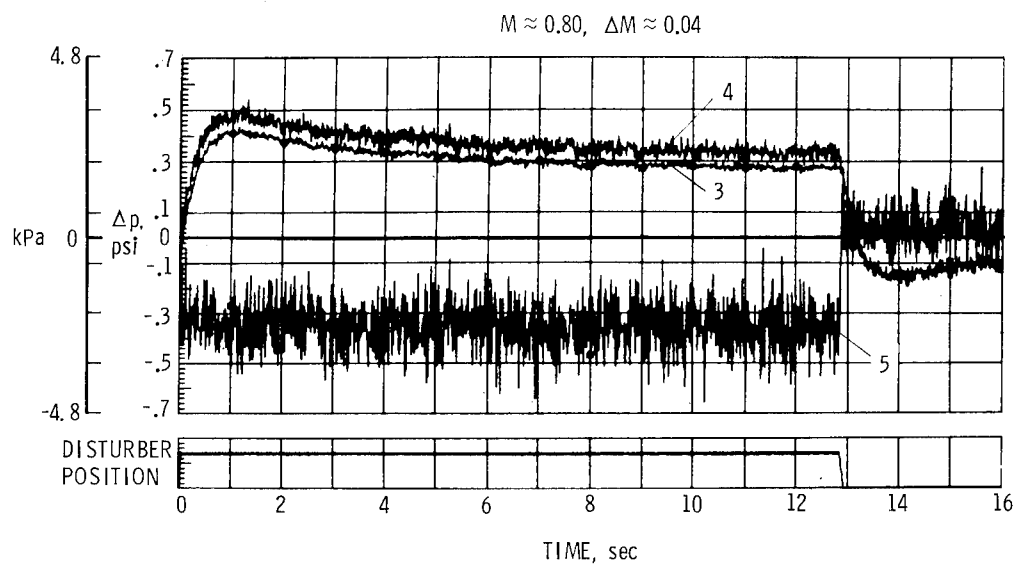
Figure 10.- Change in test section/plenum pressure produced by a test section disturbance.

ERROR,
°R

TEMPERATURE, 1.0 ⌐ .6

K   °R

167 ⌐ 300 ⌐ .8

161 ⌐ 290 ⌐ .4

.2

155 ⌐ 280 ⌐ 0

-.2

150 ⌐ 270 ⌐ -.4

-.6

-.8

144 ⌐ 260 ⌐ -1.0 ⌐ -.6

0   10   20   30
sec

167 K TO 150 K
TEMPERATURE   300 °R TO 270 °R
PRESSURE   75 psia 517 kPa
MACH NUMBER 0.8

ERROR
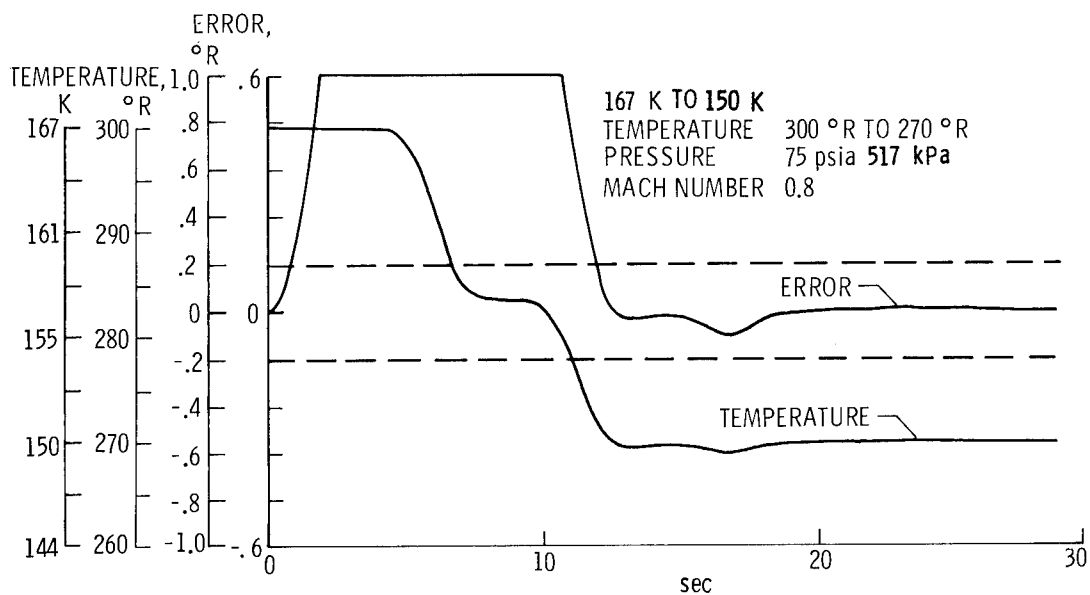
TEMPERATURE

Figure 11.- Response to commanded temperature change.

PRESSURE,   ERROR,
kPa psi   psi kPa

524 ⌐ 76 ⌐ 1.0 ⌐ 6.9

510 ⌐ 74 ⌐ .6

496 ⌐ 72 ⌐ .2

0   0

483 ⌐ 70 ⌐ -.2

469 ⌐ 68 ⌐ -.6

455 ⌐ 66 ⌐ -1.0 ⌐ -6.9

0   10   20
sec

517 kPa TO 490 kPa
PRESSURE   75 psia TO 71 psia
TEMPERATURE   300 °R 167 K
MACH NUMBER 0.8

ERROR
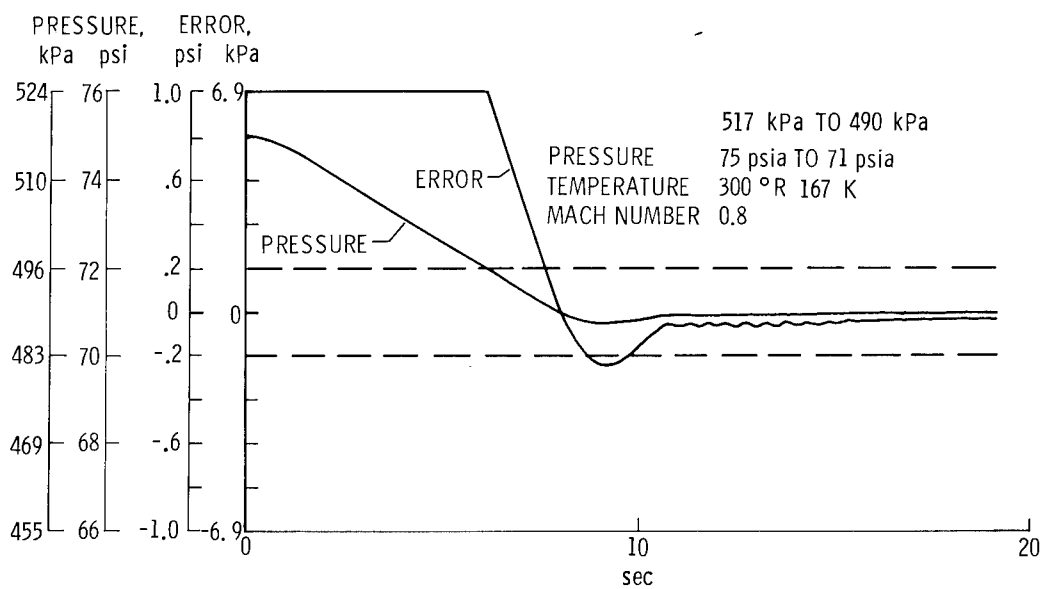
PRESSURE

Figure 12.- Response to commanded pressure change.

246

MACH

.80 ┌ ERROR
            .008
                         MACH NUMBER   0.8 TO 0.7
.78 ┤   TEMPERATURE   167 K
            .004   PRESSURE   517 kPa

.76 ┤   0

          -.002

.74 ┤

          -.004   ERROR

.72 ┤
          -.008   MACH

.70 ┤

.68 └   -.012
                              10   20
                              sec
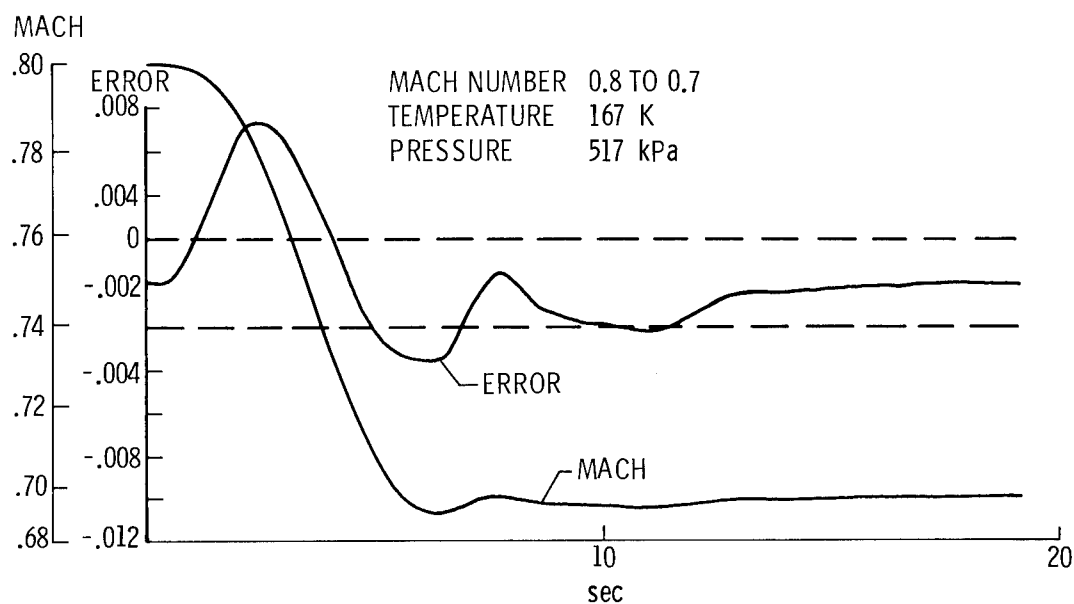
Figure 13.- Response to commanded Mach number change.

```
┌──────────────┐      ┌──────────────┐                                    ┌──────────┐
│ DISTRIBUTED  │      │ NTF ON-SITE  │────────────────────────────────────│  FINAL   │
│  PARAMETER   │─────▶│  COMPUTER    │                                     │   NTF    │
│    MODEL     │      │              │                                     │ CONTROLS │
└──────────────┘      └──────────────┘                                     └──────────┘
┌──────────────┐      ┌──────────────┐      ┌──────────────┐
│   OPTIMAL    │      │  STRAWMAN    │      │    FINAL     │
│  CONTROLS    │─────▶│  OPTIMAL     │─────▶│   OPTIMAL    │
│    MODEL     │      │  CONTROLS    │      │   CONTROLS   │
└──────────────┘      └──────────────┘      └──────────────┘
┌──────────────┐      ┌──────────────┐      ┌──────────────┐
│15 VOL. LUMPED│      │    BASIC     │      │    NTF       │
│  PARAMETER   │─────▶│  CONTROLS    │─────▶│   START      │
│    MODEL     │      │   DESIGN     │      │    UP        │
└──────────────┘      └──────────────┘      └──────────────┘
┌──────────────┐      ┌──────────────┐      ┌──────────────┐      ┌──────────┐
│   PLENUM     │      │0.3 CRYOTUNNEL│      │0.3 CRYOTUNNEL│      │   0.3    │
│  DYNAMICS    │─ ─ ─▶│  RESPONSE    │─────▶│  2 VOLUME    │─────▶│ CONTROL  │
│   TESTS      │      │   TESTS      │      │   MODEL      │      │ DESIGN   │
└──────────────┘      └──────────────┘      └──────────────┘      └──────────┘
```
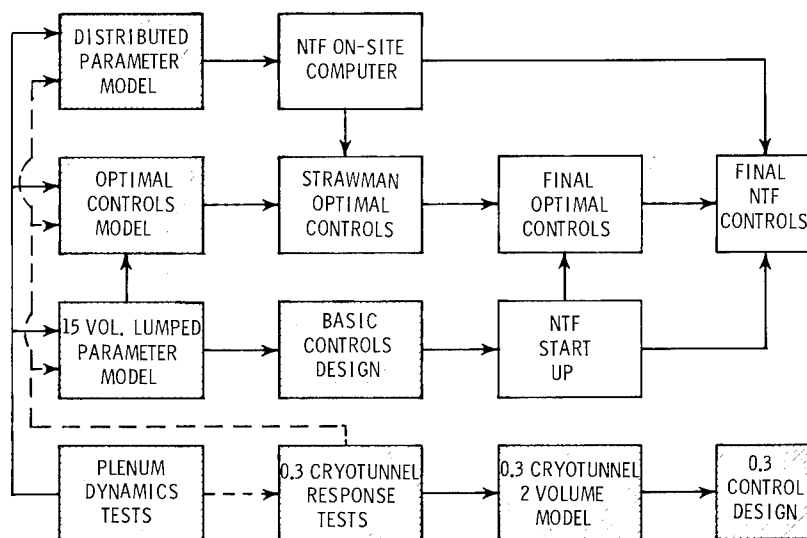
Figure 14.- Overall math model approach.

A DESCRIPTION OF THE NATIONAL TRANSONIC FACILITY PROCESS CONTROL SYSTEM

James A. Osborn
Langley Research Center

SUMMARY

High productivity and energy efficiency have been emphasized in the design of the National Transonic Facility. To support these goals a three level hierarchial control system has been designed to provide fast response, flexibility, and automation. The control system utilizes dedicated analog controllers, individual digital microcomputers, and a larger supervisory computer. Standard commercial hardware is used throughout.

INTRODUCTION

The National Transonic Facility (NTF) is a large transonic, closed circuit wind tunnel designed to provide high Reynolds number testing. To achieve the desired high Reynolds numbers liquid nitrogen (LN_2) is injected into the tunnel stream, cooling the test gas to cryogenic temperatures. The liquid nitrogen cost at a typical test condition will be $606 per minute.[1] This high energy cost has driven us to provide an energy efficient design. For the control systems we have emphasized three areas: fast response, flexibility, and automation. This paper will describe how the NTF control system has been configured to provide these features. But, first an overview of the NTF process systems will be presented. It will be followed by a description of the design objectives and the three level hierarchial control system.

NTF OVERVIEW

The NTF is a fan driven, closed circuit wind tunnel. The tunnel layout and identification of major tunnel components are shown in Figure 1.

Mach number is controlled by varying fan speed or inlet guide vane angle. For the high Reynolds number range (high power) a synchronous motor is used to supplement the power of two variable speed induction motors. Here Mach number is controlled with inlet guide vanes only.

Stagnation temperature is controlled by adjusting the flow of liquid nitrogen injected into the tunnel. Two parallel valves are used to handle the

---

[1]Mach = 0.7, Pressure = 620 kPA (90 psia), Temperature = 139 K (250° R).

nominal flow range of 0.38 to 38 m³/min (100 to 10,000 GPM) which is used to offset the heat generated by the fan.

Control of stagnation pressure is achieved by varying the flow of gaseous nitrogen (GN$_2$) vented from the tunnel. Two 61 cm (24-inch) butterfly valves are paralleled to provide the required control range.

Model attitude is adjusted by positioning a vertical strut mount to vary sting angle (model pitch). A roll coupling, when combined with pitch, provides yaw capability.

Aerodynamic flow through the slotted test section will be fine tuned by 12 individual walls and flaps: a top and bottom test section wall, two pairs of model support walls - top and bottom, and three pairs of reentry flaps - top, bottom, and side.

The tunnel can also be operated using air as a test medium. A water cooled heat exchanger is used to control stagnation temperature by dissipating the heat added by the fan. Tunnel temperature is controlled by a three-way valve which varies water temperature at the cooling coil inlet.

The NTF process has a number of characteristics which provide formidable challenges to the control system design. There is a significant amount of cross coupling between the temperature, Mach number, and pressure control loops. For instance a step change in temperature will upset or disturb both the regulation of Mach number and pressure.

There are transport delays associated with the temperature control loop. Liquid nitrogen injected at the spray bar requires from 2 to 12 seconds to travel around the tunnel and influence the temperature sensor in the settling chamber.

The dynamic behavior of a slotted wall test section at transonic speeds and wind tunnel fan aerodynamics are difficult to analyze. All these characteristics complicate the development and implementation of control algorithms.

DESIGN OBJECTIVES

To provide energy efficiency the NTF control system has emphasized three features: automation, fast response, and flexibility.

Automation is used to automatically sequence the tunnel through a series of test points. It eliminates the need for operators to manually enter setpoints for each of the twenty-two individual control loops. If setpoints were entered manually, the tunnel would expend considerable amounts of energy while waiting for the operators to enter the setpoints.

Fast response is an important feature since the tunnel spends a significant portion of its operating time moving from one test point to the next

250

test point. The energy consumed during most changes is wasted and nonproductive. Shortening the transient response time results in energy savings.

Flexibility will allow the NTF control system to accommodate new control algorithms or control strategies. When the NTF design was initiated in 1975 it was recognized that we were in our infancy in understanding the complex dynamics of a cryogenic transonic wind tunnel. As more analysis is completed and operating experience is gained there will be successive generations of improved control algorithms. A flexible control system will readily accommodate these algorithms.

HIERARCHIAL CONTROL

The control of the NTF process is accomplished through a three level hierarchial control system, see Figure 2. The lowest or first level of control is devoted to the positioning of control devices, typically a valve position or actuator position. Typical NTF control variables are Inlet Guide Vane (IGV) angle, GN_2 Vent Valve position, and LN_2 Injection Valve position. An analog controller is used for this level.

The second level is devoted to the control of individual process variables such as stagnation pressure, stagnation temperature, Mach number, etc. Because these control algorithms are sophisticated and complex, a microcomputer is used for this service.

The third level provides the coordinated command of all 22 control variables. This activity is entitled "Test Direction". This level also implements "Optimal Control" of the tunnel flow process. A supervisory computer is used for this level.

The second and third levels are new approaches to wind tunnel control at Langley Research Center (LaRC). Each level of control will be discussed in more detail, see Figure 3.

Analog Controller

An analog controller is used for the first level of control. Its primary function is to provide rapid response and inner loop stability. Control response requirements range as high as 3 Hz. High inner loop gain tends to minimize the effects of hardware nonlinearities and provide high immunity to disturbance inputs.

The first level often consists of cascaded control loops. An example is the inlet guide vane positioning system. This is an electro-hydraulic servo system utilizing a two stage servovalve to position the tandem set of guide vane actuators. The two inner feedback loops are:

- Second stage spool position feedback
- Pressure compensation feedback

Each is provided to assure stability and rapid response of the positioning system.

Microcomputer

Control of process variables is provided by the second level of control which is implemented with a microcomputer. Its primary function is to implement the sophisticated control algorithms that have been developed to provide rapid tunnel response to setpoint changes. These algorithms, which have been developed using classical control methods, utilize both feedback and feed forward compensation, see Figure 4. Data from other control loops is used to support the compensation algorithms. Figure 5 shows a block diagram of the Mach number control algorithm. A discussion of the algorithm is presented below.

A setpoint smoothing function transforms step inputs into a smooth half cosine wave output with zero slope at each end. This tends to reduce the cross coupling between control loops, to reduce the tendency of the loop to "ring" or oscillate, and to reduce drive motor power transients imposed on the electrical power system. The characteristics of the smoothing curve are a function of tunnel temperature and Mach number.

The feedback control compensation utilizes a variable gain proportional plus integral algorithm. The gains are adjusted as a function of Mach number and temperature. The magnitude of the error signal input to this algorithm is limited by a "limit" routine. The limiting action permits the use of high gains for good steady state regulation while reducing the tendency of the loop to "ring" or oscilliate.

A feed forward algorithm is used to predict the guide vane angle as a function of Mach number setpoint, temperature, and fan speed. This is a three dimensional interpolation routine based on computed fan performance data. After the NTF has been operated, this data will be updated based on actual measured fan performance.

Another significant feature of this level of control is the ability to provide continuously adjustable setpoint limits to the controlled variables. This feature can be used to implement fan stall protection and to prevent high transient thermal stresses in tunnel internal structures. The NTF has a limit on the time rate of change of the gas stream temperature to prevent high transient thermal stresses from being imposed on the tunnel internal structural components. The thermal stress will be monitored by using thermocouples mounted on the tunnel internal components. The occurrence of high thermal stress will limit or clamp the LN_2 valve position to reduce the thermal stress.

252

The microcomputer also supports the interface between the operator and control system, see Figure 3. Operator setpoint inputs for either the process variable or the controlled variable are made in the microcomputer based on inputs from the control panel. The micro also converts feedback signals to engineering units and drives the digital panel displays.

Supervisory Computer

The supervisory computer provides the highest level of control. Both "Test Direction" and "Optimal Control" are implemented at this level.

"Test Direction" is the coordinated command of all process variable setpoints. It permits the automation of a research run by directing the sequential execution of all test points. Each test point is represented by the setpoint value for each process variable. A list of these test points constitutes a research run. A typical train of events is as follows:

1. Computer sends process variable setpoints to the respective microcomputers or to "optimal control".

2. Computer monitors process response to detect when all variables have reached their setpoint.

3. Computer initiates a "take data" command to the data acquisition system.

4. Upon receipt of a "data complete" signal, computer returns to Step 1 and repeats the steps.

The supervisory computer will also execute the NTF "Optimal Control" algorithm. Currently under development, this algorithm will optimally control the NTF pressure, temperature, and Mach number processes to minimize the energy costs for changing tunnel operating conditions (moving from one test point to another). Algorithm execution will require the on-line real time solution to a set of simultaneous equations in matrix form. Provision is being made to accommodate algorithm outputs of either process variables (Mach, Temperature, Pressure) or control variable (IGV angle, LN_2 valve position, GN_2 valve position).

"Optimal Control" is based on modern control theory. It is the ultimate control tool for minimizing the energy required to change test points. The large computation load required to execute an optimization algorithm can only be found in a medium scale computer. This computer with its CRT, card reader and printer peripherals also provides a much better man-machine interface for the "test direction" operation.

Hardware

An overview of the hardware that is used to provide the hierarchial control previously described is shown in Figure 6. It consists of one supervisory computer which commands five microcomputers which in turn support twenty-two analog controllers.

Each microcomputer has specific functions as noted below:

Microcomputer   1

  - Mach Number Control
  - Fan Stall Limits

Microcomputer   2

  - Temperature Control
  - Internal Structure Temperature Limits

Microcomputer   3

  - Pressure Control

Microcomputer   4

  - Drive Speed Control

Microcomputer   5

  - Test Section Configuration and Model Control

      - Pitch
      - Roll
      - Test Section Walls   - 2 loops
      - Model Support Walls - 4 loops
      - Reentry Flaps   - 6 loops

Specific hardware characteristics are described below:

The analog controllers are standard servovalve electronic controllers. They are standard in two respects: First they are commercial off-the-shelf hardware sold by servovalve manufacturers and are compatible with NTF control elements; Second they are similar to existing controllers in use at Langley Research Center. Our technicians are familiar with the operation and maintenance of these devices.

Microcomputers used by NTF will have the following characteristics:

254

1. High Level Language (FORTRAN) Capability: This will lower software costs. We estimate that our software costs will be approximately twice the hardware costs.

2. 8 Bit Microprocessor: With an 8 bit microprocessor we can utilize existing support hardware, spare parts, trained technicians, and previously developed software modules. With a dedicated math board support package the 8 bit processor has computing speeds that are comparable with the new 16 bit microprocessors. The 8 bit microprocessor will support our control algorithms in a cost effective manner.

3. Permanent Memory: Program security and protection from inadvertent operator errors is provided by using Programmable Read Only Memory (PROM).

The supervisory computer has been selected to be compatible with other NTF and Langley Research Center hardware. This will allow lower software and maintenance costs. The capability to support a FORTRAN '77 compiler will provide the versatility offered by this latest version of the high level language. A more detailed description of this computer is provided by another conference paper entitled "The National Transonic Facility Data System Complex" (Reference 1).

CONCLUDING REMARKS

To provide energy-efficient operation, the NTF will have a highly automated and integrated process control system. It is a hierarchial three level configuration using high response analog controllers in the control element positioning loops, individual digital microcomputers for the primary control loop regulation and stability, and a medium scale digital computer to provide optimal control and test direction of a predefined research run with the operator as an observer. The control system will be flexible to readily accommodate future generations of control algorithms. Standard commercial hardware will be used throughout.

REFERENCE

1. Bryant, Charles S.: The National Transonic Facility Data System Complex. Cryogenic Technology, NASA CP-2122, 1980. (Paper 18 of this compilation.)
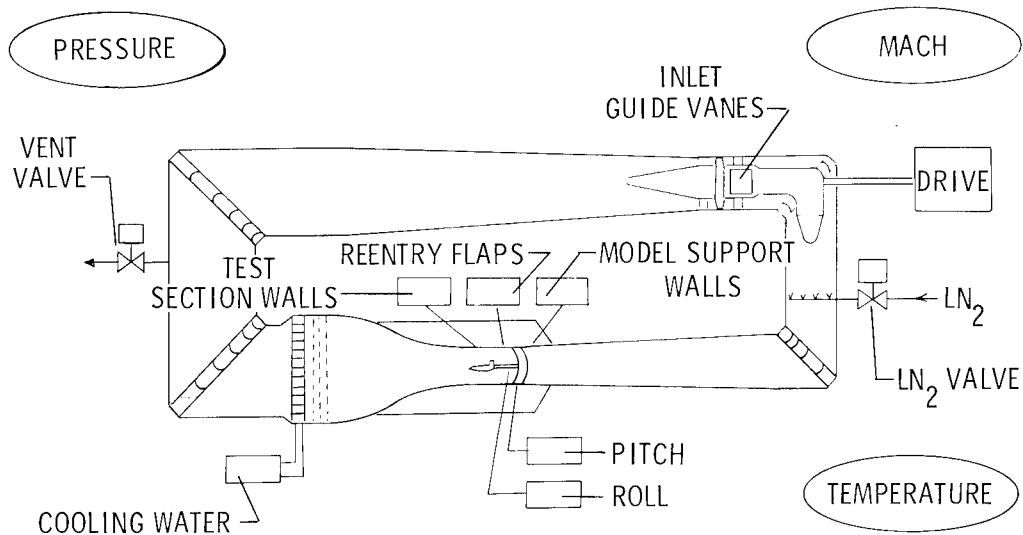
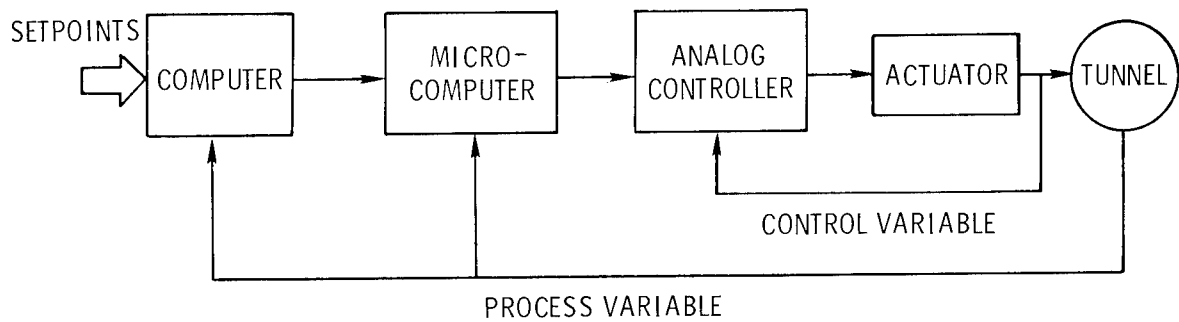Figure 1.- NTF process controls overview.

Figure 2.- NTF hierarchial control. Typical control loop.
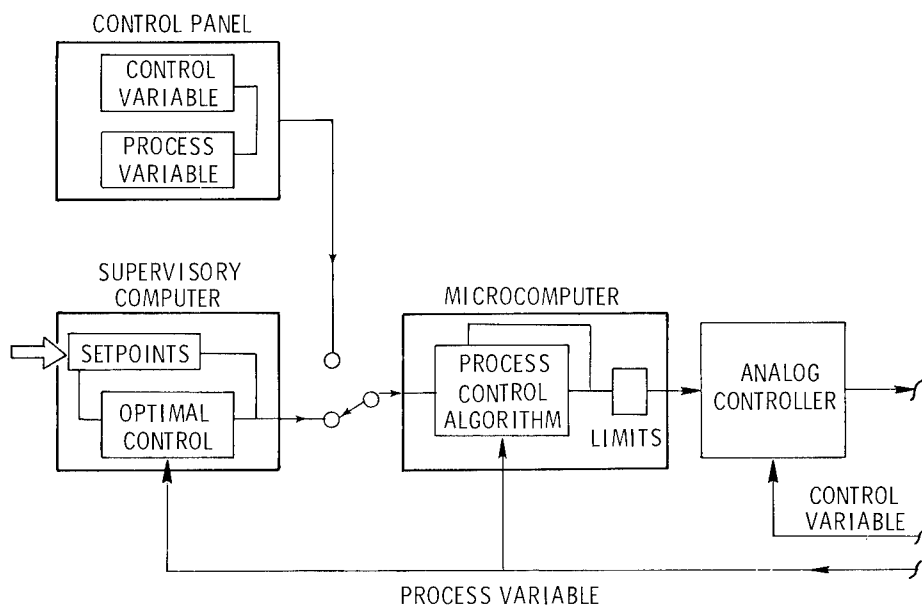
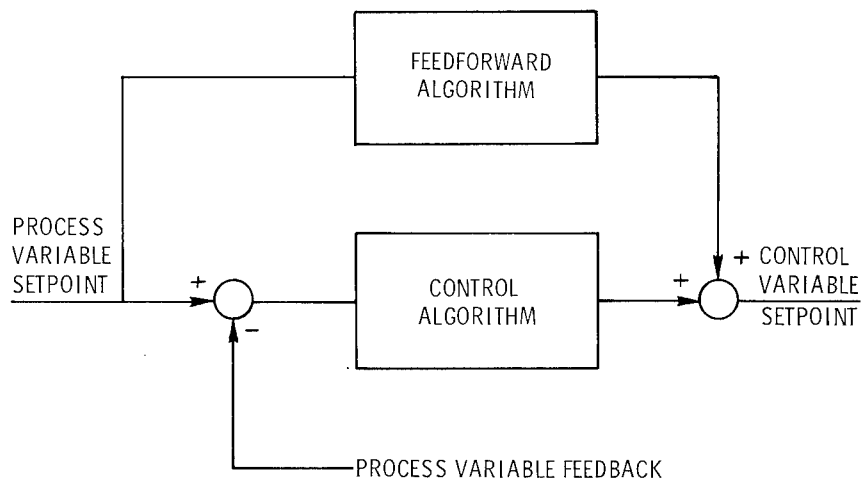Figure 3.- NTF controller details.
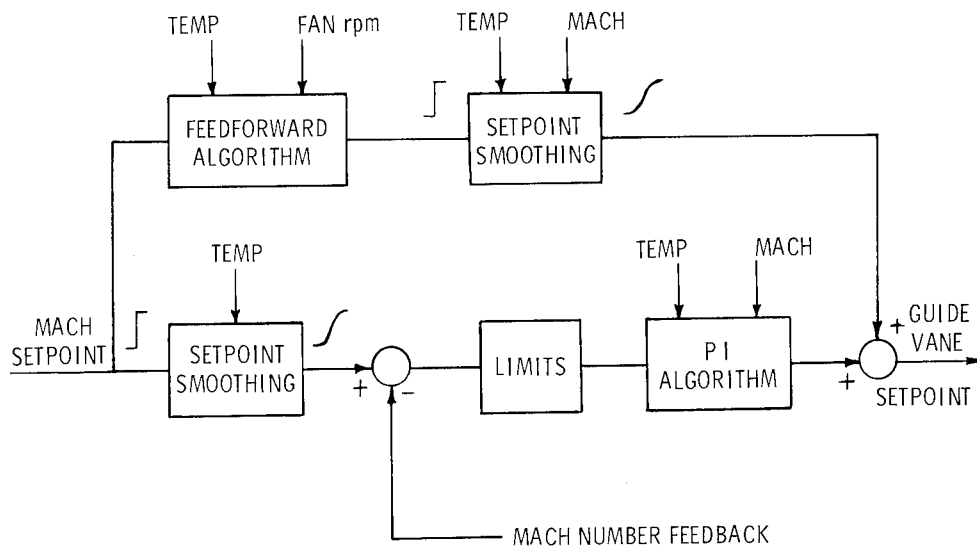

Figure 4.- Process control algorithm.

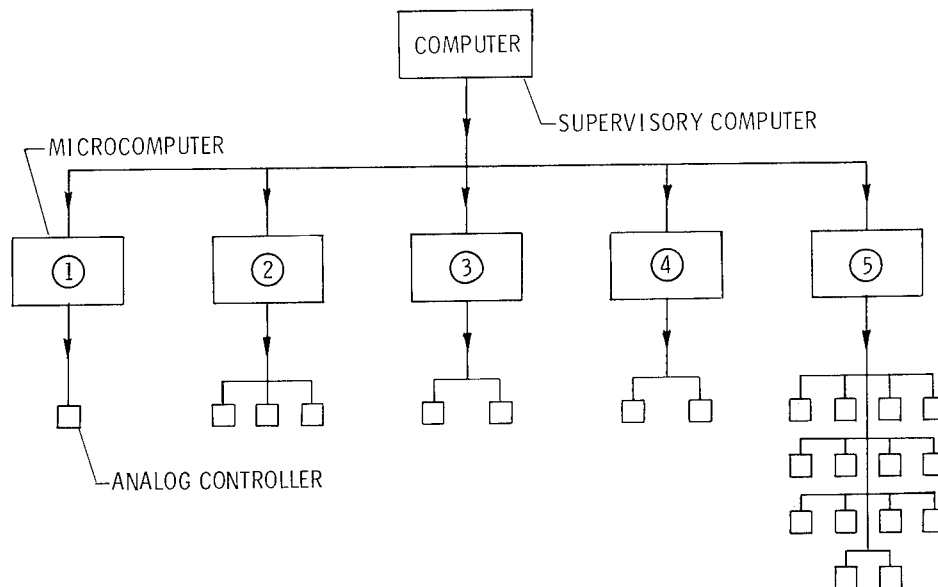Figure 5.- Mach number control algorithm.

Figure 6.- NTF control hierarchy.

DEVELOPMENT OF JOINING TECHNIQUES
FOR FINNED TUBE HEAT EXCHANGER
FOR A CRYOGENIC ENVIRONMENT

John D. Buckley and
Paul G. Sandefur, Jr.
NASA Langley Research Center

SUMMARY

Three joining methods were considered for use in fabricating cooling coils for the National Transonic Facility. After analysis and preliminary testing, soldering was chosen as the cooling coil joining technique over mechanical force fit and brazing techniques. Charpy V-Notch Tests, cyclic thermal tests (ambient to $77.8^{\circ}K$ ($140^{\circ}R$)) and tensile tests at cryogenic temperatures were performed on solder joints to evaluate their structural integrity. It was determined that low temperature solder can be used to ensure good fin to tube contact for cooling coil applications.

INTRODUCTION

It has been shown (reference 1) that the cryogenic wind tunnel concept permits high Reynolds numbers to be obtained at relatively low energy consumption levels compared to other high Reynolds number wind tunnel concepts. However, despite this relatively economical use of energy, the overall consumption of energy in high Reynolds number tunnels is high, primarily because of the use of liquid nitrogen injection for cooling (reference 2). If a conventional chilled-water heat exchanger were used for cooling in the ambient temperature mode of operation instead of liquid nitrogen injection, it has been estimated that the consumption of energy in this mode would be reduced by an order of magnitude. The cost of the energy would be reduced even further. In addition to the advantages in energy consumption, the benefits of using a conventional heat exchanger for cooling would also include the capability to use air as well as nitrogen as the test gas in the ambient temperature mode. Figure 1 shows the location of the cooling coil in the National Transonic Facility. It will be used when operating under ambient conditions using air; however, it will not be used when operating under cryogenic conditions. Tests performed on round and elliptical tube and fin cooling coil specimens, measured as a function of Reynolds number based on tube hydraulic diameter, showed an apparent aerodynamic advantage of elliptical tube shape compared to round shape for pressure loss and turbulence characteristics (reference 3). Figure 2 shows a segment of the cooling coil used in the NTF. The tube and fin structures are arranged in rows four deep in the direction of the fluid flow and are fabricated in gangs .914 meters (3 feet) and .457 meters (1.5 feet) across as shown in Figure 3. The diameter of the cooling coil is approximately 12.1 meters (40 feet).

Upon completion of the design and definition of the expected thermo-mechanical and thermodynamic loads, when operating this tunnel, inquiries were made with industry having this expertise. Industry indicated that the uniqueness of this one-of-a-kind cooling coil heat exchanger would require study and development. Because of the need for this heat exchanger in the NTF, the NASA Langley Research Center engaged in a study of the materials and fabrication technology as related to cooling coils exposed to cyclic cryogenic atmosphere. Two interdependent areas of concern became evident: (a) the 12.1 meters (40 feet) diameter suggesting the potential need for segmented lengths of cooling coil requiring tube to tube joints and (b) the effect of cyclic thermal excursions at cryogenic temperatures and cryogenic to ambient temperatures on joints and joint bonding materials.

JOINING METHODS, MATERIALS, AND TEST PROCEDURES

Table I shows the joining methods considered for fabricating the NTF cooling coils. Mechanical force fit is the technique most commonly used in industry to fabricate cooling coils. This method was ruled out early in the study when analysis indicated that thermal cycling in a cryogenic atmosphere would loosen the interface between the tube and fin components making up the cooling coil decreasing the heat transfer efficiency of the system. A second method eliminated early in the study was the dip brazing of aluminum (Table I and Table II). This technique was dropped because of corrosion experienced with aluminum tubing used in similar circumstances. Vacuum brazing of as drawn (hard copper) oxygen free copper (Table I and Table II) brazed with a braze alloy composed of 72% silver and 28% copper was accomplished in a vacuum braze furnace at .00133 newton/meter^2 (10^{-5} torr) at a maximum temperature of 1097.6^0K (1960^0R). Figure 4 shows the braze test specimen with fins, tubes and joints. The joints were required in the specimen because joints would be needed in the full scale cooling coil. There are no vacuum braze furnaces in the United States capable of brazing a cooling coil over 12.1 meters (40 feet) in length with the configuration required for NTF. Two low temperature solders (Table II) were also evaluated using as drawn (hard copper) oxygen free copper. The advantages of using low temperature solder were the low temperature and the availability of furnaces that will allow for fabricating 12.5 meters (41 feet) long (diameter) cooling coils. A major disadvantage when using high tin solders is the brittleness of these solders when subjected to temperatures at and below their ductile-brittle transition temperature of 173.6^0K (310^0R). Tensile load tests were performed on copper tube specimens (Figure 5), joined at the center to evaluate solder alloy compositions (Table II) in cryogenic atmospheres. Cryogenic tensile tests were performed in a cold box - Instron tensile test facility. Cyclic cryogenic tests consisted of two steps. Tensile specimens (Figure 5) were submerged in liquid nitrogen, held in place until thermal equilibrium was reached, raised out of the nitrogen into a furnace at 355.6^0K (635^0R), again held in position until thermal equilibrium was reached, and then the cycle repeated for a predetermined number of cycles. Upon completion of the

desired number of thermal cycles the specimens were removed and tested (ambient conditions) in tension in the Instron testing machine. Thermal cycle tests made on a segment of the NTF cooling coil to evaluate the integrity of the fin to tube bond used the thermal cyclic technique described above for the tensile specimens (Figure 6). Upon completion of the thermal cycles the specimen was examined with a metallograph to observe the presence of cracks at the fin-tube interface.

RESULTS AND DISCUSSION

As described earlier in this paper, Mechanical Force Fit and Dip Brazing were eliminated after analysis of these techniques. Upon completion of vacuum brazing a hard copper specimen brazed with 72% silver and 28% copper, this technique was dropped. The specimen (Figure 7) was so ductile after brazing that copper cooling coils fabricated using this technique would be considered structurally unacceptable. Because soldering techniques would allow fabrication at low temperatures (453.6^oK (810^oR)) and eliminate the need for joints, it was considered the most promising method for manufacture of the cooling coils. The solder material now had only one major function and that was to maintain its thermal interface between cooling coil fin and tube when subjected, though not in use, to cryogenic cycling. The results of a literature search are summarized in Table III. The data indicates that solder alloys having a major tin constituent become brittle and eventually crack when subjected to cyclic heating and cooling between 397.6^oK (710^oR) and 77.78^oK (140^oR). Charpy V-Notch Tests were performed on the two solder alloys chosen for this structure to substantiate data from the literature. The V-Notch Tests showed both alloys had acceptable toughness at room temperature but had very low impact strength at 77.78^oK (140^oR).

Because the cooling coil would have no impact loads and would operate in ambient conditions, several additional tests were performed to evaluate the integrity of the tube to fin solder joint. Tensile load tests were performed on copper tube specimens (Figure 5) joined at the center with solder alloy composition shown in Table II. Tensile tests were used as the criteria for solder joint acceptability since a cracked specimen, assuming a crack in the solder joint resulted from specimen exposure to cycling at cryogenic temperatures, would have a lower tensile strength than a specimen with no flaws. Figure 8 shows solder joint strength as a function of temperature. The curves show the expected increase in strength to the ductile-brittle transition temperature where the strength then falls off (reference 4). The important point observed in these curves was that the solder joint strength (low notch toughness, Table IV) at cryogenic temperatures approximated or was stronger than the solder joint tested at room temperature (good notch toughness, Table IV). Figure 9 shows joint strength of specimens pulled at ambient temperature after up to 5000 cyclic cryogenic exposures between 77.78^oK (140^oR) and 355.6^oK (635^oR). Lines

faired through data points for the two solder alloys evaluated showed no appreciable change in the strength of the solder joints. Finally, the typical segment of a fin-tube cooling coil (Figure 6) cycled 5000 times between 77.78°K (140°R) and 355.6°K (635°R) showed no cracks at the tube-fin interface when examined with a metallograph.

CONCLUSIONS

The results of this study indicate the following conclusions:

1. Cyclic cryogenic exposure did not affect the room temperature strength of the low temperature solder joint.

2. The low temperature solders in the joints tested did not show cracking when submitted to cyclic exposure below their ductile-brittle transition temperature.

3. Low temperature solder can be used to ensure good fin-to-tube contact for cooling coil applications.

REFERENCES

1. Kilgore, Robert A.; Goodyer, Michael J.; Adcock, Jerry B.; and Davenport, Edwin E.: The Cryogenic Wind-Tunnel Concept for High Reynolds Testing, NASA TN-D-7762, November 1974.

2. Polhamus, E. C.; Kilgore, R. A.; Adcock, J. B.; and Ray, E. J.: The Langley Cryogenic High Reynolds Nubmer Wind-Tunnel Program, Astronautics and Aeronautics, Vol. 12, No. 10, October 1974, pp. 30-40.

3. Johnson, W. G., Jr. and Igoe, W. B.; Aerodynamic Characteristics at Low Reynolds Numbers of Several Heat-Exchanger Configurations for Wind-Tunnel Use, NASA TM-80188, December 1979.

4. Taffee, R. I.; Minarcek, E. J.; Gonser: "Low Temperature Properties of Lead Base Solders and Soldered Joints" Metals Progress, December 1948, pp. 843-845.

TABLE I.- JOINING METHODS

- **MECHANICAL FORCE FIT**

- **BRAZING**
    - A. DIP BRAZING
    - B. VACUUM FURNACE BRAZING

- **SOLDERING**
    - A. 95% TIN – 5% SILVER
    - B. 63% TIN – 37% LEAD

TABLE II.- COOLING COIL MATERIALS

TUBE AND FIN ALLOYS	BRAZE ALLOYS	SOLDER ALLOYS	JOINING TECHNIQUES
6061 ALUMINUM	89% ALUMINUM 11% SILICON		DIP BRAZING
OXYGEN FREE COPPER	72% SILVER 28% COPPER		VACUUM BRAZE (HARD-COPPER)
OXYGEN FREE COPPER		{ 95% TIN, 5% SILVER } { 63% TIN, 37% LEAD }	LOW TEMPERATURE FURNACE SOLDER (HARD-COPPER)

263

TABLE III.- SOLDER DATA - ELECTRICAL CONNECTIONS

- TIN SOLDER TESTS

    — 63 TIN - 37 LEAD

    — 95 TIN - 5 ANTIMONY

- CYCLED BETWEEN 77.8 K (140°R) - 355.6 K (635°R)

- SOLDER WIRE CONNECTIONS BECAME BRITTLE AND DEVELOPED CRACKS RESULTING IN NOISY ELECTRICAL OUTPUT

TABLE IV.- ASTM CHARPY V-NOTCH TEST DATA

SOLDER MATERIALS

TEMPERATURE K (°R)	QUANTITY	95% TIN – 5% SILVER IMPACT VALUE J (FT-LB)	63% TIN – 37% LEAD IMPACT VALUE J (FT-LB)
ROOM TEMP.	6	51.68 (38)	25.84 (19)
355.6 (635)	6	51.68 (38)	25.84 (19)
77.8 (140)	6	.544 (0.4)	1.22 (0.9)
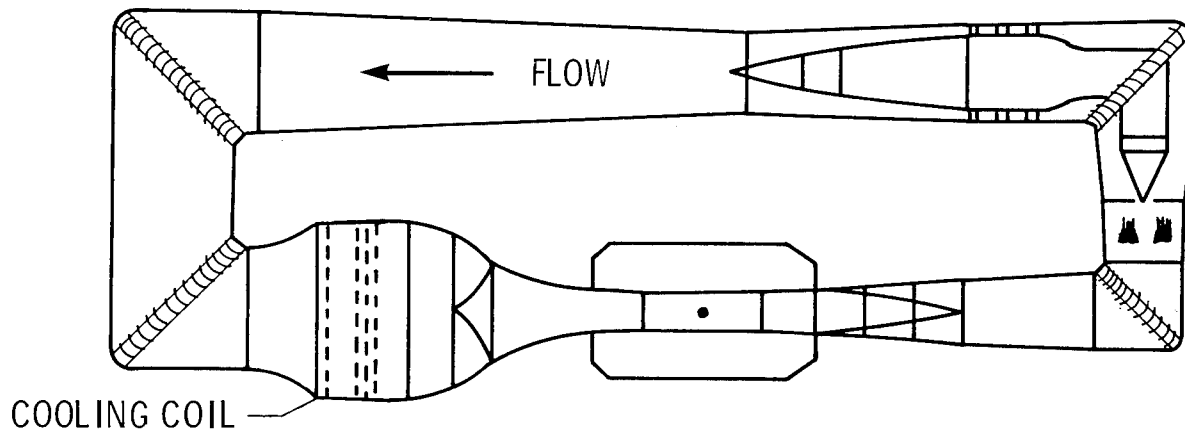
Figure 1.- Location of cooling coils in NTF.
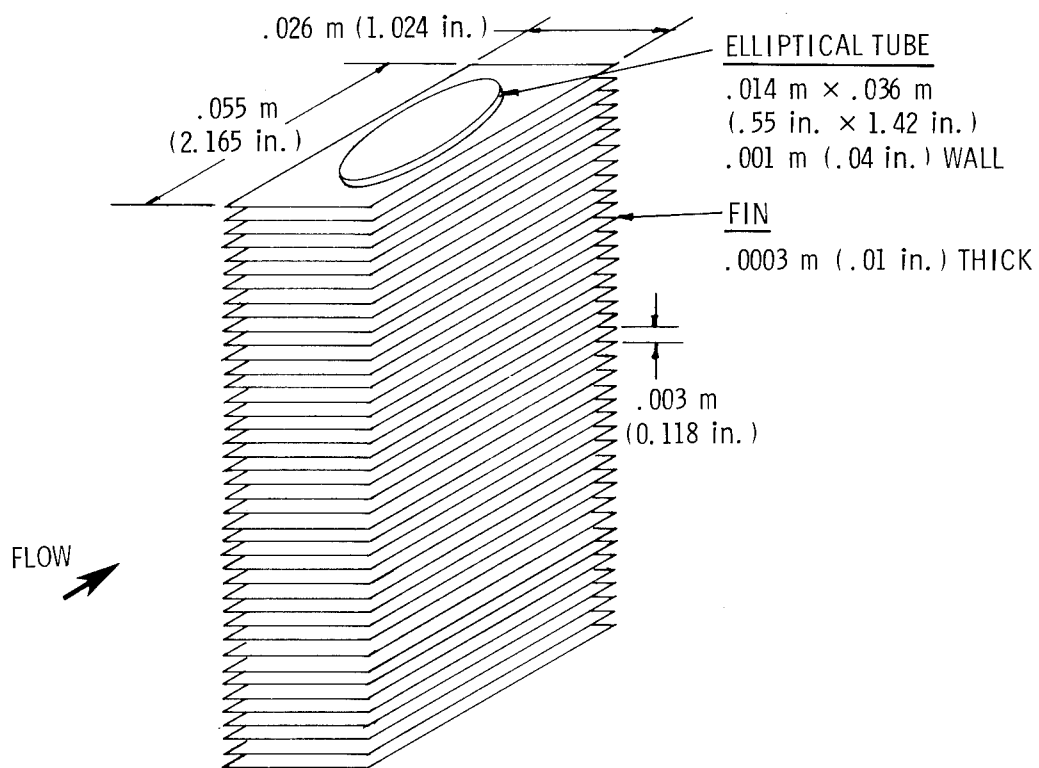
Figure 2.- Fin-tube concept showing section of NTF cooling coil.
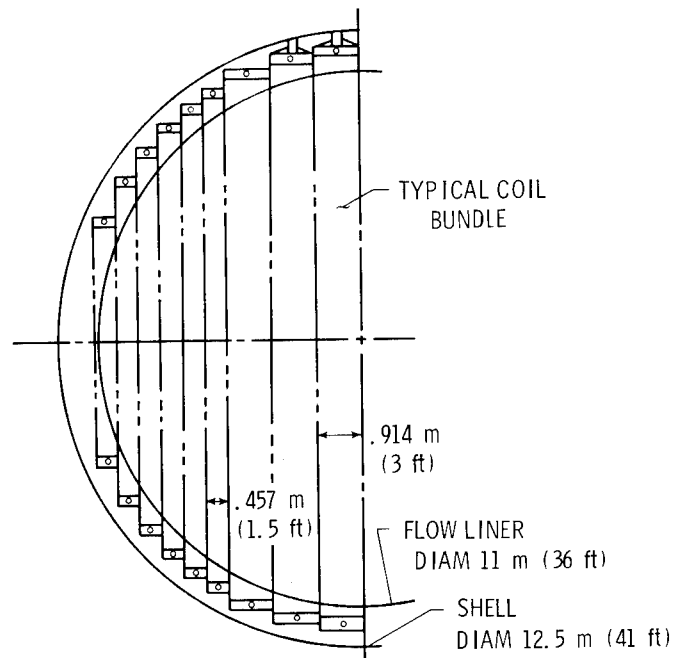
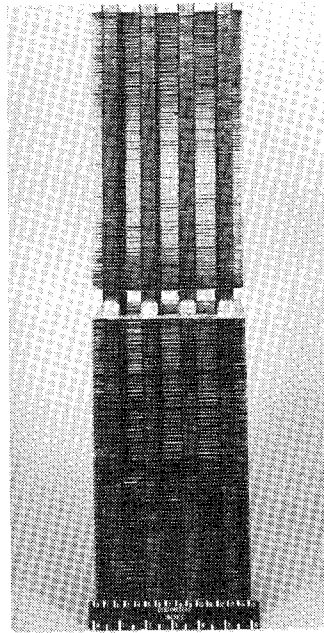Figure 3.- Cross section of NTF tunnel showing cooling coil.

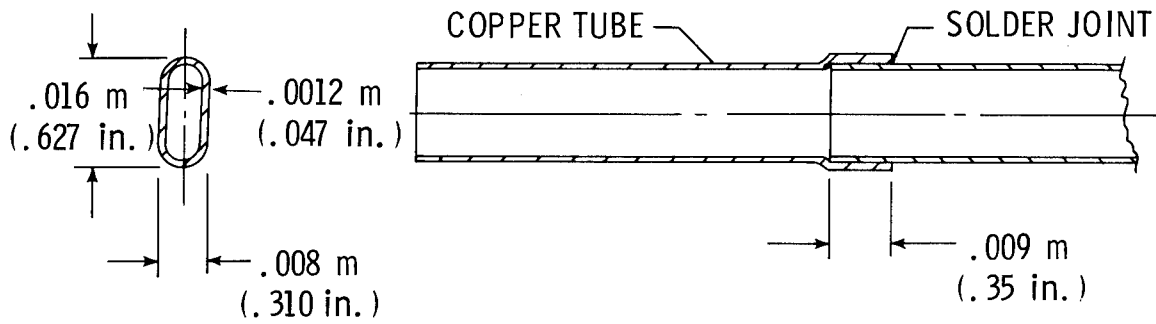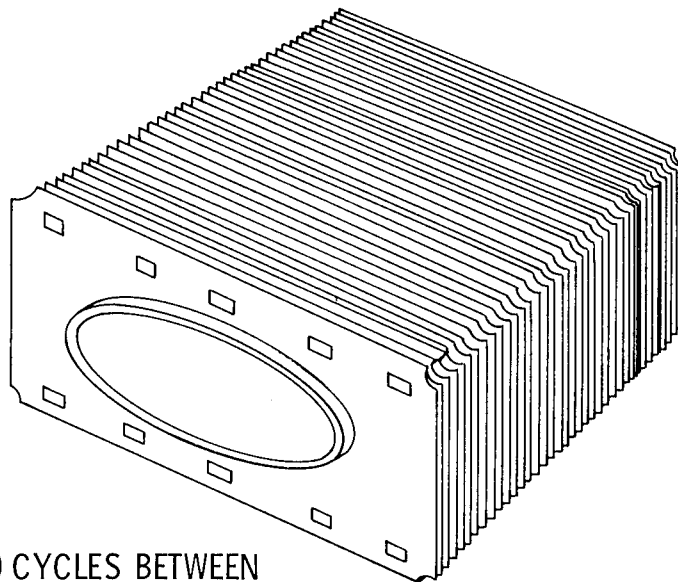Figure 4.- Braze test specimen showing fin-tube and tube to tube joints.

Figure 5.- Copper tube solder joint tensile load test specimen.

5000 CYCLES BETWEEN
77.8 K (140°R) AND 355.6 K (635°R)

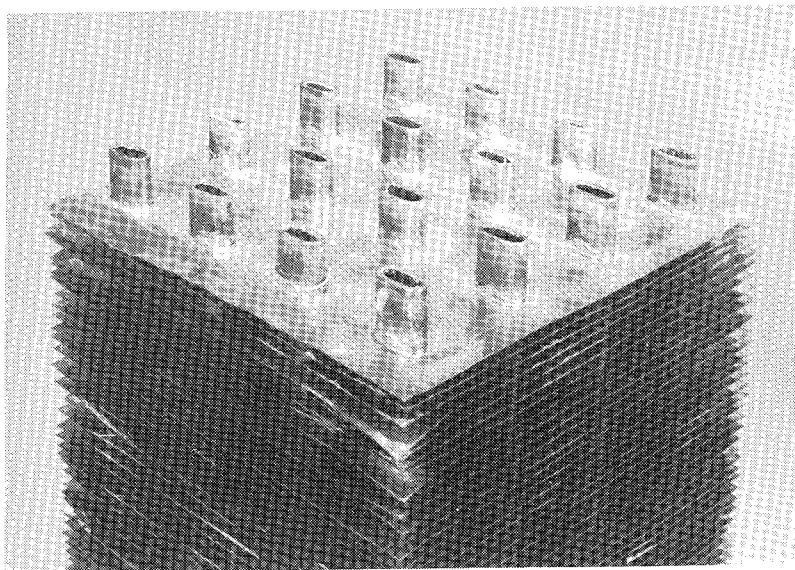Figure 6.- NTF cooling coil thermal cycle test specimen.

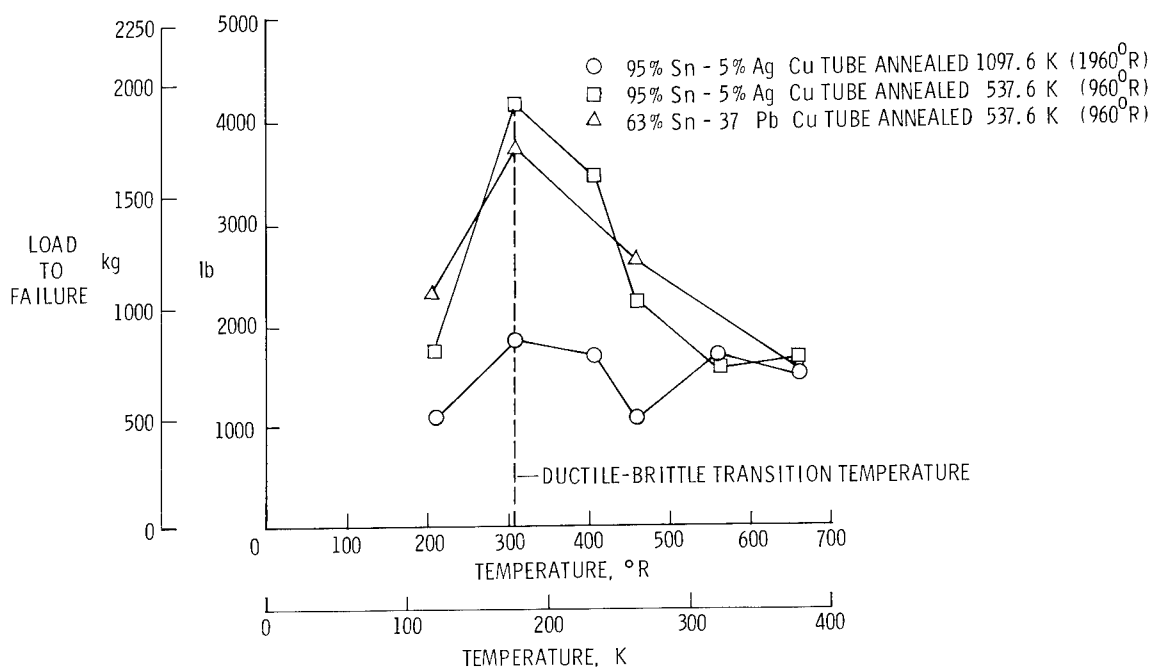Figure 7.- Tube and fin specimen after vacuum braze at 1097.6 K (1960°R).

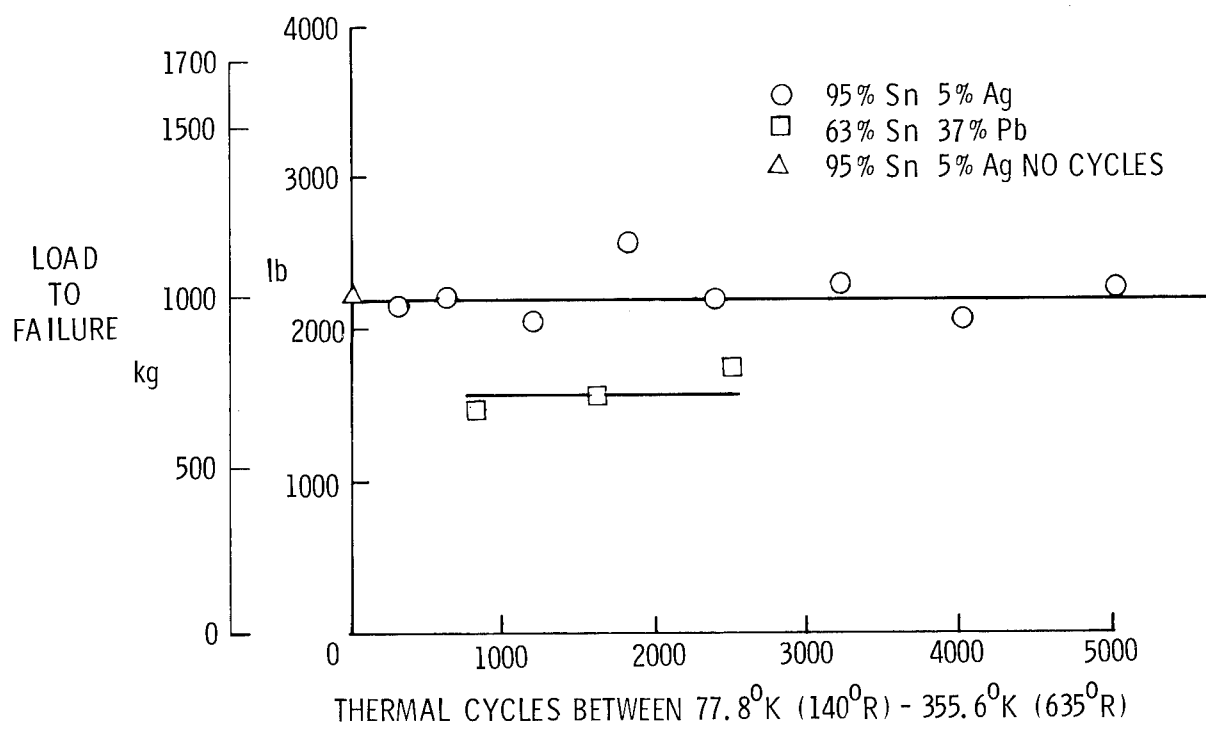Figure 8.- Solder joint strength as a function of temperature.

Figure 9.- Solder joint strength pulled at ambient temperature after thermal cyclic exposure between 77.8 K – 355.6 K ($140^{o}R$ – $635^{o}R$).

CRYOGENIC GASEOUS NITROGEN

DISCHARGE SYSTEM

George W. Ivey, Jr.
Langley Research Center

SUMMARY

A system design is discussed in this paper which safely discharges cryogenic gaseous nitrogen at flow rates ranging from 0 to 907 kg/sec (2000 lbm/sec) into the atmosphere near commercial and residential areas. The gaseous discharge is from a cryogenic wind tunnel where the stagnation pressures and temperatures of the test medium ranges from 1.0155×10^5 to 8.9632×10^5 N/m^2 (14.7 to 130 psia) and 77.8 K to 353 K, respectively. A three stream fan/ejector system is employed to mix ambient air with the nitrogen discharge such that the mixture is delivered to the system exit at a sufficient elevation with the appropriate mixture ratio and momentum to insure proper dispersal of the negatively buoyant plume. The design limits or attenuates the noises generated at cryogenic temperatures by the system. Safety considerations and hazard controls were major factors considered in the design.

INTRODUCTION

The National Transonic Facility (NTF) is a continuous flow transonic wind tunnel that uses pressurized cryogenic gaseous nitrogen as the flow medium for testing models at Reynolds numbers comparable to those of full scale aircraft. A liquid nitrogen injection system injects liquid nitrogen (LN_2) into the tunnel, after which the LN_2 is vaporized by the heat of compression of the drive fan. Conditions of constant pressure, temperature, and Mach number in the test section are obtained by controlling the amount of injected LN_2 and exhausting that same amount in cryogenic gaseous form. Inasmuch as the cryogenic GN_2 exhaust contains no oxygen and produces fog, it was necessary to devise a system that would exhaust the discharge into the atmosphere safely.

A discharge system for safely dispersing the gaseous nitrogen (GN_2) exhaust of the NTF into the atmosphere is described in this paper. An artist's rendering of this system and the NTF is shown in figure 1.

The system was designed for normal operational discharge flow rates ranging from 0 to 426 kg/sec (940 lbm/sec) and emergency flow rates up to 907 kg/sec (2000 lbm/sec). The stagnation temperature of the flow ranges from 77.8 K to 353 K. A three stream fan/ejector system using the tunnel stagnation pressure as its major energy source was selected based on its performance over the broad tunnel operational temperature and pressure ranges including startup and shutdown transients.

The fan/ejector was designed to safely disperse the cryogenic GN_2 into the atmosphere with no adverse effects on human, animal, or plant life. The three stream mixing approach insures that prior to release into the atmosphere, at least one part of air is mixed with one part of nitrogen. A muffler installed within the discharge flow system and a surrounding acoustic enclosure reduces the discharge throttling process noises and the fan noises to an acceptable level in the surrounding environment.

FAN/EJECTOR OPERATION AND PERFORMANCE

The three stream fan/ejector system's basic components include an exhaust vessel which contains a muffler; secondary air inlet nozzle; four fans with outlet ducting and silencers; exhaust stack (mixing tube); and acoustic enclosure as shown in figure 2. Ambient air premixed with the discharge GN_2 within the stack provides an O_2 concentration greater than 10% by volume upon release into the atmosphere. Secondary air is induced into the stack by the ejector pumping action of the primary jets. The primary jet is the GN_2 discharge at the higher mass flow rates and the fan air at the lower flow rates. Momentum is transferred from the primary jet to the other two flow streams to achieve proper mixing and a high stack exit momentum.

All three streams enter the stack at the mixing plane as shown in figure 2. These streams are symmetrically arranged. The GN_2 circular jet is surrounded by the fan air and secondary air annular jets. This arrangement limits ice formation by maintaining an ambient air flow along the interior stack surface until the mixing process is essentially complete. The mixing is accomplished within 80% of the stack height.

A literature survey yielded information on only two stream ejectors (references 1 and 2). Consequently, the three stream fan/ejector analytical model and computer code were developed at Langley Research Center which defined the fluid dynamic performance of the system. The overall fluid dynamic performance is characterized in figure 3 by the mass flow ratio and the exit velocity envelopes. The mass flow rate ratio is defined as the ratio of the ambient air flow rate to the cryogenic GN_2 flow rate.

The mass flow rate ratio is shown as a function of the GN_2 mass flow rate and stagnation temperatures. The upper and lower curves show how the fan/ejector performs at normal operating stagnation temperatures of 353 K and

111 K, respectively. These curves are bounded on the right by the tunnel emergency operating limit line. The dash line near the right is the tunnel normal operating limit line. As shown in figure 3, the mass flow ratio is greater than one for any GN_2 discharge rate such that the oxygen content by volume is always greater than 10%. In the region controlled by the fans, the mass flow rate ratio increases rapidly as the GN_2 discharge rate approaches zero. In the ejector controlled region the mass flow rate ratio decreases slowly as the GN_2 discharge increases. Even though the fans do not control the ejector action at the higher GN_2 discharge rates, the fans do provide additional energy to the exhaust flow. This energy addition is primarily responsible for the slower decrease in the mass flow rate ratio with increasing GN_2 discharge rates than would be expected for a conventional two stream ejector system.

Similarily, the exit velocity envelope is shown as a function of discharge flow rate and stagnation temperature. The minimum exit velocity at 23.8 m/sec (78 ft/sec) corresponds to only the fan air flow when there is no GN_2 discharge. The maximum velocity is 145 m/sec (475 ft/sec) which occurs during a tunnel emergency condition at 353 K and corresponds to a mass flow ratio at two. For normal operations, the maximum velocity of 73 m/sec (240 ft/sec) occurs for a GN_2 discharge rate of 426 kg/sec (940 lbm/sec) at a 111 K stagnation temperature.

PLUME DISPERSION

The discharge system was designed to premix one part of GN_2 with at least one part of air at any normal operational condition, such that a breathable mixture is released at the top of the stack. During the design, it was determined that a high exit momentum was required to disperse the negatively buoyant plume such that fogging at ground level is minimized.

As shown in figure 4, this exit momentum increases the plume O_2 concentration and temperature by inducing large quantities of ambient air into the turbulent mixing region of the plume. By increasing the plume temperature, fog formation is minimized and the effects of negative buoyancy forces are reduced. The maximum plume height is increased by the high momentum and allows more time for ambient air to diffuse into the plume after the turbulent mixing process is complete. This high momentum also reduces the wake effects of surrounding buildings on the exhaust plume.

A two-stage atmospheric dispersion model was developed to describe the plume dispersal in the atmosphere. The model includes the negative buoyancy of the plume and divides the plume into two stages: an initial stage treated as a jet with Gaussian spreading of properties in the radial direction; and a second stage with vorticity and drifting with the meteorological wind

direction. The dispersion model predicts O_2 concentrations of at least 19% by volume for all operating conditions. Prior to the plume approaching ground level, the O_2 concentration approaches 21% by volume, the temperature approaches ambient conditions, and the fog formation dissipates for most conditions. However, at low wind speeds (less than 6.4 km/hr) and high relative humidities (greater than 95%), the plume may approach ground level prior to dissipating. The minimum plume height at which dissipation is analytically predicted to occur is shown in figure 5 as a function of the GN_2 discharge rate at relative humidities of 90 and 95% at wind speeds of 3.6 to 6.4 km/hr (2 to 4 mph). At 95% relative humidity, the plume dissipates at less than 15.24 m above ground level. A concern for excess fogging detrimentally affecting vision at ground level arises when the plume descends below 15.2 m (50 ft). The NTF Environmental Impact Statement states that tunnel operations will be restricted when these conditions exist.

NOISE SOURCES AND CONTROL

The major noise sources of the discharge system are the throttling process, fans, primary jet, and the mixing process noises. The NTF Environmental Impact Statement established that these sources would not violate a criteria of 66 dBA at a residential trailer park located about 137 m (450 ft) from NTF. The worst case discharge noise levels at 137 m (450 ft) with and without acoustic treatment is shown in figure 6 for each major noise source. The throttling noise propagating down the exhaust piping is attenuated by a 3.05 m (10 ft) dia., 9.8 m (32 ft) long annular muffler, using a bulk absorber as the acoustic attenuation material. The throttling noise radiating through the piping upstream of the muffler is attenuated by a 7.6 m (25 ft) high steel enclosure about the discharge system. The fan/ejector systems' outlet and inlet fan noise are controlled by a cylindrical silencer and the enclosure, respectively. The mixing noise generated by the fan/ejector primary is controlled by limiting the ejector Mach number to .7. The overall sound pressure level with and without acoustic treatment is 91 dBA and 65 dBA, respectively. With the acoustic treatment, the noise level of 65 dBA satisfies the 66 dBA noise level requirement.

CONCLUSIONS

The fan/ejector discharge system meets all the design requirements which include fog formation and dissipation, O_2 concentration, and the noise levels at 37 m (450 ft) from the exhaust stack. It is concluded that a design has been achieved which safely disperses large quantities of cryogenic GN_2 associated with the NTF operation, into the atmosphere.

REFERENCES

1. Kastner, L. J.; and Spooner, J. R.: An Investigation of the Performance and Design of the Air Ejector Employing Low-Pressure Air As the Driving Fluid. Institution of Mechanical Engineers Proceedings, Vol. 162, no. 2, pp. 149-166, 1950.

2. Bird, R. Byron; Stewart, Warren E.; and Lightfoot, Edwin N.: Transport Phenomena. John Wiley and Sons, Inc., New York, Ch. 7 and Ch. 15, 1960.
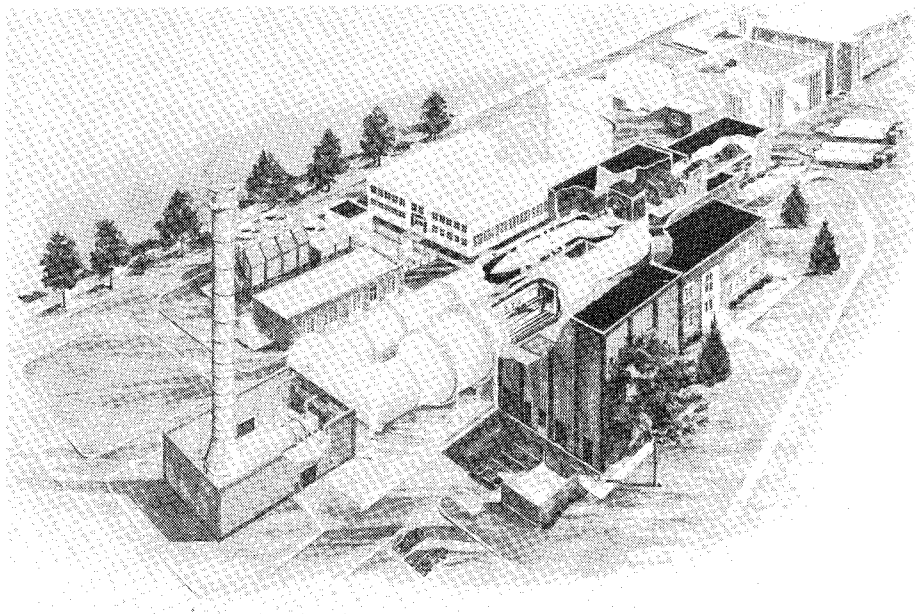
Figure 1.- Cryogenic GN_2 discharge system.

STACK

MUFFLER

MIXING PLANE

SECONDARY AIR

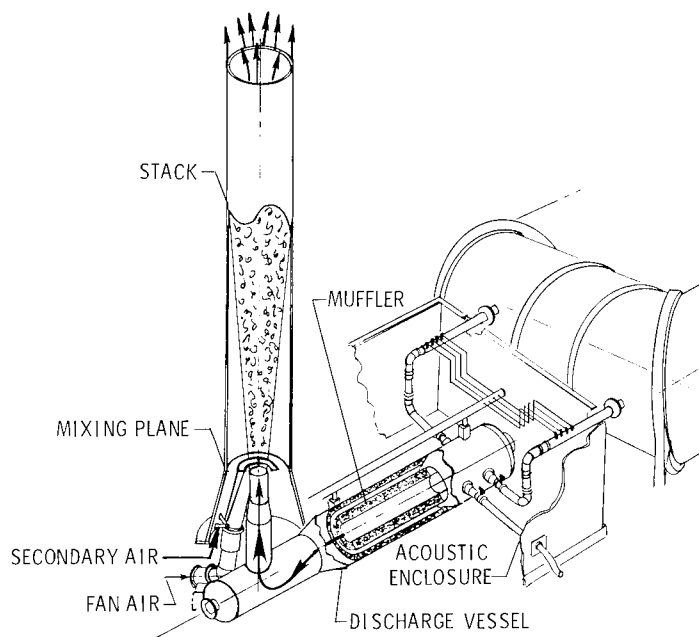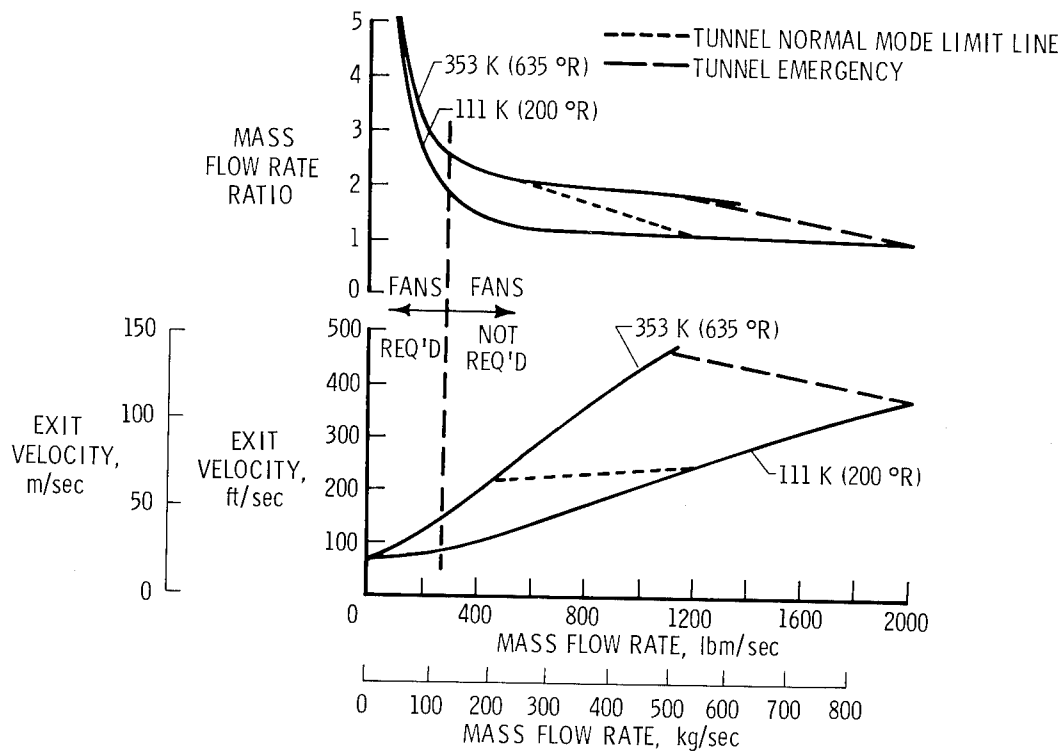FAN AIR

ACOUSTIC ENCLOSURE

DISCHARGE VESSEL

Figure 2.- Discharge system elements.

Figure 3.- Aerodynamic performance envelopes.

Figure 4.- Stack exit flow.

N$_2$ TEMPERATURE = 111 K (200 °R)
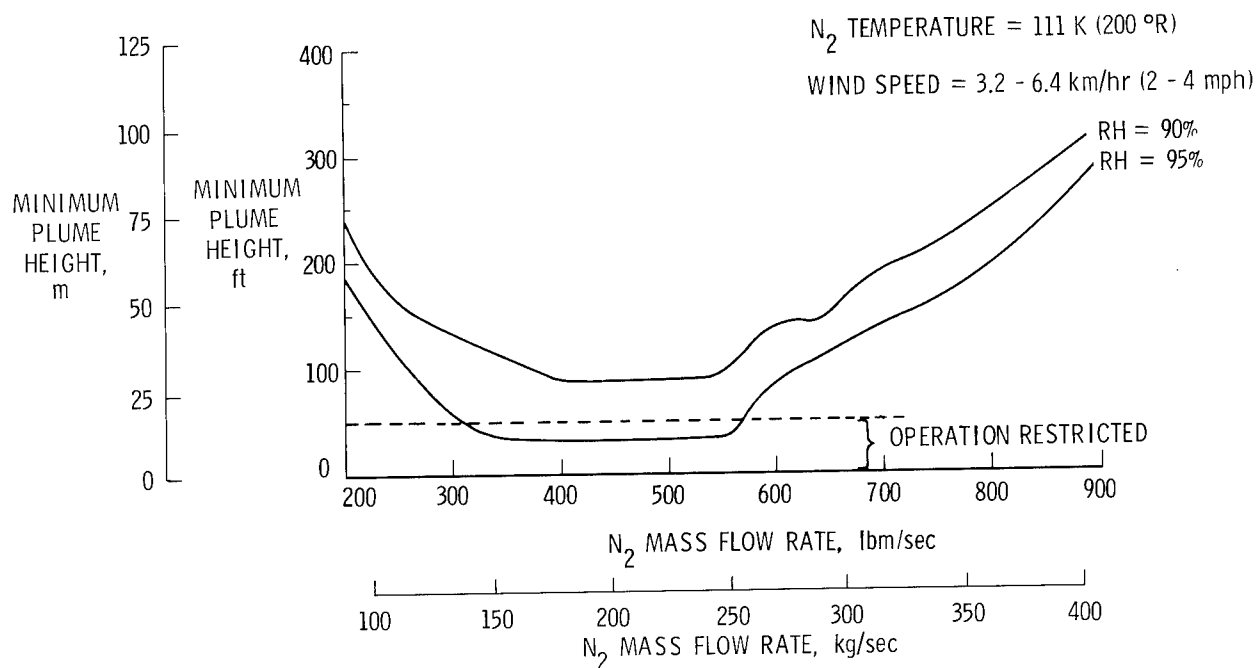
WIND SPEED = 3.2 - 6.4 km/hr (2 - 4 mph)
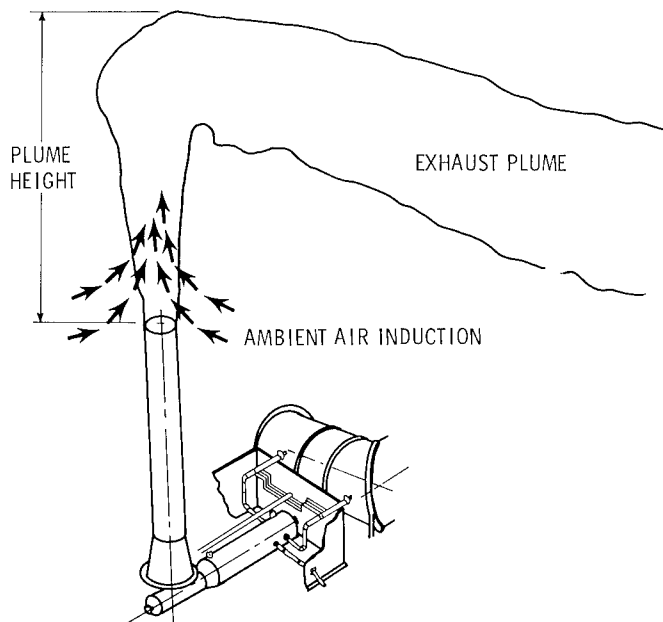
Figure 5.- Exhaust plume height.

NOISE SOURCES	NO TREATMENT	TREATMENT	WITH TREATMENT
THROTTLING PROCESS			
● FLOW NOISE - STACK EXIT	91	MUFFLER	60
● NOISE RADIATED-VESSEL	77	ENCLOSURE	60.4
FANS' FLOW NOISE			
● OUTLET-STACK EXIT	60	SILENCER	55.5
● INLET	69	ENCLOSURE	48.4
PRIMARY JET AND MIXING PROCESS			
● FLOW NOISE - STACK EXIT	60	LIMIT EXIT MACH NO.	60
OVERALL SOUND POWER LEVEL	91		65.3

Figure 6.- Discharge noises (dBA at 137 m (450 ft)).

1. Report No. NASA CP-2122, Part I	2. Government Accession No.	3. Recipient's Catalog No.
4. Title and Subtitle CRYOGENIC TECHNOLOGY		5. Report Date March 1980
		6. Performing Organization Code
7. Author(s)		8. Performing Organization Report No. L-13547
		10. Work Unit No. 505-31-53-01
9. Performing Organization Name and Address NASA Langley Research Center Hampton, VA 23665		11. Contract or Grant No.
		13. Type of Report and Period Covered Conference Publication
12. Sponsoring Agency Name and Address National Aeronautics and Space Administration Washington, DC 20546		14. Sponsoring Agency Code

15. Supplementary Notes

16. Abstract

The proceedings of the NASA Conference, Cryogenic Technology, held at the Langley Research Center on November 27-29, 1979, are reported in this NASA conference proceedings. The proceedings contain 29 papers which address different engineering problems associated with the design of mechanisms and systems to operate in a cryogenic environment. The focal point for entire engineering effort was the design of the National Transonic Facility, which is a closed-circuit cryogenic wind tunnel. The papers covered a variety of subjects including thermal structures insulation systems, noise, seals, controls, instrumentation, and materials. Papers also addressed design, fabrication, and instrumentation problems for models to be tested in a cryogenic medium.

17. Key Words (Suggested by Author(s)) Cryogenic technology Cryogenic wind tunnel Cryogenic seals Cryogenic insulation Cryogenic wind-tunnel models	18. Distribution Statement FEDD Distribution Subject Category 31
19. Security Classif. (of this report) Unclassified	20. Security Classif. (of this page) Unclassified	21. No. of Pages 284	22. Price* $11.00

Available: NASA's Industrial Application Centers

National Aeronautics and
Space Administration

Washington, D.C.
20546

SPECIAL FOURTH CLASS MAIL
BOOK

Postage and Fees Paid
National Aeronautics and
Space Administration
NASA-451

U.S.MAIL

NASA

POSTMASTER: If Undeliverable (Section 158
Postal Manual) Do Not Return